

Studies into the Role of Peptidoglycan Glycolylation in Mycobacterial Dormancy and Resuscitation

Jessica Loraine

Thesis submitted to The University of Leicester for the
degree of Doctor of Philosophy

June 2013

Department of Infection, Immunity and Inflammation
College of Medicine, Biological Sciences and
Psychology
University of Leicester
University Road, Leicester, LE1 7RH

ABSTRACT

Studies into the Role of Peptidoglycan Glycolylation in Mycobacterial Dormancy and Resuscitation

Jessica Loraine

A third of the global population are estimated to be latently infected with *Mycobacterium tuberculosis* (*Mtb*). This latent infection is most likely caused by non-replicating bacilli. Resuscitation-promoting factors (Rpfs) are secreted muralytic enzymes which are important for replication *in vivo* and are involved in resuscitation of dormant bacilli and reactivation of chronic tuberculosis. The precise mechanism of resuscitation remains unknown; however their enzymatic activity is essential for resuscitation and growth stimulatory effects.

In mycobacterial peptidoglycan, muramic acid is present in acetylated and glycolylated forms. Glycolylation occurs in the cytoplasm during synthesis of peptidoglycan precursors by action of a UDP-N-acetylmuramic acid hydroxylase (NamH). The significance of glycolylation for mycobacterial growth and persistence is unknown.

The overall aims of this study were to investigate the importance of peptidoglycan glycolylation in mycobacterial dormancy and resuscitation. Rpfs are the key enzymes involved in these processes, it was therefore predicted they might be adapted for recognition and cleavage of glycolylated peptidoglycan. *Mtb* NamH was over-expressed in *E. coli* in order to obtain glycolylated peptidoglycan and investigate its digestion by recombinant Rpfs. Recombinant Rpf was active by zymography but failed to release soluble muropeptides from different types of peptidoglycan.

The role of peptidoglycan glycolylation in stimulation of mycobacterial growth and resuscitation of non-culturable bacilli was investigated in *M. smegmatis*: *Mtb* Rpfs were shown to stimulate growth in wild type and $\Delta namH$ *M. smegmatis*, indicating that Rpf activity was not influenced by peptidoglycan glycolylation. *Mtb* Rpfs were also able to stimulate resuscitation of non-culturable *M. smegmatis*. The $\Delta namH$ mutant failed to produce non-culturable cells, therefore its resuscitation could not be investigated.

A $\Delta namH$ *Mtb* mutant showed no significant difference in replication *in vitro* and in cultured macrophages; however it was more sensitive to isoniazid treatment. Overall these results indicate that peptidoglycan glycolylation is important for maintenance of cell wall structure and antimicrobial resistance.

ACKNOWLEDGEMENTS

I would like to thank my supervisor Dr Galina Mukamolova for her support and advice throughout my PhD, as well as the funding bodies: BBSRC, MRC and the University of Leicester for providing the opportunity to work on this project. In addition I would like to thank members of lab 213b and 136 for all their help and support; I would particularly like to mention Dr Barbara Rieck and Dr Obolbek Turapov for their input.

I would also like to thank M. Pavelka and M. Young for materials provided, W. Vollmer and J. Biboy for their help with peptidoglycan purification and identification as well as E. Salina for her assistance with resuscitation experiments.

Additionally I would like to thank my progress review panel members Dr Helen O'Hare and Prof Mike Barer who were extremely attentive and offered advice throughout my PhD. I would like to thank Su-min Lee for his time spent training me in the containment lab as well as Andrew Bell and Abdul Binjomah for their microscopy advice and assistance. Many thanks also to Nino Iakobachvili, Gregory Forrest, Kathryn Pugh, Helen Lewis and Asel Sarybaeva for their friendship and encouragement.

Finally I would like to thank my family and friends for their support.

LIST OF COMMON ABBREVIATIONS

ADC	Albumin Dextrose Catalase
Ala	Alanine
AG	Arabinogalactan
APS	Ammonium persulphate
Arg	Arginine
ATP	Adenosine Triphosphate
BCIP/NBT	5-bromo-4-chloro-3'-indolyphosphate p-toluidine salt/nitro-blue tetrazolium chloride
Bp	Base pair
cAMP	cyclic Adenosine Monophosphate
cDNA	complementary DNA
CFU	Colony Forming Unit
CMBT	5-Chloro-2-mercaptobenzothiazole
Da	Dalton
D-Glu	D-iso-Glutamic acid
DMEM	Dulbecco's Modified Eagle's Medium
DMSO	Dimethyl sulfoxide
DNA	Deoxyribonucleic acid
dsDNA	double stranded DNA
ELISA	Enzyme linked immunosorbant assay
ES	Electrospray
ESAT-6	Early secreted antigenic target 6
ETB	Ethambutol
FAS-II	Fatty acid synthase-II
GC-MS	Gas chromatography mass spectrometry
gDNA	Genomic DNA
Gly	Glycine
HIV	Human immunodeficiency virus
IGRA	Interferon-gamma release assays
INZ	Isoniazid
IPTG	Isopropylthio- β -galactoside
LA	Luria agar
LAM	Lipoarabinomannan
LB	Lysogeny broth
LC-MS	Liquid chromatography mass spectrometry
LPS	Lipopolysaccharide
LTBI	Latent TB Infection
Lys	Lysine
mAGPc	Mycolyl-arabinogalactan-peptidoglycan complex
MALDI-ToF	Matrix-assisted laser desorption/ionisation-time of flight
mDAP	<i>meso</i> -Diaminopimelic acid
MDR	Multi-drug resistant
MDP	Muramyl Dipeptide
mHdeB	Modified Hartman's-de Bont

MOI	Multiplicity of infection
MPN	Most probable number
mRNA	Messenger RNA
MS	Mass spectrometry
MTBC	Mycobacterium tuberculosis complex
NAAT	Nucleic acid amplification test
NAM	N-acetylmuramic acid
NamH	N-acetylmuramic acid hydroxylase
NAG	N-acetyl glucosamine
NGM	N-glycolyl muramic acid
NOD	Nucleotide-binding oligomerisation domain receptors
NRP	Non-replicating persistence
NTM	Non-tuberculosis mycobacteria
OD	Optical density
PBS	Phosphate buffered saline
PCR	Polymerase chain reaction
PG	Peptidoglycan
PknB	Protein kinase B
PM	Permethylation
PZA	Pyrazinamide
qPCR	Quantitative PCR
RIF	Rifampicin
RipA	Rpf interacting protein A
RNA	Ribonucleic acid
Rpf	Resuscitation promoting factor
Rp-HPLC	Reverse phase high performance liquid chromatography
rRNA	Ribosomal RNA
RT	Room temperature
SDS	Sodium dodecyl sulphate
SDS-PAGE	SDS polyacrylamide gel electrophoresis
TBDB	Tuberculosis database
Tc	Tetracycline
TCA	Tricarboxylic acid cycle
TEMED	N, N, N', N'-tetramethylethylenediamine
TNF α	Tumour necrosis factor α
TST	Tuberculin skin test
UDP	Uridine diphosphate
WHO	World health organisation
WT	Wild type
XDR	Extensively drug resistant

LIST OF FIGURES

Figure 1: TB Incidence Rates, Estimated (2010).....	3
Figure 2: TB Incidence Rates, Estimated (2011).....	4
Figure 3: Estimated HIV Prevalence in New TB Cases.....	5
Figure 4: Site of Action of the Four Primary Anti-tuberculosis Drugs	12
Figure 5: Hypothetical Phylogeny of MTBC	18
Figure 6: Schematic of mAGPc within the Mycobacterial Cell Wall.....	22
Figure 7: Schematic of NamH Glycolylation of PG Precursors	24
Figure 8: An Adapted Schematic Depicting Electron Transfer in a Three Component Rieske Oxygenase System	25
Figure 9: Structure of NAG-NAM-Pentapeptide	28
Figure 10: Structural Schematic showing <i>Mtb</i> 's Rpf A-E Domains.....	36
Figure 11: A PG Schematic Showing the Proximity of Rpf Binding and Glycolylated PG	38
Figure 12: The Potential Role of Rpf released Muropeptides as Signalling Molecules.....	41
Figure 13: A Schematic Showing Peptidoglycan Hydrolases	58
Figure 14: A Schematic 'Van Deemter plot'	60
Figure 15: A Schematic Showing MALDI-ToF Geometry	62
Figure 16: A Schematic for Permethylation of Carbohydrates	76
Figure 17: Microscopy and Growth Analysis of pET15b- <i>namH</i> and pET15b ...	78
Figure 18: Western Blot of Total Cell Extracts Developed with Anti- PolyHis Antibody.	80
Figure 19: Anti-PolyHis Western Blot Showing Soluble and Insoluble Fractions of IPTG Induced pET15b- <i>namH</i> BL21.....	82
Figure 20: Growth Analysis of pBAD- <i>NamH</i> TOP10 after 0.02% Arabinose Induction	83
Figure 21: Western Blot using Anti-PolyHis Antibodies Showing IPTG Induced TOP10 pBAD- <i>namH</i> Insoluble and Soluble Protein Fractions.	85
Figure 22: pET15b BL21 Mutanolysin Digested rp-HPLC Muropeptide Profile	88
Figure 23: pET15b- <i>namH</i> and Control Cellosyl Released Muropeptide Profiles rp-HPLC Chromatograms.	90
Figure 24: Mass Spectrum of Peak 4 from Cellosyl Digested pET15b- <i>namH</i> BL21 PG	91
Figure 25: rp-HPLC Chromatogram Showing Mutanolysin Derived Muropeptides from 0.02% Arabinose Induced pBAD- <i>namH</i> TOP1093	
Figure 26: Lysozyme Digested pET15b- <i>namH</i> and pET15b PG Separated by rp-HPLC	94
Figure 27: HPLC Chromatograms Showing Mutanolysin Released Muropeptides from both pET15b and pET15b- <i>namH</i> Isolated PG ..	96

Figure 28: LCMS ES Data Showing Hydrolysed Muropeptides from NAM, pET15b and pET15b- <i>namH</i>	98
Figure 29: A Schematic of the Functional Groups for both pET15b- <i>namH</i> and pET15b Muramic acid Available for Methylation.....	100
Figure 30: MALDI-ToF Spectra of Permethylated Hydrolysed PG Samples.....	102
Figure 31: Lysozyme Sensitivity of pET15b- <i>namH</i> BL21 (DE3).....	104
Figure 32: SDS-PAGE of Purified Recombinant pETM-11-RpfB _{ΔDUF} BL21 (DE3).	107
Figure 33: Muralytic Clearance Bands of <i>M. luteus</i> Cell Wall; Digested by Recombinant RpfB _{ΔDUF}	108
Figure 34: rp-HPLC Chromatogram of RpfB _{ΔDUF} Digested pET15b- <i>namH</i> Isolated PG	110
Figure 35: rp-HPLC Chromatogram of RpfB Digested <i>M. smegmatis</i> PG	111
Figure 36: Example of an Amplification Cycle (A) Showing Fluorescence Output and a Standard Curve (B)	126
Figure 37: Melting Curves of cDNA qPCR Samples	128
Figure 38: Colony PCRs from <i>M. smegmatis</i> <i>rpf</i> -pMIND Strains.....	133
Figure 39: Anti-PolyHis ELISA Absorbance Data for Recombinant <i>Mtb</i> RpfB _{ΔUF}	135
Figure 40: ELISA Absorbance Data using Anti-PolyHis Antibodies for Dialysed RpfB _{ΔDUF}	136
Figure 41: ELISA Absorption Data using Anti-PolyHis Antibodies of <i>M. smegmatis</i> Strains in 7H9	138
Figure 42: qRT-PCR Mean Expression Data	140
Figure 43: Bioscreen Growth Curves of <i>M. smegmatis</i> Strains in 7H9.....	142
Figure 44: Bioscreen Growth Curves of Δ <i>namH</i> <i>M. smegmatis</i> Strains in 7H9	144
Figure 45: Sauton's Growth Curves for <i>M. smegmatis</i> Rpf Overexpressing Strains.....	146
Figure 46: Sautons Growth Curve Data for Δ <i>namH</i> <i>M. smegmatis</i> Rpf Strains	147
Figure 47: <i>M. smegmatis</i> pMIND- <i>M. luteus</i> Rpf Resuscitation in a Variety of Media	150
Figure 48: Log ₁₀ MPN Resuscitation Data for Wild Type <i>M. smegmatis</i> Rpf Strains.....	152
Figure 49: Δ <i>namH</i> Knockout Construct Structure.....	165
Figure 50: Schematic Showing Generation of an <i>Mtb</i> Δ <i>namH</i> Mutant	166
Figure 51: Assembly for Southern Hybridisation Transfer to Nylon Membrane	176
Figure 52: DNA gel Showing Restriction Digested DNA Fragments of FR12pNIL2.....	183

Figure 53: Schematic of Diagnostic Primer Sites in <i>Mtb namH</i> Mutant	185
Figure 54: DNA gels Showing PCR Products using <i>namH</i> -test Primers	186
Figure 55: Southern Blots of Wild Type and $\Delta namH$ <i>Mtb</i> Digested gDNA	188
Figure 56: Wild Type and $\Delta namH$ <i>Mtb</i> Growth Analysis in 7H9 and Sautons Media	190
Figure 57: Single Colony Images of Wild Type and $\Delta namH$ <i>Mtb</i>	191
Figure 58: Phase Contrast Microscopy Images of Macrophage Infection at MOI 1	192
Figure 59: Macrophage Survival and Replication Data for Wild Type and $\Delta namH$ <i>Mtb</i>	193
Figure 60: Percentage Killing in Wild Type and $\Delta namH$ <i>Mtb</i> against Antimicrobial Treatment	195
Figure 61: Log ₁₀ MPN Data for WT and $\Delta namH$ <i>Mtb</i> after Isoniazid Treatment	196
Figure 62: Muropeptide Schematic	211
Figure 63: Mass Spectrum and Fragmentation of Mutanolysin Released Muropeptides from <i>E. coli</i> PG	213
Figure 64: Melting Curves for Wild Type and $\Delta namH$ <i>M. smegmatis</i> pMIND- <i>rpfA-E</i> cDNA Samples and <i>Mtb</i> gDNA Standards using 16S rRNA Primers ..	215
Figure 65: Melting Curves for Wild Type and $\Delta namH$ <i>M. smegmatis</i> pMIND- <i>rpfA</i> cDNA Samples and <i>Mtb</i> gDNA Standards using RpfA Primers	215
Figure 66: Melting Curves for Wild Type and $\Delta namH$ <i>M. smegmatis</i> pMIND- <i>rpfB</i> cDNA Samples and <i>Mtb</i> gDNA Standards using RpfB Primers	215
Figure 67: Melting Curves for Wild Type and $\Delta namH$ <i>M. smegmatis</i> pMIND- <i>rpfC</i> cDNA Samples and <i>Mtb</i> gDNA Standards using RpfC Primers	216
Figure 68: Melting Curves for Wild Type and $\Delta namH$ <i>M. smegmatis</i> pMIND- <i>rpfD</i> cDNA Samples and <i>Mtb</i> gDNA Standards using RpfD Primers	216
Figure 69: Melting Curves for Wild Type and $\Delta namH$ <i>M. smegmatis</i> pMIND- <i>rpfE</i> cDNA Samples and <i>Mtb</i> gDNA Standards using RpfE Primers	216

LIST OF TABLES

Table 1: Drug-Resistant TB Classifications.....	13
Table 2: Classification of Non-Tuberculosis Mycobacteria Commonly Infecting Humans	20
Table 3: Polyacrylamide Gel Components	52
Table 4: Bacterial Strains used in this Chapter	64
Table 5: Constructs and their Corresponding Primer Pairs	65
Table 6: Molecular Ions of Selected <i>E. coli</i> Muropeptides	89
Table 7: The Predicted PM Mass Peaks for pET15b and pET15b- <i>namH</i> Muramic Acid.	101
Table 8: Bacterial Strains used in this Chapter	120
Table 9: Primer Sequences and their Corresponding PCR Product Size	122
Table 10: qRT-PCR Primer Sequences and Amplicon Sizes	125
Table 11: Definition of Terms.....	131
Table 12: The Calculated PCR Products for Each Rpf Construct.....	134
Table 13: qRT-PCR Copy Numbers of Wild Type and Δ NamH-pMIND <i>M.</i> <i>smegmatis</i> <i>Mtb</i> Rpf Overexpressing Strains and the Calculated Mean Expression Ratios	141
Table 14: Statistical Analysis of <i>M. smegmatis</i> Rpf Strains in 7H9	143
Table 15: Statistical Analysis of Δ <i>namH</i> <i>M. smegmatis</i> Growth in 7H9	145
Table 16: CFU and Log ₁₀ MPN Data in WT and Δ <i>namH</i> <i>M. smegmatis</i>	153
Table 17: MICs of the Front-line Anti-Tuberculosis Drugs	169
Table 18: Bacterial Strains	171
Table 19: Primers Sequences and the Resulting Amplicon Sizes	171
Table 20: Antimicrobial Concentrations for Percentage Killing Experiments.....	180
Table 21: Diagnostic Restriction Digests of FR12pNIL2 and their Calculated Sizes	182
Table 22: Amplicon Sizes in WT and Δ <i>namH</i> <i>Mtb</i> using Different Primers	185
Table 23: Restriction Digest Fragment Sizes Predicated for Wild Type <i>Mtb</i> and Δ <i>namH</i> <i>Mtb</i>	187
Table 24: Resuscitation Index and CFU Counts after INZ Treatment ..	197

TABLE OF CONTENTS

Abstract.....	ii
Acknowledgements	iii
List of Common Abbreviations	iv
List of Figures.....	vi
List of Tables.....	ix
Chapter 1: Introduction.....	xv
1.1 General Introduction.....	1
1.2 Global Burden of TB.....	2
1.2.1 The effect of HIV on TB prevalence	4
1.3 Clinical Symptoms.....	6
1.4 Diagnostics	7
1.5 Tuberculosis Treatment	9
1.6 Emergence of Drug Resistance	12
1.7 Pathophysiology.....	14
1.8 Mycobacteria.....	16
1.8.1 MTBC.....	17
1.8.2 Non-Tuberculosis Mycobacteria	18
1.8.3 Cell Wall Architecture	20
1.8.3.1 Mycobacterial PG and NamH.....	22
1.9 Latent Tuberculosis Infection and Non-Replicating Persistence	28
1.9.1 <i>In Vitro</i> and <i>In Vivo</i> Dormancy Models.....	30
1.9.2 Reactivation and Resuscitation.....	33
1.9.2.1 Resuscitation Promoting Factors.....	34
1.9.2.2 Muropeptides as Signalling Molecules	39
1.10 Aims and Objectives	43
Chapter 2: Materials and Methods	44
2.1 Reagents and Media	45
2.1.1 Media	45
2.2 Bacterial Stocks	46
2.2.1 Cultivation Techniques	46
2.2.2 CFU Plating and Counting.....	47

2.3 Buffers and Solutions	48
2.4 Generation of Bacterial Overexpression Strains	49
2.4.1 PCR.....	49
2.4.2 Restriction Digestion and Ligation	50
2.4.3 Transformation	50
2.4.4 Plasmid DNA Purification	51
2.4.5 Transformation and Electroporation into Expression Hosts.....	51
2.5 Protein Expression and Immunological Detection	52
2.5.1 SDS-PAGE.....	52
2.5.2 Western Blot.....	53
Chapter 3:	55
Generation of Glycolylated Peptidoglycan in <i>E. coli</i>	55
3.1 Introduction	56
3.1.1 Techniques used for Isolation and Analysis of PG.....	56
3.1.2 NamH and RpfB	62
3.1.3 Aims.....	63
3.2 Materials and Methods.....	64
3.2.1 Organisms used in this Chapter.....	64
3.2.2 Bacterial Strains.....	64
3.2.3 Generation of Overexpressing Strains	64
3.2.4 Expression Conditions	65
3.2.5 Confirmation of Protein Expression	65
3.2.1 Purification of Recombinant <i>Mtb</i> RpfB by Affinity Chromatography .	66
3.2.2 Zymography	68
3.2.3 Microscope Settings and Image Analysis	68
3.2.1 Lysozyme Sensitivity	69
3.2.2 PG Purification.....	69
3.2.3 Muropeptide Analysis	72
3.3 Results	77
3.3.1 PET15b- <i>namH</i> ; Growth Characteristics and Protein Expression	77
3.3.2 NamH Solubility	81
3.3.3 Determination of NamH's Functionality.....	86

3.3.4	Did pET15b- <i>namH</i> BL21 (DE3) have a Reduced Sensitivity to Lysozyme?	103
3.3.5	RpfB Muropeptide Products	106
3.4	Discussion	112
3.4.1	Overexpression of NamH	112
3.4.2	PG Purification and Analysis to Determine NamH Functionality	112
3.4.3	MS Techniques to Analyse Glycolylation	113
3.4.4	RpfB Released Muropeptides	114
3.5	Conclusion	115
3.6	Future Work	116
Chapter 4:	<i>Mtb</i> Rpfs are able to Stimulate Growth in Δ <i>namH</i> <i>M. smegmatis</i> .	117
4.1	Introduction	118
4.1.1	Aims	119
4.2	Materials and Methods	120
4.2.1	Generation of Overexpressing Strains	121
4.2.2	Confirmation and Quantitation of Protein Expression	122
4.2.3	Growth Studies	130
4.2.4	<i>M. smegmatis</i> Non-Culturability Model	131
4.2.5	MPN	132
4.3	Results	132
4.3.1	Generation of <i>M. smegmatis</i> RpfA-E Overexpression Strains	132
4.3.2	Protein Expression	134
4.3.3	Rpf Growth Stimulation Experiments	142
4.3.4	Does Glycolylation Play a Role in Resuscitation of Rpf-Dependent Cells? 148	
4.4	Discussion	154
4.4.1	Generation of <i>Mtb</i> Rpf Overexpression Strains in <i>M. smegmatis</i> ..	154
4.4.2	Rpf Expression Analysis	154
4.4.3	Growth Studies	157
4.4.4	Resuscitation of Non-Culturable Cells	160
4.5	Conclusion	161
Chapter 5:	163

Generation and Phenotypic Characterisation of <i>Mycobacterium tuberculosis</i> <i>namH</i> Deletion Mutant	163
5.1 Introduction	164
5.1.1 Generation of an <i>Mtb</i> Knockout Mutant	164
5.1.2 Southern Hybridisation	166
5.1.3 <i>Mtb</i> ; Intracellular Survival and Replication	167
5.1.4 <i>Mtb</i> Drug Susceptibility	169
5.1.5 Aims.....	170
5.2 Materials and Methods.....	171
5.2.1 Bacterial Strains.....	171
5.2.2 Generation of a $\Delta namH$ Mutant in <i>Mtb</i> H37Rv.....	172
5.2.3 <i>Mtb</i> Genomic DNA Purification	174
5.2.4 Diagnostic PCR	174
5.2.5 Southern Hybridisation	175
5.2.6 Growth Studies	177
5.2.7 Macrophage Infection Studies	178
5.2.8 Microscopy.....	179
5.2.9 Antimicrobial Killing and Recovery.....	180
5.3 Results.....	182
5.3.1 Generation and Confirmation of an <i>Mtb</i> $\Delta namH$ Mutant	182
5.3.2 $\Delta namH$ <i>Mtb</i> has a Slight Growth Defect and Increased Clumping.	189
5.3.3 Does Glycolylation Play a Role in Intracellular Survival?	191
5.3.4 Antimicrobial Killing.....	194
5.3.5 Does Glycolylation Play a Role in <i>Mtb</i> Recovery After Antimicrobial Treatment?	196
5.4 Discussion.....	198
5.4.1 $\Delta namH$ <i>Mtb</i> Mutant Confirmation.....	198
5.4.2 Growth Characterisation	199
5.4.3 $\Delta namH$ <i>Mtb</i> Intracellular Survival.....	199
5.4.4 Antimicrobial Killing.....	201
5.4.5 The Role of Glycolylation in <i>Mtb</i> Resuscitation.....	202
5.5 Conclusion	204
Chapter 6: Final Conclusions and Future Work.....	205

6.1 Final Conclusions.....	206
6.2 Future Work	208
Appendices	210
Appendix 1: Muropeptide Schematics and Fragmentation.....	211
Appendix 2: qRT-PCR Melting Curves.....	215
References.....	217

CHAPTER 1: INTRODUCTION

1.1 GENERAL INTRODUCTION

Around a third of the world's population are infected with *Mycobacterium tuberculosis* (*Mtb*), the causative agent of human tuberculosis (TB, tubercles bacillus) (Kaufmann, 2008, WHO, 2012). *Mtb* is a member of the *Mycobacterium tuberculosis complex* and has a high lipid content in the cell wall. TB is most commonly associated with the lungs (pulmonary TB), although extra-pulmonary TB (affecting bone, kidneys and lymph nodes) is widely recognised. Transmission of TB is accomplished during coughing or sneezing by droplets containing bacteria and it is hence a contagious disease.

Manifestation of *Mtb* infections can vary, reflecting a multitude of influencing factors, including those of the person infected (for example, age and immune status), those of the organism (virulence) as well as the interactions between the host and the microbe (Cole, 2005). While these are important considerations, it has also been shown that infection with *Mtb* in healthy individuals can lead to a latent tuberculosis infection (LTBI) that is asymptomatic and can remain so for life. The statistics for those who develop the disease suggests that only 1 in 10 people infected will develop the active disease (Cardona and Ruiz-Manzano, 2004). Current diagnostic techniques include classic methods, such as X-ray, physical examination, tuberculin skin test (TST), microscopy of sputum samples, sputum culture as well as modern techniques; PCR and IGRAs (interferon gamma release assays) (Mazurek et al., 2010).

Up until the late 20th century TB was considered close to elimination as a global health threat, however, the emergence of drug resistance and co-infection with HIV led to resurgence of TB, and in 1993 the World Health Organisation announced TB as a global health emergency (WHO, 2011). In 2010 there were an average 8.8 million incident cases of TB with 1.1 million deaths

occurring as a result of non-HIV related TB, and an additional 0.35 million HIV associated deaths (WHO, 2011). TB is currently the second most deadly infectious disease worldwide, the most deadly being HIV (WHO, 2012). Together these data demonstrate why TB is an important and deadly modern day disease, however not so long ago TB was considered an ancient disease, which no longer posed a threat to modern day society.

The earliest human remains, in which the presence of *Mtb* DNA was confirmed by PCR, were discovered in a Neolithic settlement in the Mediterranean and are about 9000 years old (Hershkovitz et al., 2008). These findings pre-date the previous earliest evidence of human tuberculosis by roughly 3000 years; researchers discovered molecular evidence of *Mtb* in an ancient Egyptian mummy (Nerlich et al., 1997).

Mtb was first discovered to be the etiological agent of human TB in 1882 by Robert Koch, who was then awarded the Nobel Prize in Medicine for his work. Koch developed a stain allowing visualisation of mycobacteria under a microscope and a procedure for cultivation of *Mtb in vitro*. Koch demonstrated the ability of *Mtb* culture, grown *in vitro*, to produce animal infections replicating the pathophysiology of the disease in humans (Murray, 2004), thus demonstrating for the first time that TB was caused by *Mtb* bacilli.

1.2 GLOBAL BURDEN OF TB

In recent years the WHO have announced TB as the second leading cause of death worldwide due to an infectious disease. The WHO has been dedicated to combating the 'TB problem', producing 16 reports which provided a greater depth of knowledge regarding the global TB situation. The 2011 report emphasised the need and aim of the WHO to reduce the incidence rate of TB by the year 2015 by 50%, however it also demonstrated that the total number

of the global population infected with TB has been falling since 2006 (WHO, 2011).

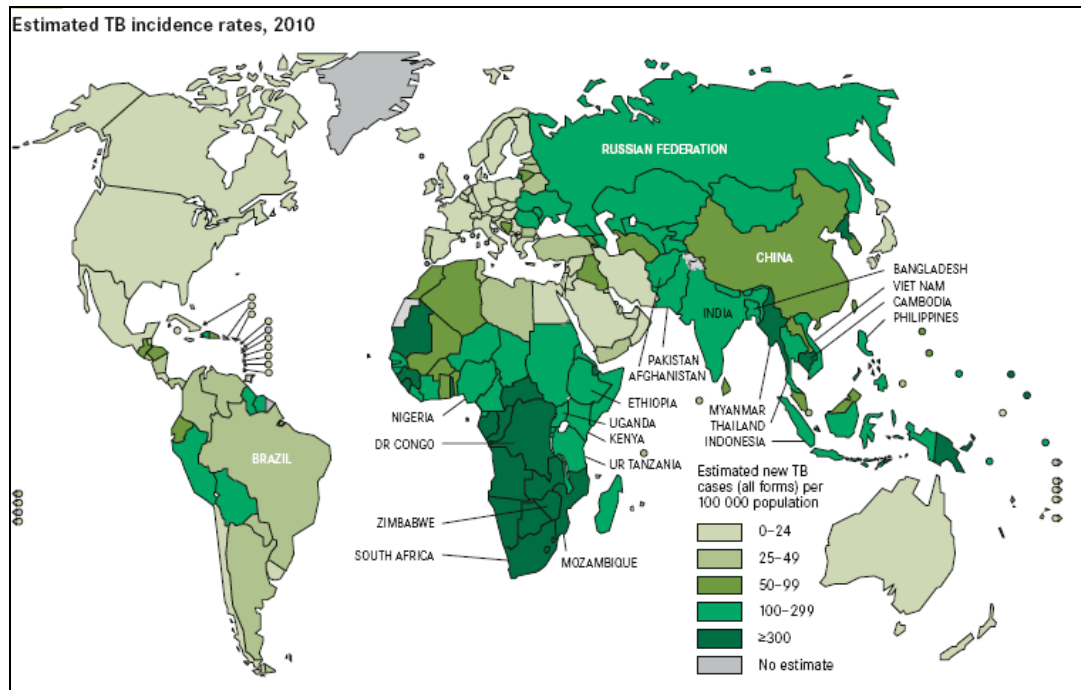


FIGURE 1: TB INCIDENCE RATES, ESTIMATED (2010)

The above figure was adapted from Global tuberculosis control: WHO report 2011 and demonstrates the predicted incidence rates of TB worldwide in 2010 based on TB surveillance data and expert opinion using Equation 1.

These data (Figure 1) can then be compared to the estimated incidence of TB reported by the WHO in the recently published 2012 TB report, shown in Figure 2 (WHO, 2012). Incidence is defined as the number of new and relapse cases of TB within a year, by the WHO (WHO, 2011). There are no direct measurements of TB incidence, due to the large sample sizes required, and hence the WHO estimates incidence rates for the majority of countries based on a combination of TB surveillance (linked through health care systems) and expert opinion at regional workshops using the following equation:

EQUATION 1:

$$\text{Incidence} = \frac{\text{case notification}}{1 - \text{underreporting}}$$

Global TB report, 2011 and 2012

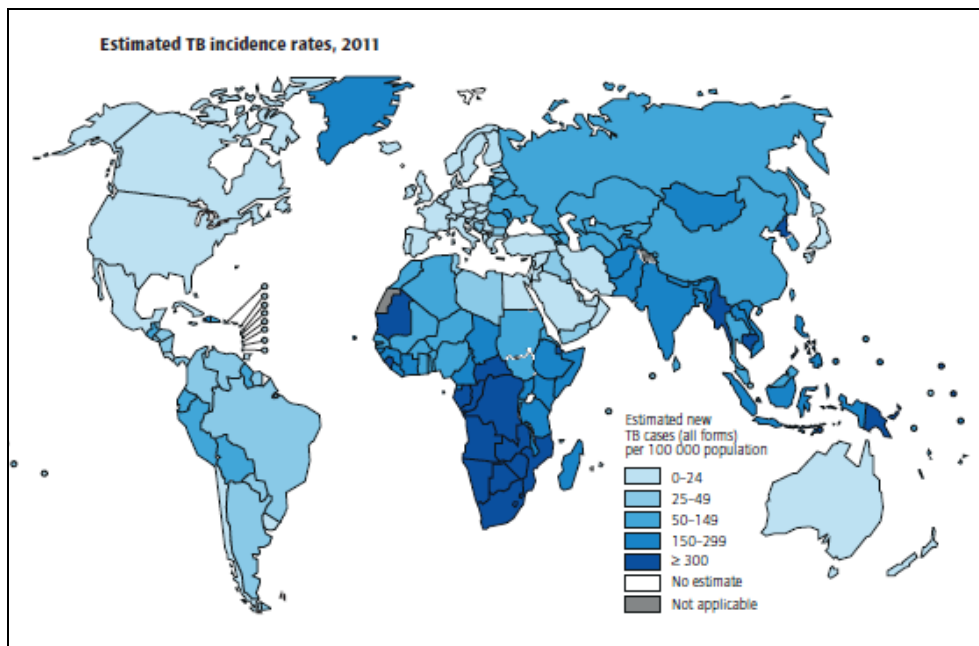


FIGURE 2: TB INCIDENCE RATES, ESTIMATED (2011)

The above figure was adapted from the WHO's Global TB report, 2012. The data is based on TB surveillance systems and expert opinion using Equation 1.

From Figure 1 and Figure 2 it can be observed that certain areas which had no estimated TB incidence data in the WHO's 2011 report have since been investigated; for example Greenland now has a high (>300 TB cases per 100,000 population) incidence estimate. The countries previously investigated do not appear to have changed drastically from the prior report to the latest. However, the 2015 goal to halt and reverse the TB epidemic has now been achieved (WHO, 2012). From the TB incidence rates and the data included in the WHO's annual TB reports the global burden of TB is shown to be highest in Asia and Africa, with India and China accounting for about 40% of all TB cases (WHO, 2012).

1.2.1 THE EFFECT OF HIV ON TB PREVALENCE

Individuals living with HIV who are infected with TB are estimated to be 21-34 times more likely to develop active TB compared to HIV-negative people (WHO, 2011). In 2010 1.1 million people infected with TB were HIV-positive, this figure remained the same in 2011 (WHO, 2012, WHO, 2011). Part of the Global Plan is to test all TB patients for HIV, whilst this is still a work in progress there have been improvements, these highlighted in the 2011 WHO Global TB report, with the greatest achievements in South Africa. In the most recent report the WHO state that globally, 40% of TB patients had a documented HIV test result. Of the HIV-positive TB patients, 80% live in Africa (WHO, 2012).

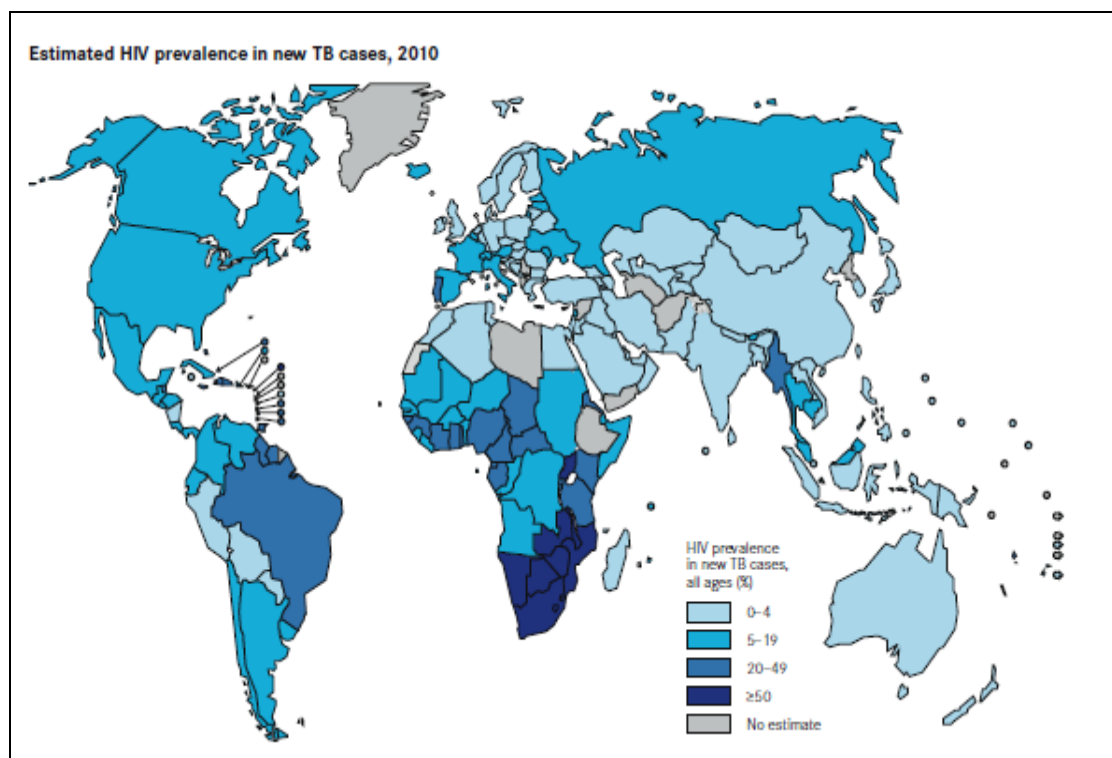


FIGURE 3: ESTIMATED HIV PREVALENCE IN NEW TB CASES

The figure was adapted from WHO Global TB report, 2011 and shows the global percentage of HIV prevalence in new TB cases for all ages.

The number of deaths due to TB is a useful indicator of the severity of HIV on TB epidemiology (Mukadi et al., 2001). However, HIV-positive TB related deaths are difficult to account for as they are documented as HIV deaths with contributory causes, which are

often unknown (WHO, 2011). The co-infected (HIV and TB) population in sub-Saharan Africa (estimated to 68% of the total number infected) are predicted to have a 30% life time risk of developing active tuberculosis (Mukadi et al., 2001, Dyer, 1992). Therefore the effect of HIV on TB epidemiology, and hence prevalence and control is significant.

1.3 CLINICAL SYMPTOMS

The majority of tuberculosis infections present as pulmonary disease due to the progression of an initial infection. It has also been shown that infection with *Mtb* in healthy individuals can lead to a latent tuberculosis infection (LTBI) that is asymptomatic and can remain so for life. If reactivation occurs this may also lead to pulmonary disease. Tuberculosis is spread through airborne droplet nuclei containing *Mtb* which can remain airborne for hours (Frieden et al., 2003). Introduction of these organisms into the lungs leads primarily to respiratory infection.

A persisting cough is a common symptom of pulmonary TB, as the disease progresses sputum may be produced as a result of increased inflammation and necrosis (Wejse et al., 2008). However, during early stages of active disease symptoms tend to be non-specific and can include fatigue, weight loss, night sweats and a mild fever (Knechel, 2009). If the disease progresses and becomes extensive then shortness of breath may occur due to a reduced lung capacity (Knechel, 2009).

Extra-pulmonary TB can occur as a result of dissemination of bacterial cells into the blood stream, leading to non-specific symptoms of weight loss and fatigue. Alternatively infection may occur in the central nervous system potentially leading to meningitis, most common symptoms as a result of this are headaches and changes in mental faculties (Yoon et al., 2004, Knechel, 2009).

1.4 DIAGNOSTICS

Historically diagnostics for TB have been somewhat cumbersome, time-consuming and insufficient. Laboratory based culture methods, over several weeks, are currently the highest standard method of diagnosis (Storla et al., 2008). There have been recent advancements in rapid diagnostics for active, latent and drug-resistant *Mtb*; however, the accuracy, accessibility and cost of these remain to be determined fully. Ziehl-Neelsen stained sputum samples, examined by microscopy remains one of the most commonly used diagnostic tests for *Mtb* due to the relative cheapness (McNerney et al., 2012). However, this is a poor standard diagnostic test, with severely limited sensitivity particularly within young children (Cuevas et al., 2012). A major failing of this technique however is the inability to detect extra pulmonary TB (Cuevas et al., 2012). The use of the automated system: BACTEC™ MGIT™ has been developed to detect the growth of mycobacteria (Tortoli et al., 1999).

The ability to determine drug-resistant TB infections would be extremely beneficial, not only to provide the correct treatment for the individual but to prevent incorrect treatment ultimately increasing resistance and potential transmission (Zumla and Maeurer, 2012). Where capable, laboratories are able to increase the speed and accuracy of active TB diagnosis through rapid culture techniques, radiography, and nucleic acid amplification tests (NAATs) amongst other methods (Lawn and Zumla, 2011). Use of multiple techniques and invasive biopsies increases sensitivity, unfortunately most of these resources are not available in the countries which need them most (McNerney et al., 2012).

A recent development in TB diagnostics has been the introduction of a 1-day diagnosis, which means multiple samples are taken on a single day rather than having to take samples on multiple visits to a clinic (Cuevas et al., 2011). This makes sample collection a lot

simpler. Research into serological tests has provided several potential antibody-based methods, however further studies have demonstrated an overall poor sensitivity and specificity (Steingart et al., 2007). Interferon- γ release assays (IGRAs) have existed for several years, detecting, via interferon- γ secreted in response to *Mtb* antigens, the presence of past or present *Mtb* infection (Wallis et al., 2010).

Two well-known commercial IGRA systems; QuantiFERON-TB Gold In-Tube assay (QFT-GIT) and T-SPOT.TB have been developed to detect interferon- γ after incubation with several *Mtb* specific antigens such as: early secretory antigen target-6 (ESAT-6) and culture filtrate protein-10 (CFP-10) (Majlessi et al., 2005, Sester et al., 2011). Despite vast interest, hype and numerous clinical studies these tests are unable to distinguish between latent and active TB (Cattamanichi et al., 2011). Therefore they are ultimately no more specific or useful than the tuberculin skin test (TST).

NAATs were investigated as a means of distinguishing between active and latent TB. GeneXpert MTB/RIF is an automated platform which runs real time polymerase chain reaction experiments, producing results within 2 hours (Boehme et al., 2010). This is also combined with the ability to determine sensitivity to Rifampicin (Boehme et al., 2010). Owing to multiple studies demonstrating false positive RIF resistance the WHO recommends using a second RIF resistance test alongside GeneXpert MTB/RIF (Blakemore et al., 2010).

A urine-based dip-stick diagnostic test for *Mtb* was developed, it is rapid, cheap and detects LAM antigenuria providing positive or negative readings (Lawn and Zumla, 2011). Work has also been carried out into detecting mycobacteria in sputum by gas chromatography (O'Sullivan et al., 2012). Current efforts are focused on development of robust and cheap techniques to diagnose TB in resource poor countries.

1.5 TUBERCULOSIS TREATMENT

After discovery of the causative agent of TB, the next challenge was to find a treatment effective against *Mtb*. It was another 40 years before the work by Albert Schatz in the laboratory of Selman Waksman led to the isolation of streptomycin in 1944 (Waksman et al., 1945). Streptomycin is a bactericidal agent and its mode of action was found to be inhibition of protein synthesis, however, it was not long before antibiotic resistance occurred (Shaila et al., 1973). In the following 20 years after the first application of streptomycin as an anti-tuberculosis agent, a further four antimicrobials active against *Mtb* were discovered, these still comprise the four leading anti-tuberculosis drugs used today.

In 1952 both isoniazid (INZ) and pyrazinamide (PZA) were introduced for TB treatment; isoniazid was actually synthesised 40 years earlier but its potential as an anti-tuberculosis agent was not realised (Bernstein et al., 1952). InhA, an 2-trans-enoyl-acyl carrier protein reductase, was identified as a potential target of INZ based on the homology of this protein to *E. coli*'s EnvM protein (which plays a role in fatty acid biosynthesis) (Banerjee et al., 1994). It was hypothesised that this enzyme might be involved in mycolic acid biosynthesis and it was later confirmed by Jacob's group (Vilcheze et al., 2000), who demonstrated that this protein belongs to the fatty acid synthetase II (FAS-II) system in *Mtb* (Marrakchi et al., 2000, Vilcheze et al., 2000). Inactivation of this enzyme resulted in cell lysis and accumulation of saturated fatty acids consistent with the findings from INH treated cells (Vilcheze et al., 2000).

Isoniazid therefore affects synthesis of mycolic acids, core components of the mycobacterial cell wall thus inhibiting growth and resulting in cell lysis, hence INZ is highly efficient in killing of mycobacteria (Takayama et al., 1972). INZ is a prodrug and is activated by a catalase peroxidase (KatG) (Metcalf et al., 2008,

Zhang et al., 1992). Resistance can occur by increased expression of InhA or through mutations which reduce affinity for NADH, as well as mutations in KatG or defects in NADH dehydrogenase (Miesel et al., 1998).

Pyrazinamide which was also discovered in 1952 was originally thought to disrupt the plasma membrane and energy metabolism in *Mtb* (Zhang et al., 2003). Pyrazinamide (PZA) is a pro-drug and its active constituent (pyrazinoic acid; POA) has been shown to be more effective on slower or non-replicating bacilli (Shi et al., 2011). A recently published article identified a ribosomal protein S1 (RpsA) as a target of POA. RpsA is involved in *trans*-translation; which is believed to be dispensable in actively growing bacteria but vital for non-replicating bacilli under stressful conditions (Shi et al., 2011, Keiler, 2008). This may therefore explain PZA's effectiveness on slower replicating organisms. PZA, in combination with INH and Rif ultimately reduces the treatment time for TB.

Two other front line drugs, ethambutol (EMB) and rifampicin (RIF) were discovered in 1961 and 1966, respectively. Rifampicin, a derivative of rifamycin B, prevents transcription of bacterial DNA to RNA by inhibition of the RNA polymerase (Levin and Hatfull, 1993). Rifampicin specifically targets the β -subunit of RNA polymerase (*rpoB*) and has a high bactericidal activity against replicating and non-replicating *Mtb* bacilli (Telenti et al., 1993). Ethambutol inhibits growth of replicating mycobacteria and was found to target and inhibit arabinosyltransferase EmbC and thus the biosynthesis of arabinogalactan (Goude et al., 2009, Takayama and Kilburn, 1989). The four drugs (ethambutol, pyrazinamide, rifampicin and isoniazid) are included in standard anti-tuberculosis drug regimen, worldwide.

Several novel antimicrobial agents active against mycobacteria have been recently discovered, including benzothiazinones (BTZ)

and dinitrobenzamide (DNB) derivatives (Ribeiro et al., 2011). BTZs have been shown to target DprE1 protein which is involved in arabinose synthesis (Makarov et al., 2009) and DNBS have been found to block the same pathway, resistance occurs through mutations within DprE1 in both cases and recent studies indicate DNBS may target DprE1 as well (Ribeiro et al., 2011). TMC207, a diarylquinoline compound and the first compound in novel class of anti-tuberculosis drugs targets bacterial ATP synthase and has bactericidal and sterilising activity (Matteelli et al., 2010, Andries et al., 2005). Mutations within mycobacterial ATP synthase have been shown to cause resistance to TMC207 in mycobacteria (Segala et al., 2012, Andries et al., 2005).

According to the latest WHO anti-tuberculosis treatment guidelines the two most frequently prescribed regimens are either a combination of EMB, RIF and INZ or the same with the addition of PZA. The course for this antimicrobial treatment is usually 6 months long with a variation of the drugs prescribed depending on the stage of treatment. For example, in the early stage of treatment all four drugs will be implemented to maximise elimination of bacteria, whilst during the final four months only Rif and INZ are prescribed to eliminate non-replicating bacteria which may persist within the patient (WHO, 2009). Of course the effectiveness of the treatment may differ depending on the stage of the infection, the strain of bacteria, the health of the host, and how strictly the course has been followed.

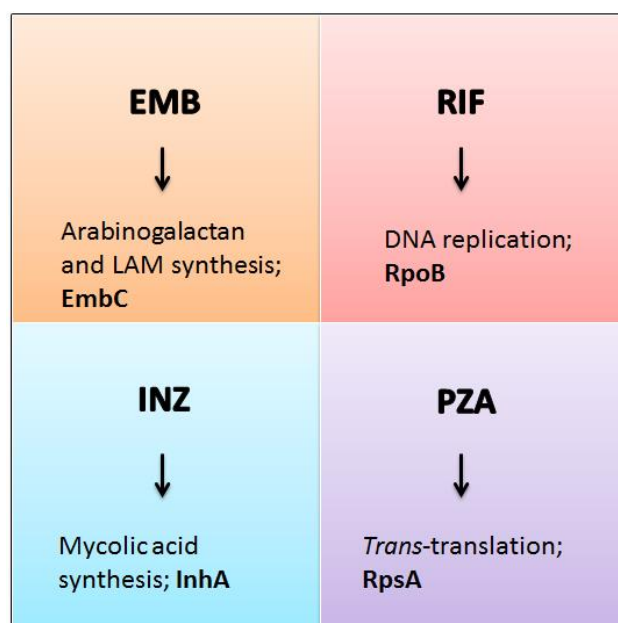


FIGURE 4: SITE OF ACTION OF THE FOUR PRIMARY ANTI-TUBERCULOSIS DRUGS

The four major first-line anti-tuberculosis drugs are depicted, indicating their specific site of action.

1.6 EMERGENCE OF DRUG RESISTANCE

Drug resistance in *M. tuberculosis* is the direct result of chromosomal mutations which, in a clinical environment, arise as a consequence of poor drug adherence, inaccurate prescriptions and selection pressure due to drug supply (Zhang and Yew, 2009). Drug tolerance, or delayed bacterial killing, has been demonstrated *in vitro* for EMB, INH and RIF with increased tolerance observed after prolonged exposure and it is believed to be associated with dormant or non-replicating bacteria (Wallis et al., 1999). However, recent findings by Wakamoto and colleagues challenge this by showing that INZ tolerance depended on the catalase expression in growing cells rather than on the physiological state of mycobacteria (Wakamoto et al., 2013). Multiple drug resistance pumps (including Rv0342 and Rv1258) were also found to participate in the development of drug tolerance to INH and EMB (Colangeli et al., 2005, Adams et al., 2011).

TABLE 1: DRUG-RESISTANT TB CLASSIFICATIONS

State of Resistance	Definition
Mono-resistance	Strains resistant to <i>one</i> of five first-line drugs
Poly-resistance	Strains resistant to <i>two or more</i> but not both INZ and Rif
Multidrug-resistant (MDR)	Strains resistant to <i>both</i> INZ and Rif
Extensively drug-resistant (XDR)	Strains resistant to <i>both</i> INZ and Rif, a fluoroquinolone and at least <i>one</i> second-line injectable drug

*Table adapted from previously published work (Chan et al., 2009)

The two major and most commonly referenced forms of drug-resistant *Mtb* are MDR and XDR. Resistance can also be defined as primary or acquired; primary resistance referring to infection with a resistant strain of *Mtb* whereas the term acquired indicates that the patient has been receiving drug treatment and hence 'acquired' resistance (Jassal and Bishai, 2009). This has since been redefined to resistance either among new cases or previously treated cases as several cases, in which treatment had previously been administered were shown to be a result of transmission of a drug-resistant strain (Van Rie et al., 2000, Jassal and Bishai, 2009). The molecular mechanisms for most forms of drug resistance have been determined.

As outlined in Table 1; MDR-TB will require treatment with second-line drugs in order to eliminate resistant bacteria, whilst XDR-TB will rely on less potent second-line drugs due to resistance, potentially with severe side effects (such as hearing loss), prolonged treatment and reduced effectiveness (Seddon et al., 2012, Chan et al., 2009). In 2011 there were 310,000 estimated cases of MDR-TB among pulmonary TB patients; 60% of these cases were found within China, India and the Russian Federation

(WHO, 2012). An average proportion of 9% of all MDR-TB cases were found to contain XDR-TB, and XDR-TB has been identified in 84 countries so far (WHO, 2012). The emergence of drug-resistant *Mtb* has been well known since the introduction of streptomycin (Zhang and Yew, 2009). The modern drug regimen therefore implements a combination of anti-tuberculosis drugs for a long period of time. However, as discussed above, there is an increasing population of MDR and XDR-TB which can no longer be treated with the standard first-line drug treatment. Hence there is a current demand for new anti-tuberculosis drugs.

1.7 PATHOPHYSIOLOGY

Tuberculosis is spread through airborne droplet nuclei with particle diameters of 1-5 μ m containing *Mtb* which can remain airborne for hours (Frieden et al., 2003). Once bacteria have entered the distal airways they come into contact with alveolar macrophages, the cell wall component lipoarabinomannan (LAM) interacts with macrophage receptors including the mannose receptor and complement receptor 3 (Nicod, 2007, Welin et al., 2008). LAM is a key virulence factor for *Mtb* and can inhibit phagosomal maturation through the incorporation of mannose capped LAM from *Mtb* into the macrophage cell membrane and by preventing the recruitment of endosomal tethering molecule, EEA1 (Welin et al., 2008, Vergne et al., 2003). Blocking of phagosomal maturation into phagolysosome is essential for *Mtb* replication and survival in macrophages (Vergne et al., 2003).

The complement system is important for phagocytosis of mycobacteria, protein C3 binds to the cell wall and promotes mycobacterial recognition (Ferguson et al., 2004). Phagocytosis then leads to a cascade of events ultimately determining whether the infection is controlled or active tuberculosis is established (Frieden et al., 2003). During this time proteolytic enzymes and cytokines, produced by macrophages, attempt bacterial

degradation. Cytokines result in the attraction of T-cell lymphocytes which interact further with macrophages due to the presence of antigens on their surfaces, this stage can last between 2 and 12 weeks (van Crevel et al., 2002). At this stage the infection can be identified via a skin test.

The next stage of *Mtb* infection is formation of granulomas as a result of an accumulation of activated T-cell lymphocytes and macrophages and thus generation of a microenvironment, in which an early necrotic lesion forms (Frieden et al., 2003, Nicod, 2007). Mycobacteria have the ability to adapt to, and survive in this environment, resulting in caseous necrosis; with characteristically low pH, low O₂ and low nutrient availability (Dheda et al., 2005). At this stage lesions can become calcified as a result of the immune response, however, if the immune system is less effective this will progress to active primary tuberculosis (Dheda et al., 2005). If the infected individual is immune compromised then this lesion can become liquefied and leach into blood or lymphatic systems. Patients infected with *M. tuberculosis* may then expectorate droplets, containing tuberculosis bacteria which can be transmitted to individuals in close contact; thus propagating the disease (Richeldi et al., 2004).

Clinically, infection with *Mtb* on an individual basis can progress slightly differently as a result of host interactions and strain variation, amongst other variables. A possible outcome of infection can be harbouring a population of 'dormant' bacilli, a state believed to be associated with latent TB. Although they do not pose a risk of transmitting the disease whilst the bacteria are in this state, these individuals are at risk of reactivation and development of active disease at a later stage (WHO, 2011).

The cytokine and chemokine signals in *Mtb* infection are critically important in protective immunity; it is the organisation of T-lymphocyte sensitisation and monocyte attraction that determines

the outcome of infection (Jo et al., 2003). Interferon- γ has been shown through *ex vivo* studies, as well as through mutational work to be important; a mutation in receptor 1 caused severe mycobacterial infection (Jouanguy et al., 1996). The cytokines: Tumour necrosis factor α (TNF- α) and multiple interleukins have been highlighted as potentially important for control of tuberculosis infection, with Interferon- γ playing a crucial role in TNF- α secretion by macrophages and hence granuloma formation (Frieden et al., 2003).

1.8 MYCOBACTERIA

Mycobacteria are aerobic, unicellular rods and generally classified as Gram-positive due to their cell wall composition but are often referred to as acid fast bacilli due to their staining abilities (M. Madigan, 2009). A high C-G content is another characteristic feature of mycobacteria, and they are known to contain unique lipids called mycolic acids providing the bacteria with a 'waxy' coat and resulting in their acid-fastness (M. Madigan, 2009). Acid-fast Ziehl-Neelsen stain comprises a mixture of a dye (fuchsin) and phenol used to penetrate the lipids which are then decolourised with an acid-alcohol solution followed by a counter stain used for visualisation (M. Madigan, 2009). Mycolic acids are a group of long chain, branched fatty acids that are attached to peptidoglycan of the mycobacterial cell wall (Brennan and Nikaido, 1995).

Mycobacteria tend to undergo filamentous growth but can become fragmented into rods/coccoid forms. Based on their growth characteristics, mycobacteria can be divided into two groups: fast or slow growers (M. Madigan, 2009). *Mtb* is classed as a slow grower, taking weeks for development of visible colonies on agar. The slow growth of *Mtb* led to increased usage of *Mycobacterium smegmatis* as a model organism for research, an example being research into resuscitation of non-culturable cells (Shleeva et al., 2004). The morphology of the colonies when visible could be

described as 'wrinkled', a potential effect of high lipid content, with a tendency to clump due to the hydrophobicity of the cell (M. Madigan, 2009). *Mtb* resistance to chemicals is used for isolation from patient sputum.

1.8.1 MTBC

Mtb belongs to the *Mycobacterium tuberculosis* complex (MTBC), which consists of the additional following bacteria: *Mycobacterium africanum* and *Mycobacterium canettii* (human pathogens), *Mycobacterium bovis* (bovine), *Mycobacterium caprae* (goats), *Mycobacterium pinnipedii* (seals) and *Mycobacterium microti* (rodents) (Homolka et al., 2010). It is well known that all members of this group have significantly similar genomic sequences (greater than 99.95%), however, this genomic similarity is not reflected in clinical outcomes (Achtman, 2008). There is ever increasing evidence to demonstrate that strain variation has significant impact on infection, specifically virulence (Firmani and Riley, 2002, Palanisamy et al., 2009). *M. bovis* has a wide spectrum of hosts for infection, including humans (Brosch et al., 2002). It was originally hypothesised that *Mtb* evolved from *M. bovis*, however, this was prior to full genome sequencing of *Mtb* (Stead et al., 1995).

Subsequent hybridisation assays identified multiple regions, of varying size absent from *M. bovis* yet present within *Mtb* H37Rv (Gordon et al., 1999). This was the first step in understanding the phylogenetic history of *Mtb*, which is still not fully known. No unique genomic sequence within *M. bovis* was consistently found to be absent within *Mtb* (Gordon et al., 2001). Using a combination of spoligotyping, single-nucleotide polymorphisms (SNP) and through the generation of bacterial artificial chromosome libraries the ancestry and evolution of MTBC has been investigated (Gordon et al., 1999, Mostowy et al., 2002). Spoligotyping is a commonly used PCR based hybridisation assay to examine genetic diversity (Brudey et al., 2006).

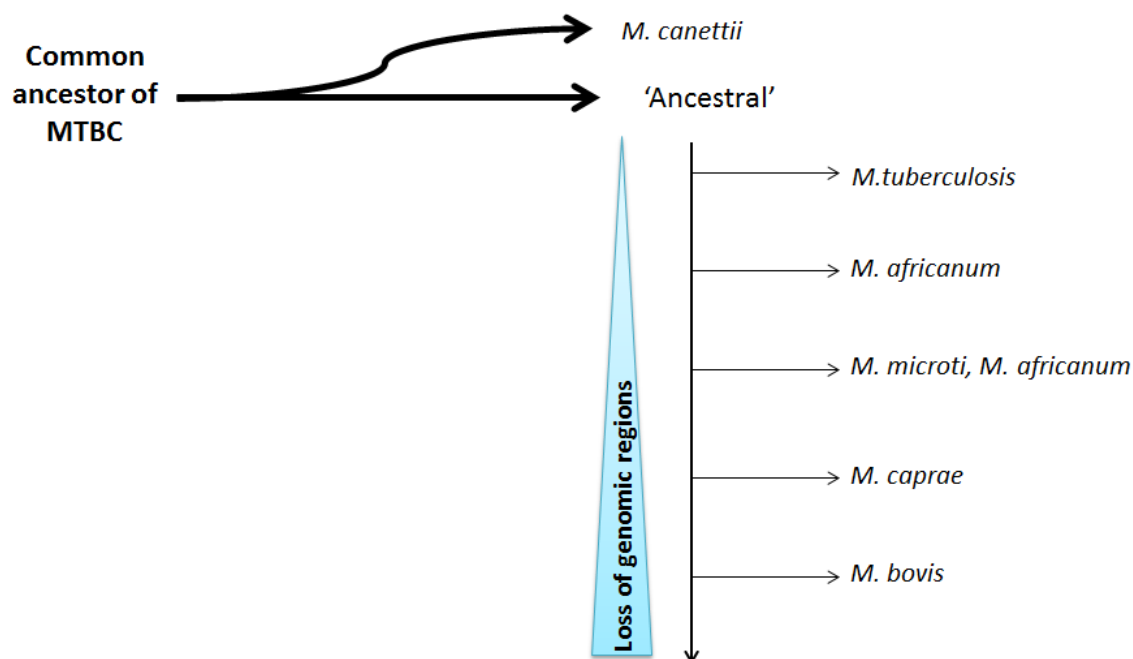


FIGURE 5: HYPOTHETICAL PHYLOGENY OF MTBC

The above figure is adapted from previous work (Brosch et al., 2002, Smith et al., 2009, Mostowy et al., 2002). Hypothetical phylogeny of MTBC was based on loss of genomic regions, classed as deleted regions and sequence polymorphisms. Deletions accumulate in both vertical and horizontal directions, increasing from top to bottom and left to right. Isolates of *M. africanum* could not be classified within a single group due to inconsistent deletions.

Genomic deletions have been shown to potentially represent genetic events; in combination with SNP analysis, studies using isolates from varying geographic locations and obtained from a variety of hosts, compared deleted regions to investigate MTBC phylogeny (as shown in Figure 5) (Mostowy et al., 2002, Kato-Maeda et al., 2001). It was therefore concluded that *Mtb* did not evolve from *M. bovis*, but that an *M. africanum* → *M. bovis* lineage diverged from a progenitor of a modern day *M. tuberculosis* strain (Brosch et al., 2002). Due to a lack of the deletions both *Mtb* and *M. canettii* appear to resemble the original TB ancestor most closely, and hence this pathogen may have already been adapted to infection in humans (Brosch et al., 2002).

1.8.2 NON-TUBERCULOSIS MYCOBACTERIA

Non-tuberculosis mycobacteria (NTM) consist of one hundred mycobacteria which are not members of MTBC and are not *M. leprae* (Griffith et al., 2007, Wu. S.T, 2009, Ventura et al., 2007). A large proportion are pathogens and can be divided into four groups according to the Runyon system (Wu. S.T, 2009). This system classifies bacteria based on the following criteria: rate of growth, colony morphology and pigmentation (Koh et al., 2002). Groups I, II and III within this classification system are termed 'slow growers' these are then subdivided; I: photochromogens (light dependant pigment producers), II: scotochromogens (pigment producers in absence of light) and III: nonchromogens whilst group IV are fast growing organisms (Wu. S.T, 2009).

These bacteria are ubiquitous within the natural environment, and while no evidence of transmission between humans has been found the symptoms associated with infection may appear, clinically, similar to that of TB and therefore classification is important (Tabarsi et al., 2009, Koh et al., 2002). There is, however, evidence for animal to human transmission and if incorrectly diagnosed as TB then treatment will most likely fail to eradicate the infection as numerous NTM are resistant to antimicrobial treatments including first-line anti-tuberculosis drugs and β -lactams (Tabarsi et al., 2009, Utrup et al., 1995).

Some of the NTM most commonly causing human infection are listed below, in Table 2. However, due to the latest advancements, including the use of DNA probes and microarrays allowing large scale analysis, these classifications are becoming less and less important (Ventura et al., 2007). Due to the poor response of NTM to the first-line anti-tuberculosis drugs many NTM infections may be diagnosed as MDR-TB. A recent study found that 11.43% of the patients referred as MDR-TB were in fact NTM infections (Tabarsi et al., 2009). It is therefore of high clinical significance to identify the causative agent of infection in patients with TB symptoms.

TABLE 2: CLASSIFICATION OF NON-TUBERCULOSIS MYCOBACTERIA COMMONLY INFECTING HUMANS

		Non-Tuberculosis Mycobacteria
Slow Growing	Group I	<i>M. kansasii</i>
		<i>M. marinum</i>
	Group II	<i>M. gordonae</i>
		<i>M. scrofulaceum</i>
	Group III	<i>M. avium</i> complex; <i>M. avium</i> and <i>M. intracellulare</i>
		<i>M. terrae</i> complex; <i>M. ulcerans</i> and <i>M. xenopi</i>
Rapidly Growing	Group IV	<i>M. fortuitum</i>
		<i>M. chelonae</i>
		<i>M. abscessus</i>

*Adapted from previously published work (Koh et al., 2002).

1.8.3 CELL WALL ARCHITECTURE

Gram-positive cell walls consist of peptidoglycan, polysaccharides and many other components such as teichoic acids, while lacking the characteristic outer membrane belonging to Gram-negative bacteria (Salton, 1964). Gram-positive bacteria also have a higher peptidoglycan content and lack lipopolysaccharide (LPS) (Salton, 1964). However, while mycobacteria are generally considered as Gram-positive bacteria, their cell wall has some important differences, including the high lipid content and very low permeability.

An asymmetric lipid bilayer model, proposed by Minnikin in the 1980's has recently been supported by structural data using NMR and X-ray diffraction techniques (Hong and Hopfinger, 2004b, Hong and Hopfinger, 2004a). Mycolic acids, present within mycobacteria, affect the cells permeability, due to their long branched hydrocarbon chains, of which the *meso* chain can be 40-60 carbon atoms long (Jarlier and Nikaido, 1994, Hong and Hopfinger, 2004b). The perpendicular position, length and hydrophobicity of these structures have been shown to form a tightly packed layer covalently linked via ester bonds to arabinogalactan (AG) with the average distance between mycolic acids around 7.3 Å (Hong and Hopfinger, 2004a). Mycolic acids are commonly found in the following actinobacteria: *Tsukamurella* species, *Rhodococcus* species, *Corynebacterium* species, *Gordonia* and *Nocardia* species amongst a few others (Onaka et al., 2011).

Based upon GC-MS data, structural information has been obtained regarding AG, which exists within the cell wall in the furanose form and is attached to peptidoglycan through a disaccharide phosphate linker. Attached to two thirds of the terminal hexa-arabinofuranosides, in clusters of four and attached through 1-5 bonds are the mycolic acids (Brennan and Nikaido, 1995). AG is a polymer consisting of arabinofuranose and galactofuranose, with galactan being made up of a linear chain of approximately 30 alternating 5 or 6 linked β -D-galactofuranose units.

Attached at carbon-5 of these units are arabinan chains that are made up from 5-linked α -D-arabinofuranose units that can be branched at positions 2 or 3 (McNeil et al., 1990). Together these components form the mycolyl-arabinogalactan-peptidoglycan complex (mAGPc) creating an effective permeability barrier and aiding drug resistance, a schematic of which is shown in Figure 6.

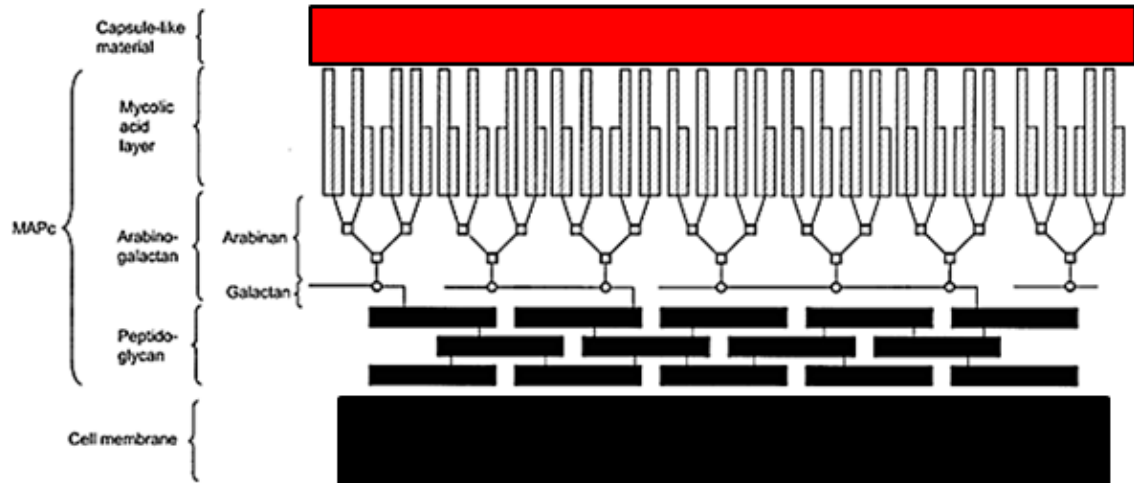


FIGURE 6: SCHEMATIC OF MAGPC WITHIN THE MYCOBACTERIAL CELL WALL

The above figure depicts a schematic representation of the most widely accepted structural orientation of the mycobacterial cell wall. This figure was adapted from previously published work (Crick et al., 2001).

1.8.3.1 MYCOBACTERIAL PG AND NAMH

Mtb has A1 γ type peptidoglycan architecture, the same classification as *Escherichia coli* (Schleifer and Kandler, 1972, Li et al., 1998). The peptidoglycan (PG) of most bacteria consists of the repeating disaccharide unit: N-Acetyl-Glucosamine- β 1-4-N-Acetyl-Muramic acid (NAG-NAM:) (Dover et al., 2007). These PG saccharides form repeating units creating long polysaccharide chains; these chains are cross-linked by peptide stems which vary in amino acid content between species and types of bacteria. Mycobacteria tend to have a pentapeptide stem consisting of: L-Alanine (Ala) attached to the lactyl acid moiety of NAM which is then followed by D-isoglutamic acid (D-Glu), meso-diaminopimelic acid (mDAP), D-Alanine and finally a terminal D-Alanine (as shown in Figure 7 and Figure 9). The terminal D-Ala may be lost when adjacent polysaccharide chains form peptide cross links via mDAP and D-Ala of two opposing peptide stems (Blackburn and Clarke, 2000).

Mycobacterial peptidoglycan is characterised by several modifications. One of these modifications takes place at the N-acetyl group of NAM as a result of an N-Ac-Muramic hydroxylase (NamH), resulting in an N-glycolylated group, as depicted in Figure 7 (Mahapatra et al., 2005, Raymond et al., 2005). This modification is found in all mycobacteria, excluding *M. leprae* which contains a *namH* pseudogene and therefore does not produce NGM (Mahapatra et al., 2008).

Another modification of the mycobacterial PG is the presence of peptide cross links in a 3-3 position, rather than the more common 4-3 cross link, produced by L-D transpeptidases (Lavollay et al., 2008, Gupta et al., 2010a). Mycobacterial PG can also be amidated at the carboxylic acid group on both mDAP and D-Glu on the peptide stem (Mahapatra et al., 2008). In *M. leprae* the L-Ala residues are substituted with glycine as is true for other types of bacteria and the peptide cross links may also contain glycine linkers (usually penta-glycine in *E. coli*) (Draper et al., 1987).

NamH belongs to a family of Rieske type monooxygenases, utilising a co-factor (such as NADPH) for the transfer of an oxygen group. Glycolylation of muramic acid by NamH is believed to result in insensitivity to lysozyme and potentially other lytic enzymes (Amano and Williams, 1983, Lavollay et al., 2008). Glycolylation of the muramyl peptidoglycan precursors and incorporation into mature peptidoglycan has only been identified in actinobacteria, such as mycobacteria, *Nocardia kirovani* and *Micromonospora* (Schleifer and Kandler, 1972, Hett and Rubin, 2008).

Generation of a *namH* knockout mutant in *M. smegmatis* by M. Pavelka's group demonstrated an increased sensitivity to antibiotics and lysozyme, this was enhanced during growth in rich medium (Raymond et al., 2005). This increased sensitivity was also enhanced when the cells reach stationary phase and the authors suggest that glycolylation may be a survival technique and

mechanism to prevent cell lysis and death (Raymond et al., 2005). It has recently been shown that N-glycolyl-muramyl-dipeptide resulted in significantly increased recognition of NOD2 mediated TNF secretion in mice compared to its non-glycolylated counterparts (Coulombe et al., 2009). These findings highlight the importance of glycolylation for mycobacterial adaptation *in vitro* and *in vivo*.

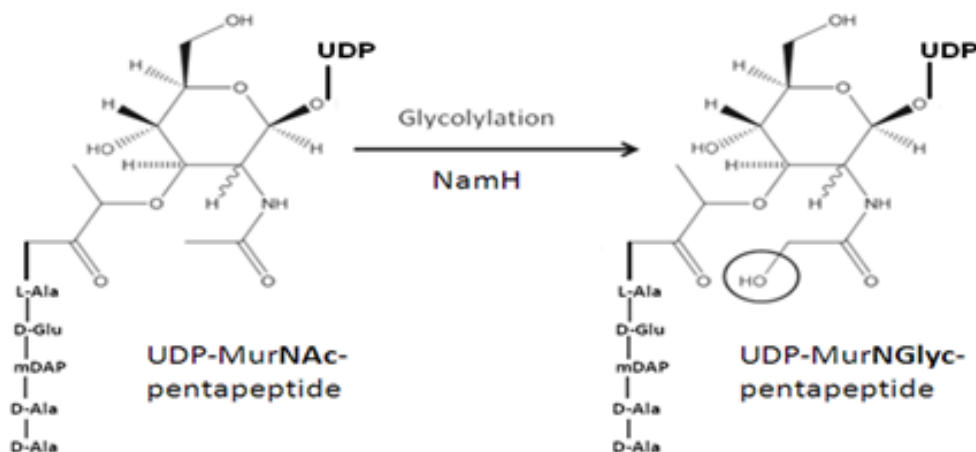


FIGURE 7: SCHEMATIC OF NAMH GLYCOLYLATION OF PG PRECURSORS

A schematic representing NamH activity at UDP-NAM PG precursors is depicted. The above schematic was created using ChemBioDraw.

The *namH* gene consists of 1,551 nucleotides and encodes a protein of 516 amino acid residues with a molecular mass of 57,615 Da (Reddy et al., 2009). As discussed earlier, NamH is a Rieske type monooxygenase enzyme, containing a 2Fe-2S domain and is primarily found in certain aerobic Actinomycetes (Coulombe et al., 2009). There has been little characterisation of this protein, however, studies investigating other Rieske type monooxygenases with the same catalytic domain have been carried out. Monooxygenases catalyse the incorporation of one oxygen atom into the substrate, in Rieske type monooxygenases this is facilitated by Fe ions ($\text{Fe}^{3+}/\text{Fe}^{2+}$) and other cofactors. One of the Fe ions is usually in coordination with two histidine residues and the other Fe ion, with two cysteine residues (D'Ordine et al., 2009)

a flat rhombic cluster is then formed by two sulphide bridges between the two sulphur ions and iron ions (D'Ordine et al., 2009).

In order to activate O_2 molecules by reducing agents, cofactors (for example NAD(P)H) are often required to enable protein interactions and thus allow this process (D'Ordine et al., 2009). The Rieske domain receives electrons from a reductase and/or a ferredoxin and can then drive the reduction of O_2 , as shown in Figure 8 (Lipscomb and Hoffman, 2005, D'Ordine et al., 2009). Hence they are made up of either 2 or 3 component systems (Ferraro et al., 2005).

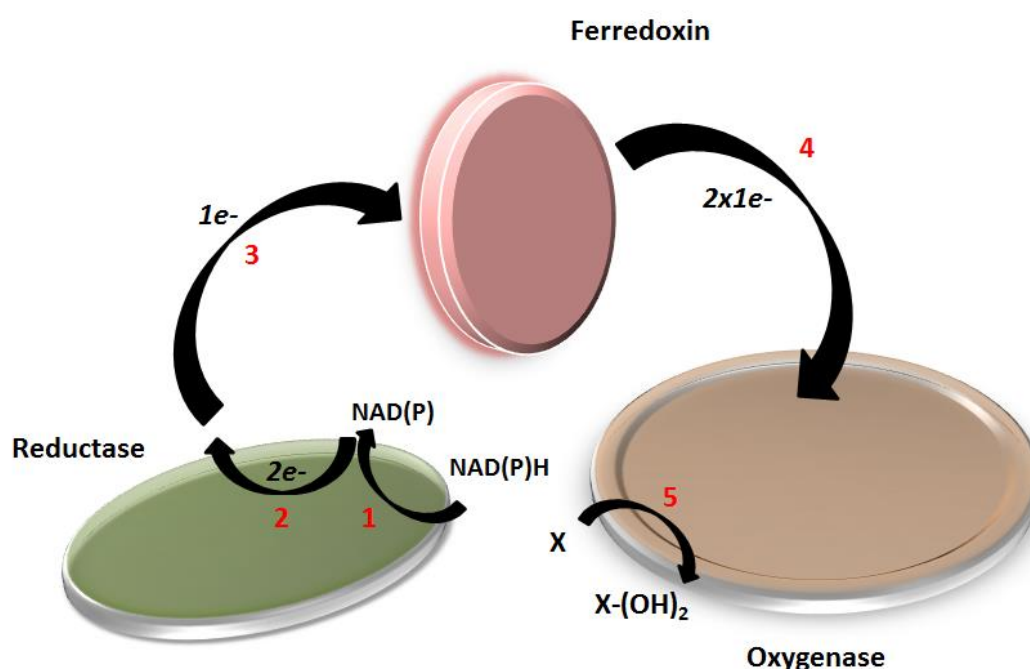


FIGURE 8: AN ADAPTED SCHEMATIC DEPICTING ELECTRON TRANSFER IN A THREE COMPONENT RIESKE OXYGENASE SYSTEM

Schematic showing electron transfer in a three component Rieske oxygenase system adapted from (Ferraro et al., 2005). Numbers indicate the reaction progress from reductase to oxygenase and the electron transfer, where X is the substrate in question.

The gene downstream of *namH* in *Mtb* (Rv3819), which is within the same operon, overlaps with *namH* by 3 base pairs; this led to

the postulation that this could encode for a protein potentially important for NamH activity. Using NCBI online freeware, sequence similarity searches using the sequence data for Rv3819 were carried out. Results with the highest hits were either orthologues within other mycobacterial species or hypothetical proteins, however, a hit with a 32% sequence identity, was a NADH dehydrogenase subunit from *Rhodothermus marinus* DSM 4252. This protein is involved in shuttling electrons from NADH to Fe-S centres, hence Rv3819, by extension may be involved in electron transfer for the enzymatic activity of NamH. In *M. smegmatis* the *namH* ortholog also overlaps with the downstream gene (MSMEG_6411) by 3 base pairs and this gene encodes a protein with roughly 70% similarity to Rv3819 in *Mtb*. This is also the case in *M. bovis*. In *M. leprae* this gene (ml0084c) is annotated as a pseudogene, as is the ortholog of *namH* (ml0085c); although there is no overlap between the two genes.

Expression and regulation data for *namH* (available from TBDB (Boshoff et al., 2004, Reddy et al., 2009) demonstrated that treatment with s-nitrosoglutathione and chlorpromazine stimulated *namH* expression whilst triclosan and benzamide both resulted in decreased levels of expression. Further studies comparing expression profiles of null mutants compared to WT H37Rv showed decreased expression of *namH* in a Δ sigE mutant when grown in 7H9 medium or during macrophage infection and another study using an aprC mutant strain showed decreased *namH* expression compared to wild type under standard growth conditions (Fontan et al., 2008, Abramovitch et al., 2011). TBDB indicates Rv0081 (a transcription regulator) and Rv0767c (a hypothetical protein) as probable regulators of rv3818, as determined by ChIP sequencing experiments (Reddy et al., 2009).

As demonstrated by Figure 7, the addition of a hydroxyl group to the muramic acid residue which results in altered structural interactions as well as 3D conformations has been hypothesised to

be the cause of lysozyme resistance in mycobacteria, due to increased hydrogen bonding (Gupta et al., 2010a). It has also been suggested to be important for the activity of Rpf (a muralytic enzyme) in mycobacteria. However, based on protein sequence searches, using the online NCBI blast system, as well as published peptidoglycan analyses, *Micrococcus luteus* (the organism in which the first Rpf was identified) does not contain a *namH* homologue or glycolylated PG (Schleifer and Kandler, 1972, Hett and Rubin, 2008, Young et al., 2010).

As mentioned previously peptide cross links may form between adjacent mDAP residues (in a 3-3 orientation), as a result of two L, D-transpeptidases found in *Mtb*; Ldt_{Mt1} (Rv0116c) and Ldt_{Mt2} (Rv2518c) (Lavollay et al., 2008, Gupta et al., 2010a). Despite having a functional homologue, Ldt_{Mt2} (Rv2518c) has been shown to be important for virulence and drug resistance (Gupta et al., 2010a).

The percentage of peptide cross-linking in mycobacteria verses bacteria such as *E. coli* is massively increased from about 30% (in *E. coli*) to ~80% (in *Mtb*), providing stability and resilience to the cell (Matsushashi, 1966). The bond linkages differ also, in *E. coli* they are predominantly 4 to 3 whereas in mycobacteria the percentage of 3 to 3 cross links increases upon entrance into stationary phase, reaching about 80% (Gupta et al., 2010a, Lavollay et al., 2008). Both of these structural features are thought to result in antimicrobial resistance as well as decreased lysozyme sensitivity.

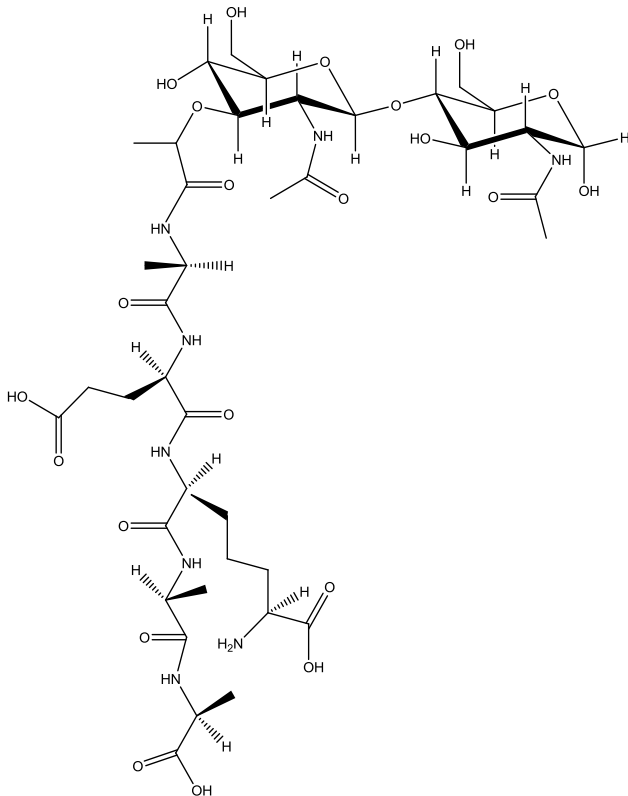


FIGURE 9: STRUCTURE OF NAG-NAM-PENTAPEPTIDE

A schematic of NAM-NAG with Ala-D-Glu-mDAP-Ala-Ala pentapeptide attached via NAM lactyl moiety is shown. This was created using ChemBioDraw.

1.9 LATENT TUBERCULOSIS INFECTION AND NON-REPLICATING PERSISTENCE

As previously discussed a possible outcome of infection with *Mtb* is the ability of the host immune response to control the infection, leaving a population of cells which are still viable and may result in active TB in the future (Parrish, Dick et al. 1998; Grange, Brunet et al. 2011). It has also been disputed whether the levels of post-primary TB infections and hence LTBI actually reflect latent TB or if it is simply a matter of re-infection (Cardona and Ruiz-Manzano, 2004). Clinical evidence of latency primarily stems from TST data which demonstrates the long time frame between infection with *Mtb*

and disease establishment, as well as a means of testing for LTBI (Kleinert et al., 2012, Lawn et al., 2011). Due to the lack of evidence to support the presence of viable *Mtb* bacilli in individuals harbouring LTBI, the current hypothesis as to the formation of LTBI is due to a population of dormant or non-replicating cells (NRP).

The first evidence to support the presence of dormant bacteria was found upon the introduction of antimicrobial chemotherapy through the surgical removal of pulmonary lesions from smear negative patients. These lesions demonstrated both non-viable (but microscopically detectable) and viable cells (from ~20% of patient samples) from lesions 'blocked' (a dense, anaerobic environment) for up-to several years (Wayne and Hayes, 1996, Wayne and Sohaskey, 2001). This aided the hypothesis of a population of NRP cells within the host due to immune response, which upon cultivation were found to be both viable and non-viable.

Mtb bacilli have been shown to be able to adapt to stressful conditions occurring at sites of host defence, by reducing their metabolic activity and transitioning to a dormant state, often referred to as non-replicating persistence (NRP). Dormancy enables mycobacteria to survive stresses and reduces initiation of the immune response (Cardona and Ruiz-Manzano, 2004, Barry et al., 2009). Hence dormancy is defined as: 'a reversible state of low metabolic activity in which cells can exist for extended periods without division' (Kaprelyants et al., 1993).

When environmental conditions are favourable for growth, resuscitation of bacilli can occur and the time period before this resuscitation can vary greatly (Kaprelyants et al., 1993). Dormant bacilli associated with latent infection have been shown to be less susceptible to antimicrobial treatment due to physiological changes and therefore are of clinical significance in the eradication of TB (Zhang, 2004). In recent years there has been an increase in research into bacterial gene expression upon entry to dormancy

within *in vitro* models, using laboratory strains as well as sputum samples. This has led to the discovery of several important mechanisms required for long term survival, whilst it has also shown discrepancies between expression levels in cultured versus sputum obtained *Mtb* and currently leaves many questions unanswered (Dahl et al., 2003, Deb et al., 2009).

1.9.1 *IN VITRO* AND *IN VIVO* DORMANCY MODELS

Several *in vitro* models of dormancy have been developed. Examples include non-replicating persistence under microaerophilic conditions (Wayne and Sohaskey, 2001), starvation in PBS (Betts et al., 2002), incubation in prolonged stationary phase (Shleeva et al., 2002, Smeulders et al., 1999), the Hu-Coates high dose RIF model (Hu et al., 2000) and a multiple stress model (Deb et al., 2009). A recent publication using *Mycobacterium tuberculosis* 18b, a Streptomycin (STR)-dependent mutant, demonstrated that when grown in the absence of STR bacilli entered a viable but non-culturable state. *In vitro* experiments were then performed using approved and experimental tuberculosis drugs, several of which were found to be active (Zhang et al., 2012). Common features of NRP mycobacteria are the loss of acid-fastness, phenotypic drug resistance and a reduced level of ATP or metabolism (Deb et al., 2009, Betts et al., 2002, Wayne and Hayes, 1996, Gengenbacher and Kaufmann, 2012).

Dormant mycobacteria are believed to be more difficult to eradicate, therefore using *in vitro* and *in vivo* dormancy models to further understand this phenomenon may lead to progress in the eradication of dormant cells. Wayne used *Mtb* cells grown in microaerophilic conditions, as a means of inducing non-replicating persisters and found an initial 10-fold increase in glyoxylate synthesis, most likely for required for the regeneration of NAD necessary for replication before oxygen limitation prevented further growth (Wayne and Lin, 1982). In a later study examining hypoxia

the group found two stages of non-replicating persistence (NRP). Stage 1 was found to occur rapidly when the reducing level of dissolved O₂ reached ~1% saturation, when the dissolved concentration reached 0.06% saturation the bacilli entered an anaerobic state, which they designated NRP 2 (Wayne and Hayes, 1996). In this model respiration fell upon entry into NRP 2 as did growth rate, however, cultures demonstrated spontaneous resuscitation when reintroduced into favourable growth conditions (Wayne and Hayes, 1996).

A recent multiple stress model for the production of dormant *Mtb* bacilli using the following conditions: low oxygen (5%), high CO₂ (10%), nutrient starvation and acidic pH (5.0), found that *Mtb* lost culturability and acid fastness, accumulated triacylglycerol (TG) and wax esters (WE) and then developed phenotypic antibiotic resistance (Deb et al., 2009). Nutrient starvation (Betts et al., 2002) is another model of *in vitro* dormancy investigated using *Mtb*, the work demonstrated growth arrest, reduced respiration and antimicrobial resistance.

In vivo, animal models have been used to demonstrate immunological and post-antimicrobial latency, as demonstrated by a mouse model revealing recrudescence as a result of age-related reduced immunity and a mouse model demonstrating entry to the latent state after pyrazinamide treatment (Orme, 1988, McCune et al., 1956). The three commonly used animal models in *Mtb in vivo* work are: Rabbit, Mouse and Guinea pig, with the mouse model being the model of choice in most cases (Gupta and Katoch, 2009). Each model has its benefits and drawbacks; the mouse model mimics the human immune response the most closely, while the rabbit is the only model which can result in cavitation and the guinea pig is the most susceptible to infection with *Mtb*, however, despite several guinea pig studies it is generally considered that these animals do not harbour latent infections (Patel et al., 2011, Dharmadhikari and Nardell, 2008). Models using untreated infected

mice were the first to demonstrate that, within cells, the nutrient content was not the limiting factor triggering latency leading to the discovery of the role of the immune response (Wayne and Sohaskey, 2001).

Historically, the Cornell latency *in vivo* model is a platform for which many of today's *in vivo* studies into mimicking latent disease and reactivation of mycobacterial infection have been based. This model and variations of it involve infection of mice with *Mtb* followed by antimicrobial treatment until no bacilli are able to be detected in the lungs (apparent sterility). At this stage mice show no sign of disease, however upon immune-suppression through NOD2 suppression, TNF- α neutralisation or INF- γ neutralisation reactivation of disease occurred (McCune et al., 1956, McCune and Tompsett, 1956, Scanga et al., 1999).

However, it has been argued that this model does not reflect the *in vivo* state in humans of *Mtb* infection as early drug treatment may influence the immune response of the host (Flynn and Chan, 2001). The Hu-Coates *in vivo* model uses mice infected with *Mtb* and treats with PZA to induce bacterial persistence, demonstrating the presence of mRNA and 16S rRNA transcripts within persisting *Mtb* bacilli, whilst *in vitro* studies and RIF treatment presented the same findings (Hu et al., 2000).

Use of an artificial granuloma *in vivo* mouse model, achieved through subcutaneous implantation, results in the formation of granulomatous lesions and an altered bacterial physiological state with a dormancy-like phenotype (Karakousis et al., 2004). Gene expression analysis of bacilli within these lesions demonstrated induction of *dosR* (Rv3133c) and multiple members of the DosR regulon, currently thought to have a role in the transition to dormancy (Karakousis et al., 2004). There are more modern versions of the Cornell mouse model, as well as other animal

models, yet none which fully mimic *Mtb* infection in humans; therefore to understand latency, further improvement is needed.

A key finding from *in vivo* work is the role played by the host immune system in controlling TB, authors found that *Mtb* continues to replicate throughout chronic infection in mice and is restrained by the immune system (Gill et al., 2009). Understanding reactivation of disease due to bacterial resuscitation is of upmost importance in the eradication of TB, key issues of eliminating NRP cells are their phenotypic drug resistance as well as their ability to survive for extended periods of time (Gold et al., 2012). Bacterial factors, such as Rpf have been shown to play a role in resuscitation of NRP cells, in addition to Rpf resuscitation it has been suggested that phospholipids may lead to reactivation of dormant bacilli (Cardona and Ruiz-Manzano, 2004).

1.9.2 REACTIVATION AND RESUSCITATION

Persisting populations are highly heterogenic and contain bacilli in various physiological states. Kaprelyants and colleagues suggested distinguishing surviving bacteria in three types: 1) viable 2) dormant and 3) “non-culturable” owing to their culturability. Non-culturable dormant bacilli are not capable of forming a colony on agar without a re-activation (resuscitation) step whereas non-viable cells are utterly incapable of doing so (Kaprelyants et al., 1993). *In vitro* dormant cells can be generated via long stationary phase growth and they require re-activation or resuscitation before ‘normal’ growth can be resumed. Alternatively ‘persister’ cells are often referred to in the literature and tend to refer to non-replicating cells which when transferred to favourable media spontaneously resuscitate (Wayne and Hayes, 1996).

A resuscitation procedure may vary depending on bacterial species. Dormant *M. luteus* cells were resuscitated by addition of sterile culture supernatant obtained from growing cultures of the

same organism (Mukamolova et al., 1998b). A resuscitation promoting factor secreted into *M. luteus* culture supernatant was then identified as a secreted protein and shown to be active at picomolar concentrations (Mukamolova et al., 1998a). Later it was shown that dormant mycobacteria could be also resuscitated by culture supernatant of recombinant Rpf (Sun and Zhang, 1999, Shleeva et al., 2002).

1.9.2.1 RESUSCITATION PROMOTING FACTORS

Rpf proteins are secreted muralytic enzymes shown to resuscitate dormant bacterial cells and to stimulate bacterial growth through peptidoglycan degradation (Mukamolova et al., 1998a, Mukamolova et al., 2006). This has been well established for multiple bacterial species including *Mtb* which encodes five different Rpf proteins (A-E) (Downing et al., 2005, Mukamolova et al., 2006, Ruggiero et al., 2009, Mukamolova et al., 2002b, Mukamolova et al., 1998b). The domain structure for each of these proteins is shown in Figure 10. The predicted mechanism for PG degradation and resuscitation is cleavage of the β 1,4-glycosidic linkage between alternating NAM-NAG residues (or NGM-NAG). *M. luteus* contains a single Rpf protein which is essential for growth of this bacterium (Mukamolova et al., 2002a).

Rpfs have been shown to display functional redundancy, however, deletion of 3 of the 5 Rpf-like genes resulted in an attenuated strain in a mouse model incapable of resuscitation *in vitro* (Downing et al., 2005). Deletion of all Rpf genes resulted in severe growth and persistence defects in a mouse model of tuberculosis (Kana et al., 2008). Yet, the subsequent deletion of both RpfB and RpfA in *M. tuberculosis*, or even a single deletion (RpfB) prevented the resulting strains from growing in stressful conditions (i.e. oxygen depletion) (Downing et al., 2005, Mukamolova et al., 2002b, Russell-Goldman et al., 2008).

Whilst individual RpfB were found dispensable for *in vitro* and *in vivo* growth, RpfB was solely indispensable for resuscitation *in vivo*, and RpfB were shown to be differentially expressed (Tufariello et al., 2006, Tufariello et al., 2004). A study using a Δ ABCDE *Mtb* strain demonstrated the role of Rpf in β -lactam tolerance and outer membrane permeability (Wivagg and Hung, 2012). Overall RpfB have been found to be dispensable for growth *in vitro*; however, have been shown to be important for growth and persistence *in vivo*. Double and triple *rpf* mutant strains were shown to be attenuated in their ability to disseminate to mouse lungs, as well as diminished in their ability to reactivate after immune suppression through an intraperitoneal administered mouse model (Biketov et al., 2007).

Recent work has demonstrated the clinical importance of RpfB in human TB; a large proportion of bacilli isolated from sputum were found to be RpfB-dependent (Mukamolova et al., 2010). In a separate study *Mtb* RpfB were found to be immunogenic by their ability to induce INF- γ production in the blood of TST-positive healthy individuals who had been in close contact with TB patients; RpfB-specific T-cell responses were shown to be maintained for several decades in non-progressors (Mukamolova et al., 2010, Commandeur et al., 2011).

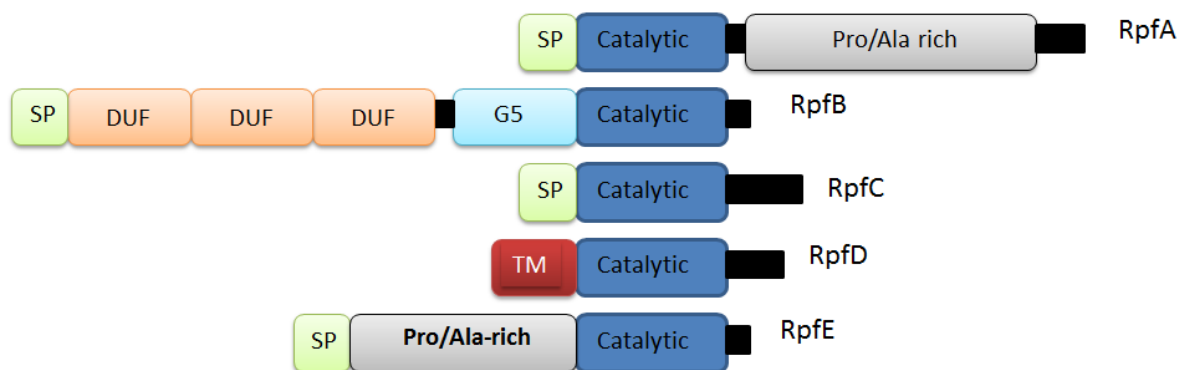


FIGURE 10: STRUCTURAL SCHEMATIC SHOWING *MTB*'S RPF A-E DOMAINS

The above schematic demonstrates the structural domains of all 5 *Mtb* Rpf proteins. The abbreviations shown in the figure are as follows: SP; signal peptide, DUF; domain of unknown function, TM; transmembrane domain and Pro/Ala-rich; proline and alanine rich region. This figure was adapted from work previously published using the PFAM database (Ruggiero et al., 2011).

The Rpf-like proteins in *Mtb* are annotated as lytic transglycosylases (a class of muramidase), which cleave the β 1,4-glycosidic bond between NAM and NAG (Reddy et al., 2009). This results in the formation of a 1,4-anhydro ring at the NAM residue whilst lysozymes (another type of muramidase), which can be one of four types, cleave the β 1,4-glycosidic bond resulting in a product with a terminal reducing NAM residue (Holtje and Tomasz, 1975), (Wyckoff et al., 2012, Vollmer et al., 2008). As depicted in Figure 10 all five *Mtb* Rpf proteins contain a catalytic domain, this domain has a conserved active site glutamine residue essential for muralytic activity (Cohen-Gonsaud et al., 2005). Crystallography has also demonstrated the binding of this active site to peptidoglycan (Ruggiero et al., 2009). Figure 10 was adapted from previously published work (Ruggiero et al., 2011), this work used the PFAM database. (Lavollay et al., 2008, Raymond et al., 2005)

There have been studies since, using Prosite, SignalP and TMHMM servers, which suggest slightly altered protein structures (Sigrist et al., 2013, Petersen et al., 2011, Krogh et al., 2001). For example, using these databases RpfA and D are predicted to be secreted

whilst RpfB is thought to be anchored to the outer surface of the cell membrane, RpfC has a secretory signal predicted using SignalP but does not have a predicted TM helix and RpfE has a weakly predicted TM helix and a strongly predicted signal sequence (Gupta, 2012).

RpfB, a 362 amino acid protein, contains a lipid membrane lipoprotein anchor at the N terminal and a conserved Rpf region located near its C terminal (Mukamolova et al., 2002b, Ruggiero et al., 2009, Ruggiero et al., 2007). RpfB has a G5 domain, which can be found in many proteins and is believed to be involved in binding NAG, and in the case of RpfB is thought to result in the attachment to the peptide crosslinks within peptidoglycan allowing the active catalytic site to interact with NAG-NAM and cleave the glycosidic bond (Ruggiero et al., 2007, Ruggiero et al., 2009). Thus, due to the close proximity and likely interaction of the predicted Rpf binding site and NGM/NAM peptidoglycan moiety, it could be possible for this modification to play a role in Rpf action, this structural orientation is shown in Figure 11.

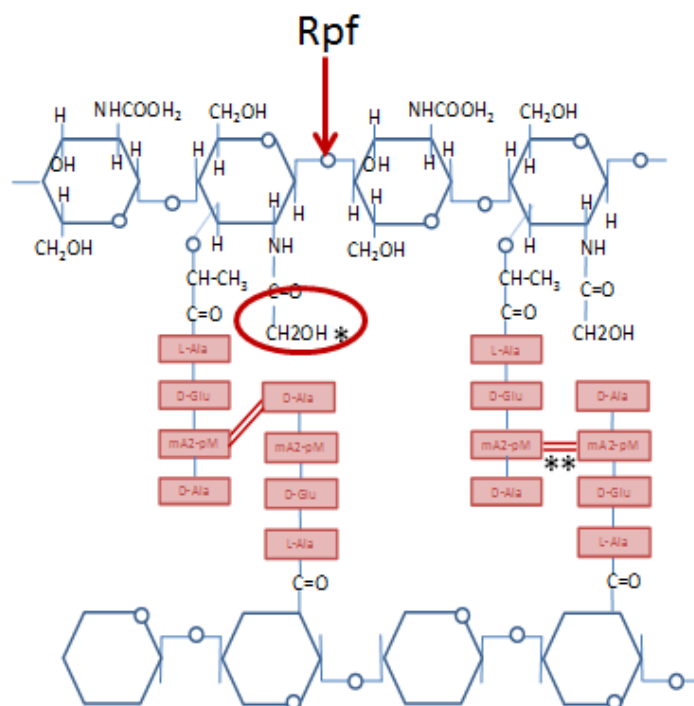


FIGURE 11: A PG SCHEMATIC SHOWING THE PROXIMITY OF RPF BINDING AND GLYCOLYLATED PG

The above schematic demonstrates the hydroxylation of the muramyl residue within mycobacterial PG resulting in CH_2OH in place of the methyl group, this is highlighted in red and by a single *. This is shown in relation to the proximity of the predicted binding site of Rpf within PG. ** indicates the 3-3 peptide cross links commonly found within mycobacterial PG.

Expression of *Mtb* Rpfs in the lungs of infected mice and in human tissue has been confirmed previously (Tufariello et al., 2004, Davies et al., 2008). A study examining the expression profile of *Mtb* Rpfs under different environmental stresses found that at the onset, and throughout resuscitation all Rpfs were expressed, with maximum ratios for RpfA and RpfD, whereas RpfC was consistently expressed during the different growth stages as well as during nutrient starvation (Gupta et al., 2010b). Interestingly, Gupta found that acid stress induced expression of Rpfs D and E whilst hypoxia resulted in increased expression levels of RpfC and RpfE. Their findings therefore contribute to the work of others indicating the varying roles of the mycobacterial Rpfs and hence the suggestion

of differential regulation for *Mtb* RpfS (Gupta et al., 2010b). Previous work has shown variation in expression levels of *Mtb* RpfS in a growth-phase-dependent manner (Mukamolova et al., 2002b, Tufariello et al., 2004).

More recent work on Rpf regulation has further demonstrated the non-uniform expression and regulation previously hinted at by deletion studies (Kana et al., 2008). RpfA, as previously discussed, is positively regulated by a homologue of cAMP receptor family protein (Rickman et al., 2005), whilst RpfC has been shown to be up regulated by SigD (Raman et al., 2004) and RpfE down regulated after vancomycin treatment (Provvedi et al., 2009, Kana and Mizrahi, 2010).

A riboswitch candidate has been identified upstream of *rpfA* in *Mtb*, although no ligand has yet been identified these are commonly associated with the regulation cell of wall processes (Arnvig and Young, 2012). RpfB (and E) interact with an endopeptidase with L-D specificity known as Rpf interacting protein (RipA) for synergistic degradation of mycobacterial PG, promoting growth and resuscitation of dormant cells (Kana and Mizrahi, 2010, Kana et al., 2008, Hett et al., 2008). Through the use of knockout mutants, the importance of RpfS in the physiological establishment of chronic TB infections, as well as in the reactivation of disease has been demonstrated.

1.9.2.2 MUROPEPTIDES AS SIGNALLING MOLECULES

Muropeptides are products released via the breakdown of PG, whether this is a result of enzymatic hydrolysis (i.e. lysozyme), antibiotic treatment or in the course of growth and division. Muropeptides are classed as a minimum of one NAM and one amino acid residue (Traub et al., 2006, Stewart-Tull and White, 1964). Muramic acid is universal throughout both Gram-positive and negative bacteria, only absent from cells devoid of a cell wall as well as specific Archaeobacteria (Salton, 1964). Generally

speaking Gram-negative bacteria release few muropeptide products due to peptidoglycan recycling whereas Gram-positive bacteria are thought to release a greater amount, mycobacterial peptidoglycan recycling has yet to be firmly established (Vollmer et al., 2008, Mahapatra et al., 2005).

Using reverse phase HPLC (rp-HPLC) the complexity of muropeptides or murein has been identified. In *E. coli* more than 80 variations of muropeptides have been identified, this is partly due to the differing peptide chain lengths as well as a result of an unusual cross linking. This is caused by a transpeptidase with L-D specificity (Blackburn and Clarke, 2000) This, combined with the 1,6-anhydro form of muramic acid, presents a large variety of muropeptide fragments that will be produced via enzymatic digestion (Jacobs et al., 1994, Kraft et al., 1998).

Muramidases (a type of autolysin), such as lysozyme, specifically hydrolyse the β -1 to 4 glycosidic bond and release NAG and NAM residues. Lytic transglycosylases (another type of autolysin known as exoglycosylases) are not hydrolases but cleave the β -glycosidic linkages by progressively degrading the murein strands and producing 1,6-anhydro-NAM residues (Blackburn and Clarke, 2000, Kraft et al., 1998). However, it is unknown at which end this degradation begins at.

Variation in muropeptides is increased in mycobacteria due to the presence of *namH* gene (*rv3818*), which encodes UDP-MurNAc-pentapeptide monooxygenase, it results in the glycolylation modification of the PG and is thought to increase hydrogen bonding and therefore the stability of the cell wall (Raymond et al., 2005). The *namH* gene has been identified in all other mycobacterial genomes, and hence all mycobacteria contains glycolylated PG, excluding *M. leprae* which contains a pseudogene (Mahapatra et al., 2008). It can therefore be argued that this modification may play a role in dormancy and resuscitation of

mycobacteria; if Rpf released mucopeptides act as signalling molecules then the addition of a hydroxyl group could have a major influence on the resuscitation activity, as shown in Figure 12. Alternatively this modification may be important for Rpf activity.

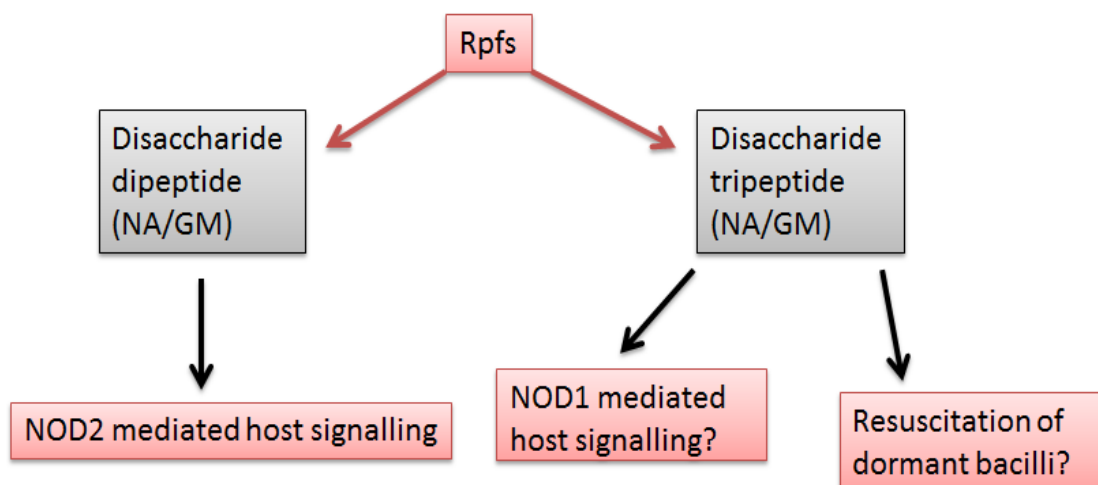


FIGURE 12: THE POTENTIAL ROLE OF RPF RELEASED MUROPEPTIDES AS SIGNALLING MOLECULES

Rpf mucopeptide products and their known and predicted roles in NOD signalling, as well as in resuscitation are depicted. This figure is based on previously published data (Kana and Mizrahi, 2010).

Muramyl dipeptide (MDP) has been found to be the smallest structural component of PG to have an adjuvant effect (Boneca, 2005). After phagocytosis mucopeptides are released and exert an immune response via a signalling cascade, leading to altered gene expression (Traub et al., 2006). The recognition of bacterial structures is required for an immune defence activity to occur and this is carried out by pattern recognition receptors (PRRs), toll-like receptors (TLRs) are a well-known example of a family of these (Traub et al., 2006). It was previously thought that mucopeptide fragments acted via this family of PRRs, however, it has recently been discovered that cytoplasmic receptors NOD1 and 2 can act as receptors. NOD1 recognises Gram-negative PG breakdown

products while NOD2 is believed to recognise MDP (Chamaillard et al., 2003, Girardin et al., 2003a).

Muropeptides, in addition to being immune-modulators are signalling molecules for β -lactamase expression in *E. coli* (Jacobs et al., 1994). Recently a postulated 'scout' model of resuscitation has been suggested (Gengenbacher and Kaufmann, 2012); in this model scouts are limited in LTBI and the environment they sense is not supportive of growth, if the environment becomes more hospitable (i.e. caseating granuloma) then scouts, perhaps through Rpf action, resuscitate higher levels of bacteria leading to active disease (Gengenbacher and Kaufmann, 2012).

The muropeptide fragments released as a consequence of PG degradation (e.g. Rpf muralytic activity) have recently been linked to endospore germination in *B. subtilis* via binding to protein kinase C (PknC) extracellular domains; penicillin and serine threonine kinase associated domains (PASTA, 3 are present in *B. subtilis*) which are attached to a trans-membrane spanning region and exposed at the membrane surface (Shah et al., 2008). The minimal structure found necessary for germination was a disaccharide tripeptide. *Mtb* contains a PknB domain (linked to 4 PASTA domains) that is structurally homologous to eukaryotic S/T kinases (Barthe et al., 2010). It has been suggested that binding of these fragments causes a signalling cascade and leads to resuscitation from dormancy as well as promoting cell growth, in PknB muropeptide binding to the PASTA domains was shown to be dependent on the amino acid composition of the stem peptide (Mir, 2001 PLoS Path) and (Shah and Dworkin, 2010).

A recent study by Coulombe et al found that, if the muropeptide signalling molecule MDP contained a glycolyl group the inflammatory response via NOD2 was much stronger, indicating the potent immunogenic potential of mycobacterial cell wall molecules and perhaps how this modification could play an as yet unknown

role in resuscitation (Coulombe et al., 2009). In a recent publication, a truncated *M. luteus* Rpf protein was used to generate muropeptide products from both *M. smegmatis* and *M. tuberculosis*, these products had stimulatory activity on non-culturable cells at levels comparable to recombinant Rpf (Nikitushkin et al., 2013). Using specific Rpf inhibitors, Rpf-dependent resuscitation was inhibited, indicating that Rpf products may act as a substrate for Rpf rather than as a direct stimulant of resuscitation (Nikitushkin et al., 2013).

1.10 AIMS AND OBJECTIVES

The overall aims of this study were to investigate the role of glycolylation of muramic acid in mycobacterial PG in relation to Rpf action. It was also hypothesised that Rpfs may be adapted to, and more efficient at degrading mycobacterial PG.

The following objectives were therefore undertaken:

- Generation of model mycobacterial PG in *E. coli* in order to investigate release of muropeptides by recombinant Rpf
- Individual over-expression of all 5 *Mtb* Rpfs in both wild type and $\Delta namH$ *M. smegmatis* to examine the role of glycolylation in Rpf growth stimulation and resuscitation
- Generation a $\Delta namH$ *M. tuberculosis* mutant to examine any growth phenotype, antimicrobial sensitivity and the role of this modification in intracellular survival within murine macrophages

CHAPTER 2: MATERIALS AND METHODS

2.1 REAGENTS AND MEDIA

All reagents used were purchased from Fisher Scientific UK Ltd (Loughborough) or Sigma-Aldrich Company Ltd (Gillingham, Dorset) unless otherwise stated. Media for growth studies were purchased from Sigma-Aldrich Company Ltd (Gillingham, Dorset) or Becton, Dickinson and Company Ltd (Oxford).

2.1.1 MEDIA

LB medium was prepared by dissolving 10g tryptone, 5g yeast extract and 10g NaCl per 1L dH₂O; pH was adjusted to 7.5 using 10mM NaOH before sterilisation by autoclaving at 121°C. LA was made as described with the addition of 15g agar and boiling in a microwave prior to sterilisation.

7H9 Middlebrook medium was prepared by dissolving 4.7g 7H9 powder (Becton, Dickinson and Company Ltd) in 900ml ddH₂O containing 2.5g glycerol, before sterilisation by autoclaving. 10% (v/v) Albumin-dextrose-catalase (ADC) supplement and 0.05% (w/v) Tween 80 were added to 7H9 media prior to use.

7H10 Middlebrook agar was prepared by dissolving 19g of 7H10 powder (Becton, Dickinson and Company Ltd) in 900ml ddH₂O containing 6.25g of glycerol; this was then boiled in a microwave prior to sterilisation by autoclave. 10% (v/v) ADC was added prior to use.

Sauton's medium was prepared by adding the following to 800ml ddH₂O: 0.5g KH₂PO₄, 0.5g MgSO₄·7H₂O, 4g L-asparagine, 0.05g ferric ammonium citrate, 2g citric acid, 10ml glycerol and 0.1ml of 1% (w/v) ZnSO₄ solution. The pH was adjusted to 7.2-7.4 using NaOH and the volume made up to 1L prior to sterilisation. Medium was supplemented by 0.05% (w/v) Tween 80 and in some cases by 10% (v/v) ADC.

Diluted Sauton's medium was prepared by adding the following (per litre): 0.25g KH_2PO_4 , 0.7g $\text{MgSO}_4 \cdot 7\text{H}_2\text{O}$, 1g L-asparagine, 6ml glycerol, 0.025g ferric ammonium citrate, 1g citric acid and 50 μl of a 1% (w/v) ZnSO_4 . pH was adjusted to 7.0 before sterilisation by autoclaving.

Broth E was prepared by adding 5 peptone, 1.5g yeast extract, 1.5g beef extract and 5g NaCl to 1L of dH_2O before sterilisation by autoclaving. For mycobacterial cultivation 0.05% (w/v) Tween 80 was added prior to use.

mHdeB medium (modified Hartman's-deBont) was prepared as previously described (Shleeva et al., 2004) by adding (per litre): 11.8g $\text{Na}_2\text{HPO}_4 \cdot 12\text{H}_2\text{O}$, 1.7g citric acid, 20g $(\text{NH}_4)_2\text{SO}_4$, and 30ml glycerol were mixed, filter sterilised and supplemented with 0.05% (w/v) Tween 80 and 1% (v/v) of trace elements solution. The trace elements solution contained the following components (per litre): 1g EDTA, 10g $\text{MgCl}_2 \cdot 6\text{H}_2\text{O}$, 0.1g $\text{CaCl}_2 \cdot 2\text{H}_2\text{O}$, 0.04g $\text{CoCl}_2 \cdot 6\text{H}_2\text{O}$, 0.1g $\text{MnCl}_2 \cdot 2\text{H}_2\text{O}$, 0.02g $\text{Na}_2\text{MoO}_4 \cdot 2\text{H}_2\text{O}$, 0.2g $\text{ZnSO}_4 \cdot 7\text{H}_2\text{O}$, 0.02g $\text{CuSO}_4 \cdot 5\text{H}_2\text{O}$ and 0.5g $\text{FeSO}_4 \cdot 7\text{H}_2\text{O}$.

ADC was prepared by dissolving 50g Bovine serum albumin (Fraction V), 20g D-glucose, 8.5g NaCl and 40g catalase in 1L ddH_2O before filter sterilising.

DMEM-Dulbecco's Modified Eagle Medium (Life Technologies Ltd, UK) was supplemented with 10% (v/v) foetal calf serum (FCS) (Life Technologies Ltd, UK) and 2mM L-glutamine.

2.2 BACTERIAL STOCKS

200 μl of 70% (v/v) glycerol was added to 800 μl of exponential culture in 1.5ml cryogenic tubes (Nalgene, Fisher). After careful mixing, stocks stored at -80°C .

2.2.1 CULTIVATION TECHNIQUES

E. coli

Cultivation of bacterial starter cultures began with inoculation of 5ml LB in 20ml sterile universal tubes (with or without antibiotics) either by picking a single colony from LA plates or by addition of 100µl from a thawed frozen stock. These 5ml starter cultures were then incubated at 37°C, with 200rpm shaking overnight.

M. smegmatis

Bacterial starter cultures were inoculated as above; however, Broth E, Sauton's or 7H9 media were used. These were then grown under the same conditions as before but incubated for 3 days or until they reached a desirable OD. When required, antibiotics were added as follows: 20ng/ml tetracycline (in 70% EtOH) or 50ng/ml kanamycin or hygromycin.

M. tuberculosis

Cultivation was performed in accordance with the Codes of Practice set out for work within the Category III suite. All manipulations with *Mtb* were performed within class I or II microbiological safety cabinets, using approved Standard Operating Procedures (SOP). 7H9 or Sauton's liquid media and 7H10 agar plates were used for growth of *Mtb*. 5ml starter cultures were inoculated with 500µl of thawed bacterial stock and grown in 20ml universals sealed with Nescofilm (Osaka, Japan) and double bagged before incubation at 37°C with 100rpm shaking for up to 21 days. Larger scale cultures were grown in 50ml Flacon tubes or 1L roller bottles; roller bottles were placed on a rolling mechanism at 37°C with constant mixing.

2.2.2 CFU PLATING AND COUNTING

All CFU counts were performed using a standard liquid droplet method, bacterial cultures were serially diluted in appropriate medium, mixed and triplicate 10µl spots were carefully placed onto

duplicate segmented LA or 7H10 agar plates and allowed to dry before inversion and sealing in Nescofilm. Plates were then incubated statically at 37°C until CFUs became visible; normally 3 days for *M. smegmatis* and 3 weeks for *Mtb*. CFU counts (per ml) were calculated using the following formula:

$$CFU \text{ count/ml} = \text{average count in } 10 \mu\text{l spot} \times 100 \times \text{dilution factor}$$

2.3 BUFFERS AND SOLUTIONS

PBS (Phosphate Buffered Saline) was prepared by dissolving 1 PBS tablet (Sigma-Aldrich); in 200ml ddH₂O. The obtained buffer contained 0.01 M phosphate buffer (pH 7.4), 0.0027 M potassium chloride and 0.137 M sodium chloride. This solution was then autoclaved.

10x TAE buffer is made by dissolving 48.4g Tris base in 800ml ddH₂O before adding 11.4ml of glacial acetic acid (17.4M) and 3.7g ethylene-diamine-tetra-acetic acid (EDTA). This solution was then made up to 1L with ddH₂O. Prior to use this solution was diluted 1 in 10 with ddH₂O.

TE buffer is composed of 10mM Tris HCl, pH 8.0; 1mM EDTA

20x SSC buffer (saline sodium citrate) is made by dissolving 0.3M sodium citrate and 3M NaCl in ddH₂O, pH was adjusted to pH 7.0.

Washing buffer contained of 0.1 M Maleic acid (pH 7.5), 0.15 M NaCl; 0.3% (w/v) Tween 20.

Detection buffer contained 0.1 M Tris-HCl (pH 9.5), 0.1 M NaCl.

4x SDS sample buffer was composed of 40% (v/v) glycerol, 240mM Tris HCl; pH 6.8, 8% (w/v) SDS, 0.04% (w/v) bromophenol blue and 5% β-mercaptoethanol dissolved in dH₂O.

10x SDS Running buffer was prepared by dissolving 144g glycine, 36.3g Tris base and 10g of SDS in up to 1L of dH₂O; pH 8.3.

Transfer buffer was prepared by adding 25mM Tris base, pH 8.3; 192mM glycine and 20% (v/v) MeOH per 1L dH₂O.

Tris Buffered Saline (TBS) consisted of 0.1M NaCl and 20mM Tris, pH 7.5.

Tris buffered saline Tween (TBST): 0.1% (w/v) Tween 20 was added to TBS.

2.4 GENERATION OF BACTERIAL OVEREXPRESSION STRAINS

2.4.1 PCR

Gene coding sequences were amplified from bacterial genomes using corresponding forward and reverse primers (for details see Table 5, Table 9 and Table 19). The following components are required for amplification:

0.25µM Forward primer
0.25µM Reverse primer
<2ng/µl template DNA
40µM dNTP mix
Platinum Taq Polymerase*
10x buffer
2mM MgSO₄
DMSO**
DNase free H₂O

* Platinum® Taq High fidelity polymerase (Invitrogen) was used to amplify genes for cloning. ** DMSO was used when required (at 10% (v/v)). For all diagnostic PCR reactions the above components were used with the following alterations: GoTaq® polymerase (Promega) was used in combination with 5x reaction buffer.

Samples were mixed and aliquoted into 0.2ml flat cap PCR tubes (Fisher, UK) and placed in a PCR thermocycler under the conditions below.

Initial denaturation 94°C 4 minutes

Denaturation	94°C	30 seconds		X29 cycles
Annealing	55°C*	30 seconds		
Extension	68°C	30 seconds**		

Final extension 72°C 2 minutes

*The annealing temperature was usually -5°C of the T_m of the primer pair. ** 30 seconds per 500bp being amplified

2.4.2 RESTRICTION DIGESTION AND LIGATION

Once amplified an aliquot of the PCR mixture was analysed by gel electrophoresis. Samples were loaded on a gel containing 1% (w/v) agarose and 0.5µg/ml ethidium bromide. The DNA fragments were visualised by exposure of the gel under UV light. The remaining PCR product was purified using a QIAquick kit (Qiagen). This amplified DNA and the plasmid DNA were digested using specific restriction enzymes (NEB), samples were ran on a DNA gel, excised and gel purified using QIAEX II extraction kit (Qiagen). If DNA concentrations were low samples were concentrated by vacuum drying. Ligation reactions were then set up as follows:

Plasmid DNA (100ng)
 Insert DNA (100ng)
 T4 DNA ligase (1µl)
 T4 rapid ligation buffer (5µl)
 DNase free H₂O (To make 10µl)

Reagents were mixed well and incubated at RT overnight.

2.4.3 TRANSFORMATION

Constructs were transformed into competent α -select gold standard cells (Bioline Reagents Ltd, London). A 25µl aliquot of cells, thawed on ice, was mixed well with 3µl of the ligation mixture and incubated on ice for 15 minutes. This tube was then placed at 42°C for 45 seconds before briefly being placed back onto ice. 400µl of LB medium containing 10mM MgSO₄ was added to the mixture,

followed by incubation at 37°C with 200rpm shaking for 1 hour. After incubation the mixture was plated onto appropriate agar and incubated as described earlier.

2.4.4 PLASMID DNA PURIFICATION

Several single colonies were picked and used to inoculate 5ml aliquots of LB with the appropriate antibiotic. Tubes were incubated overnight, once in stationary phase cultures could be used for plasmid DNA purification. Cultures were spun down at 12,000xg for 15 minutes in a bench top centrifuge before plasmid DNA was extracted using a GeneElute™ miniprep kit (Sigma-Aldrich) which uses a spin column to bind DNA. DNA was then eluted using DNase and RNase free H₂O and checked for the presence of insert DNA by restriction digests and gel electrophoresis.

2.4.5 TRANSFORMATION AND ELECTROPORATION INTO EXPRESSION HOSTS

E. coli

Transformation into expression hosts such as BL21 (DE3), TOP10 or LMG194 were performed as previously described for DH5α cells.

M. tuberculosis

Competent cells of *M. tuberculosis* were generated using *Mtb* H37Rv grown in 7H9 medium supplemented with 10% (v/v) ADC and 0.05% (w/v) tween 80, bacteria were harvested at OD 1.2 and washed by centrifugation (at 2000xg for 20 minutes at 20°C) in 10% glycerol, this was performed three times. Cells were then resuspended in 3ml of 10% glycerol. For electroporation, 2mm cuvettes (Eppendorf, UK) were used with 400µl aliquots of cells mixed well with 3µl of DNA (5-10µg for non-replicating plasmids and 1µg for replicating plasmids) before being transformed at 1000Ω and 2500V. Electroporated cells were removed in a total

volume of 3ml medium for overnight shaking incubation at 37°C. These cells were then plated onto 7H10 in the following dilutions: undiluted, 10^{-1} and 10^{-2} . Using wild type H37Rv *Mtb* cells which contained no additional DNA a negative control was also grown and plated on both types of plates and kept at 37°C.

M. smegmatis

A similar protocol to the *Mtb* method above was followed for *M. smegmatis* cells, with the following differences: cells were kept on ice for 1.5 hours (all centrifugation steps were performed at 4°C), 7H9 medium was used without the addition of ADC, 100µl aliquots of cells were used for electroporation with 3µl of 1µg DNA of each construct and incubation at 37°C was carried out for 3 hours before plating onto 7H10 plates containing an appropriate antibiotic.

2.5 PROTEIN EXPRESSION AND IMMUNOLOGICAL DETECTION

2.5.1 SDS-PAGE

E. coli samples were prepared as described (Chapter 3). Positive and negative controls were used on each gel and several candidate clones were analysed. A 12% separating polyacrylamide gel was made and a loading gel was stacked on top, as described in Table 3.

TABLE 3: POLYACRYLAMIDE GEL COMPONENTS

Component	Loading Gel	Lower Gel (12%)
Acrylamide 30% (v/v)	1.98ml	6.0ml
0.5M Tris HCl pH 6.8	3.78ml	N/A
1.5M Tris HCl pH 8.8	N/A	3.75ml
10% (w/v) SDS	150µl	150µl
TEMED	15µl	7.5 µl
10% (w/v) APS	75µl	75 µl
dH₂O	9ml	5.0ml

The above components were placed, prior to solidification, into gel casting implements with a comb inserted into the loading gel to create sample wells. Once set gels were placed into an

electrophoresis tank, filled with 1x SDS running buffer. 4x SDS sample loading buffer was added to protein samples to give a 1x final concentration. Samples were heated to 90-95°C for 10 minutes in order to denature proteins before brief centrifugation, up to 25µl of the final solution was added to each well. Gels were run at 180V for up to 2 hours. If staining, gels were placed in fixing solution (50% MeOH and 10% acetic acid) for 1 hour prior to placing gels into Coomassie blue stain (0.1% Coomassie Brilliant Blue R or G, 50% MeOH and 10% acetic acid) for 1 hour, gels were then destained (40% MeOH and 10% acetic acid) and proteins visualised. Gels could alternatively be used for Western blotting.

2.5.2 WESTERN BLOT

Prior to loading the SDS-PAGE gel, Precision Plus Protein™ (Bio-Rad, Hertfordshire) standards were used if the resulting gel needed to be used for Western blotting. Within a semi-dry blotter (Cleaver Scientific Ltd) an SDS-PAGE gel was placed onto a Nitrocellulose membrane, which had been placed onto a small stack of Whatman Ltd paper soaked in transfer buffer. Once assembled this construct was topped with further wet Whatman Ltd paper and the lid secured. Transfer was then performed at 20V for 1 hour. The equipment was disassembled and the membrane placed in 5% (w/v) milk solution for 15 minutes to block unspecific binding.

The membrane was briefly washed in TBS before being placed in 2% (w/v) milk containing primary antibody. This was carried out using monoclonal anti-polyHis antibodies (Sigma) raised in mouse (1:3,000 dilution) or anti-Rpf antibodies raised in sheep (1:1000 dilution) (as previously described (Mukamolova et al., 2002b)). The membrane was incubated in primary antibody for an hour and a half, at room temperature with constant agitation before being washed 3 times in TBST. Secondary antibody; anti-mouse or anti-rabbit IgG alkaline phosphatase (1:10,000 dilution) in 2% (w/v) milk

solution was added and incubated for 30 minutes before repeating the washing stage. BCIP/NBT substrate dissolved in 10ml H₂O was poured over the membrane until the band of interest could be observed clearly. The reaction was then terminated by rinsing in dH₂O.

CHAPTER 3:
GENERATION OF GLYCOLYLATED PEPTIDOGLYCAN IN *E.*
COLI

3.1 INTRODUCTION

This chapter describes attempts to generate glycolylated peptidoglycan (PG) in *E. coli*. The aim of this part of the project was to investigate (1) feasibility of generating of model mycobacterial PG in *E. coli* by over-expressing NamH, an enzyme responsible for glycolylation of muramic acid within *Mtb* and (2) the importance of this modification for activity of muralytic enzymes, in particular *Mtb* RpfB.

3.1.1 TECHNIQUES USED FOR ISOLATION AND ANALYSIS OF PG

3.1.1.1 PURIFICATION OF PEPTIDOGLYCAN

Purification of PG from *E. coli* cells can be carried out using several well-established protocols (Glauner, 1988, Vollmer and Bertsche, 2008). Purified PG is digested with muralytic enzymes (such as lysozyme or mutanolysin) to generate PG fragments called muropeptides. Muropeptides are separated by reverse-phase high pressure liquid chromatography (rp-HPLC) and their molecular weight and composition are analysed by mass spectrometry (MS). These methods were originally developed for *E. coli* PG and later adapted for isolation and analysis of muropeptides from other bacteria.

The standard procedure for purification includes boiling cells in the presence of SDS to prevent activation of muralytic enzymes and to remove proteins. Harvested PG sacculi are washed to remove SDS and treated with amylase and pronase to eliminate contamination with glycogen and lipoproteins. In Gram-positive bacteria such as *Bacillus subtilis* or *Staphylococcus aureus* PG is treated with hydrofluoric acid to remove teichoic acids (Endl et al., 1984).

Mycobacterial PG purification is more complicated, time consuming and requires a greater biomass to yield pure PG in the amounts sufficient to generate and analyse muropeptides. The structurally complex mycobacterial cell wall is the major cause of this and in order to purify mycobacterial PG mycolyl-arabinogalactan, which is covalently attached to the PG, must be removed. Initial steps include purification of mAGP; cells are lysed by sonication or French press before proteolytic digestion and mAGP is extracted with ethanol diethyl ether (Petit et al., 1969, Mahapatra et al., 2008). In addition to this method, removal of mycolic acids by saponification under reflux, which breaks the ester bonds has been shown to result in mycolic acid release (Toubiana et al., 1979, Parish and Stoker, 1998). AG removal is carried out by incubation in sulphuric acid and insoluble PG harvested by centrifugation (Mahapatra et al., 2008).

3.1.1.2 GENERATION OF MUROPEPTIDES

Mutanolysin is a commonly used N-acetylmuramidase, cleaving the β 1-4 glycosidic PG bonds and releasing muropeptide products. The purified enzyme is available from Sigma-Aldrich and it generates a mixture of muropeptides which can then be separated by HPLC. Other muramidases commonly used for PG cleavage include cellosyl (very similar to mutanolysin); a class of muramidase which is able to hydrolyse O-acetylated and N-deacetylated PG, and a muramidase isolated from *Chalaropsis* (Gally et al., 1991, Vollmer et al., 2008). Other classes of enzymes capable of cleaving within bacterial PG are: endopeptidases which cleave bonds within the peptide stems (e.g. DD-, LD-, and DL-Endopeptidases), Carboxypeptidases (also DD-, LD- and DL-Carboxypeptidases) which hydrolyse peptide bonds to remove C-terminal D- or L-amino acids and N-acetylmuramyl-L-ala amidase which hydrolyses the peptide bond between the lactyl group of NAM and L-ala (Vollmer et al., 2008). Examples are depicted in Figure 13.

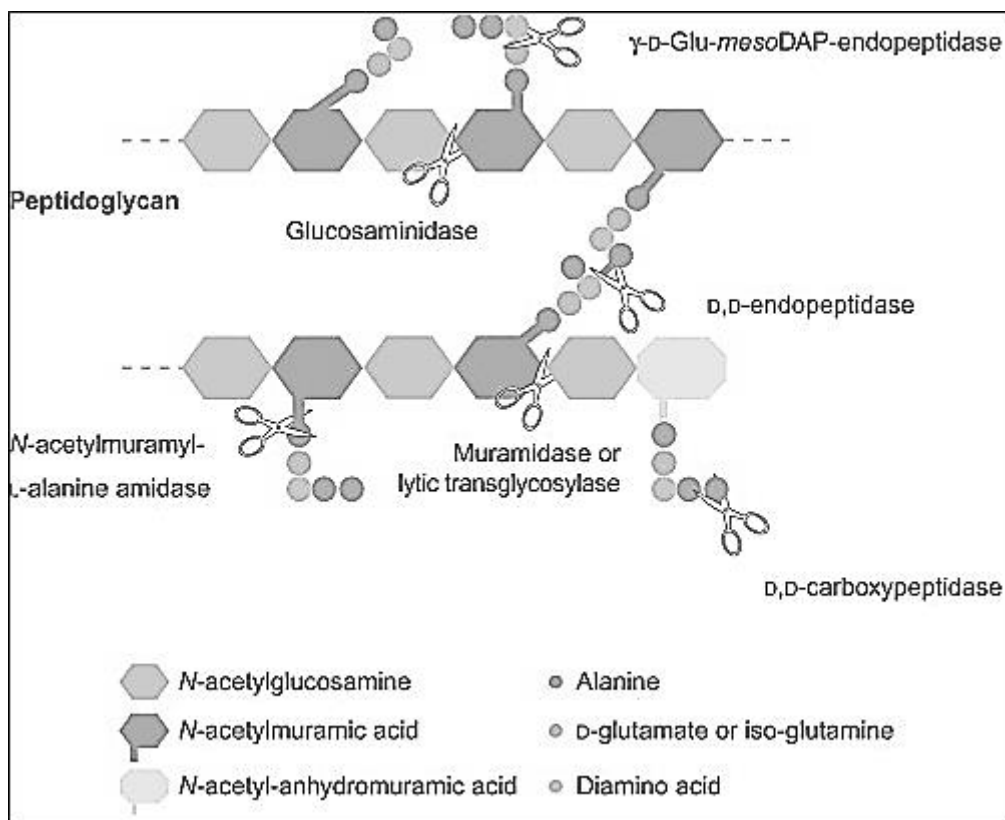


FIGURE 13: A SCHEMATIC SHOWING PEPTIDOGLYCAN HYDROLASES

The schematic was adapted from previously published work (Boneca, 2005). The scissors shown indicate the bond being hydrolysed.

3.1.1.3 ANALYSIS OF MUROPEPTIDES

3.1.1.1.1 BY RP-HPLC

The original method of muropeptide detection was paper chromatography which permitted identification of disaccharide and larger complexes but did not allow analysis of their composition (Olijhoek et al., 1982). Determination of amino sugars was originally carried out by acid hydrolysis and analysis using an amino acid analyser (Krulwich et al., 1967). HPLC is a well-established method of muropeptide separation and combination with mass spectrometry (MS) has resulted in the vast increase in the knowledge of PG structures. A recent publication demonstrated the ability of using fluorescently labelled muropeptides to analyse PG by gel electrophoresis (Young, 1996). This group argues that

HPLC is technically demanding and aimed to produce a rapid and equally effective method of analysing PG structure, however HPLC is still the core method used today.

Rp-HPLC is a powerful analytical technique used for the separation and purification of various compounds. It is based on the principle of binding the material in question to a specific packing material within the column (the solid phase) and gradually eluting these compounds, based on their binding ability to the column, by an increasing gradient (mobile phase). These compounds are then detected by a UV detector and the resulting chromatograms displayed. Choosing the correct column, buffers and protocol allows you to manipulate how these products are eluted.

HPLC is limited by how the flow rate within the system and column efficiency influence one another (Swartz, 2005). In most systems a faster flow rate will reduce column efficiency and a balance must therefore be found. This relationship can be graphically displayed, and is referred to as a so-called 'Van Deemter plot' (a schematic of which is shown in Figure 14), allowing optimisation of chromatography (Horvath et al., 1967). There are a variety of HPLC methodologies, using various buffer systems and columns; in this chapter a gradient based system has been described. This uses a linear gradient of an increasing organic based buffer, thus maximising the elution potential (Kaliszan et al., 2004).

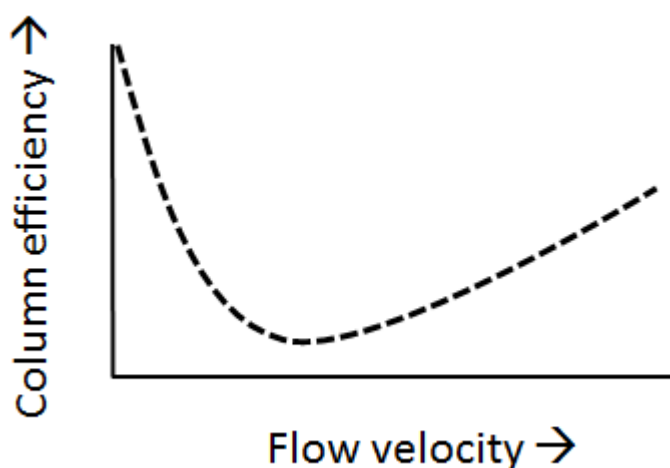


FIGURE 14: A SCHEMATIC ‘VAN DEEMTER PLOT’

Depicting how flow rate and column efficiency are related (Horvath et al., 1967).

C18 columns, as suggested by the name, contain silica particles attached to 18 Carbon molecules which will bind (based on hydrophobic/polar interactions) with a variety of compounds, in this instance mucopeptides. Two C18 columns were used for the HPLC analysis in this chapter; Hypersil ODS and Prontosil 120-3-C18, both have the same dimensions and pore size but differ in their particle size. The most commonly used particle size; 5 μ m belongs to the ODS column used here, whereas the Prontosil column has a slightly smaller size of 3 μ m. Particle size is important, influencing separation of peaks by increasing the surface area, however, this results in higher back pressure. Essentially the pressure required to maximise the velocity (or flow rate) is inversely proportional to the square of the particle size (Yoshida and Majors, 2006).

Muralytic digestion of PG and separation of mucopeptides by HPLC is the conventional method to study PG composition and structure. In experiments described in this chapter C18 columns were used for binding and separating mucopeptides based on their hydrophobicity. Mucopeptides are eluted using an organic based solvent system; weaker hydrophobic interactions lead to faster

elution and hence elution patterns can be predicted to a certain extent.

3.1.1.1.2 MASS SPECTROMETRY

Mass spectrometry (MS), an important analytical technique, determines the mass to charge ratio of a variety of species; here used to determine the mass of muropeptide fragments from *E. coli*. Matrix-assisted laser desorption/ionisation time of flight (MALDI-ToF) causes desorption of samples by a UV laser, which generates a variety of species that can then be ionized and eventually detected (as depicted in Figure 15). MALDI-ToF requires a matrix in order for samples to 'fly' within the machine, therefore there are visible peaks found in the resulting spectra belonging to this matrix. These peaks are easily distinguished from sample peaks by running 'blank' matrix controls and determining the masses of the species generated in the spectrometer and then excluding these results from further analysis. LCMS meanwhile, combines HPLC for separation with mass analysis by mass spectrometry.

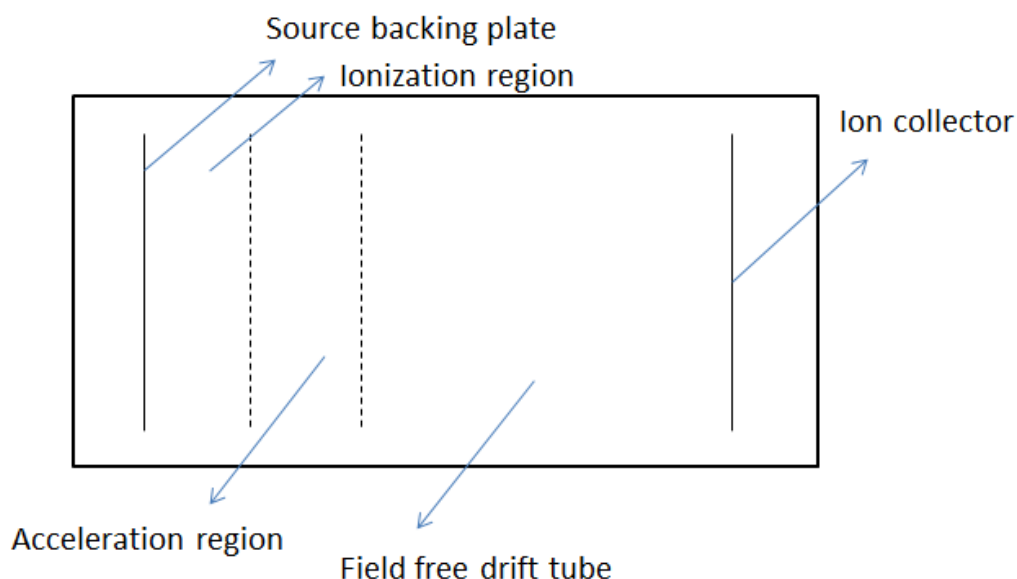


FIGURE 15: A SCHEMATIC SHOWING MALDI-TOF GEOMETRY

Adaptation of a MALDI-ToF schematic (W. C. Wiley, 1955), demonstrating the different components of a MALDI machine.

3.1.1.1.2.1 PERMETHYLATION

Permethylation, as previously described (Ciucanu, 1984), uses NaOH and methyl-iodide to drive the reaction. Permethylation results in addition of a methyl group through the formation of a methyl ester and is a base catalysed reaction. Therefore the choice of base is important; however this is limited by the solvent. DMSO is a suitable solvent in this case as most polysaccharides are highly soluble in it, it is readily commercially available and is water-free (Price, 2008). NaOH has poor solubility in DMSO so a suspension has to be made; this can lead to under methylation. A different method, in order to overcome this problem is to use sodium hydride, however this must be stored under oil and is quite difficult to handle (Price, 2008).

3.1.2 NAMH AND RPFS

Rpfs, as discussed in Chapter 1, are muralytic enzymes; capable of cleaving mycobacterial PG and, resuscitating dormant bacteria,

the precise mechanism of which is not fully understood. Rpf's are annotated as lytic transglycosylases, which cleave bacterial PG resulting in formation of a 1,6-anhydro ring at NAM residues; these have been purified and identified by rp-HPLC and Mass spectrometry. In order to identify Rpf muropeptide products, a model system using *E. coli* cells was implemented. Glycolylation of the muramic acid residues is a modification found in all mycobacterial species (excluding *M. leprae* as it contains a pseudo *namH* gene, (Mahapatra et al., 2008); the proximity of this modification and that of the *Mtb* Rpf predicted binding and cleavage site led to the hypothesis that *Mtb* Rpf's may be adapted to, and more efficient at cleaving glycolylated PG.

Therefore in order to investigate the muropeptides released from PG by Rpf the following was undertaken: (1) generation of glycolylated PG within *E. coli*; this was implemented as a means of overcoming the need to purify the waxy, hydrophobic and notoriously difficult to purify mycobacterial PG. In order to achieve this *Mtb*'s *namH* gene was amplified and expressed in *E. coli*. (2) Purification of mycobacterial PG and analysis of Rpf released muropeptides.

3.1.3 AIMS

To develop a method of reliably producing and analysing glycolylated PG, in order to examine recombinant *Mtb* Rpf products the following was undertaken:

- Generation of NamH overexpressing strains in *E. coli*
- Optimisation of PG purification methodology
- Separation and identification of muropeptide products
- Analysis of muropeptides released from modified and wild type *E. coli* PG by recombinant *Mtb* RpfB

3.2 MATERIALS AND METHODS

3.2.1 ORGANISMS USED IN THIS CHAPTER

All *E. coli* strains were grown in LB medium containing the appropriate antibiotic and inducer unless otherwise stated. *M. smegmatis* was grown in Sauton's medium. All medium was prepared as previously described in chapter 2.

3.2.2 BACTERIAL STRAINS

TABLE 4: BACTERIAL STRAINS USED IN THIS CHAPTER

Strain	<i>E. coli</i> Host	Plasmid/Inducer	Source
BL21(DE3)	BL21 (DE3)	N/A	Laboratory stock (Bioline)
BL21(DE3) pET15b	BL21 (DE3)	pET15b/IPTG	This study
BL21(DE3) pET15b-<i>namH</i>	BL21 (DE3)	pET15b/IPTG	This study
BL21(DE3) pETM-11-RpfB_{ΔDUF}	BL21 (DE3)	pETM-11/IPTG	Provided by Prof Mike Young (Aberystwyth)
TOP10 pBAD_{HisA}	TOP10	pBAD/arabinose	This study
TOP10 pBAD_{HisA}-<i>namH</i>	TOP10	pBAD/arabinose	
LMG 194 pBAD_{HisA}	LMG 194	pBAD/arabinose	This study
LMG 194 pBAD_{HisA} -<i>namH</i>	LMG 194	pBAD/arabinose	This study

3.2.3 GENERATION OF OVEREXPRESSING STRAINS

All plasmids for the over-expression of *namH* were generated following the procedures outlined in Chapter 2. The inserts were sequenced by GATC. Once confirmed, these plasmids were transformed into protein expression strains BL21, TOP10 or LMG194 (shown in Table 4). Plasmids were maintained using

50µg/ml ampicillin. The primers shown in Table 5 were used for the generation of NamH expressing constructs. pBAD, TOP10 and LMG194 were purchased from Invitrogen (UK).

TABLE 5: CONSTRUCTS AND THEIR CORRESPONDING PRIMER PAIRS

Construct	Amplicon size (bp)	Primer
pET15b-<i>namH</i>	1,551	F: 5'cgaaag <u>CTCGAG</u> gtgcaggtcacaagcgttggt R: 5'cgtaga <u>GGATCC</u> catggccgtgaactgcgtag
pBAD_{HisA}-<i>namH</i>	1,562	F: 5'cag <u>GCTAGC</u> gaaaggtagctgtg R: 5'cta <u>GTCGAC</u> catggccgtgaac
pET15b-3818-3819	1,883	pET15b- <i>namH</i> forward primer R:5'cact <u>GGATCC</u> tcacgttcggtggagggcgca

Introduced restriction sites are shown in italic capitals.

3.2.4 EXPRESSION CONDITIONS

All *E. coli* pre-cultures used to seed subsequent cultures for expression were in a final volume of 5ml LB. 50µl of stationary phase culture was used to seed subsequent 10ml LB cultures. Strains carrying the pET15b plasmid were maintained by adding 50µg/ml ampicillin and were induced by adding 1mM IPTG (unless otherwise stated) which in turn directs T7 RNA polymerase gene expression and hence the gene of interest (Novagen, 2003b). Strains bearing the pBAD plasmid were maintained using 50µg/ml ampicillin and were induced by adding 0.02% (w/v) arabinose (unless otherwise stated). All cultures were grown at 37°C with continuous shaking at 200rpm. All growth curves were generated by taking 1ml samples and analysed spectrophotometrically at 600nm, samples with an OD of 0.8 and above were diluted in fresh medium before measurements.

3.2.5 CONFIRMATION OF PROTEIN EXPRESSION

Sodium dodecyl sulphate polyacrylamide gel electrophoresis (SDS-PAGE) was carried out using a 12% polyacrylamide gel (as previously described in Chapter 2), before being transferred to a nitrocellulose membrane for Western blot analysis using anti-polyHis antibodies (Chapter 2). 1ml samples were obtained from pre- and post-induction time points. Bacteria were collected by centrifugation in a microcentrifuge at 12,000g, resuspended in 50µl dH₂O and heated at 90°C for 15 minutes. After re-centrifugation the supernatants were removed to a new 1.5ml eppendorf tube and 10µl of 6x sample buffer was added; 12µl samples were then loaded onto the polyacrylamide gel for analysis. In the case of pETM-11-RpfB_{ΔDUF} expression samples were taken from cultures induced overnight at 15°C with 200rpm shaking.

3.2.5.1 SEPARATING THE SOLUBLE AND INSOLUBLE PROTEIN FRACTIONS

To separate the soluble fraction, 1ml of sample was taken, centrifuged at 12,000g for 5 minutes and the resulting pellets resuspended in 100µl of the following buffer: 20mM Tris HCl, pH 7.9; 50mM NaCl; 1xBugBuster (Novagen®) and incubated at room temperature for 5 minutes. Glass beads were added and samples vortexed for 20 seconds. Centrifugation was repeated for 15 minutes. Supernatants were transferred to a fresh tube and 35µl of 4x sample buffer was added. Insoluble fractions were prepared by using the pellets remaining after soluble protein isolation and resuspending in 100µl of the following buffer: 20mM Tris HCl, pH 7.9; 50mM NaCl; 8M urea. After incubation for 5 minutes, sample buffer was added as described above.

3.2.1 PURIFICATION OF RECOMBINANT *MTB* RPF B BY AFFINITY CHROMATOGRAPHY

2L flasks, each containing 500ml LB media, were inoculated with 5ml of pETM-11-RpfB BL21 and cultures were grown until OD_{600nm}= 0.4-0.7 with 200rpm shaking before induction with 1mM IPTG was

carried out. This was incubated at 15°C with 150rpm shaking for 16-18hrs. Bacteria were collected using a Beckman centrifuge (4000g, 30 minutes at 4°C) and the pellets were resuspended in buffer containing 30mM Tris HCl pH 7.2 and kept on ice while 30 cycles of sonication (30 seconds on followed by 30 seconds off) were carried out. The cell lysate was then centrifuged for 30 minutes at 50,000g and 4°C, the supernatant collected and kept on ice.

A sepharose column was prepared by adding 10ml of buffer containing 40mM NiSO₄ and 20mM Tris HCl; 150mM NaCl pH 7 to charge the column and prevent contamination. This was then washed in 20ml of buffer containing 20mM Tris HCl; 150mM NaCl pH 7 and any excess removed before adding the supernatant and allowing it to flow through and bind to the column. The column was not allowed to run dry at any point. Any unbound contaminants were removed by washing, first in 20ml of washing buffer containing 20mM Tris HCl; 150mM NaCl pH 7 and then using 50ml of the same washing buffer containing 60mM imidazole. To elute the bound protein, 500mM imidazole (in 20mM Tris HCl; 150mM NaCl buffer) was added 1ml at a time and each elution collected in 1.5ml eppendorfs. The protein concentration was then determined using a Nanodrop™ 1000 at Abs_{280nm} so that the concentration of protein could be calculated using Equation 2.

EQUATION 2: $A = E.C.L$

A= Absorbance, e= extinction coefficient*, c= concentration and l= path length. * Where e was calculated to be 40575M⁻¹ cm⁻¹ (determined using ExPASy software (Gasteiger et al., 2003).

The elution fractions containing the greatest amounts of protein were combined and added to a dialysis tube and placed in 2L dialysis buffer (25mM Tris HCl; 500mM NaCl; 20% glycerol pH 8.5) with gentle stirring for approximately 16hrs. All purification work

was carried out in a cold room. After 16hrs the RpfB protein concentration was re-measured and any protein not needed immediately was stored at -80°C. If there was a large volume then protein concentration was performed using Vivaspin 20 centrifugal concentrator (Sigma-Aldrich).

3.2.2 ZYMOGRAPHY

Activity of purified recombinant RpfB was assayed using zymography. Zymography uses lyophilised bacterial cells as a substrate, this is incorporated into a protein gel and activity of muralytic enzymes can be assessed by clearance bands within the gel. By running a normal SDS-PAGE with the addition of dried *M. luteus* cells at 0.2% (w/v) as a substrate, RpfB samples reduced with 5mM DTT were loaded into all wells. Electrophoresis at 180V for up to 2 hours was carried out and the gel cut into strips containing the protein, each strip was placed into 20ml of one of the following buffers containing 2% (w/v) Triton X100:

25mM Sodium phosphate pH 6, 6.5, 7 and 7.5

25mM Sodium citrate pH 4.5, 5 and 5.5

25mM Tris HCl pH 7, 7.5, 8 and 8.5

These strips were placed at 37°C overnight to re-nature the protein. After being incubated overnight the gels were stained in 0.1% (w/v) methylene blue in 0.01% (w/v) potassium hydroxide and placed on a shaker for 2 hours before being washed repeatedly in H₂O.

3.2.3 MICROSCOPE SETTINGS AND IMAGE ANALYSIS

A Nikon Diaphot 200 inverted microscope with 100w high pressure mercury vapour lamp was used for all images. Images were taken with a high speed Peltier-cooled Retiga Exi Fast 1394 camera (QImaging, Surrey, BC).

The software used was: InVivo v3.2.2 build 48 (Media Cybernetics, U.S.A) and ImageJ v1.4q (Staal et al., 2004) was used for image analysis. All images were stored as 12 bit tagged image files (tif) for further analysis.

3.2.1 LYSOZYME SENSITIVITY

Lysozyme sensitivity assays were carried out in triplicate over 24 hour periods, following a previously published method (Masschalck et al., 2001). Samples were washed in buffer comprising 30mM Tris HCl; pH 8, 1.3mM EDTA and adjusted to the same OD before adding 100µg/ml lysozyme and incubating for 2 hours at 37°C, after 2 hours the optical density was measured. CFU plates were prepared at several time points (as previously described; chapter 2).

3.2.2 PG PURIFICATION

A variety of PG purification methods are described below; method 1 has been adapted from a classical purification method (method 2) in order to maximise protein induction. The 3rd method is specific to the purification of mycobacterial PG.

3.2.2.1 METHOD 1

This method is based on previously published work (Glauner, 1988). 500ml culture volumes of LB media (Chapter 2) containing a final 50µg/ml ampicillin were inoculated with 5ml of overnight pre-culture. These were then grown at 37°C, 200rpm till the OD_{600nm} reached 0.4-0.7, IPTG was then added to a final concentration of 1mM. Induced cultures were grown till the OD_{600nm} reached 1.5-2. Cells were collected at 4000g in 400ml centrifuge tubes in a Beckman Coulter Avanti® J-E centrifuge using a F10 rotor for 30

minutes at 4°C. Pellets were resuspended and washed in milliQ H₂O before collection by centrifugation (as above), resulting pellets were resuspended in 20mM sodium acetate (pH 5) and added dropwise to boiling 4% (w/v) SDS for 30 minutes with mixing. Bacteria were collected and washed 3 times in milliQ H₂O, at 50,000g using a JA-25.50 Rotor for 30 minutes at 15°C in 50ml tubes.

The lysate was then resuspended in buffer comprising 100mM Tris HCl; 10mM NaCl pH 7.5 and 10µg/ml DNase I added before incubating overnight at 37°C. The samples were then washed twice and collected at 50,000g (as described above) and the remaining pellets resuspended in buffer containing 100mM Tris HCl; 10mM NaCl pH 7.5 and 50µg/ml proteinase K added to remove any protein associated with the PG, this was incubated overnight at 37°C. The remaining SDS-insoluble material was then extracted in 1% (w/v) boiling SDS for 30 minutes. The material was collected and washed 3 times at 50,000g (as described above) and the resulting PG was resuspended in minimal milliQ H₂O and lyophilised, this was then stored at -80°C.

3.2.2.2 METHOD 2

(Glauner, 1988) published a PG purification method which the following protocol is based on. Bacteria were inoculated as above and grown in 400ml LB media (Chapter 2) without antibiotics at 37°C and 200rpm till the OD_{600nm} was between 0.4-0.8. IPTG or arabinose induction was carried out when the OD_{600nm} = 0.2. Cells were then cooled on ice for up to 10 minutes. The cells were harvested by centrifugation at 4000g in Beckman Coulter centrifuge using an F10 rotor at 4°C. Using a glass pipette pellets were carefully resuspended in 6ml of ice-cold H₂O and added dropwise to 6ml of boiling 8% (w/v) SDS, with constant stirring for 30 minutes. When samples reached room temperature the sacculi of

both strains were collected by ultracentrifugation (using a TLA-100.3 rotor and bench top ultracentrifuge) for 1 hour at 90,000 rpm in 3ml Beckman tubes. Supernatants were carefully discarded and pellets resuspended in 60°C MilliQ H₂O and ultracentrifuged (as above), between 8 and 10 washes were performed and the Hayashi test carried out to determine whether samples were free from SDS.

After removal of SDS samples were resuspended in 900µl of buffer containing 100mM Tris HCl; 10mM NaCl pH 7 in a 2ml microfuge tube and 100µl 3.2M imidazole pH 7 added. 15µl of 10mg/ml α-amylase was then added to degrade high molecular weight glycogen within the sacculi. Samples were incubated for 2 hours at 37°C. 20µl of pre-incubated (at 60°C for 2 hours) 10mg/ml Pronase E was added for 1 hour at 60°C to release covalently bound lipoproteins.

1ml of 4% (w/v) SDS was added to the samples and these were heated at 100°C for 15 minutes. Samples were centrifuged and washed as before, up to 6 times and checked via the Hayashi test. Samples were resuspended in 400µl of 0.02% NaN₃ and stored at 4°C. Any stages which required overnight storage had 0.02% NaN₃ added and before continuing the samples were heated at 42°C in a water bath for 20 minutes.

3.2.2.2.1 HAYASHI TEST

In a 1.5ml eppendorf tube the following reagents were added:

335µl murein sample
7µl 0.5% methylene blue
170µl NaPO₄ pH 7.2
1ml Chloroform

Samples were mixed for 20 seconds on a vortex and brief centrifugation applied in order for phase separation to occur. The appearance of a blue colour in the chloroform layer indicated the presence of SDS, however clear or slightly pink colours indicated clearance of SDS (Hayashi, 1975).

3.2.2.3 MYCOBACTERIAL PG PURIFICATION

PG was isolated from *M. smegmatis* based on previously published methods (Mahapatra et al., 2008, Parish and Stoker, 1998, Toubiana et al., 1979). Mycobacteria were grown in Sauton's media and collected by centrifugation before resuspension in 10mM NH_4HCO_3 followed by 30 cycles of sonication (comprising 60 seconds on and 60 seconds off) before digestion with 10 μg of DNaseI at 37°C overnight. The pellet containing cell wall was then collected by centrifugation at 50,000g for 30 min 4°C, this was then resuspended in 100mM Tris 10mM NaCl; pH 7.5 buffer and added dropwise to boiling 4% (w/v) SDS before being collected and washed as described above and incubated with proteinase K (also as above) overnight at 37°C. This process was then repeated with 1% (w/v) SDS before the resulting pellet was extracted with ethanol-diethyl ether (1:1) and dried under a vacuum.

Reflux was carried out to saponify the ester linkage between mycolic acids and arabinogalactan; a 1:1 ratio of toluene:methanol (MeOH) with 2% (w/v) KOH in a final volume of 30ml with the mAGPc from *M. smegmatis* was heated at 65°C for 48 hours with constant stirring. Once cooled to room temperature the precipitating AGPc was collected by centrifugation and washed in MeOH. The pellet was then washed in MeOH twice and diethyl ether before being vacuum dried. The AG-PG was digested with 0.05N H_2SO_4 at 37°C for five days. The remaining insoluble PG was then washed four times by centrifugation and dried under vacuum.

3.2.3 MUROPEPTIDE ANALYSIS

3.2.3.1 MUROPEPTIDE SAMPLE PREPARATION

Isolated PG was resuspended in 100 μl buffer containing 80mM NaPO_4 pH 4.8 and 20 μl of 0.5 $\mu\text{g}/\text{ml}$ mutanolysin or cellosyl,

samples were incubated overnight at 37°C with 200rpm shaking. Lysozyme digestion took place in buffer comprising 25mM NaPO₄; pH 6 at 100µg/ml, 37°C overnight. RpfB digestion was performed using 100µg/ml in 40mM citric acid; pH 6.5. Samples were then boiled for 10 minutes on a dry block and centrifuged at 12,000g using a microcentrifuge. 100µl of 0.5M sodium borate (pH 9) solution was added prior to addition of solid sodium borohydrate for the reduction of muropeptide products. Samples were incubated for 30 minutes at room temperature with centrifugation at 2000g to prevent spillage. The reaction was then terminated by the addition of 20% phosphoric acid and adjusted to pH 4.0 (or between pH 3.5 and 4.5). Prior to loading of samples onto the HPLC column they were centrifuged briefly, if samples were not immediately needed they were stored at -20°C.

3.2.3.2 RP-HPLC PROTOCOL

Rp-HPLC work was carried out on an AKTA Purifier Preparative Liquid Chromatography System.

3.2.3.2.1 METHOD 1

Column: C₁₈ Genesis ODS hypersil
Column parameters:

Height: 25cm
Diameter: 0.46cm
Volume: 4.155ml
Particle size: 5µM

HPLC parameters:

Flow-Rate: 0.5ml/min
Pressure limit: 20MPa
Wavelengths: 205, 250, 280 (nm)
Elution fraction size: 1ml
Target concentration B: 100%
Length of gradient: 30 (CV)

Buffers:

Buffer A = 40mM NaH₂PO₄ pH 4.3 (and 0.1% NaN₃)
Buffer B = 40mM Na H₂PO₄; 15% MeOH pH 5.1

3.2.3.2.2 METHOD 2

Column: C₁₈ Prontosil 120-3-C18-AQ

Column parameters:

Height: 25cm
Diameter: 0.46cm
Volume: 4.155ml
Particle size: 3µM

HPLC parameters:

Flow-Rate: 0.5ml/min
Pressure limit: 20MPa
Wavelengths: 205, 250, 280 (nm)
Elution fraction size: 1ml
Target concentration B: 100%
Length of gradient: 18 (CV)

Buffers:

Buffer A = 50mM NaH₂PO₄ pH 4.31 (and 0.1% NaN₃)
Buffer B = 75mM Na H₂PO₄; 15% MeOH pH 4.95

3.2.3.3 AMMONIUM HYDROXIDE HYDROLYSIS

PG samples used for LCMS and MALDI-ToF analysis were first digested with mutanolysin (200µg/ml) and lysozyme (200µg/ml) (both obtained from Sigma-Aldrich, UK) at 37°C in 25mM Na₂PO₄; pH 6 buffer containing 0.1mM MgCl₂. Soluble mono- and disaccharides were collected by ultracentrifugation before being hydrolysed by NH₄OH. NH₄OH (30% v/v) was added (0.35µl added per µl of digested PG) and placed at 37°C for 5hrs before being put to -80°C and vacuum dried to neutralise. This method was based on work carried out by (Arbeloa et al., 2004).

3.2.3.4 LCMS

A 4000 QTRAP® LCMS/MS System was used for all LCMS work in this chapter; it is a Hybrid Triple Quadrupole/Linear Ion trap mass spectrometer. This system was used to analyse PG from different *E. coli* strains.

PG samples were dissolved in 100% methanol (MeOH) prior to analysis.

3.2.3.5 MALDI-ToF

The equipment used was a Voyager DE-STR MALDI-ToF Mass Spectrometer. A 96 well plate was used for sample spotting and the following matrices were used:

- α -cyano-4-hydroxycinnamic acid (α -cyano)
- dihydroxybenzoic acid (DHB)
- 5-chloro-2-mercaptobenzothiazole (CMBT)

All three were tested using commercially available monosaccharides found within PG and based on this data, as well as previously published work (Pfenninger et al., 1999) CMBT was selected for optimal visualisation of monosaccharides. A combination of solution constituents were tested including: ethanol (EtOH):H₂O, Chloroform:MeOH, MeOH:trifluoroacetic acid (TFA), MeOH:H₂O, acetonitrile (ACN):0.1% TFA, ACN:H₂O, EtOH and EtOH:H₂O:tetrahydrofuran (THF). Typically solutions of CMBT in EtOH:H₂O:THF were prepared at 10g/L concentrations.

Matrix to sample ratios were also tested using the matrices mentioned above and commercially available N-acetyl glucosamine (NAG) and N-glycolyl muramic acid (NAM) standards at 10 μ g/ml concentration. Matrix and samples were mixed in 5:1 ratio (matrix to sample) and 1 μ l of the mixture was spotted onto the plate. Several replicas per sample were prepared as were matrix controls for each spot. Isolated PG samples were hydrolysed by NH₄OH prior to spotting.

3.2.3.6 PERMETHYLATION

Permethylation was carried out as previously described (Ciucanu, 1984, Kang et al., 2005). For optimisation experiments 10µl of a 9mM NaOH suspension was added to 10µg NAG dissolved in 30µl DMSO. 5.6µl of methyl-iodide was then added and samples placed on a vortex for 20 minutes, samples were also taken every 5 minutes. 0.5ml of chloroform was added to samples and mixed well by vortexing, the aqueous phase was removed and the organic phase washed twice in water. Samples could then be concentrated by vacuum drying. This was then repeated using 5µl of hydrolysed PG samples from both *E. coli* strains. The reaction schematic is shown in Figure 16. Samples were then analysed by MALDI-ToF.

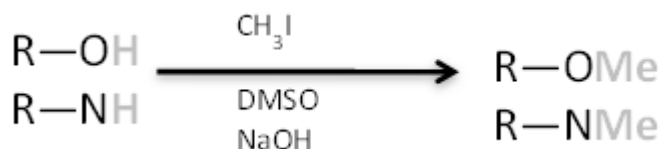


FIGURE 16: A SCHEMATIC FOR PERMETHYLATION OF CARBOHYDRATES

The permethylation reaction for the conversion of free amino and hydroxyl groups under CH₃I, DMSO and NaOH conditions is shown. Adapted from (Ciucanu, 1984)

3.3 RESULTS

The pET vector is a commercially available system for the cloning and expression of foreign proteins within *E. coli*. DH5 α is an ideal strain for initial cloning steps due to high efficiency of transformation. Once the clone had been generated a new host suited to protein expression, was required. BL21(DE3) is the main host adopted in this chapter, advantages of this were: the presence of *lacI* gene, *lacUV5* promoter and the gene for T7 RNA polymerase (Novagen, 2003b).

3.3.1 PET15B-*NAMH*; GROWTH CHARACTERISTICS AND PROTEIN EXPRESSION

The *E. coli* expression strains; pET15b BL21 and pET15b-*namH* BL21 were generated as described (Chapter 2). Briefly; pET15b-*namH* forward and reverse primers (Table 5) were used for the PCR amplification of *namH* (*rv3818*), 5 μ l of PCR product was analysed by gel electrophoresis and the remaining product purified using a commercially available QIAquick kit (Qiagen, UK); purified PCR product and pET15b plasmid were digested, ligated and transformed into DH5 α cells. The presence of the insert was confirmed by diagnostic colony PCR. Purified DNA was sent for sequencing before transformation into the BL21 expression host. Growth analysis was performed using a successful clone to assess toxicity.

The growth characteristics of both BL21 (DE3) pET15b and pET15b-*namH* were examined in LB media, 1mM IPTG was added to induce expression via T7 RNA polymerase. Previous work using *M. smegmatis namH* found overexpression of this protein to be toxic to *E. coli* (Raymond et al., 2005); *M. tuberculosis namH* was

used in an attempt to overcome toxicity issues. The growth phenotype of pET15b-*namH* BL21 was therefore analysed.

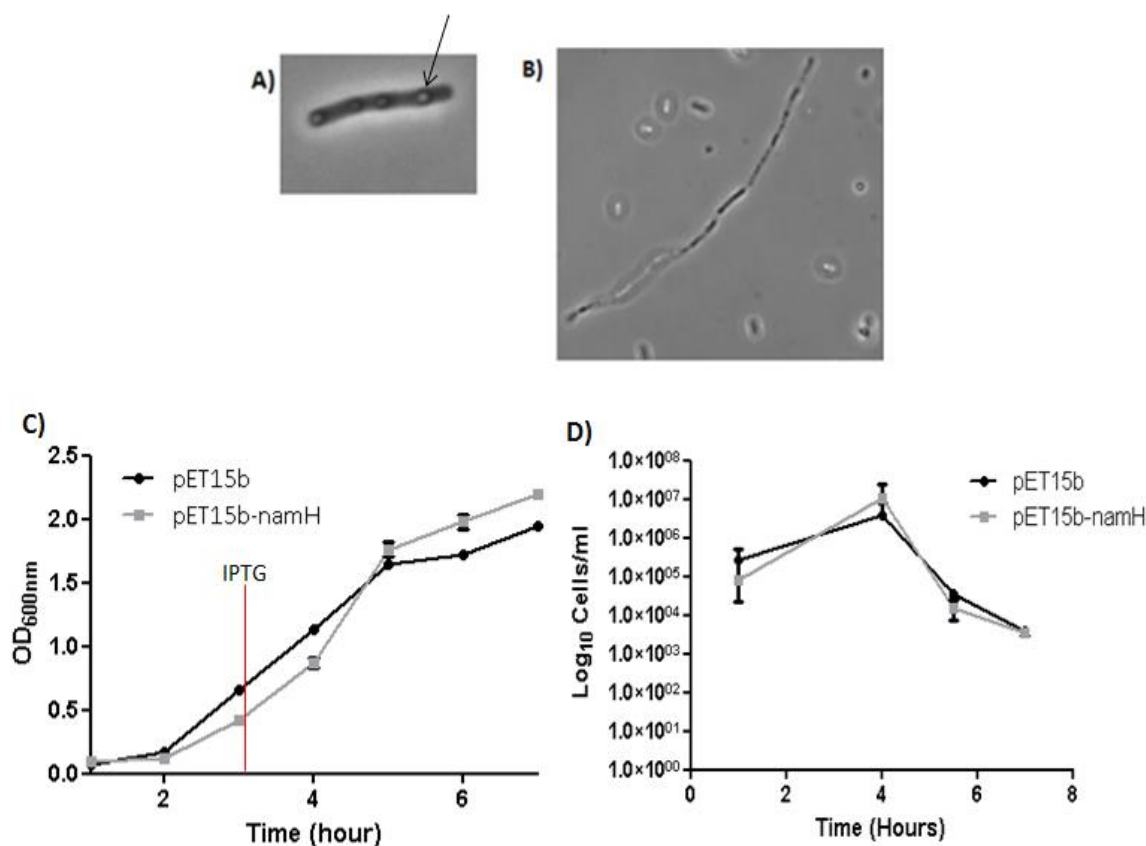


FIGURE 17: MICROSCOPY AND GROWTH ANALYSIS OF pET15b-NAMH AND pET15b

Figures A and B show microscope images of pET15b-*namH* BL21 1 hour post IPTG induction, a Nikon Diaphot 200 inverted microscope with 100w high pressure mercury vapour lamp was used for all images. Inclusion bodies are indicated by an arrow. C) Bacteria were cultured in LB medium as previously described (Chapter 2). 1mM IPTG was added as indicated by the red line in the above figure. OD measurements were prepared by taking 1ml samples and analysing spectrophotometrically at 600nm; samples were diluted once they reached OD 0.8. D) CFU counts were analysed in a separate experiment by serial dilution; the time shown indicates time after induction. The results shown are the average value of duplicate experiments. All error bars show standard deviation.

As shown in Figure 17, C *Mtb* NamH does not appear to be toxic to *E. coli*, OD values are initially consistent with, or slightly reduced compared to pET15b BL21 and once induced by IPTG cells

continue to replicate. Due to the increased energy cost to the cell for the overexpression of NamH, it would be expected that pET15b-*namH* BL21 cells, once induced, would have a reduced growth rate in comparison to the control strain. pET15b-*namH*, prior to and for a short period after induction, has a slightly reduced growth rate in comparison to pET15b BL21, however after 2 hours of IPTG induction this trend is no longer observed and pET15b-*namH* has a consistently greater OD than pET15b. The CFU counts (in D) reflect a similar trend in both pET15b and pET15b-*namH* BL21: there is a rapid increase during log phase which begins to decrease as the cells enter stationary phase, the rapid drop in CFU counts could reflect a loss of plasmid and hence a reduced bacterial survival on antibiotic containing plates. These data both indicate that *Mtb* NamH was not toxic to *E. coli*.

Bacteria were inspected under the microscope and pET15b-*namH* BL21 demonstrated long chains of bacilli (Figure 17, B), cells also had bubble-like shapes possibly indicative of inclusion bodies (Figure 17, A). Comparative pET15b BL21 cells did not demonstrate these chains of cells or bubble-like formations. The increase in turbidity represented by higher OD readings from post IPTG induction could therefore be a result of bacterial structures as this increase was not reflected in CFU counts (Figure 17, D).

pET15b-*namH* contains a 6xHistidine N-terminal tag, allowing detection of protein expression by Western blot using anti-polyHis antibodies (Sigma). Samples for protein expression experiments were taken at several time points in order to determine optimal expression conditions prior to large scale expression. Negative and positive controls were also included; the empty pET15b BL21 strain was used as a negative control and a pETM-11-RpfB $_{\Delta DUF}$ strain overexpressing a His-tagged RpfB $_{\Delta DUF}$ was used as a positive control. The optimal expression time for pET15b-*namH* BL21 was

found to be 2 hours, protein expression from this time point is shown in Figure 18.



FIGURE 18: WESTERN BLOT OF TOTAL CELL EXTRACTS DEVELOPED WITH ANTI-POLYHIS ANTIBODY.

From left to right: 1) BL21 (DE3) pET15b-*namH*, 2) protein marker, 3) RpfB Δ DUF (positive control) and 4) BL21 (DE3) pET15b. All crude cell extracts were prepared from cells grown in LB medium, at 37°C with 200rpm shaking, after 2 hours of 1mM IPTG induction. Samples were loaded onto a 12% polyacrylamide gel and once separated by electrophoresis proteins were transferred to a nitrocellulose membrane for Western blot analysis.

As can be observed in Figure 18, NamH expression was confirmed by Western blot. There is a band visible in lane 1 (pET15b-*namH* BL21) corresponding to slightly greater than 50 kDa but lower than the 75 kDa marker. The predicted size of NamH (including the His-tag) is 58.45 kDa. Therefore it can be concluded that: owing to the specificity of this technique, the lack of bands present within the negative control and the molecular weight of the main band detected, NamH is being expressed. The lower molecular weight band, produced by pET15b-*namH* BL21 (DE3) bacteria, is most likely a result of protein degradation.

Samples taken at later time points produced a more intense band of the lower molecular weight product which was indicative of a higher level of protein degradation. Earlier time points produced equally bright bands and a two hour induction was found to be the optimal expression condition (Figure 18). Two hour protein induction produced no further degradation products than shorter induction times and allowed detectable protein expression.

3.3.2 NAMH SOLUBILITY

Growth analysis and examination of pET15b-*namH* BL21 under the microscope indicated the presence of inclusion bodies, therefore after examining the expression of NamH in pET15b-*namH* BL21 crude cell extract by Western blot using anti-polyHis the expression level of soluble protein was investigated. This was done by separating the insoluble and soluble fractions from bacteria. Proteins were separated by SDS-PAGE and detected by Western blot using anti-polyHis antibodies. Attempts to increase the level of soluble protein expressed were undertaken. Samples were grown at a variety of temperatures (15°C-37°C), length of induction was varied (1 hour-overnight) and the concentration of inducer altered (0.05-1mM); the optimal expression obtained is shown in Figure 19.

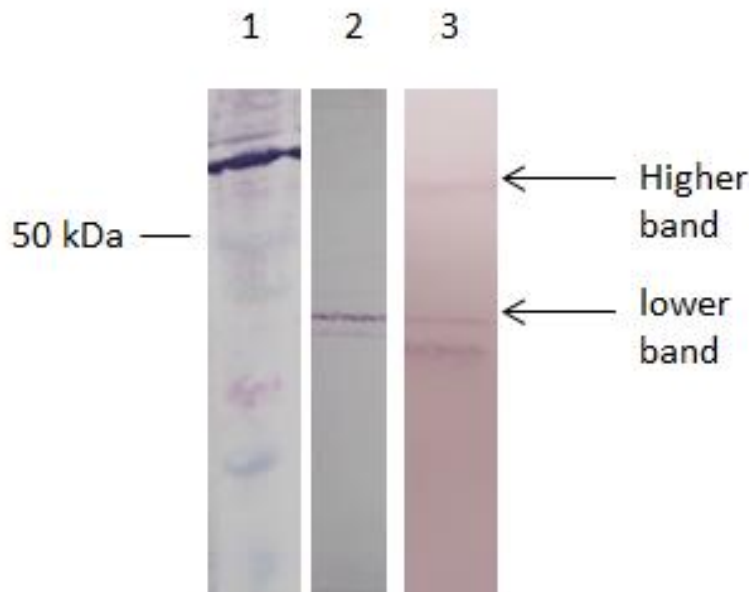


FIGURE 19: ANTI-POLYHIS WESTERN BLOT SHOWING SOLUBLE AND INSOLUBLE FRACTIONS OF IPTG INDUCED pET15b-*NAMH* BL21

The above figure shows the soluble fraction (lane 2) and the insoluble fraction (lane 3) of pET15b-*namH* BL21 cells grown in LB medium and induced with 1mM IPTG for 4 hours at 37°C. 1ml samples were taken from 10ml cultures for preparation of different fractions. A band at the expected mass of NamH is indicated and referred to as 'higher band', a lower molecular weight band; likely to be a degradation product is referred to as the 'lower band'.

Figure 19, which depicts the soluble and insoluble protein fractions expression levels of NamH in pET15b-*namH* BL21 cells after IPTG induction, suggests a much greater level of insoluble compared to soluble protein. Both soluble (lane 2) and insoluble protein fractions (lane 3) contain low molecular weight bands (indicated in the above figure) which are likely to be products of protein degradation. The lower molecular weight band present in pET15b-*namH* soluble fraction appears to be more intense than the full length protein (lane 2). Figure 19 indicates the greatest yield of soluble NamH based upon these experiments, and in order to overcome this low solubility issue a new construct was generated using the pBAD_{HisA} system. This system provides more stringent control

of expression and could potentially increase the level of soluble NamH.

pBAD-*namH* was generated using the corresponding primers (pBAD-*namH* F and R) shown in Table 5, once NamH had been amplified and examined by DNA gel electrophoresis the PCR product was purified and digested using NheI and Sall restriction enzymes. Commercially available pBAD_{HisA} was likewise digested and gel extracted, the resulting insert and linear plasmid were ligated and transformed into DH5 α , once successfully sequenced purified DNA was used to transform this construct into a TOP10 expression host. Growth analysis in LB medium was then carried out under various arabinose induction concentrations, 0.02% arabinose induction is shown in Figure 20.

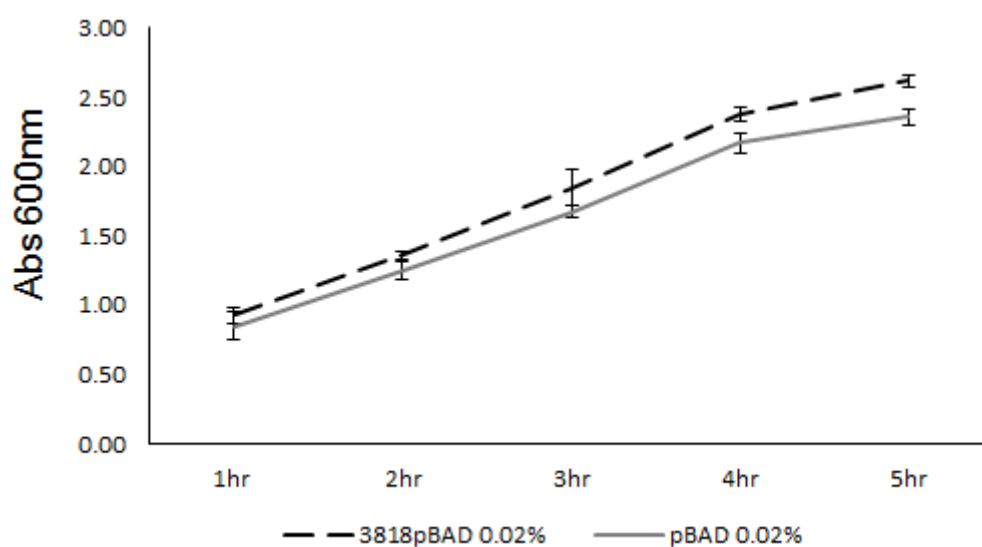


FIGURE 20: GROWTH ANALYSIS OF pBAD-NAMH TOP10 AFTER 0.02% ARABINOSE INDUCTION

Cultures were induced with 0.02% (w/v) arabinose. 1ml samples were taken at hourly intervals and analysed spectrophotometrically at 600nm. Samples were diluted once an OD of 0.8 or higher was reached. The results shown are the average of duplicate samples, error bars show standard deviation.

A very similar growth trend is observed for both pBAD-*namH* TOP10 and the corresponding pBAD control after arabinose induction. The overall growth pattern here is also very similar to that observed for pET15b-*namH* BL21 (Figure 17). Log phase growth, immediately after induction, shows a slight discrepancy between the two constructs; pET15b-*namH* initially has a lower OD compared to the control, this is no longer true 2 hours post induction whereas pBAD-*namH* consistently has a slightly greater OD compared to pBAD TOP10.

However, the slight increase in OD of pBAD-*namH* in Figure 20 is not statistically significant (p value of 0.06 or higher); many of the error bars overlap. Growth analysis using higher arabinose concentration for induction showed a slightly reduced rate of growth, equally in both pBAD-*namH* and pBAD TOP10 strains. Using this new construct and a more stringent expression system the solubility of the NamH protein was examined by Western blot using anti-polyHis antibodies.

Using a variety of growth conditions: temperature (15°C-37°C), inducer concentration (0.02-0.1%) and induction time (1 hour-overnight) pBAD-*namH* protein expression was examined. The soluble and insoluble protein fractions of bacteria were separated and loaded onto a gel to determine optimal expression conditions to increase the yield of soluble protein.

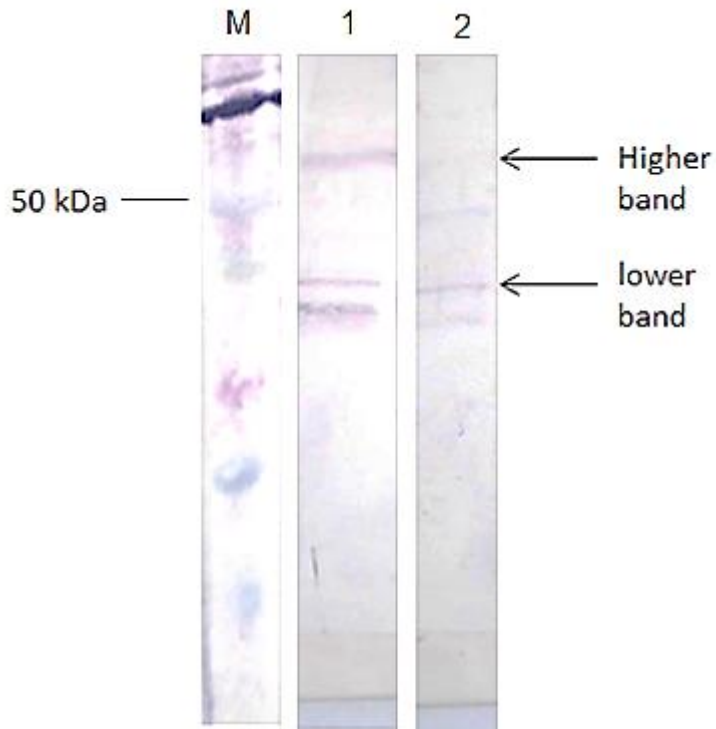


FIGURE 21: WESTERN BLOT USING ANTI-POLYHIS ANTIBODIES SHOWING IPTG INDUCED TOP10 pBAD-*NAMH* INSOLUBLE AND SOLUBLE PROTEIN FRACTIONS.

The marker lane is indicated by the letter M. Lane 1: pBAD-*namH* insoluble fraction and lane 2: pBAD-*namH* soluble fraction. Protein induction was carried out using 0.02% arabinose overnight at 19°C. Samples of insoluble and soluble protein fractions were isolated as described previously. Samples were loaded onto polyacrylamide gels for SDS-PAGE analysis before transfer to nitrocellulose membrane for Western blot. A band at the expected mass of NamH is indicated and referred to as 'higher' band, a lower molecular weight band; likely to be a degradation product is referred to as the 'lower band'.

Solubility of recombinant NamH was examined using the pBAD-*namH* TOP10 strain under a variety of conditions; Figure 21 demonstrates the greatest level of soluble protein identified. The major protein band was detected in the insoluble fraction by Western blot using anti-polyHis antibodies. A similar intensity of soluble protein as that shown in Figure 19 was observed. Again a

low molecular weight band could be observed in both the soluble and insoluble fractions (indicated in Figure 21) and is most likely a result of protein degradation.

It therefore appears that use of this more stringent expression system did not improve NamH solubility. In addition to TOP10 expression host the pBAD-*namH* construct was also cloned into a LMG194 strain which is suited to expression of toxic proteins and expression levels can be reduced by the addition of glucose, however solubility expression studies using this construct also failed to increase the level of soluble NamH (data not shown).

As previously discussed *rv3819* overlaps by 3 nucleotides with *namH* and encodes a protein which could potentially influence the activity of NamH by aiding electron transfer. Therefore co-expression of NamH and Rv3819 in *E. coli* was undertaken in a further attempt to increase solubility and to possibly increase activity. This strain was generated using the primers shown in Table 5, XhoI and BamHI restriction enzymes were used prior to ligation into pET15b and transformation into DH5 α . Purified plasmid DNA was sequenced and used for transformation into BL21 (DE3) expression host.

Unfortunately examination of these cells under the microscope indicated high levels of inclusion bodies and hence this construct was not used for further investigations. The low level of soluble protein identified in the pET15b-*namH* expression strain, whilst not ideal, indicated the presence of some soluble protein and was therefore used in further experiments to examine whether NamH was functional.

3.3.3 DETERMINATION OF NAMH'S FUNCTIONALITY

Despite the low level of soluble NamH protein, identified by Western blot using anti-polyHis antibodies, determination of

activity was undertaken. There were several methods available to determine whether this protein was functional: a direct enzymatic activity assay, analysis of PG structure and indirect biological assays. Since the aim of this work was the generation of glycolylated PG this was the first line of investigation.

3.3.3.1 PURIFICATION OF PG USING METHOD 2

In order to obtain pure PG and produce wild type *E. coli* muropeptide profiles that correspond to those of published results a well-established purification method was followed (Method 2) (Glauner et al., 1988). Using the following strains the muropeptide profiles were investigated by rp-HPLC: pET15b BL21 (DE3), *pET15b-namH* BL21 (DE3) and BL21 (DE3) (containing no plasmid).

Using the control strain pET15b BL21, PG purification was first analysed by rp-HPLC to determine the purity and pattern of mutanolysin released muropeptides. This chromatogram was then compared to published *E. coli* muropeptide profiles for peak identification. As shown in Figure 22 the observed muropeptide peaks have been labelled according to published chromatograms of cellosyl digested *E. coli* PG (Glauner et al., 1988). Cellosyl is a muramidase from *Streptomyces coelicolor* which hydrolyses the glycosidic bond in PG and has very similar activity to mutanolysin (from *Streptomyces globisporus*) but is no longer commercially available.

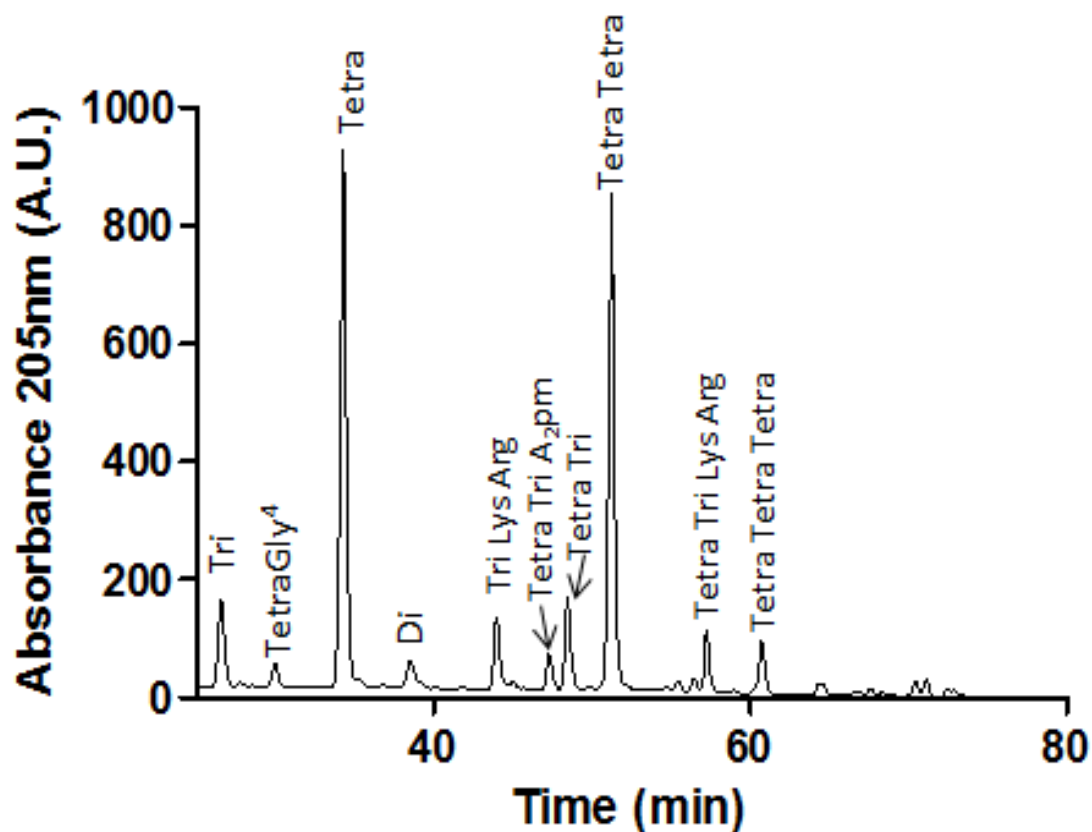


FIGURE 22: PET15B BL21 MUTANOLYSIN DIGESTED RP-HPLC MUROPEPTIDE PROFILE

PG from pET15b BL21 was purified according to Method 2 and digested with 0.5 μ g/ml mutanolysin in 80mM NaPO₄ pH 4.8 at 37°C overnight. Samples were reduced using NaBH₄ and neutralised by phosphoric acid. A 200 μ l sample was ran using a C18 prontosil column in 50mM NaH₂PO₄ pH 4.31 and eluted using a linear gradient of 75mM Na H₂PO₄; 15% MeOH pH 4.95. Di, disaccharide dipeptide; Tri, disaccharide tripeptide; Tetra, disaccharide tetrapeptide; Tetra Tetra, Tetra cross linked to Tetra; Gly⁴, glycine residue in position 4 of peptide side chain; Lys Arg, Lys-Arg residue from lipoprotein.

TABLE 6: MOLECULAR IONS OF SELECTED *E. COLI* MUROPEPTIDES

Muropeptide	Mass ([M+H]⁺/[M+Na]⁺)
Disaccharide Tripeptide	870.9/892.9
Disaccharide Dipeptide	698.68/720.68
Disaccharide Tripeptide-Lys-Arg	1155.27/1177.27
Disaccharide Tetrapeptide	942.5/964.5
Disaccharide Tetrapeptide-Tetrapeptide	1405/1427
Disaccharide Tetrapeptide-Disaccharide Tripeptide	1794.0/1816.0
Disaccharide Tetrapeptide-Disaccharide Tetrapeptide	1865.0/1887.0
Disaccharide Tetrapeptide-Disaccharide Tripeptide-Lys-Arg	2079.24/2101.24
Disaccharide Tetrapeptide-Disaccharide Tetrapeptide-Disaccharide Tetrapeptide	2789.79/2811.79

The mass of several of the major *E. coli* muropeptides are shown in Table 6, these were taken from previously published work (de Jonge et al., 1989, Tuomanen and Cozens, 1987, Ottolenghi et al., 1993, Pfanzagl et al., 1996, De pedro et al., 1993).

Schematic examples of muropeptide structures are shown in Appendix 1: Muropeptide Schematics and Fragmentation. Not all muropeptides previously identified by Glauner in 1988 were observed in Figure 22, and the structural identity of those of low intensity was inferred by comparison to the two main peaks associated with *E. coli* PG (Tetra and Tetra-Tetra). Figure 22 therefore demonstrates that use of this method to purify and analyse *E. coli* PG produces muropeptide profiles matching previously published work. Investigation of PG isolated from pET15b-*namH* BL21 was then undertaken to detect the presence of glycolylated muropeptides.

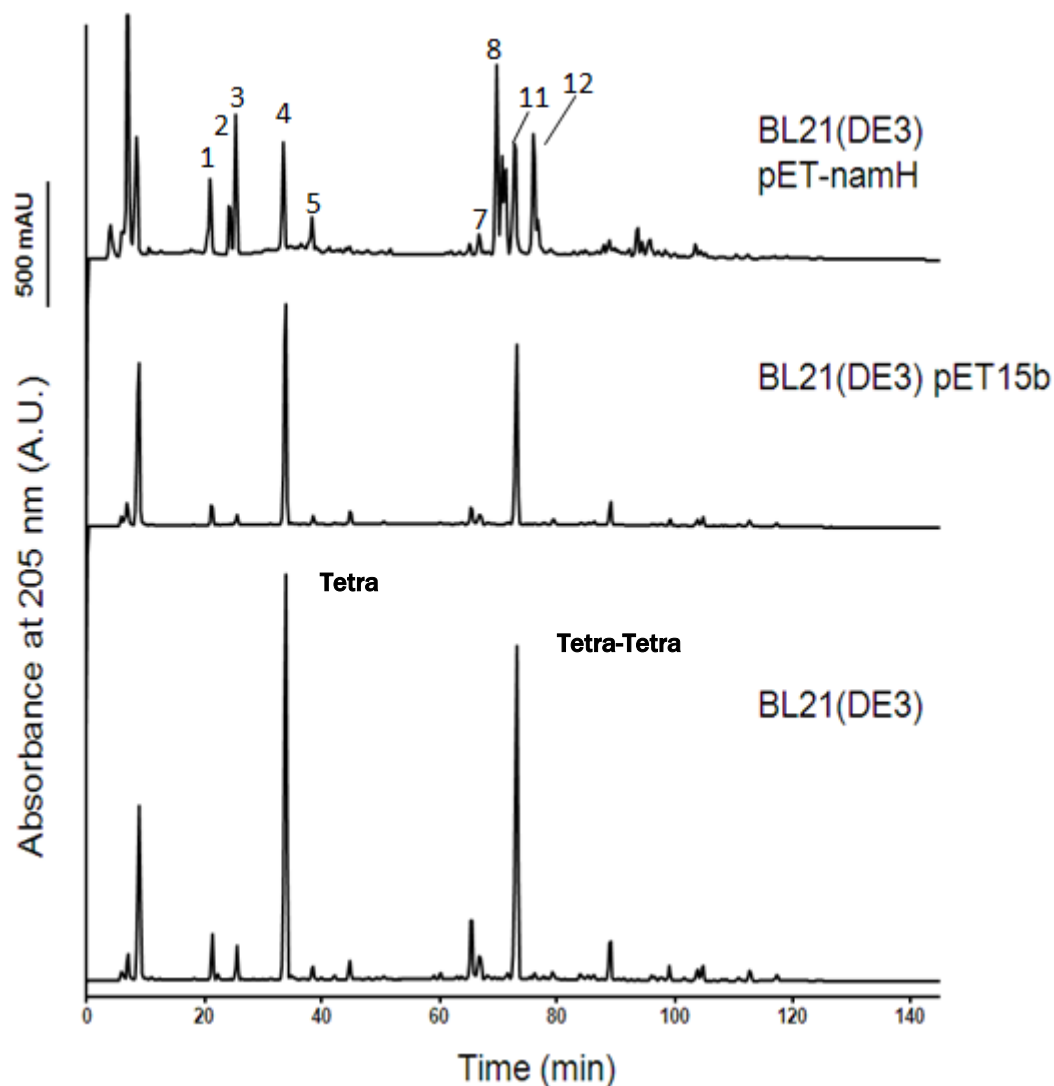


FIGURE 23: PET15B-NAMH AND CONTROL CELLOSYL RELEASED MUROPEPTIDE PROFILES RP-HPLC CHROMATOGRAMS.

HPLC chromatograms of cellosyl digested PG for the following strains (from top to bottom): pET15b-*namH*, pET15b and BL21 (DE3) *E. coli*. Absorbance was measured at 205nm, 180 μ l of NaBH₄ treated samples were loaded onto a C18 Prontosil column and HPLC was performed in 50mM NaH₂PO₄ pH 4.31 and eluted using a linear gradient of 75mM Na H₂PO₄; 15% MeOH pH 4.95. All pET15b-*namH* peaks with 100mAU or higher were collected for MS analysis, these are labelled 1 to 12.

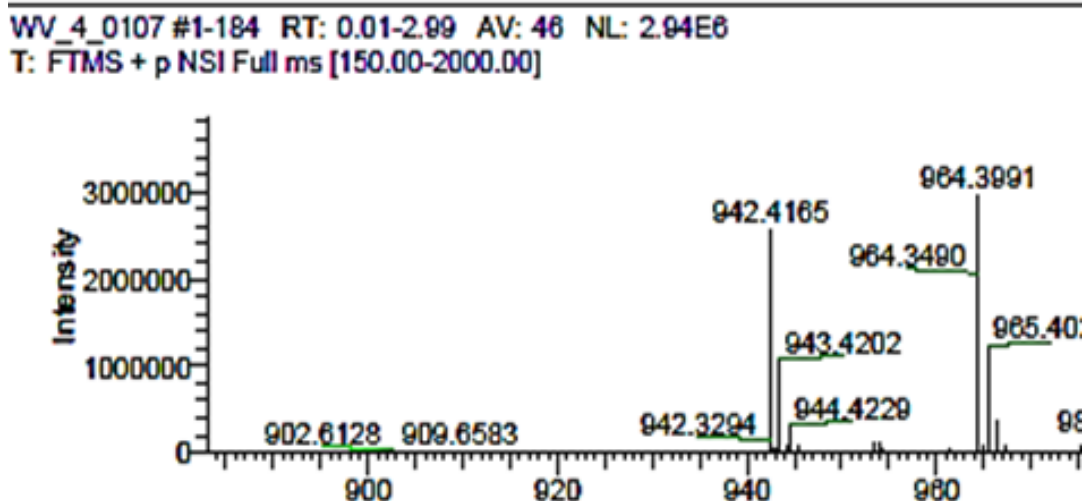


FIGURE 24: MASS SPECTRUM OF PEAK 4 FROM CELLOSYL DIGESTED pET15b-NAMH BL21 PG

Peak 4 (shown in Figure 23) of cellosyl digested pET15b-*namH* BL21 PG was analysed by MS at the University of Newcastle. Mass peaks at 942.4 and 964.39 were then structurally identified.

As shown in Figure 23, the mucopeptide profile of the NamH expressing BL21 strain was different in comparison to both control strains. In addition, the mucopeptide profiles of the control strains match those of previously published work; each contains the two main peaks (labelled Tetra and Tetra-Tetra in Figure 23) which were described in Figure 22. pET15b-*namH* cellosyl released mucopeptides retain the Tetra and possibly the Tetra-Tetra peaks. Peak 4 was analysed by MS, the results of which are shown in Figure 24. The peaks eluted slightly earlier than the Tetra-Tetra peak in Figure 23 (pET15b-*namH*) could correspond to Tetra-Tri- A_2pm , Tetra-Tetra-Gly⁴ and Tetra-Tri based on previously published structural data (Glauner et al., 1988). However, these series of peaks were usually observed at very low levels but here appear to be massively increased. There were several other peaks which no longer match those of previously published *E. coli* mucopeptide chromatograms, including a peak eluted prior to the

Tetra muropeptide. Unfortunately, the muropeptide profile shown in Figure 23 for pET15b-*namH* could not be replicated in subsequent purifications.

The fractions collected were analysed by Fourier Transform MS (FTMS) at the University of Newcastle. Most muropeptide peaks collected did not produce MS peaks correlating to known muropeptide masses. Analysis of peak 4 (numbered in Figure 23), which was predicted to correspond to the *E. coli* Tetra muropeptide, resulted in the FTMS spectrum shown in Figure 24.

The peaks shown in Figure 24 (964 and 942) correspond to the $[M+H^+]$ and $[M+Na^+]$ of Tetra (disaccharide tetrapeptide) respectively. MS analysis of the remaining muropeptides produced poor quality data; the fractions which did produce MS peaks did not correspond to known muropeptide masses. It therefore appears that pET15b-*namH* does not consistently produce enough soluble protein to result in glycolylated PG detectable by rp-HPLC. An example of fragmentation of a muropeptide is shown in Appendix 1: Muropeptide Schematics and Fragmentation.

Using pBAD-*namH* TOP10 (and the corresponding pBAD control) PG was purified according to Method 2 and mutanolysin digested muropeptides analysed and separated by rp-HPLC.

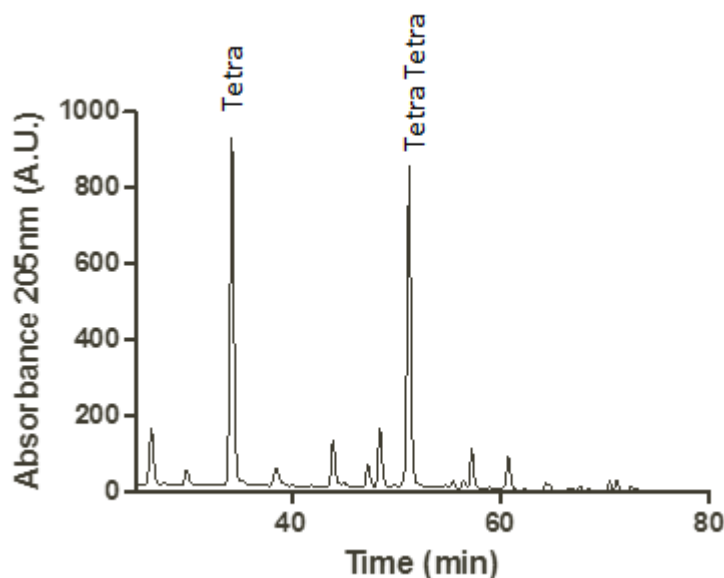


FIGURE 25: RP-HPLC CHROMATOGRAM SHOWING MUTANOLYSIN DERIVED MUROPEPTIDES FROM 0.02% ARABINOSE INDUCED PBAD-*NAMH* TOP10

PG was purified and mutanolysin digestion carried out as previously described. 200 μ l of NaBH₄ reduced sample was loaded onto a C18 Prontosil column and HPLC was performed in 50mM NaH₂PO₄ pH 4.31 and eluted using a linear gradient of 75mM NaH₂PO₄; 15% MeOH pH 4.95.

As shown in Figure 25, the resulting muropeptide profile of mutanolysin digested pBAD-*namH* TOP10 corresponds strongly to that of wild type *E. coli* PG (Figure 22 and Figure 23). This pattern of muropeptides was consistently observed and it can hence be concluded that under these conditions glycolylation of the PG in NamH expressing *E. coli* does not occur. This was most likely a consequence of a low level of soluble NamH and a short expression time. Therefore due to the irreproducibility of an altered muropeptide profile for NamH expressing strains an alternative method of PG purification was implemented.

3.3.3.2 AN ALTERNATIVE PG PURIFICATION METHOD

3.3.3.2.1 LYSOZYME DIGESTION

PG was isolated as described in Method 1; in comparison to the previous PG purification method this method harvested cells at a later stage of growth after a greater length of induction. Once purified, samples were digested with 200 µg/ml lysozyme overnight prior to analysis by rp-HPLC.

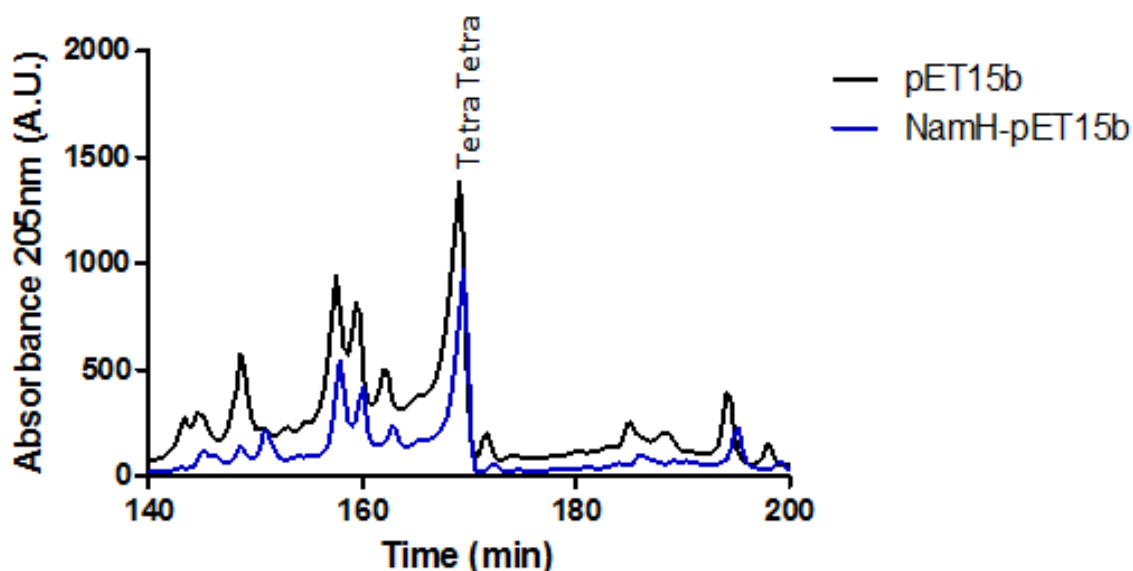


FIGURE 26: LYSOZYME DIGESTED PET15B-NAMH AND PET15B PG SEPARATED BY RP-HPLC

A C18 hypersil column was used and rp-HPLC was carried out (as described previously) in 40mM NaH₂PO₄ pH 4.3 and 200µl of NaBH₄ treated samples were loaded. Elution was carried out by a linear gradient of 40mM NaH₂PO₄; 15% MeOH pH 5.1. Isolated PG from both pET15b and pET15b-*namH* strains were digested at 37°C in phosphate buffer and 200 µg/ml lysozyme overnight. Absorbance was recorded at 205nm.

As depicted in Figure 26, there was a highly similar pattern of muropeptides released from lysozyme treatment of both pET15b and pET15b-*namH* isolated PG, however there was no longer the standard *E. coli* peaks observed; with the exclusion of Tetra-Tetra possibly. The above results were highly reproducible and therefore the loss of these distinctive peaks and the reduction in peak resolution was most likely a result of impure PG.

The similarity of muropeptide profiles observed in Figure 26 could signify the digestion of non-modified PG due to the insensitivity of glycolylated murein to lysozyme. Due to the potential 'lysozyme insensitivity' of the NamH overexpressing strain it could be postulated that this enzyme may not result in cleavage of the glycosidic bond in which the attached muramic acid residue is glycolylated (Mahapatra et al., 2005). Hence the PG cleaved by lysozyme, and the resulting products, may represent the non-glycolylated proportion of PG. This would therefore appear identical to that of wild type *E. coli* PG. However, a matching *E. coli* muropeptide pattern was not evidence enough to conclude that this was the case. Mutanolysin digested pET15b-*namH* was then investigated using the modified purification method.

3.3.3.2.2 MUTANOLYSIN RELEASED MUROPEPTIDES

Mutanolysin was used in an attempt to generate modified muropeptides from the NamH overexpressing strain. A shift in retention to the column would be expected as a result of an additional hydroxyl group on the muramic acid residue, as this would influence the polarity and binding of the muropeptide to the column. It could be postulated that a glycolylated muropeptide may have slightly decreased retention to the column than its acetylated homologue due to the increased polarity.

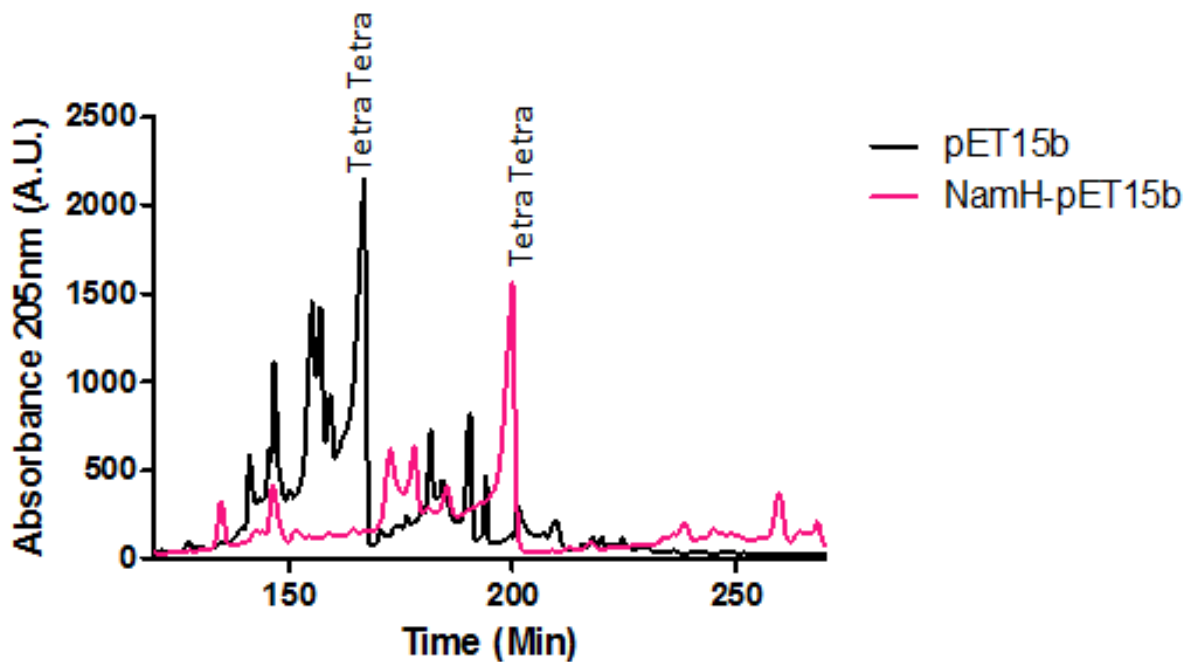


FIGURE 27: HPLC CHROMATOGRAMS SHOWING MUTANOLYSIN RELEASED MUROPEPTIDES FROM BOTH pET15b AND pET15b-NAMH ISOLATED PG

A C18 hypersil column was used and rp-HPLC was carried out (as described previously) in 40mM NaH₂PO₄ pH 4.3 and 200µl of NaBH₄ treated samples were loaded. Elution was carried out by a linear gradient of 40mM NaH₂PO₄; 15% MeOH pH 5.1. Isolated PG from both pET15b and pET15b-*namH* strains were digested at 37°C in 80mM NaPO₄ pH 4.8 with 0.5µg/ml mutanolysin overnight. Absorbance was recorded at 205nm.

Figure 27 demonstrates the muropeptide profile of mutanolysin digested PG from pET15b and pET15b-*namH* strains, separated by rp-HPLC. Again there was loss in peak resolution and in the number standard peaks observed (compared to Figure 22), however the profile shown in Figure 27 for pET15b (black) matches that of pET15b when digested by lysozyme, as shown in Figure 26. This altered muropeptide profile was highly reproducible.

There was a clear shift in retention to the column between the two samples, with an increased retention observed for pET15b-*namH* released muropeptides. From Figure 27 it appears as though there was a structural difference between the PG of the two strains in

question, however the glycolylation of pET15b-*namH* murein led to the hypothesis that a reduced retention to the column which was the opposite of that observed. The observed muropeptide profile in Figure 27 was extremely reproducible, as was that observed in Figure 26, for lysozyme released muropeptides.

It therefore appears that under these conditions and using this purification method a consistent altered muropeptide profile was observed for pET15b-*namH* expressing *E. coli* when digested by mutanolysin. Analysis by mass spectrometry was therefore necessary to confirm the presence of glycolylated murein.

3.3.3.3 BL21 (DE3) PET15B-NAMH ANALYSIS BY MASS SPECTROMETRY

3.3.3.3.1 LCMS

In order to examine the PG structure of pET15b-*namH* further, PG samples were first hydrolysed and then analysed by LCMS.

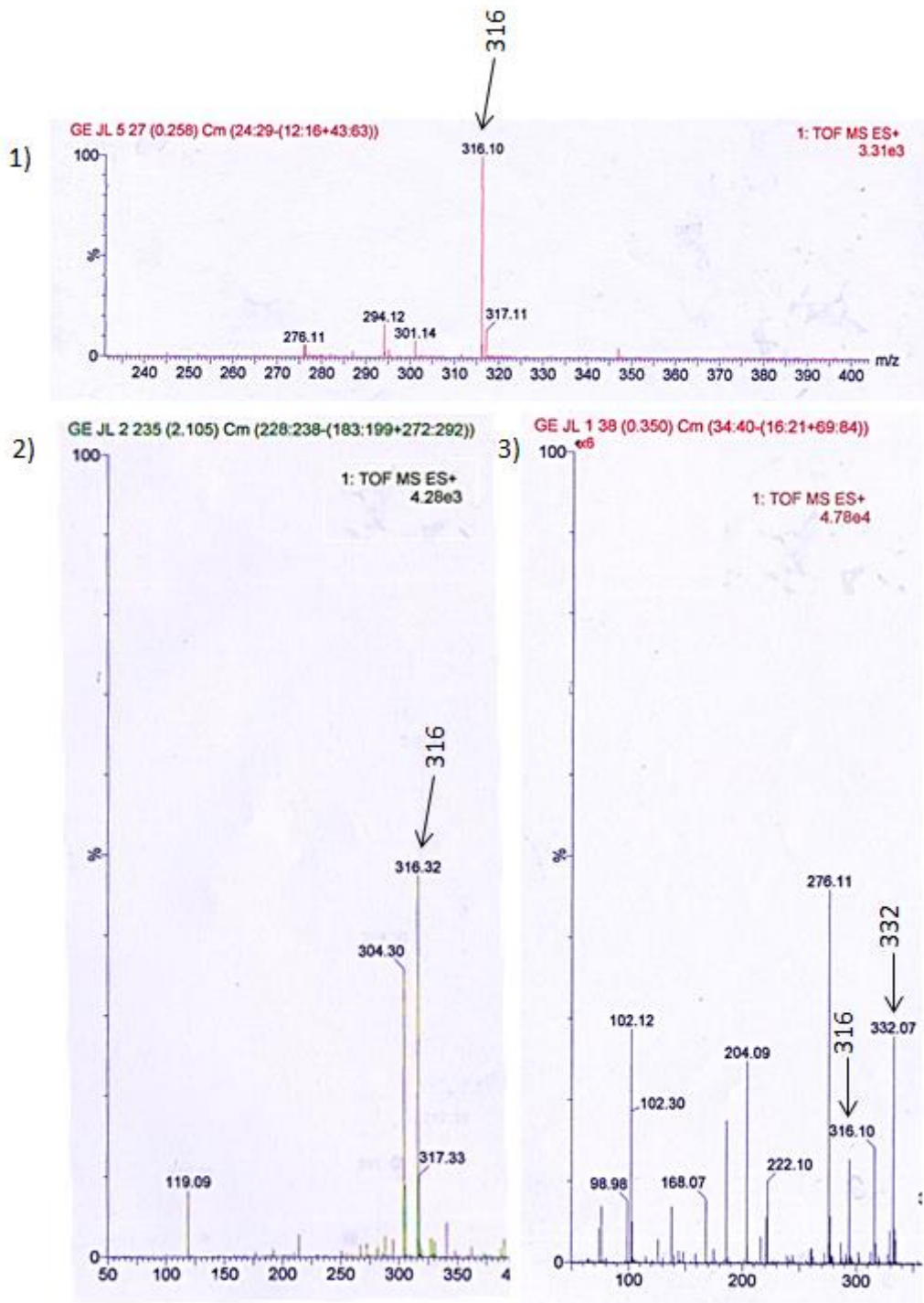


FIGURE 28: LCMS ES DATA SHOWING HYDROLYSED MUROPEPTIDES FROM NAM, PET15B AND PET15B-NAMH

Spectra from top to bottom: 1) NAM, 2) pET15b and 3) pET15b-*namH*. Both 2) and 3) were NH_4OH hydrolysed PG samples and 1) was $10\mu\text{g/ml}$ commercially available NAM. All samples were dissolved in 100% MeOH and were run in the positive mode. Only the ES data has been included.

Commercially available N-acetyl muramic acid (NAM) (at 10µg/ml), as depicted in Figure 28 image 1, was ran on LCMS, the ES data is displayed in Figure 28. Figure 28 image 1 has a major peak at 316 Da, which corresponds to the molecular weight of NAM with a Na⁺ adduct. N-glycolylation of NAM, as result of NamH (to NGM), was predicted to produce a peak with a mass increase of 16 Da; resulting in a peak of 332 Da (including a Na⁺ adduct). From Figure 28, image 2, it can be observed that a peak of the same mass (316 Da) was present within BL21 (DE3) pET15b hydrolysed PG. However, when pET15b-*namH* hydrolysed PG was analysed, this no longer had a major peak at 316 Da but (as shown in Figure 28, image 3) had a peak at the expected mass of 332 Da and a less intense peak at 316 Da. These spectra suggest the presence of both glycolylated and acetylated muramyl residues within pET15b-*namH* BL21 PG.

3.3.3.4 CHEMICAL MODIFICATION AND MALDI-TOF ANALYSIS

Detection of the predicted MS peaks (Figure 28) indicated the presence of glycolylated muramic acid residues within PG of the pET15b-*namH* strain, however, in order to confirm that the 332 Da peak corresponded to NGM, chemical modification of hydrolysed PG was performed. Permethylation (PM) was initially optimised using commercially available N-acetyl glucosamine (NAG). Permethylation is a base-catalysed reaction resulting in methylation (usually through the formation of methyl esters). However, as discussed previously, using NaOH as a base may lead to under methylation. This was observed when NAG was permethylated, hence the resulting spectrum contained mass peaks corresponding to NAG (un-methylated) as well as the masses corresponding to methylation of 1 to 5 groups. Using hydrolysed PG samples the resulting mass shifts due to PM could be

predicted. These predicted masses are shown in Table 7 and correspond to the PM at the highlighted groups in Figure 29.

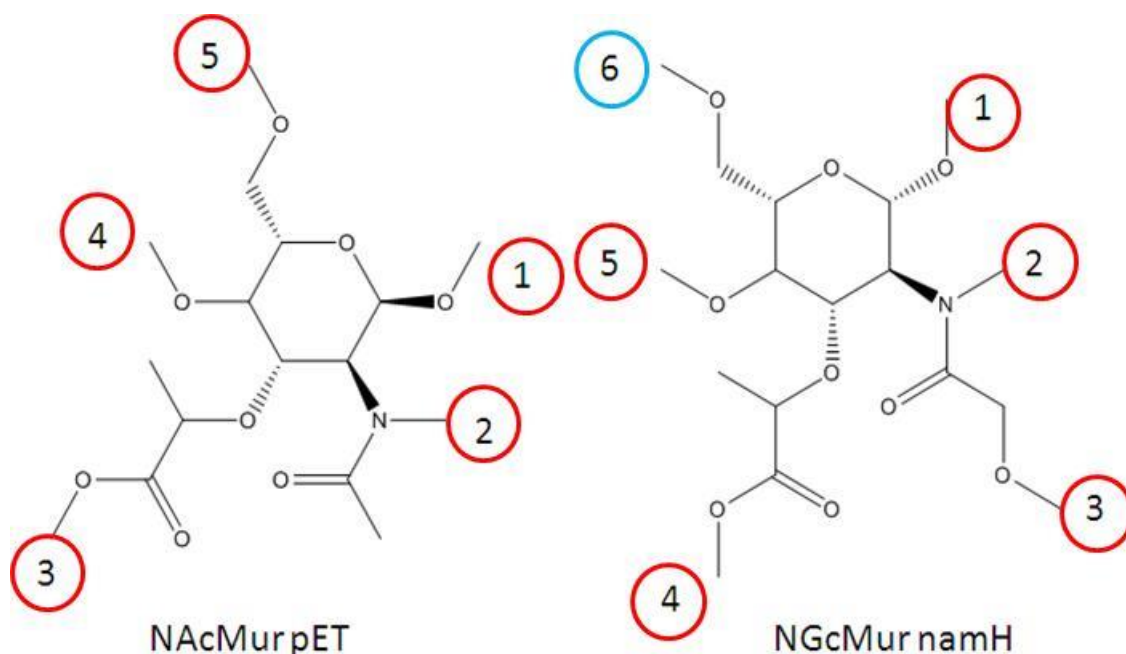


FIGURE 29: A SCHEMATIC OF THE FUNCTIONAL GROUPS FOR BOTH PET15B-NAMH AND PET15B MURAMIC ACID AVAILABLE FOR METHYLATION.

A schematic created using ChemBioDraw highlights the functional groups that are available for methylation (circled in red), due to the predicted presence of an additional hydroxyl group in NamH a 6th group should therefore be available (circled blue).

As shown in Figure 29, the additional hydroxyl group present within glycolylated muramic creates an extra functional group available for methylation. By doing so a new set of mass peaks were generated (shown in Table 7) allowing a more direct assessment of pET15b-*namH* PG structure.

TABLE 7: THE PREDICTED PM MASS PEAKS FOR pET15B AND pET15B-NAMH MURAMIC ACID.

PM state	pET15b (Da)	pET15b- <i>namH</i> (Da)
N/A	316	316 and 332
1	330	330 and 346
2	344	344 and 360
3	358	358 and 374
4	372	372 and 388
5	386	386 and 402
6	N/A	416

As can be observed in Table 7, there were two sets of predicted mass peaks expected for pET15b-*namH*, this was due to the previously discussed inefficiency of the NamH enzyme; *Mtb* PG has been predicted to contain roughly 70% glycolylated muramic acid and hence does not result in complete glycolylation of the PG (Mahapatra et al., 2005). The presence of NAM and NGM in the PG of pET15b-*namH* BL21 was therefore expected.

Hydrolysed PM and non-PM samples were analysed by MALDI-ToF. The reason for using this technique was a combination of factors: firstly, the low volume of permethylated samples was more suited to MALDI-ToF, secondly the chemicals used for this reaction could influence how these samples would fly within the ES machine and thirdly with the series of mass peaks expected and identification against the matrix background should be significantly improved. Additionally, the increase in the mass of expected peaks moves the range of masses being examined and thus reduces the noise background associated with the lower molecular weight region.

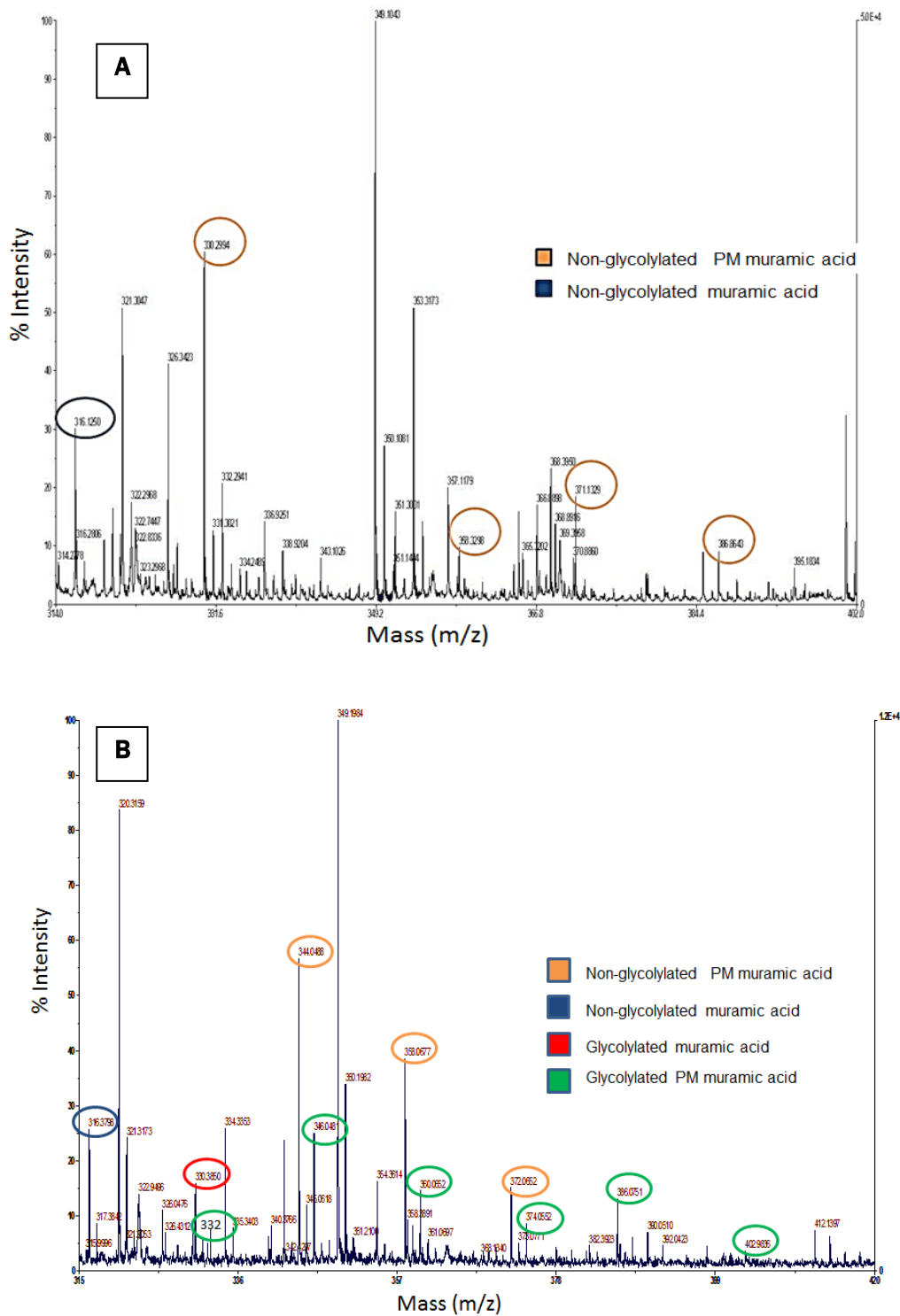


FIGURE 30: MALDI-TOF SPECTRA OF PERMETHYLATED HYDROLYSED PG SAMPLES.

pET15b and pET15b-*namH* (A and B respectively) hydrolysed samples were permethylated. Samples were mixed with a 10g/L solution of CMBT (prepared in EtOH:H₂O:THF) in a 1:5 ratio and spotted onto a 96 well plate.

From Figure 30, A) the predicted mass peaks (Table 7) for methylation of the individual functional groups within pET15b muramic acid have been highlighted (yellow rings). In comparison to this, Figure 30, B) shows the resulting spectrum of permethylated pET15b-*namH* hydrolysed PG. From this figure the predicted mass shifts of both NAM and NGM (Table 7) can be observed, however some of the higher molecular weight peaks appear to have a low abundance. Additionally, both spectra show a similar pattern; a greater intensity of residues with fewer PM groups, decreasing in intensity further as the number of PM groups increases. This trend was also observed in the NAG control and was indicative of under-permethylation; potentially as a result of using NaOH as the base catalyst. It should also be noted that in CMBT matrix control MALDI-ToF spectra, the peaks observed in Figure 30 corresponding to PM NAM residues (both NAM and NGM), were not present. These data indicate the presence, at a low level, of both NAM and NGM in pET15b-*namH* BL21 PG. A second line of investigation was to use a biological assay to distinguish the presence of NGM.

3.3.4 DID PET15B-NAMH BL21 (DE3) HAVE A REDUCED SENSITIVITY TO LYSOZYME?

Determination of NamH activity was further investigated by biologically assessing pET15b-*namH* lysozyme sensitivity. Mycobacteria are highly resistant to several cell wall enzymes; including lysozyme (Kanetsuna, 1980, Amano and Williams, 1983). It has been demonstrated that glycolylation of the PG within *M. smegmatis* results in a reduced susceptibility to β -lactams and other drugs with cell wall targets (Raymond et al., 2005). Therefore it was hypothesised that glycolylation may influence the cells susceptibility to lysozyme. Lysozyme sensitivity of both pET15b and pET15b-*namH* strains was tested, as successful incorporation

of N-glycolylated murein into pET15b-*namH* PG may have resulted in a predicted decreased sensitivity to lysozyme.

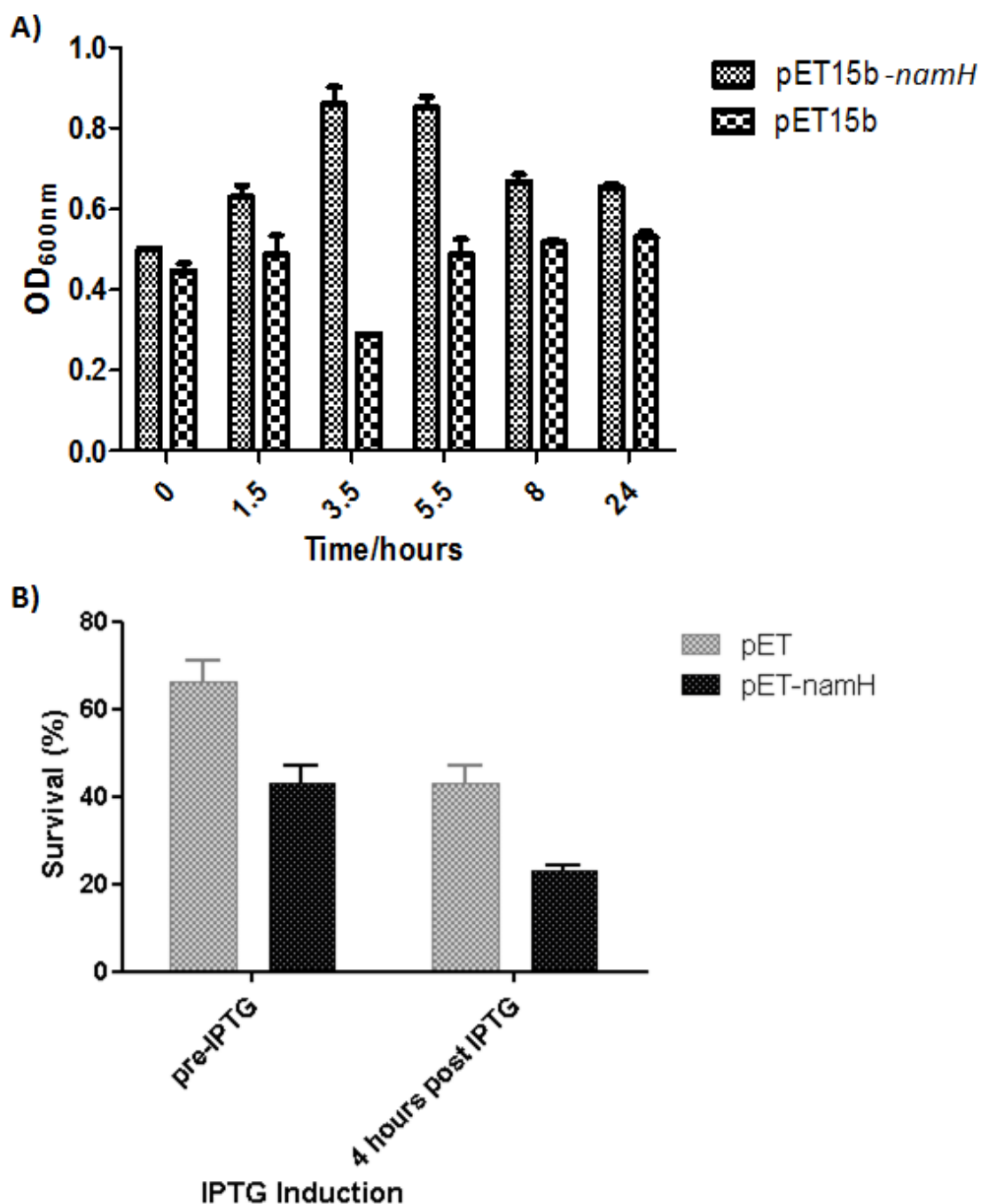


FIGURE 31: LYSOZYME SENSITIVITY OF PET15B-NAMH BL21 (DE3).

pET15b-*namH* BL21 (DE3) and pET15b BL21 (DE3) were grown in LB medium with 1mM of IPTG. Bacteria were washed and the OD standardised in 30mM Tris HCl; pH 8.0, containing 1.3mM EDTA before 100µg/ml lysozyme was added and samples incubated at 37°C. OD measurements were taken after 2 hours at each time

point. Figure A shows the OD after lysozyme treatment at different growth stages and B shows the percentage survival after lysozyme treatment, determined by CFU counts (the variance between the starting CFU counts was not statistically significant (p value 0.77)).*The variation in percentage survival between the two strains at both times points was statistically significant.

Figure 31 demonstrates a consistent OD, and at certain time points an increase in OD when pET15b-*namH* expressing cells were exposed to lysozyme. This increase in OD mirrors the increasing NamH expression time until stationary phase is reached and the OD drops to pre-IPTG induction levels. This pattern was not observed in the pET15b control strain. Overall this could indicate that pET15b-*namH* has a reduced sensitivity to lysozyme indicative of this strain harbouring modified PG. Uninduced NamH also has a slightly elevated OD compared to the control.

However, by examining percentage survival (Figure 31, B) it is clear that the increase in OD observed for pET15b-*namH* was not found in CFU counts; pET15b-*namH* lysozyme survival data was consistently lower than the pET15b control strain at both time points. Using a student's T-Test the variance between the starting CFU counts (before lysozyme treatment) of two datasets was determined not to be statistically significant (p value 0.77). However, the variance in percentage survival between the two strains was found to be statistically significant (p values: 0.04 and 0.02 pre-IPTG and 4 hours post IPTG respectively) at both time points. Therefore pET15b-*namH* appears to be more sensitive to lysozyme, as determined by percentage survival. Again this is true for uninduced NamH cells.

The increase in OD consistently observed in pET15b-*namH* could be a result of chains of cells as previously shown in Figure 17 (B), cellular debris due to cell lysis or perhaps due to clumping as cultures expressing pET15b-*namH* had a tendency to clump. An alternative biological assay to test the presence of glycolylation

would have been to assess the antimicrobial effect of penicillin; as glycolylation has previously been shown to result in decreased sensitivity to penicillin (Raymond et al., 2005). Unfortunately the use of plasmids carrying ampicillin resistance genes (pET15b and pBAD) prevented this line of investigation.

Altogether these findings indicate that a small percentage of PG within pET15b-*namH* expressing BL21 may contain glycolylated muramyl residues, however it does not appear that this level of modification can be observed consistently by rp-HPLC. Use of a more sensitive but non-quantitative method; mass spectrometry resulted in consistent observation of NGM within pET15b-*namH* expressing BL21 only. This strain was therefore used in an attempt to generate Rpf muropeptide products alongside confirmation of the presence of this modification.

3.3.5 RPF B MUROPEPTIDE PRODUCTS

3.3.5.1 PURIFICATION AND MURALYTIC ACTIVITY OF RECOMBINANT *MTB* RPF B

To investigate whether *Mtb* RpfBs were more efficient at digesting glycolylated PG, recombinant *Mtb* RpfB_{ΔDUF} was purified by affinity chromatography and analysed by SDS-PAGE for purity before the muralytic activity was tested. This was carried out using an optimal refolding buffer, by zymography. RpfB was ideal for this assay as it can be purified from the soluble fraction and is expressed at a high level under IPTG.

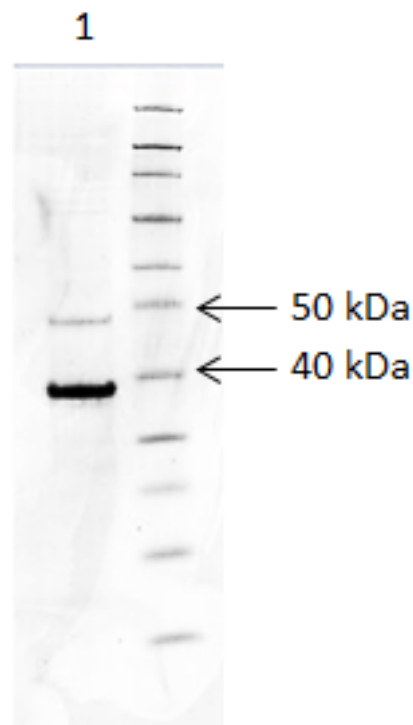


FIGURE 32: SDS-PAGE OF PURIFIED RECOMBINANT PETM-11-RPFB_{ΔDUF} BL21 (DE3).

RpfB_{ΔDUF} was purified as previously described and analysed by SDS-PAGE. 10 μ l of purified RpfB_{ΔDUF} (post dialysis) in 5mM DTT and sample buffer was loaded onto a 12% gel. The gel was stained in colloidal blue overnight. RpfB was dialysed into 25mM Tris HCl; 500mM NaCl; 20% glycerol pH 8.5.

Figure 32 shows purified recombinant *Mtb* RpfB_{ΔDUF}, the purified fractions were pooled and concentrated to generate 1mg/ml solution. The expected mass of RpfB_{ΔDUF} is 18.74 kDa, however as can be observed in Figure 32 the recombinant protein runs at roughly 40 kDa. This is consistent with previously published gel filtration work on this protein (Ruggiero et al., 2009). Renaturation was first optimised and muralytic activity was then assessed by zymography.

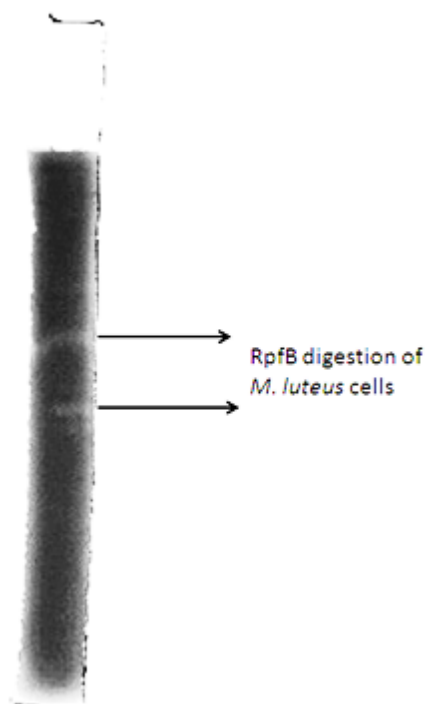


FIGURE 33: MURALYTIC CLEARANCE BANDS OF *M. LUTEUS* CELL WALL; DIGESTED BY RECOMBINANT RPF_{ΔDUF}.

20µg of recombinant RpfB_{ΔDUF} was loaded into all lanes of an SDS-PAGE gel containing lyophilised *M. luteus* cell wall. After electrophoresis the gel was cut into strips and each placed in different renaturation buffers. Gel strips were then stained and clearance bands observed after several washes. The strip shown was renatured in 25mM Tris HCl pH 8.5 in the presence of 2% (w/v) Triton X100.

The muralytic activity of recombinant RpfB was demonstrated by zymography (Figure 33). The following buffers were used: 25mM Sodium phosphate pH 6, 6.5, 7 and 7.5, 25mM Sodium citrate pH 4.5, 5 and 5.5 and 25mM Tris HCl pH 7, 7.5, 8 and 8.5. Clearance bands were observed when RpfB was renatured in 25mM Tris HCl pH 8.5. Using the same buffer but with lower and higher pH (pH 6 and 8), clearance bands were also observed; these were less intense and less reproducible upon subsequent protein purifications. The isoelectric point calculated for RpfB is 5.22 (Reddy et al., 2009), suggesting that the protein was negatively charged under the conditions in which muralytic activity has been shown. The presence of multiple clearance bands corresponds well

to the bands observed after protein purification (Figure 32). This additional, high molecular weight band could indicate the presence of a dimer. Once muralytic activity was confirmed this recombinant protein was used to study muropeptide products.

3.3.5.2 MODEL MUROPEPTIDE PRODUCTS OF RPF B

Purified and active recombinant RpfB was then used to digest isolated PG from pET15b-*namH* and pET15b strains, using the same method for mutanolysin digestion. Released muropeptides were then analysed by rp-HPLC and no muropeptide peaks were observed when pET15b PG was used as the substrate. When pET15b-*namH* PG was used there were multiple peaks consistently observed, however these peaks had variable chromatogram profiles and were of extremely low intensity indicating their unreliability.

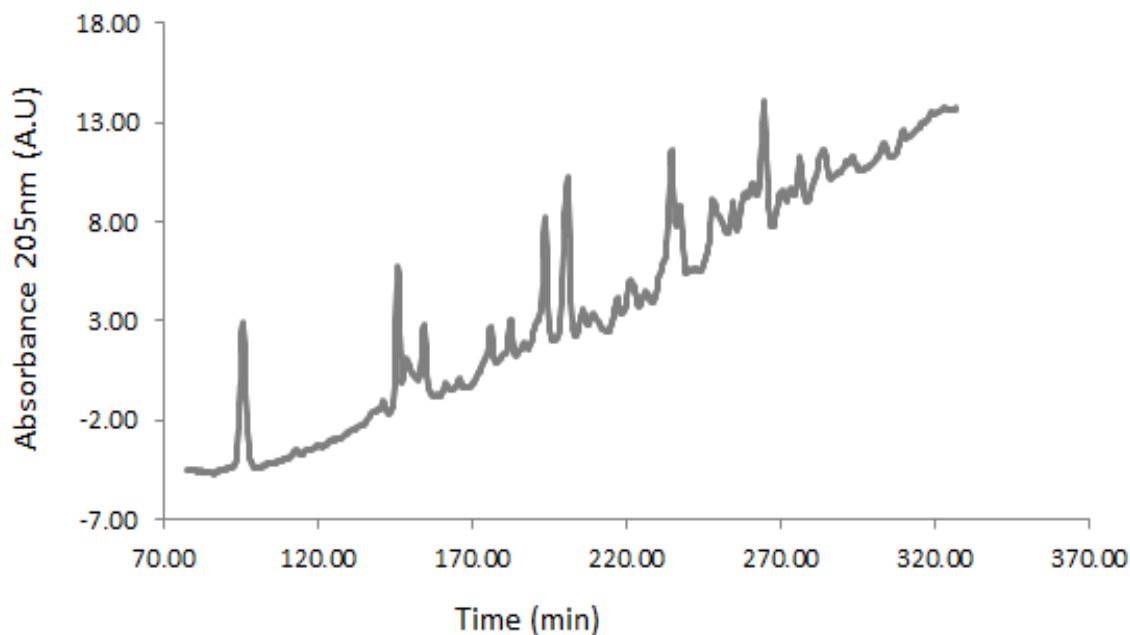


FIGURE 34: RP-HPLC CHROMATOGRAM OF RPF_B Δ DUF DIGESTED PET15B-NAMH ISOLATED PG

PG digestion was carried out using 100 μ g/ml RpfB in 40mM citric acid; pH 6.5 at 37°C overnight. A C18 hypersil column was used and rp-HPLC was carried out in 0.1% formic acid pH 4.2. Elution was carried out by a linear gradient of 0.1% formic acid, 15% MeOH; pH5.2. Absorbance was recorded at 205nm.

An example of the muropeptide profile produced by RpfB digestion of pET15b-*namH* BL21 PG is shown in Figure 34. Low intensity peaks can be observed, these peaks were also highly inconsistent and could indicate that RpfB has released muropeptide products which were too large and therefore did not bind well to the column. This could also explain the lack of peaks observed in pET15b BL21 RpfB digested PG.

Using *M. smegmatis* PG recombinant RpfB was used to generate a muropeptide profile by rp-HPLC. The results of one such experiment are shown in Figure 35. Similar to the muropeptide profile of RpfB digested pET15b-*namH* BL21, the peaks observed were of low intensity and irregular.

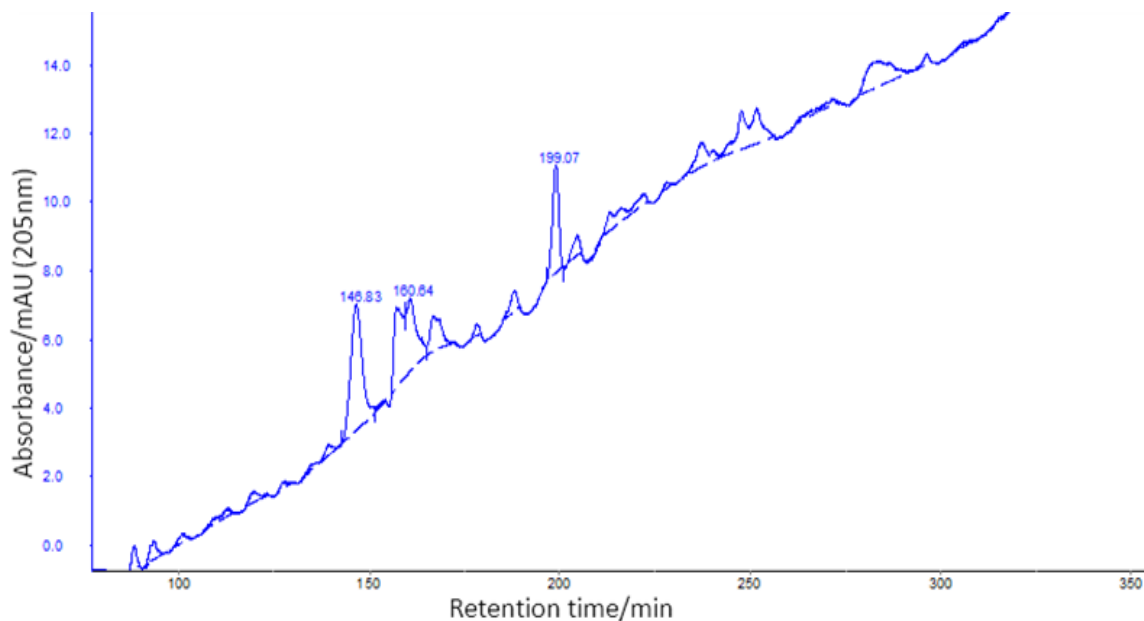


FIGURE 35: RP-HPLC CHROMATOGRAM OF RPF B DIGESTED *M. SMEGMATIS* PG

PG was purified as described previously (Mycobacterial PG Purification). PG digestion was carried out using 100 μ g/ml RpfB in 40mM citric acid; pH 6.5 at 37°C overnight. A C18 hypersil column was used and rp-HPLC was carried out in 0.1% formic acid pH 4.2. Elution was carried out by a linear gradient of 0.1% formic acid, 15% MeOH; pH5.2. Absorbance was recorded at 205nm.

Similarly to pET15b-*namH* BL21 RpfB digested muropeptide profile, the lack of consistent high intensity peaks could be the result of fragments which were too large and hence hindered the binding to the column. Due to the waxy complex nature of mycobacterial cell wall it is also possible that PG contained impurities which may have increased the size of RpfB products. Overall recombinant RpfB has been shown to be expressed by SDS-PAGE and active by zymography. Analysis of RpfB digested muropeptides indicates that products were too large to bind to column and only low intensity and variable peaks were observed.

3.4 DISCUSSION

3.4.1 OVEREXPRESSION OF NAMH

The first aim of this project was to generate an *E. coli* strain overexpressing *Mtb namH*. Overexpression of the *M. smegmatis* NamH protein within *E. coli* had previously been shown to be toxic (Raymond et al., 2005). Once *namH* was successfully cloned into BL21 (DE3) using a pET15b plasmid the first aim was to determine whether *Mtb* NamH was toxic to *E. coli*. It was found by growth analysis that *Mtb* NamH is not toxic to *E. coli*. Subsequent to this, protein expression needed to be confirmed. Protein expression trials were examined by Western blot using anti-polyHis antibodies and demonstrated a 2 hour optimal expression time. NamH solubility experiments showed a low level of soluble protein and microscope images had previously shown bubble-like formations which may represent inclusion bodies (Garcia-Fruitos et al., 2005).

As the primary aim was to generate glycolylated PG within *E. coli* by overexpressing *Mtb* NamH, a greater yield of soluble protein would be beneficial. Therefore an alternative expression system was adopted. The pBAD system, which is a highly stringent expression vector under arabinose induction, was implemented. Growth expression was examined and showed *Mtb* NamH to be non-toxic to *E. coli* whilst protein solubility determined by Western blot using anti-polyHis antibodies showed a similarly low level as observed in pET15b-*namH*. The original construct was therefore used for determination of NamH functionality.

3.4.2 PG PURIFICATION AND ANALYSIS TO DETERMINE NAMH FUNCTIONALITY

The second aim was to purify PG to assess the presence of glycolylated muramic acid residues. A previously published method was used for *E. coli* PG purification, using pET15b BL21(DE3) as a

control, mutanolysin digested muropeptides were assessed by rp-HPLC and identified by comparison to previously published work (Glauner et al., 1988, Magnet et al., 2008). The resulting muropeptide profile matched those of previously published works on *E. coli* PG composition. This method was then used to analyse pET15-*namH* BL21 PG, the initial experiment demonstrated an altered muropeptide chromatogram. MS analysis of these peaks failed to demonstrate glycolylation and subsequent analysis showed muropeptide profiles matching wild type *E. coli*. pBAD-*namH* PG was purified and muropeptide composition was analysed by rp-HPLC, however this failed to produce altered muropeptide profiles.

Consistent altered muropeptide profiles were only achieved through alteration of the method for PG purification. Using cultures grown to a higher OD greater protein expression was achieved and therefore a greater overall level of soluble NamH. However, this also reduced the purity of the PG and resulted in an altered muropeptide profile of wild type *E. coli* PG with poorer separation. This profile was found to be consistently altered and was used as a comparison for pET15b-*namH* mutanolysin digested PG; this demonstrated a shift in retention to the column as well as an altered muropeptide profile for pET15-*namH* PG.

3.4.3 MS TECHNIQUES TO ANALYSE GLYCOLYLATION

The third aim of this project was to develop assays to directly determine the presence of glycolylation within pET15b-*namH* expressing *E. coli* PG. LC-MS and MALDI-ToF were used to analyse lysozyme, mutanolysin and NH₄OH hydrolysed muropeptides from both pET15b BL21 and pET15b-*namH* BL21. The expected mass peaks for NGM and NAM were identified by LC-MS. Samples were then permethylated to generate a set of new specific peaks which could be identified by MALDI-ToF. The

calculated peaks for NGM permethylation at all six individual functional groups were observed. This fits with published data on PM, and was most likely a result of using NaOH as the base catalyst which has poor solubility in DMSO and causes an under-methylation (Price, 2008).

These findings indicated the presence of glycolylated muramic acid within pET15b-*namH* PG; however it is likely this was at a very low level as MALDI-ToF is a very sensitive technique. Consistently altered rp-HPLC muropeptide profiles however, were not achieved without increasing the protein expression time and no LC-MS muropeptide data showed glycolylated muropeptides. Therefore it is probable that the low level of soluble NamH resulted in a negligible amount of glycolylated PG.

3.4.4 RPF B RELEASED MUROPEPTIDES

The aim of this part of the project was to analyse muropeptides released from glycolylated and wild type *E. coli* as well as mycobacterial PG by recombinant *Mtb* RpfB. RpfB was chosen due to previously published work on the structure and function of this protein (Ruggiero et al., 2009). RpfB contains a unique G5 domain, which is a PG anchor allowing attachment and interaction with the PG (Ruggiero et al., 2009). It also, like the remaining *Mtb* Rpfs, has the conserved catalytic domain, with the conserved functional glutamine; essential for muralytic activity (Kana and Mizrahi, 2010). RpfB's high solubility and level of expression lent its use as a recombinant muralytic enzyme for the digestion of PG.

RpfB was successfully purified, as evidenced by SDS-PAGE. RpfB_{ΔDUF} has a calculated mass of 18.74 kDa, however as previous authors have shown (Ruggiero et al., 2009), this protein runs at a much higher molecular weight by SDS-PAGE and gel filtration (~40 kDa). The higher molecular weight band is most likely a dimer as both bands are muralytically active; as shown by zymography. The

aim was to use purified RpfB to generate muropeptide products from wild type and glycolylated *E. coli* PG as well as *M. smegmatis*. RpfB failed to produce consistent muropeptide profiles by rp-HPLC; there was poor reproducibility and extremely low absorbance of the peaks observed from all strains analysed.

As previous work has found, RpfB synergistically interacts with and cleaves PG with Rpf interacting protein A (RipA) (Both et al., 2011, Ruggiero et al., 2010, Chao et al., 2013). Therefore it is possible that in order to generate smaller muropeptide products, visible by rp-HPLC, RpfB may require the presence of RipA (or another protein or unknown compound) to synergistically degrade PG. Since use of RipA would have produced products which were not of interest to this project, this work was not undertaken. Recent work overexpressing full length *Mtb* RpfB into the periplasm of *E. coli* resulted in cell lysis, thereby indicating that RpfB is highly active on non-glycolylated PG and may not be adapted to digestion of glycolylated PG.

3.5 CONCLUSION

Using an adapted PG purification method pET15b-*namH* BL21 consistently produced altered muropeptide profiles by HPLC. MS peaks corresponding to that of N-glycolylated muramic acid were detected and PM of these resulted in MALDI-ToF data correlating with the mass peaks calculated for PM NGM. Whilst a classical PG purification method, yielding highly pure PG but using a short induction period, failed to reproducibly achieve altered muropeptide profiles.

After examining NamH protein expression the level of soluble protein was found to be low and therefore thought to result in a small proportion of glycolylated PG which can only be identified using an alternative PG purification method and mass spectrometry analysis. Recent work in the laboratory has shown *Mtb* Rpfs to be

active against wild type *E. coli* thus rendering the need to generate model mycobacterial PG less prudent.

3.6 FUTURE WORK

In order to achieve glycolylated PG a system expressing a higher level of soluble protein would be required. One possible way that this solubility issue could be overcome would be to try an alternative tag, such as glutathione-S-transferase (GST), thioredoxin (Trx), or N utilization substance A (NusA) which are suited to expressing soluble cytosol proteins (Novagen, 2003a). Another method to increase solubility would be to change the expression host to Origami™ B or Rosetta™ allowing a more adjustable expression level within all cells (Novagen, 2003a).

As previously discussed *rv3819* overlaps the gene coding region of *rv3818* by 3 nucleotides and has 32% sequence similarity to a NADH dehydrogenase subunit from *Rhodothermus marinus* DSM 4252. Therefore this gene could play a role in electron transfer necessary for NamH monooxygenase activity. A construct co-overexpressing both Rv3818 and Rv3819 was generated; this produced a high level of inclusion bodies as judged by microscopy. Therefore glycolylation may be achieved by optimisation of protein solubility using this construct. However, with recent work demonstrating *Mtb* Rpf activity in wild type *E. coli*, generation of a NamH overexpressing strain may not be necessary as analysis of Rpf muropeptide products could potentially be investigated using wild type *E. coli*.

CHAPTER 4: *MTB* RPFS ARE ABLE TO STIMULATE
GROWTH IN Δ *NAMH* *M. SMEGMATIS*

4.1 INTRODUCTION

As previously discussed Rpf proteins are muralytic enzymes, predicted to bind PG and cleave at the β -1,4 glycosidic bond within PG (Ruggiero et al., 2011). The proximity of this cleavage site to the structural N-glycolylation modification within muramic acid led to the hypothesis that Rpfs may be more efficient at recognising and digesting glycolylated PG.

This could be addressed using two alternative approaches: (1) studying peptidoglycan cleavage by recombinant Rpfs (discussed in Chapter 3) or (2) investigation of growth stimulation and resuscitation by Rpfs in mycobacterial strains producing glycolylated and non-glycolylated PG. It was previously established that over-expression of *M. luteus* Rpf in *M. smegmatis* resulted in reproducible and reliable growth stimulation and resuscitation (Shleeva et al., 2004, Mukamolova et al., 2006). A similar approach was therefore used in this chapter.

Mtb Rpfs should therefore behave in a similar manner and all five individual *Mtb* Rpfs were cloned in pMIND plasmids, containing a tetracycline (Tc) regulated promoter and Rpfs were expressed in *M. smegmatis*. It should be noted that *M. smegmatis* contains four endogenous Rpfs, therefore an empty pMIND WT control was used throughout. The growth stimulation ability of *Mtb* Rpfs in *M. smegmatis* was first established before the role of glycolylation in Rpf action was examined by a series of growth experiments using a *namH* *M. smegmatis* knockout mutant. *Mtb* Rpfs have previously been shown to result in resuscitation of non-culturable *Mtb* cells but have not been shown to elicit the same effect in *M. smegmatis* to date. Therefore the ability of the individual *Mtb* Rpfs to resuscitate non-culturable *M. smegmatis* cells was established before examination of their ability to resuscitate Δ *namH* *M. smegmatis* cells.

This chapter will focus on the role of individual *Mtb* Rpf s in *M. smegmatis* growth stimulation and resuscitation. Techniques covered are: protein expression, expression quantification and an *M. smegmatis* model for the production of Rpf-dependent cells. There are a variety of well-known techniques for confirmation of protein expression which are readily available. Many of these techniques rely on the use of an N- or C-terminal tag for antibody recognition. In this chapter enzyme-linked immunosorbant assays (ELISA) using anti-polyHis antibodies were employed. This was utilised to examine non-quantitative levels of secreted recombinant protein by measuring the absorbance of a colour change reaction. Expression at the RNA level was quantitatively determined by qRT-PCR. This was performed by assessing the level of fluorescence intensity as a result of SYBR® green binding to increasing levels of double stranded DNA (dsDNA) as the amplification cycles progress. Relative abundance or expression ratios were determined by comparison to an internal standard or housekeeping gene; 16S rRNA.

4.1.1 AIMS

An *M. smegmatis* Δ *namH* mutant was provided by Martin Pavelka and in order to investigate whether *Mtb* Rpf s stimulate growth and resuscitation of *M. smegmatis* and to study the importance of PG glycolylation for these stimulatory effects, the following was undertaken:

- All five *Mtb* Rpf s were over-expressed under a tetracycline induced promoter in both wild type and Δ *namH* *M. smegmatis*
- Over-expression of the individual Rpf s was confirmed at the RNA and protein levels
- Growth and resuscitation phenotypes of the strains were investigated

4.2 MATERIALS AND METHODS

The bacterial strains used in this chapter are shown below, in Table 8.

TABLE 8: BACTERIAL STRAINS USED IN THIS CHAPTER

Strain	Plasmid/Inducer	Source
<i>M. smegmatis</i> mc ² 155 pMIND	pMIND/Tc	This study
Δ <i>namH M. smegmatis</i> mc ² 155	N/A	M. Pavelka at University of Rochester
Δ <i>namH M. smegmatis</i> mc ² 155 pMIND	pMIND/Tc	This study
<i>M. smegmatis</i> mc ² 155 RpfA-pMIND	pMIND/Tc	This study
<i>M. smegmatis</i> mc ² 155 RpfB-pMIND	pMIND/Tc	This study
<i>M. smegmatis</i> mc ² 155 RpfC-pMIND	pMIND/Tc	This study
<i>M. smegmatis</i> mc ² 155 RpfD-pMIND	pMIND/Tc	This study
<i>M. smegmatis</i> mc ² 155 RpfE-pMIND	pMIND/Tc	This study
<i>M. smegmatis</i> mc ² 155 <i>M. luteus</i> Rpf-pMIND	pMIND/Tc	This study
<i>M. smegmatis</i> mc ² 155 RpfA-pMIND	pMIND/Tc	This study
<i>M. smegmatis</i> mc ² 155 RpfB-pMIND	pMIND/Tc	This study
Δ <i>namH M. smegmatis</i> mc ² 155 RpfC-pMIND	pMIND/Tc	This study
Δ <i>namH M. smegmatis</i> mc ² 155 RpfD-pMIND	pMIND/Tc	This study
Δ <i>namH M. smegmatis</i> mc ² 155 RpfE-pMIND	pMIND/Tc	This study
Δ <i>namH M. smegmatis</i> mc ² 155 <i>M. luteus</i> Rpf-pMIND	pMIND/Tc	This study

*All *Mtb* Rpf overexpressing strains were cloned both with and without an N-terminal His-tag (excluding Rpf C strains which do not contain a His-tag)

4.2.1 GENERATION OF OVEREXPRESSING STRAINS

All overexpressing strains were generated following the procedures outlined in Chapter 2. Inserts were confirmed by DNA sequencing. Once confirmed, purified DNA was used to electroporate the above plasmids (Table 8) into both wild type (WT) and Δ namH *M. smegmatis* strains (as described in Chapter 2). Screening and identification of successful transformants was carried out by diagnostic PCR. Plasmids were maintained using 50 μ g/ml kanamycin or hygromycin and induction was controlled by addition of 20ng/ml Tetracycline (Tc) to culture medium.

TABLE 9: PRIMER SEQUENCES AND THEIR CORRESPONDING PCR PRODUCT SIZE

Primer /Gene no	Amplicon (bp)	Primer sequences (5'-3')
RpfA/Rv0867c	1224	F:ATC <i>GGATCC</i> CGAGAGGAATTACCTAACGT ATGA R:CAC <i>ACTAGT</i> TCA <i>ACGCGT</i> GCCGATGACGT ACGGC
RpfB/Rv1009	1089	F:AGT <i>GGATCC</i> ATGTTGCGCCTGGTAGTCGG T GCG R:ATA <i>ACTAGT</i> TCA <i>ACGCGT</i> GCGCGCACCCG CTCGTGCAGC
RpfC/Rv1884c	531	F:AGT <i>GGATCC</i> GTGCATCCTTTGCCGGCCG ACCAC R:TAT <i>ACTAGT</i> TCACATATGGCGCGGAATAC TTGCCTGAAT
RpfD/Rv2389c	465	F:AGT <i>GGATCC</i> CAGCAAGGTGGAGCTGCTAT G R:CAT <i>ACTAGT</i> TCA <i>ACGCGT</i> ATCGTCCCTGCT CCCCGAACA
RpfE/Rv2450c	519	F:TCG <i>GGATCC</i> GCGAAAGGAACAACGTTGA AGAAC R:TGC <i>ACTAGT</i> TC <i>ACGCGT</i> GCCGCGGCGGC CGCAG
<i>M. luteus</i> Rpf	696	F: TGCC <i>GGATCC</i> GCCGATCAGCGAGGA R: GTC <i>ACTAGT</i> TCAGGCCTGCGGCAG
His-Myc	N/A	F: GCA <i>ACGCGT</i> GAACAAAACTCATCTCA R: GCG <i>ACTAGT</i> TAATCTGTATCAGGCGGA
pMIND	N/A	F: TGAGTCATAGTTGCACTTTATCAT R: TCCGAATCAATACGGTCGAGA

*Restriction sites are marked in italic and highlighted as follows: *Bam*HI (Red), *Spe*I (blue) and *Mlu*I (green).

4.2.2 CONFIRMATION AND QUANTITATION OF PROTEIN EXPRESSION

4.2.2.1 ENZYME-LINKED IMMUNOSORBANT ASSAYS

ELISA experiments were carried out using a method adapted from previously published work (Shleeva et al., 2004, Britton et al., 1985). An additional step of freeze-drying supernatant from late logarithmic phase or early stationary phase culture was carried out to increase protein concentration. Dried samples were

resuspended in 1ml PBS. Into 96 well plates 100 μ l of concentrated culture supernatant was loaded into triplicate wells per *M. smegmatis* strain. Serial dilutions were then carried out into sterile PBS. Plates were incubated overnight at 4°C before the removal of supernatants by pipetting.

Wells were then washed 3 times in PBS before blocking in 4% (w/v) milk for 4 hours at 4°C. Incubation in primary anti-polyHis (Sigma) or anti-Rpf (Mukamolova et al., 2002b) antibodies (1:3,000 dilution) was carried out overnight at 4°C in 2% (w/v) milk. 3 PBS washes were then carried out before incubation with secondary antibodies (anti-mouse or anti-sheep; both with alkaline phosphatase conjugates) (1:10,000) for 1 hour at room temperature with constant shaking. 3 washes with PBS were carried out before the addition of p-nitrophenyl phosphate (pNPP liquid, purchased from Sigma-Aldrich) to each well and incubation at room temperature (in the dark) was carried out for up to 20 minutes. The reaction was measured spectrophotometrically at 405nm, using a 680 Absorbance Microplate Reader (Bio-Rad).

4.2.2.2 MYCOBACTERIAL RNA EXTRACTION

This is a method based on work previously published (Mangan et al., 1997, Li et al., 2001). 10ml mid-log phase *M. smegmatis* cultures, grown in 7H9 medium, were collected by centrifugation (2000xg, 4°C for 20 minutes). Pellets were suspended in 200 μ l of RNase free H₂O and transferred to 2ml RNase free tubes (Camlab). 1ml of Trizol® reagent (Invitrogen) was then added to each tube with 0.1mm glass beads and inverted briefly. Cells were then lysed using a reciprocal shaker (Hybaid RiboLyser Homogenizer) for 2x 45 seconds at a 6.5 speed.

Tubes were incubated at room temperature for 10 minutes. 200 μ l of chloroform was added to each tube, inverted for 30 seconds, and incubated for 10 minutes at room temperature to allow phase separation. Tubes were centrifuged at 13,000 rpm at 4°C for 15 minutes. The aqueous phase was then transferred to a new microcentrifuge tube and re-extracted with an equal volume of chloroform (centrifugation was repeated). The aqueous phase was transferred to a fresh tube and nucleic acid precipitation performed through the addition of 0.8 volume isopropanol (briefly inverted) and incubated overnight at -20°C.

The nucleic acid extractions were centrifuged as above; the supernatants were removed by pipetting. 500 μ l cold 70% ethanol (EtOH) was used to wash the nucleic acid pellets, centrifugation was repeated and EtOH removed by pipetting. Tubes were re-spun briefly, any excess EtOH was removed and tubes were air dried at room temperature for 10 minutes. Pellets were resuspended in 100 μ l RNase free H₂O.

RNA samples were then cleaned up using the commercially available TURBO DNA-free™ kit (Invitrogen). 0.1 volume of 10x TURBO DNase buffer and 1 μ l TURBO DNase were added to the RNA samples and mixed. Samples were incubated at 37°C for 20-30 minutes. Resuspended DNase inactivation reagent (0.1 volume) was added and mixed, this was incubated at room temperature for 5 minutes. Tubes were centrifuged at 10,000xg for 90 seconds; supernatants containing RNA were transferred to fresh tubes. RNA concentration was measured using a Thermo Scientific NanoDrop™ 1000 machine by loading 1 μ l drops and measuring absorbance at 260nm.

4.2.2.3 REVERSE TRANSCRIPTION

cDNA synthesis was carried using the commercially available SuperScript™ II Reverse Transcriptase kit (Invitrogen).

The following reagents were added to a microcentrifuge tube:

50-250ng random primers

0.5 μ g total RNA

0.8mM dNTP mix

Sterile H₂O

The mixture was heated to 65°C for 5 minutes and chilled on ice. Tubes were briefly centrifuged and the following added:

1x First-strand buffer

0.01M DTT

Tubes were mixed briefly and incubated at room temperature for 2 minutes. 1 μ l (200 units) of SuperScript™ II RT was added and samples mixed by pipetting before incubating at room temperature for 10 minutes. Samples were then incubated at 42°C for 50 minutes and inactivated by heating at 70°C for 15 minutes. Samples were stored at -20°C.

4.2.2.4 qRT-PCR

TABLE 10: qRT-PCR PRIMER SEQUENCES AND AMPLICON SIZES

Primer Name	Amplicon Size (bp)	Primer Sequences (5'-3')
RpfA	152	F:CGGGTTATCGAACGCAACAC R:GGTCGTTAGCGGCAAGTTCC
RpfB	138	F:TCGGATCAAGAAGGTCACCG R:GCTACCGCGAACGTCACATC
RpfC	114	F:AGCTGCCTCTCGGGAACAA R:GACCACAGTGCGATCGGAAGG
RpfD	121	F:GCAACAGATCGAGGTCGCAG R:CGAGGAACGTCAGGATGTGG
RpfE	193	F:TGGCCTACAGCGTGAAGTGG R:GAACGCAGCACGTTCTCCAGC
16S rRNA	55	F:TCCGGGCCTTGTACACA R:TAACACCCGAAGCCAGTGG

Detection, using SYBR green® (ABgene) is in real-time as fluorescence is proportional to the increase in target; an amplification curve is generated throughout each PCR cycle (Figure 36).

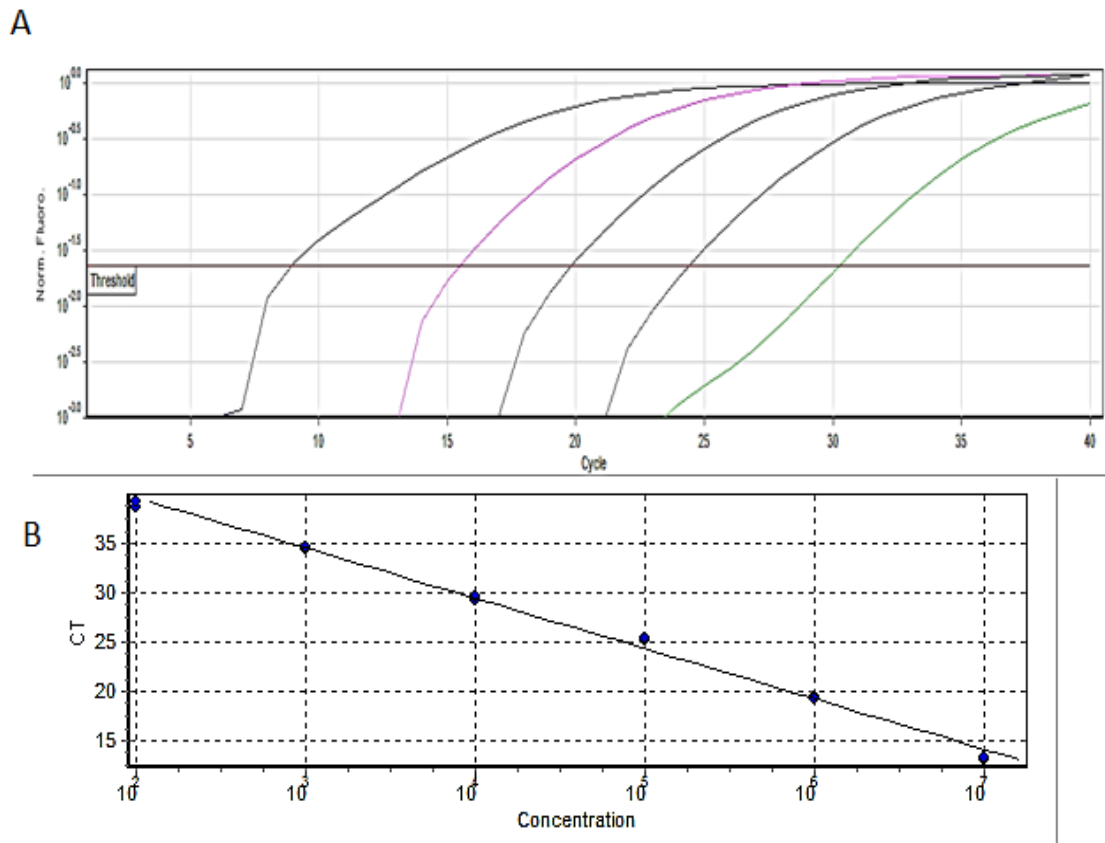


FIGURE 36: EXAMPLE OF AN AMPLIFICATION CYCLE (A) SHOWING FLUORESCENCE OUTPUT AND A STANDARD CURVE (B)

Figure 36 (A) displays the Log Fluorescence emitted from standard DNA samples plotted against the increasing cycle number as the PCR amplification reaction runs. DNA was serially diluted and each dilution ran in triplicate. (B) Shows a constructed standard curve using 16S rRNA qRT-PCR forward and reverse primers (Table 10) and serially diluted *Mtb* gDNA.

In Figure 36 (B) an example of a generated standard curve plot is shown. For each PCR run a standard curve was generated using serially diluted genomic DNA and gene specific primers. This allows the copy number to be calculated and used for quantification of gene specific expression. Therefore each standard

curve must have similar reaction efficiencies in each run in order to accurately compare samples (Heid et al., 1996). This amplification efficiency can be calculated automatically using Rotor-Gene 6000 Series software and is based on Equation 3 and Equation 4 (Pfaffl, 2004). There are indirect methods for calculating amplification efficiency, such as fitting the fluorescence data to mathematical models; however, this is not always ideal. SYBR® Green is not ideal for indirect calculations as it generates a higher background than other labelling methods which is ignored in direct methods (Stahlberg et al., 2004).

$$\text{EQUATION 3: EXPERIMENTAL AMPLIFICATION} = 10^{(-1/\text{SLOPE})}$$

$$\text{EQUATION 4: EFFICIENCY} = [10^{(-1/\text{SLOPE})}] - 1$$

Since SYBR® Green binds to any dsDNA present and is therefore non-specific; methods to overcome this were introduced. Firstly, specific primers used for the amplification of a sequence within a sample will result in a product consisting of a particular sequence and number of bases; hence by implementing a melting curve of the amplified product the specificity can be assessed. An ideal amplification curve should produce a clean, single peaked and reproducible melting curve (an example of which is shown in Figure 37) (Pfaffl, 2004).

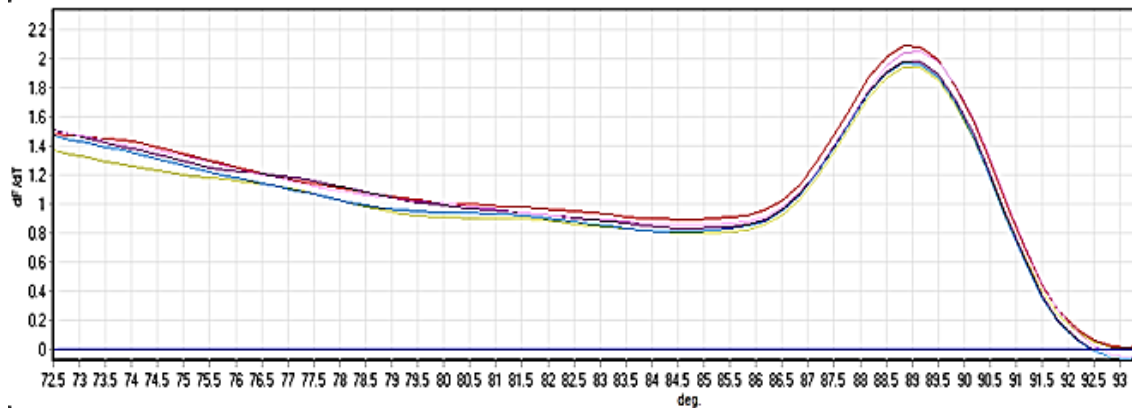


FIGURE 37: MELTING CURVES OF cDNA qPCR SAMPLES

Figure 37 shows the melting curves of several PCR amplification runs (using the same primers). Since the amplified product should be a single DNA sequence with a fixed number of bases the dissociation temperature should also be fixed. Standard melting curves, using genomic DNA should be identical to those of cDNA samples using the same primers.

Figure 37 demonstrates how melting curves of qRT-PCR cDNA samples, (amplified using the same primers) produce peaks at the same dissociation temperature as a genomic DNA control.

Absolute™ qRT-PCR SYBR® Green Mix (ABgene) was used for all qRT-PCR reactions. The following reagent mix was used for all qRT-PCR assays (total volume 25µl):

1x SYBR® Green Master-Mix
 0.07µM Forward primer
 0.07µM Reverse primer
 50ng Template cDNA
 +/- DMSO
 DNase and RNase free H₂O

For *Mtb* genomic DNA (gDNA) standards, serial dilutions in DNase and RNase free H₂O were made so that stocks could be prepared (from 1×10^7 to 1×10^1 gene copy number). 100ng of *Mtb* gDNA equals 2.25×10^8 gene copy number (4,000,000 base pair template), therefore 0.5µl of 100ng/µl gDNA diluted into 10µl gives a 1×10^7 stock which can then be serially diluted. This is based on the

average weight of a base pair (650 Da), 1 mole of base pairs equals 650g and therefore the molecular weight of the dsDNA template can be calculated, as shown in Equation 5.

$$\text{EQUATION 5: COPY NUMBER} = \frac{(\text{AMOUNT} * X 6.022 \times 10^{23})}{(\text{LENGTH} * X 1 \times 10^9 * X 650)}$$

*Where amount refers to the template (ng) and length refers to the size of the template (bp).

These stocks were then used in the above SYBR Green® reaction to generate standard curves for the quantification of gene specific expression levels. These were generated by plotting the threshold cycle (Ct), which correspond to the point at which the fluorescence threshold is reached during each cycle, against the corresponding number of gene copies; this process is automated by Rotor-gene 6000 software (Corbett).

All qRT-PCR cycles were performed using a Rotor-gene 6000 (Corbett). The following amplification cycle was implemented in all qRT-PCR runs:

95°C 15 minute hold (1 cycle)

95°C 10 seconds
55°C 15 seconds
72°C 20 seconds



X40 cycles

Melt conditions: 72°C-95°C, 1°C rise at each step.

Strips of 0.1ml Rotor-gene (Corbett Research, Qiagen) tubes were used for all reactions. All samples were run in triplicate. All runs contained a negative control with no template present. Controls using gDNA and gene of interest qRT-PCR primers were also performed.

4.2.2.5 CALCULATING MEAN EXPRESSION RATIOS

The relative expression or abundance of the individual *Mtb* RpfS was determined using the gene specific copy numbers obtained by

qRT-PCR and normalising these to the house-keeping gene encoding 16S rRNA. Sample cDNA and serially diluted *Mtb* gDNA was used to amplify 16S rRNA to normalise the sample to sample variation. The copy number of the gene of interest was divided by the 16S rRNA copy number to obtain the mean expression ratio.

4.2.3 GROWTH STUDIES

Growth studies were carried out using either 7H9 or Sauton's media (Chapter 2). Growth in 7H9, containing 50 μ g/ml kanamycin and supplemented with 0.05% (w/v) Tween 80, was performed in an automated Bioscreen C MBR plate reader (Thermo Fisher Scientific). To ensure a consistent inoculum was used throughout, all cultures were standardised to OD 1 before dilution to 10^{-1} . 10 μ l was used to inoculate 100 μ l of growth media containing 20ng/ml Tc in 100 well plates. Plates were then incubated at 37°C with continuous shaking. OD measurements at 600_{nm} were performed every 2 hours. Plates were incubated and read in a Bioscreen C MBR plate reader (Thermo Fisher Scientific).

Growth studies in Sauton's were performed using 10ml culture volumes over 7 days, samples were taken approximately every 10-24 hours. All cultures were standardised to OD 1 and a 50 μ l inoculum added to fresh Sauton's medium containing 20ng/ml Tc, 50 μ g/ml kanamycin and 0.05% (w/v) Tween 80. CFU measurements were taken for all cultures. Triple biological replicas were used in 3 independent experiments. OD measurements were taken manually and absorbance was measured at 600_{nm}. All cultures contained 20ng/ml Tc. The growth rate (h^{-1}) was calculated by plotting a log scale graph of linear growth, and generating an exponential line showing the equation of the line, in which the gradient equals the growth rate. All trend lines had an R^2 value of 0.99 and higher.

TABLE 11: DEFINITION OF TERMS

Term	Definition
Apparent lag phase (hours)	The time taken for the first OD doubling (determined as an OD of 0.2)
Final OD (600_{nm})	The highest OD reached during cell growth
Growth rate (h⁻¹)	The gradient of the slope during exponential growth

4.2.4 *M. smegmatis* NON-CULTURABILITY MODEL

The following protocol is based on a previously published method (Shleeva et al., 2004). Rich medium for the initial 5ml starter culture consisted of Broth E, containing (per litre): 5g peptone, 5g NaCl, 1.5g beef extract, 1.5g yeast extract supplemented with 0.05% (w/v) Tween 80 and 50µg/ml kanamycin. This was inoculated using *M. smegmatis* strains plated on LA 50µg/ml kanamycin plates. Once cultures had been grown for 48 hours, 330µl of this starter culture was then used to inoculate 50ml of a sub-optimal medium (modified Hartman's-deBont) mHdeB containing (per litre): 11.8g Na₂HPO₄.12H₂O, 1.7g citric acid, 20g (NH₄)₂SO₄, 30ml glycerol, 0.05% (w/v) Tween 80 plus 250µl of trace elements solution which contained (per litre): 1g EDTA, 10g MgCl₂.6H₂O, 0.1g CaCl₂.2H₂O, 0.04g CoCl₂.6H₂O, 0.1g MnCl₂.2H₂O, 0.02g Na₂MoO₄.2H₂O, 0.2g ZnSO₄.7H₂O, 0.02g CuSO₄.5H₂O and 0.5g FeSO₄.7H₂O. After 72-90 hours growth at 37°C, 200rpm shaking in 250ml glass flasks (with protrusions), 200µl undiluted culture was plated onto LA plates. Bacteria were classed non-culturable when they were unable to form colonies on solid media. Culture at this stage was used to prepare most probable number (MPN) assays.

4.2.5 MPN

MPN was carried out as previously described (Harris and Sommers, 1968). Using 48 well plates (Corning), 450 μ l of diluted Sautons medium (Chapter 2) containing 0.05% (w/v) yeast extract was aliquoted into all wells. Then, 50 μ l inoculum was added to the first row of wells before serial dilution within the plate was performed. After 2 weeks growth at 37°C the number of positive wells was recorded. Using an MPN calculator available at http://www.wiwiiss.fu-berlin.de/institute/iso/mitarbeiter/wilrich/MPN_ver2.xls, MPN counts were calculated and expressed as Log₁₀ values. Resuscitation index (RI) was calculated as follows: RI = Log₁₀ (MPN/CFU) as previously described (Mukamolova et al., 2010).

4.3 RESULTS

4.3.1 GENERATION OF *M. smegmatis* RPF-A-E OVEREXPRESSION STRAINS

Mtb Rpf over-expressing strains were generated in wild type and Δ *namH* *M. smegmatis*. *Mtb* Rpf *rpfA-E* genes were amplified by PCR using the gene specific primers shown in Table 9. The corresponding restriction enzymes shown in Table 9 (*Bam*HI and *Spe*I) were used to digest both purified PCR product and purified plasmid DNA prior to ligation and transformation into DH5 α . Several clones per transformation were used to inoculate small scale cultures, plasmid DNA was then purified and sent for sequencing and once confirmed to contain no mutations these constructs were used to generate His-tagged constructs for all Rpf constructs (excluding RpfC constructs).

This was performed by PCR using the primers His-Myc (shown in Table 9) to amplify DNA from pBAD_{gIII} plasmid DNA, PCR product was then purified and concentrated. His-Myc DNA was digested

with BamHI and MluI before ligation with similarly digested Rpf-pMIND plasmid DNA. Purified DNA was used to electroporate wild type and Δ *namH* electro-competent *M. smegmatis* cells. After 3 hours of incubation samples were plated on LA plates and resulting single colonies were picked and used directly for PCR, using pMIND primers (Table 9) to confirm the presence of corresponding *rpf* genes. The PCR products were analysed by DNA electrophoresis, as shown in Figure 38.

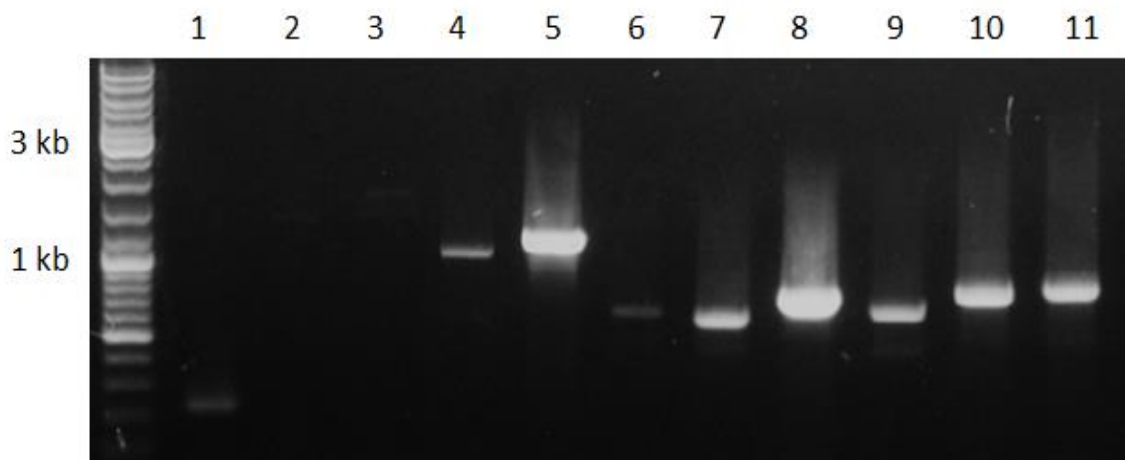


FIGURE 38: COLONY PCRS FROM *M. SMEGMATIS* RPF-pMIND STRAINS

Colony PCRs of the individual *Mtb* Rpf over-expressing strains (with or without His-tags) in wild type *M. smegmatis* were performed. The pMIND primers shown in Table 9 were used. From left to right: 1) empty pMIND control, 2) RpfA-pMIND, 3) RpfA_{His}-pMIND, 4) RpfB-pMIND, 5) RpfB_{His}-pMIND, 6) RpfC-pMIND, 7) RpfD-pMIND, 8) RpfD_{His}-pMIND, 9) RpfE-pMIND, 10) RpfE_{His}-pMIND and 11) *M. luteus* Rpf-pMIND. A DNA ladder is on the far left (GeneRuler™/Thermo Scientific).

Confirmation of successful electroporation, by colony PCR, for each Rpf strain in wild type *M. smegmatis* can be observed in the above figure. The same was carried out in Δ *namH* *M. smegmatis*. The calculated masses expected for each construct, using pMIND primers, are shown in Table 12.

TABLE 12: THE CALCULATED PCR PRODUCTS FOR EACH RPF CONSTRUCT

CONSTRUCT	SIZE OF PCR PRODUCT* (BP)	SIZE OF PCR PRODUCT +HIS (BP)	CONFIRMATION BY PCR
RPFA	1,448	1,591	YES
RPFB	1,312	1,433	YES
RPFC	733	N/A	YES
RPFD	682	820	YES
RPFE	707	845	YES
<i>M. LUTEUS</i> RPF	870	N/A	YES
pMIND	245	N/A	YES

*pMIND primers were used to calculate PCR products (Table 9).

From the calculated PCR products using pMIND primers shown in Table 12, and the observed bands of the individual Rpf clones (with or without His-tags) shown in Figure 38 it has been demonstrated that all strains have been confirmed. For example RpfB which without a His-tag, using pMIND primers was calculated to product a PCR product of 1.3kb shows a DNA band above the 1kb ladder marker whilst the His-tagged RpfB construct, predicted to have a product of 1.4kb has a DNA band above the 1.2kb band. Having confirmed the successful generation of each *M. smegmatis* Rpf strain, these clones could therefore be used for protein expression studies and characterisation.

4.3.2 PROTEIN EXPRESSION

4.3.2.1 ELISA

Protein expression of the individual *Mtb* Rpf overexpressing *M. smegmatis* strains was analysed by ELISA. This was carried out using different growth media, and bacteria were isolated during early stationary phase growth as previously described (Shleeva et al., 2004). Purified recombinant RpfB $_{\Delta$ DUF (containing a His-tag)

was run alongside culture supernatant samples as a positive control. Anti-His and anti-Rpf antibodies were both utilised for initial experiments, however owing to the presence of endogenous *M. smegmatis* Rpf proteins anti-Rpf antibodies produced a high background and anti-His antibodies were used for all subsequent protein expression studies.

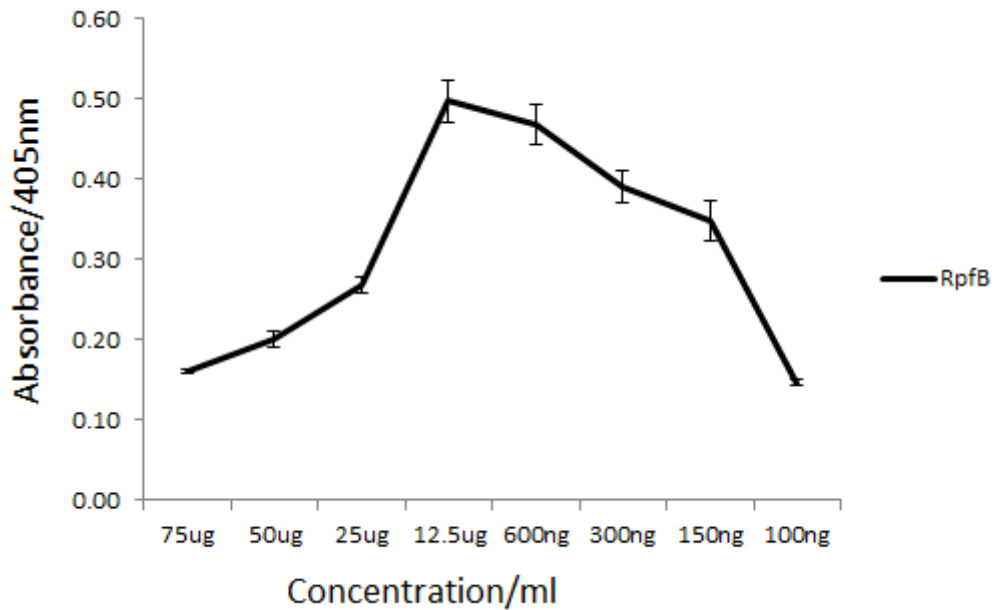


FIGURE 39: ANTI-POLYHIS ELISA ABSORBANCE DATA FOR RECOMBINANT *MTB* RPF Δ UF

Recombinant RpfB Δ DUF was serially diluted, aliquoted into 96 well plates and ELISA experiments using anti-polyHis antibodies were carried out. Once adhered to the well, washed, blocked and incubated with primary (anti-His, raised in mouse) and then secondary antibodies (anti-mouse) plates were exposed using pNPP and absorbance measured at 405nm in a microplate reader. RpfB was present in the following buffer: 25mM Tris HCl; 500mM NaCl; 20% glycerol pH 8.5.

Figure 39 shows ELISA, using anti-polyHis antibodies, absorption data for serially diluted recombinant RpfB Δ DUF. This data demonstrates a potential inhibition at high protein concentrations. This could be as a result of high buffer concentrations ultimately affecting protein adhesion to the well, or perhaps antibody

recognition. In an attempt to overcome this, RpfB was dialysed into 50mM sodium phosphate; pH 8 and ELISA experiments were repeated. This did not completely prevent the reduced absorbance at high protein concentrations as shown in Figure 40.

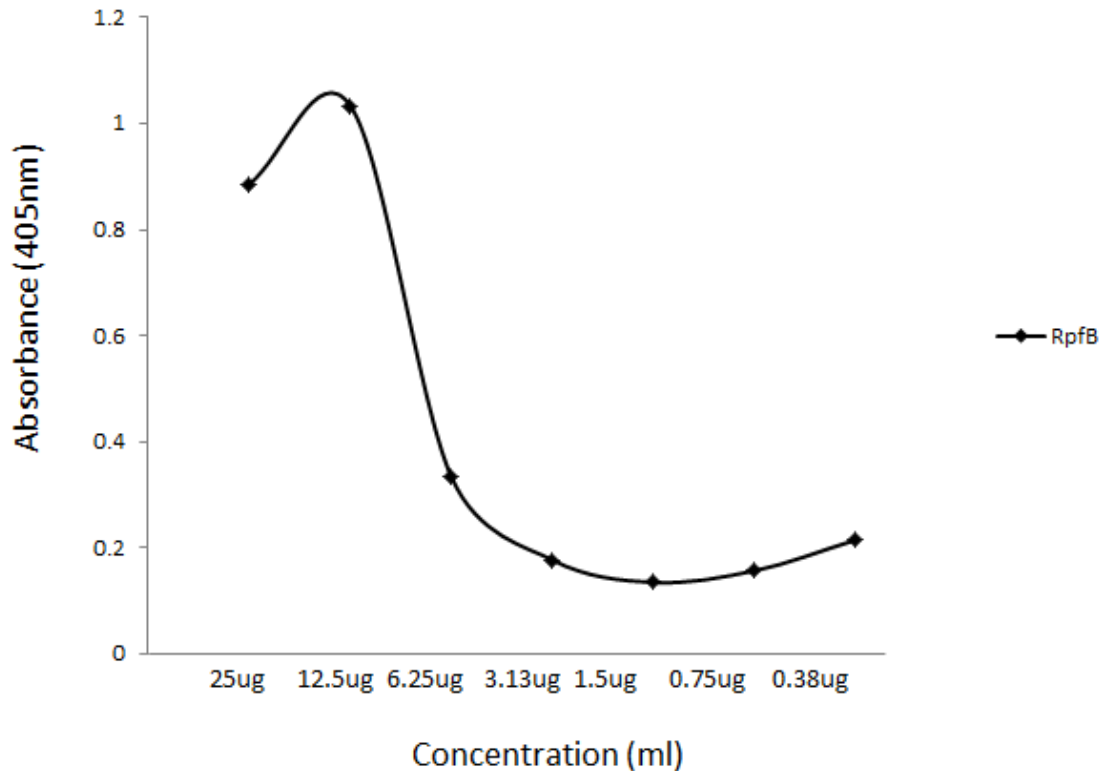


FIGURE 40: ELISA ABSORBANCE DATA USING ANTI-POLYHIS ANTIBODIES FOR DIALYSED RPF Δ DUF

Recombinant RpfB was dialysed into 50mM sodium phosphate; pH 8 and diluted in PBS before adding 100 μ l aliquots into 96 well plates at the shown concentrations. Once adhered to the well, washed, blocked and incubated with primary (anti-polyHis, raised in mouse) and then secondary antibodies (anti-mouse) plates were exposed using pNPP and absorbance measured at 405nm in a microplate reader.

Figure 40 demonstrates a similar pattern of absorbance at the higher concentrations as shown in Figure 39; a reduced absorbance. However, after dialysis into sodium phosphate buffer there is a general increase in absorbance: Figure 39 shows an absorbance of roughly 0.25 at 25 μ g/ml whilst Figure 40, after dialysis has an

absorbance >0.9 at the same concentration. Therefore whilst there was still a slight inhibition at the highest concentration after dialysis, the overall increase in absorbance indicates the previous buffer was disrupting protein adhesion or antibody recognition. Dialysed RpfB was hence used in subsequent experiments.

Concentrated culture supernatant samples could then be used in ELISA experiments, alongside diluted RpfB samples. Experiments using anti-polyHis antibodies were carried out for Rpfs A, B, D and E and the results are shown below in Figure 41.

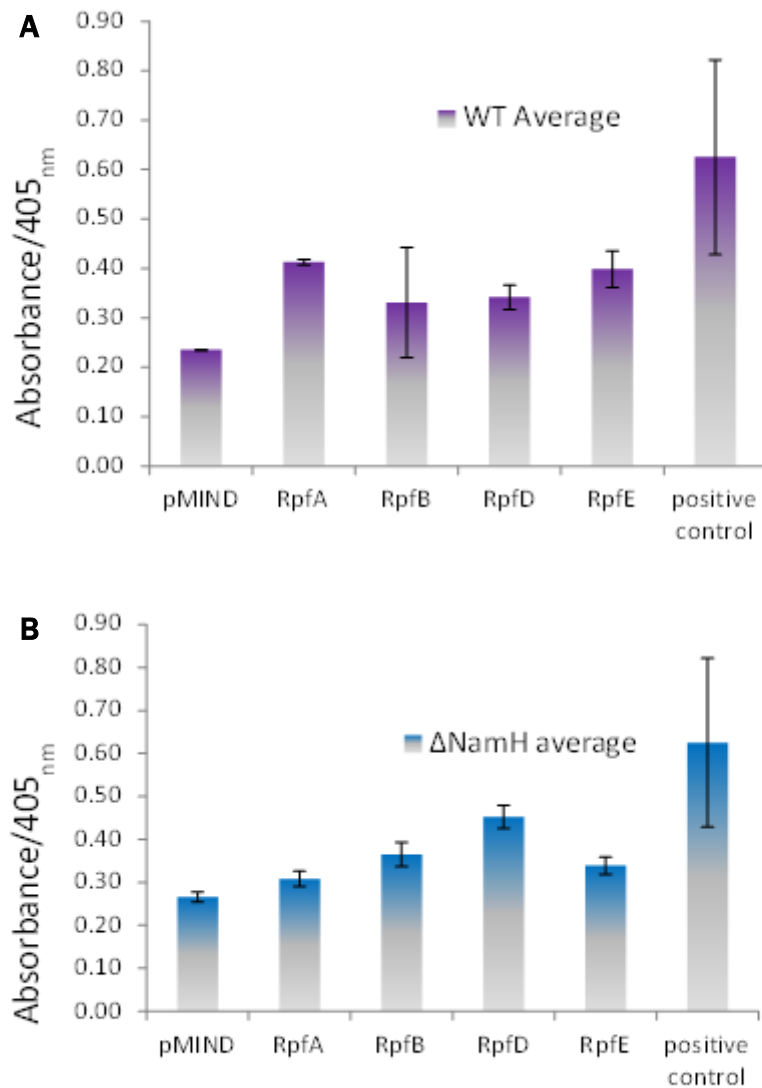


FIGURE 41: ELISA ABSORPTION DATA USING ANTI-POLYHIS ANTIBODIES OF *M. SMEGMATIS* STRAINS IN 7H9

Wild type *M. smegmatis* Rpf strains were grown in 7H9 medium (without ADC supplementation), and concentrated culture supernatants were used for ELISA experiments. The results are the average of triplicate biological replicas; the error bars show the standard deviation of the averaged absorbance. Figure 41 A) shows the results from wild type *M. smegmatis* Rpf over-expressing strains and B) from Δ *namH* *M. smegmatis* Rpf over-expressing strains. Absorbance was measured at 405nm.

Quantification of Rpf proteins by ELISA would require generation of standard curves for each individual Rpf. Due to time constraints this method was used solely to determine whether proteins were

expressed rather than the level of this expression. Figure 41 demonstrates that RpfA, B, D and E are expressed in both wild type and Δ *namH* *M. smegmatis* strains.

There is a different trend observed between the expression pattern of the individual RpfA as well as between wild type and Δ *namH* *M. smegmatis* strains. In Δ *namH* *M. smegmatis*, RpfD appears to have the greatest expression level with RpfA having the lowest level. In wild type this is reversed; RpfA has the greatest absorbance and RpfD the lowest. RpfB has a large error bar indicating the variable expression levels. It should also be taken into consideration that the expression levels analysed here correspond to secreted protein and therefore absorption data could reflect variations in this. Differences between wild type and Δ *namH* *M. smegmatis* Rpf secreted protein levels may be affected by the cell wall structure; perhaps affecting the level of protein bound to the cell wall and could reflect a difference in release from the cell wall.

The experiments shown in Figure 41 were also carried out in Sauton's medium, however due to viscosity issues the results observed were varied and of consistently poor absorption (data not shown). Additionally, anti-Rpf ELISAs were carried out for RpfC strains, as well as *M. luteus* Rpf overexpressing strains. There was a high background observed in control strains, most likely as a result of endogenous *M. smegmatis* Rpf proteins. Expression of *rpfA-E* genes was then examined by qRT-PCR.

4.3.2.2 qRT-PCR

qRT-PCR was implemented as a means of quantitatively determining the expression of all five *Mtb* Rpf genes.

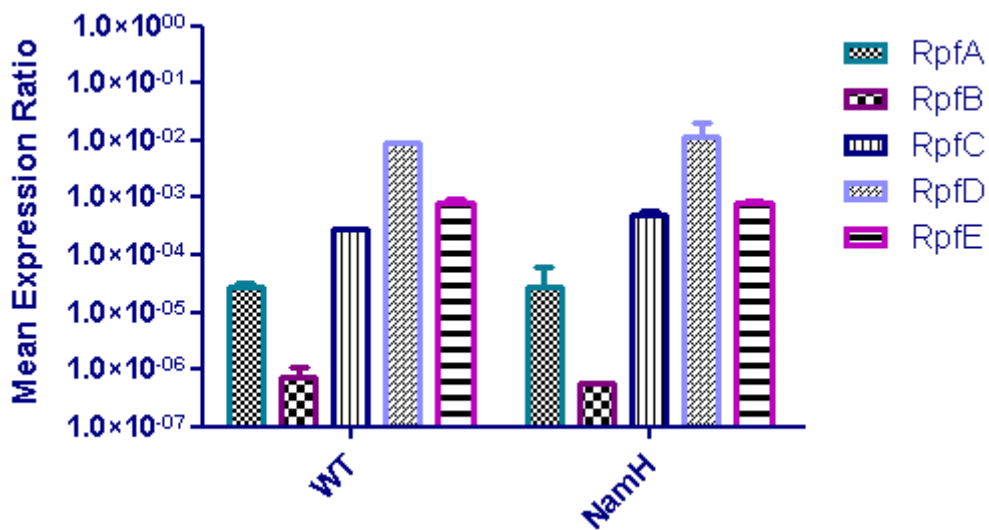


FIGURE 42: qRT-PCR MEAN EXPRESSION DATA

qRT-PCR was run on a Rotor-gene 6000 (Corbett) using cDNA samples of *M. smegmatis* Rpf strains, grown to mid-exponential phase in 7H9. The mean expression ratios were obtained by division of the copy number by 16S rRNA. Duplicate biological samples were run in triplicate, and the average is shown in the above figure. Error bars show the standard deviation. The corresponding copy numbers are shown in Table 13. All R^2 values were 0.98 or higher, reaction efficiencies were all 0.7 or higher excluding RpfA and B which were about 0.55.

qRT-PCR expression data for the individual *Mtb* Rpfs, shown in Figure 42, demonstrates that all Rpfs were expressed in both wild type and Δ *namH* *M. smegmatis*. Expression ratios were calculated as follows: copy numbers of the individual *Mtb* Rpfs were divided by copy numbers obtained for the house keeping gene 16S rRNA. All melt curves for each sample contained a single peak (shown in Appendix 2: qRT-PCR Melting Curves) and all were present at a specific dissociation temperature per primer set indicating specificity. Negative controls were carried out, whereby cDNA samples of the empty wild type and Δ *namH* *M. smegmatis* pMIND strains were run using primer sets for all *Mtb* Rpfs; they showed no amplification. Examination of contamination with plasmid DNA was easily examined by performing reverse transcription without the addition

of reverse transcriptase and including these samples as a control in each qRT-PCR run; no plasmid DNA was found.

The qRT-PCR data shows the same expression trend in both wild type and Δ namH *M. smegmatis*, with *rpfD* being the most highly expressed, followed by *rpfE* then *rpfC* and *rpfA*. *rpfB* has the lowest expression level. The low level of expression observed for both *rpfA* and *rpfB* could be due to the decreased reaction efficiencies compared to the remaining *rpf*s. Lower efficiencies could be a result of high GC content (73% and 68% in RpfA and B respectively), the presence of PCR inhibitory compounds or due to primer design. Overall there was no difference in Rpf gene expression pattern between wild type and Δ namH *M. smegmatis*.

TABLE 13: qRT-PCR COPY NUMBERS OF WILD TYPE AND Δ NAMH-PMIND *M. smegmatis* *MTB* RPF OVEREXPRESSING STRAINS AND THE CALCULATED MEAN EXPRESSION RATIOS

	Rpf	Copy Number	Mean Expression Ratio
WT	RpfA	24,089	2.74E-05
	RpfB	278	7.57E-07
	RpfC	98,354	2.78E-04
	RpfD	2,894,831	8.88E-03
	RpfE	223,146	8.25E-04
ΔNamH	RpfA	19,819	2.73E-05
	RpfB	251	5.57E-07
	RpfC	191,158	5.13E-04
	RpfD	3,617,065	1.17E-02
	RpfE	376,259	8.00E-04

The qRT-PCR expression pattern of the individual RpfS did not reflect those observed via ELISA; ELISA data indicates RpfA is the most highly expressed in wild type *M. smegmatis* whilst RpfD is

shown to be the most highly expressed in Δ *namH* *M. smegmatis*, qRT-PCR data meanwhile indicates *rpfD* as the most highly expressed in both (Figure 41). A potential explanation for this is that ELISA experiments assess levels of secreted protein whilst qRT-PCR estimates gene expression. Both methods demonstrated that all Rpf s were over-expressed in *M. smegmatis* but at different levels.

4.3.3 RPF GROWTH STIMULATION EXPERIMENTS

After confirmation of *Mtb* Rpf expression in all *M. smegmatis* strains the growth stimulatory activity of *Mtb* Rpf s against *M. smegmatis* was investigated prior to examination of the role of glycolylation in *Mtb* Rpf action. Growth analysis was performed using different cultivation media to examine the effects of *Mtb* Rpf over-expression on the growth of *M. smegmatis*.

4.3.3.1 7H9 MIDDLEBROOK MEDIUM

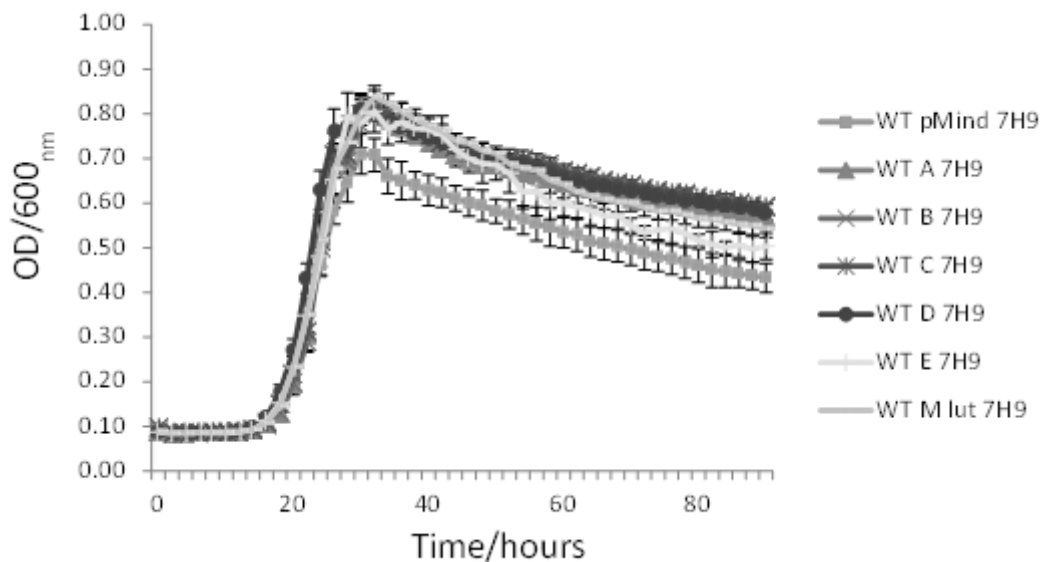


FIGURE 43: BIOSCREEN GROWTH CURVES OF *M. smegmatis* STRAINS IN 7H9

Wild type *M. smegmatis* strains over-expressing *Mtb* Rpf s were grown in 100 well microtitre plates (Oy Growth Curves AB Ltd) in a Bioscreen C MBR plate reader (Thermo Fisher Scientific) at 37°C with constant shaking, absorbance was measured at 600nm at 2

hour intervals for 4 days. Each well contained 100 μ l culture media (7H9, 20ng/ml Tc, 0.05% (w/v) Tween 80 and 50 μ g/ml kanamycin) inoculated with 10 μ l of each *M. smegmatis* strain which had been standardised to an OD_{600nm} of 1 and diluted 10⁻¹ prior to inoculation (CFU plates were prepared at this stage).

Figure 43 shows the Bioscreen growth data for wild type *M. smegmatis* Rpf over-expressing strains in 7H9 medium. The corresponding growth analysis is shown in Table 14.

TABLE 14: STATISTICAL ANALYSIS OF *M. SMEGMATIS* RPF STRAINS IN 7H9

Sample	Apparent lag phase/hours	Final OD	Growth Rate/h ⁻¹
pMIND	20 \pm 0.66	0.71	0.19
RpfA	20 \pm 0.88	0.82*	0.22*
RpfB	20 \pm 0.71	0.82*	0.21*
RpfC	18 \pm 0.88	0.81*	0.20*
RpfD	18 \pm 0.66	0.81*	0.19
RpfE	19 \pm 0.5	0.81*	0.18*
<i>M. luteus</i> Rpf	19 \pm 0.53	0.84*	0.19

*Statistically significant ($p < 0.05$ using an unpaired T-Test)

In Table 14 the apparent lag phase shows the time at which individual strains reached an OD of 0.2, whilst the p-value was calculated using a 2 tailed T-Test in Excel to determine whether the difference between the final OD of each strain compared to the pMIND control was statistically significant. P-values < 0.05 were classified as statistically significant. The overexpression of each *Mtb* Rpf resulted in a statistically significantly increased final OD compared to the control strain (Table 14).

Variations in the growth rate were also observed; Rpfs A, B and C resulted in an increase in the growth rate while RpfE had a slightly reduced growth rate. Rpfs D and *M. luteus* Rpf showed a growth rate consistent with the control strain. Examining the apparent lag phase indicates a slightly reduced lag phase in strains overexpressing RpfC and RpfD and to a lesser extent RpfE and *M.*

luteus Rpf. *Mtb* Rpfs were shown to stimulate growth in *M. smegmatis*.

After confirmation of *Mtb* Rpf growth stimulatory effects in *M. smegmatis* the ability of *Mtb* Rpf to stimulate growth in non-glycolylated PG containing Δ namH *M. smegmatis* was investigated. Rpf strains were analysed by growth in 7H9, in 100 well plates using a Bioscreen C MBR plate reader.

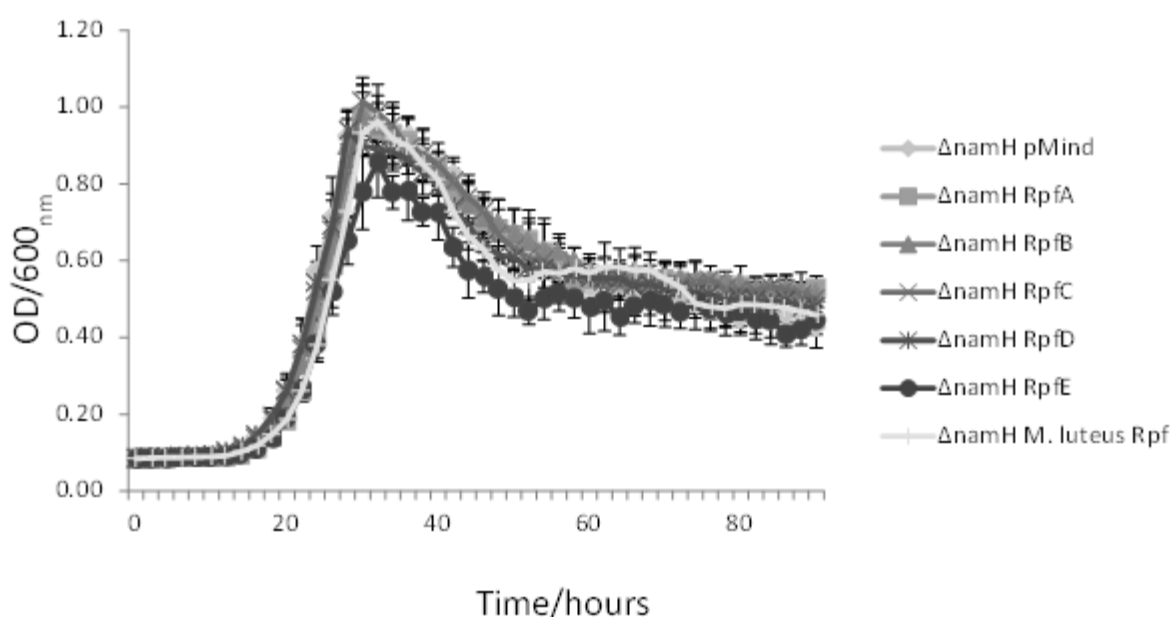


FIGURE 44: BIOSCREEN GROWTH CURVES OF Δ NAMH *M. SMEGMATIS* STRAINS IN 7H9

Δ namH *M. smegmatis* Rpf overexpressing strains were grown in 100 well microtitre plates (Oy Growth Curves AB Ltd) in a Bioscreen C MBR plate reader (Thermo Fisher Scientific) at 37°C with constant shaking, absorbance was measured at 600nm at 2 hour intervals for 4 days. Each well contained 100 μ l culture media (7H9, 20ng/ml Tc, 0.05% (w/v) Tween 80 and 50 μ g/ml kanamycin) inoculated with 10 μ l of each *M. smegmatis* strain which had been standardised to an OD_{600nm} of 1 and diluted 10⁻¹ prior to inoculation (CFU plates were prepared at this stage).

Growth data from curves shown in Figure 44 was then used for statistical analysis of individual *Mtb* Rpfs in Δ namH *M. smegmatis*.

Table 15: Statistical Analysis of Δ *namH* *M. smegmatis* Growth in 7H9

Rpf Strain (Δ <i>namH</i>)	Apparent lag phase/hours	Final OD	Growth Rate/h ⁻¹
pMIND	18±0.75	0.98	0.16
RpfA	20±0.74	0.98	0.18*
RpfB	19±0.33	0.98	0.17*
RpfC	18±0.71	1.02	0.15*
RpfD	18±0.82	0.94	0.16
RpfE	20±0.48	0.86*	0.15*
<i>M luteus</i> Rpf	20±0.55	0.96	0.17

*Statistically significant ($p < 0.05$ using an unpaired T-Test)

All values were calculated as described above. In contrast to the observations for the individual Rpf strains in wild type *M. smegmatis*, overexpression of *Mtb* Rpfs in Δ *namH* resulted in highly consistent final OD's for all strains. Excluding RpfE which has a statistically significantly reduced average final OD as determined by a type 2 unpaired t-test. There was an increase in growth rate observed for Δ *namH* *M. smegmatis* strains overexpressing RpfA, RpfB and *M. luteus* Rpf (Table 15) compared to the Δ *namH* pMIND control. RpfC and RpfE show a slightly reduced growth rate compared to the control strain. None of the *Mtb* Rpfs resulted in a reduced apparent lag phase.

Overall *Mtb* Rpfs A and B, did not reduce the apparent lag phase or increase the final OD but consistently produced a statistically significant increased growth rate and can therefore be said to stimulate Δ *namH* *M. smegmatis* growth in 7H9 medium. In order to examine these growth phenotypes further growth studies were performed in Sautons medium.

4.3.3.2 SAUTON'S MEDIUM

The reduced growth observed for Δ *namH* *M. smegmatis* in 7H9 was amplified when grown in Sautons medium; growth was not

observed till approximately 120 hours after inoculation (Figure 44). Wild type *M. smegmatis* strains also showed reduced growth in this medium compared to 7H9; growth was not observed till approximately 102 hours after inoculation (Figure 43). In addition to reduced growth rate, an increase in cell clumping (particularly within Δ *namH*) was observed, this meant that growth analysis using this medium did not produce reliable and consistent data in the small volume required for an automated plate reader. 10ml culture volumes were therefore used and hand measured via a spectrophotometer.

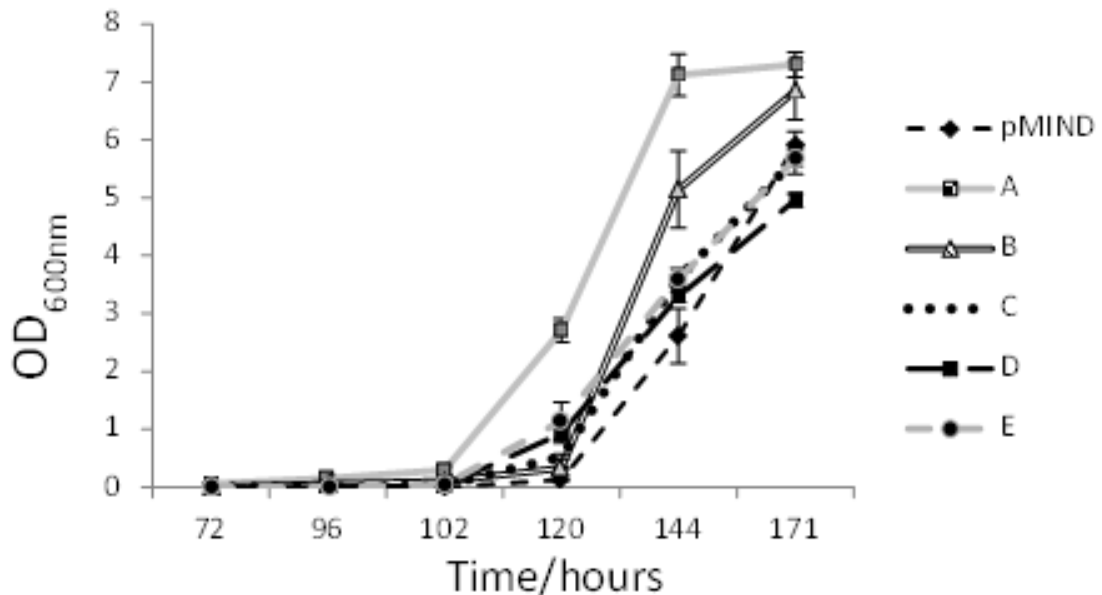


FIGURE 45: SAUTON'S GROWTH CURVES FOR *M. SMEGMATIS* RPF OVEREXPRESSING STRAINS

10ml cultures, using Sauton's medium were grown for over 7 days, samples were taken approximately every 10-24 hours. All cultures were inoculated with 50 μ l inoculum from *M. smegmatis* culture, standardised to OD 1. CFU measurements were taken for all cultures. Triple biological replicas were used in 3 independent experiments. OD measurements were taken manually and absorbance was measured at 600nm. All cultures contained 20ng/ml Tc.

When grown in Sauton's medium RpfA and RpfB (to a lesser extent) result in a curve indicating a reduced lag phase. The remaining strains were visually, highly similar in their growth patterns. Not enough data points were present to conclude accurate growth rates (R^2 values were all <0.9) or apparent lag phases. After 170 hours cultures began to visibly clump and due to sampling at different time points the volume remaining for further time points was vastly reduced, therefore final ODs were not obtained. Δ namH *M. smegmatis* Mtb Rpf strains were used under the exact same conditions in order to make a direct comparison.

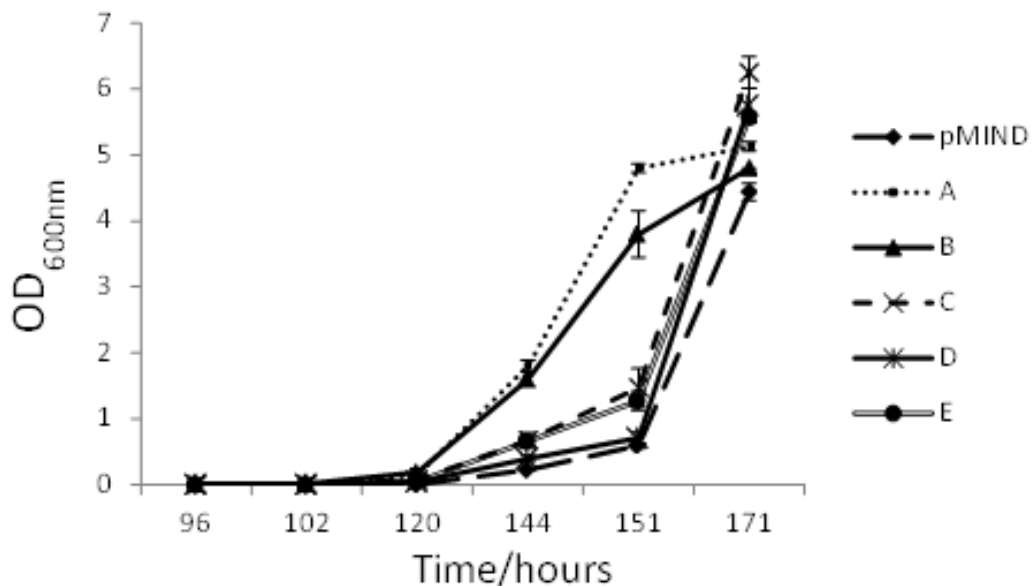


FIGURE 46: SAUTONS GROWTH CURVE DATA FOR Δ NAMH *M. SMEGMATIS* RPF STRAINS

10ml cultures, using Sautons medium were grown for over 7 days, samples were taken approximately every 10-24 hours. All cultures were inoculated with 50 μ l inoculum from *M. smegmatis* culture, standardised to OD 1. CFU measurements were taken for all cultures. Triple biological replicas were used in 3 independent experiments. OD measurements were taken manually and absorbance was measured at 600nm. All cultures contained 20ng/ml Tc for protein expression.

Δ *namH M. smegmatis* strains overexpressing RpfA and RpfB (Figure 46), when grown in Sauton's medium, result in visually increased growth rate compared to the Δ *namH* pMIND control. This pattern and the overall trend were mirrored in wild type *M. smegmatis* Sauton's growth data (Figure 45). This indicates the *Mtb* Rpfs were able to stimulate growth in both wild type and Δ *namH M. smegmatis* and fits well with the observed increase in growth rate when RpfA and RpfB were over-expressed in 7H9 medium (Table 15).

Δ *namH M. smegmatis*, when grown in Sauton's medium shows an increased lag phase for all strains compared to wild type strains in Sautons (Figure 45 and Figure 46), these results reflect those previously observed in 7H9 medium but to a greater extent (Table 15). The growth data generated (using both 7H9 and Sauton's media) demonstrated that glycolylation of mycobacterial PG did not play a role in Rpf growth stimulation. However, it remains to be determined whether this modification plays a role in resuscitation from dormancy.

4.3.4 DOES GLYCOLYLATION PLAY A ROLE IN RESUSCITATION OF RPF-DEPENDENT CELLS?

In order to investigate the effects of each individual *Mtb* Rpf on resuscitation of Rpf-dependent cells, an *M. smegmatis* non-culturability model (Shleeva et al., 2004) was implemented. This model uses a three stage growth process, culminating in 72-96 hours growth in sub-optimal growth medium (mHdeB). This produces bacteria which are no longer capable of colony formation or growth in liquid media. However, if these bacteria are supplied with exogenous Rpf (for example, in the form of culture supernatant) or possess a plasmid carrying *M. luteus* Rpf, they are able to resuscitate and grow in liquid media (Shleeva et al., 2004).

The first step was optimisation of the formation of non-culturable or Rpf-dependent cells. This was carried out using a negative and positive control for *M. smegmatis*: empty pMIND and *M. luteus* pMIND-Rpf strains. Hence, both strains should be able to form Rpf-dependent cells but only *M. luteus* pMIND-Rpf strain should be capable of spontaneous resuscitation. After 72 hours, growth was analysed by spreading 200 μ l of mHdeB grown culture onto LA plates (no antibiotic).

The absence of colonies after 3 days incubation demonstrated the non-culturability of both strains. Optimal conditions included a 48 hour pre-culture in Broth E (no antibiotic) followed by 72 hour growth in mHdeB medium for non-culturable cells to be formed. Resuscitation medium was then optimised; this was carried out by using a variety of resuscitation media and setting up MPN resuscitation plates. The medium producing the greatest MPN counts was then deemed most suitable for resuscitation. This was performed using both pMIND and *M. luteus* pMIND-Rpf *M. smegmatis* strains.



FIGURE 47: *M. SMEGMATIS* pMIND-*M. LUTEUS* RPF RESUSCITATION IN A VARIETY OF MEDIA

The figure shows the resuscitation of wild type *M. smegmatis* pMIND-*M. luteus* Rpf in a variety of media. Media from left to right: Diluted Sauton's (Sd) +tetracycline (Tc), Sd +yeast extract (YE)+Tc, Sd+ADC+YE+Tc, Sd+ADC+Tc, 7H9+ADC+Tc, Sd, Sd+YE and Sauton's+YE. The dilution factor is shown on the right (starting at 0 and ending at 10⁻⁵). 450µl of medium per well was inoculated with 50µl inoculum (cultures were grown for 72 hours in mHdB after an initial 48 hours growth in Broth E) and serial dilution was performed within the plate using 50µl volumes. *M. smegmatis* pMIND strain showed no growth in any of the media.

Figure 47 (2nd lane from the right) demonstrated that diluted Sauton's medium, containing 0.05% (w/v) yeast extract and without Tc, resulted in the greatest resuscitation. Growth was observed in 10⁻³ dilution. Growth was also observed in diluted Sautons -YE and Sautons -YE both without Tc. These three variations of Sautons medium produced growth to 10⁻²-10⁻³ and due to the greater turbidity observed in diluted Sautons +YE this was then used for all

subsequent resuscitation assays. *M. smegmatis* pMIND MPN plates (using the above media) produced no growth after 2 weeks of incubation, demonstrating that WT *M. smegmatis* endogenous Rpf do not result in resuscitation.

Using the optimised growth conditions and resuscitation medium, non-culturability and resuscitation was then performed for all wild type *M. smegmatis* Rpf overexpressing strains. The MPN values were then used to calculate $\text{Log}_{10}\text{MPN}$. MPN allows the use of positive and negative results to produce quantitative data by sample dilution, the degree at which this produces negative results can then be used to calculate the original concentration (Harris and Sommers, 1968).

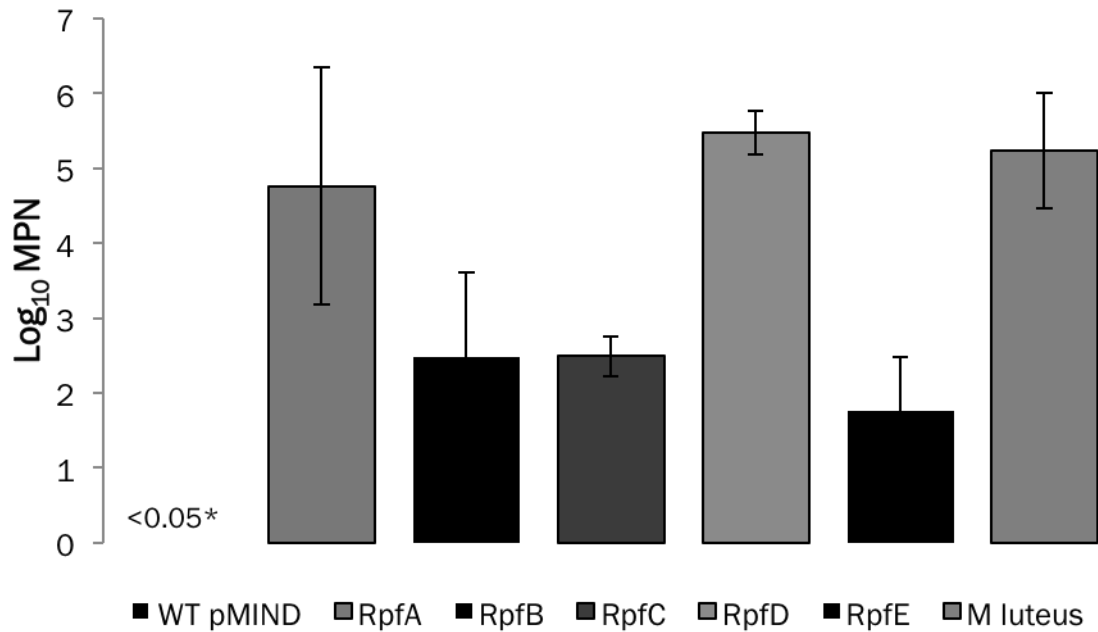


FIGURE 48: LOG₁₀ MPN RESUSCITATION DATA FOR WILD TYPE *M. SMEGMATIS* RPF STRAINS

Three independent experiments for each strain were performed; each containing triplicates per sample. The average Log₁₀ MPN values are shown here, the error bars show the standard deviation. *0.05 is the limit of detection (WT was below this limit and is therefore is shown as such). All MPN plates used diluted Sauton's medium supplemented with 0.05% (w/v) YE and were incubated, without shaking at 37°C for up to 2 weeks. All resuscitation data represent cultures which were non-culturable, determined as <10cells/ml when 200µl of undiluted culture was plated.

Figure 48 shows resuscitation of wild type *M. smegmatis* by all 5 individual *Mtb* Rpfs, the negative control (pMIND) shows no resuscitation. RpfD appears to have the greatest resuscitation potential, closely followed by the positive control; *M. luteus* Rpf. RpfB, RpfC and RpfE have relatively low resuscitation potentials compared to RpfD, as determined by MPN. Overall these data demonstrate the ability of *Mtb* Rpfs to resuscitate non-culturable *M. smegmatis* cells.

Having demonstrated this for all Rpfs in wild type *M. smegmatis* the resuscitation potential of the individual *Mtb* Rpfs within non-glycolylated *M. smegmatis* was attempted. However, after multiple

attempts to optimise formation of non-culturable cells in Δ namH *M. smegmatis* pMIND and *M. luteus* pMIND-Rpf (both pre-culture incubation and mHdeB incubation), it was determined that Δ namH *M. smegmatis* is incapable of forming of Rpf-dependent cells using the current method. This is demonstrated by the CFU and MPN data shown in Table 16.

TABLE 16: CFU AND LOG₁₀ MPN DATA IN WT AND Δ NAMH *M. smegmatis*

<i>M. smegmatis</i> Strain	Log ₁₀ CFU	Log ₁₀ MPN	Resuscitation Index (RI)
Δ namH-pMIND	4.95	5.7	0.75
Δ namH-pMIND- <i>M. luteus</i> Rpf	4.6	4.7	0.1
WT-pMIND	1*	N/A	N/A
WT-pMIND-RpfA	1*	4.8	3.8
WT-pMIND-RpfB	1*	2.5	1.5
WT-pMIND-RpfC	1*	2.5	1.5
WT-pMIND-RpfD	1*	5.5	4.5
WT-pMIND-RpfE	1*	1.8	0.8
WT-pMIND- <i>M.</i> <i>luteus</i> Rpf	1*	5.2	4.2

*This is an arbitrary value used to calculate RI due to CFU counts below the detection limit.

A possible explanation for Δ *namH M. smegmatis* being unable to form non-culturable cells using this model could be due to the increased clumping compared to wild type *M. smegmatis*, this could have resulted in cells which were protected from the environmental conditions during growth thus remaining culturable even after growth in sub-optimal medium.

4.4 DISCUSSION

4.4.1 GENERATION OF *MTB* RPF OVEREXPRESSION STRAINS IN *M. smegmatis*

A Δ *namH M. smegmatis* mutant was kindly provided by M. Pavelka (University of Rochester), previously published work using this strain demonstrated an increased susceptibility to β -lactam antibiotics as well as lysozyme (Raymond et al., 2005). This strain was generated by allelic exchange, using a suicide plasmid bearing a 500bp deletion allele, this was confirmed by Southern hybridisation (Raymond et al., 2005).

It was attempted to generate strains expressing the individual *Mtb* Rpf in Δ *namH M. smegmatis* alongside wild type *M. smegmatis*. This was achieved using the pMIND plasmid, which allowed tetracycline regulated gene expression (Blokpoel et al., 2005). Sequences were confirmed prior to electroporation and successful transformants were identified by PCR.

4.4.2 RPF EXPRESSION ANALYSIS

4.4.2.1 ENZYME-LINKED IMMUNOSORBANT ASSAY

Secreted *Mtb* Rpf protein expression was confirmed by ELISAs using anti-polyHis antibodies. This was evidenced by the absorption data shown in Figure 39. Initially there was notable inhibition at higher protein concentrations of recombinant RpfB Δ DUF possibly due to higher buffer concentrations affecting antibody

recognition, protein binding or substrate reactions; the latter appears to be the least likely due to the number of washes prior to this stage. In an effort to overcome this apparent inhibition, recombinant RpfB was dialysed into a sodium phosphate buffer. This produced a similar ELISA absorbance pattern at the highest concentration (25 μ g/ml) but overall showed an increase in absorption.

All His-tagged Rpf proteins in wild type *M. smegmatis* were found to be expressed, but at varying levels (Figure 41, a), this was also found to be true in Δ namH *M. smegmatis* (Figure 41, b). The secreted protein expression pattern, determined by ELISA, between the two strains differs; in wild type: Rpf A>E>D and RpfB is highly variable whilst in Δ namH *M. smegmatis* Rpf D>E>B and RpfA levels are relatively low. Quantification was not carried out by ELISA due to the time constraints necessary to generate standard curves for individual Rpfs.

As ELISA absorption levels are representative of secreted protein expression it was hypothesised that the difference in Rpf expression patterns between wild type and Δ namH *M. smegmatis* could be a consequence of an altered cell wall structure. Loss of glycolylated muramyl within PG may affect the overall cell wall structure and therefore could influence Rpf secretion. The loss of this functional group appeared to reduce Rpf secretion as demonstrated by ELISA data. Reduced secreted Rpf levels could be indicative of increased Rpf binding to the PG or reduced release of Rpf proteins from the cell wall.

However, RpfD has an increased level of expression compared to the remaining Rpfs. RpfD does not contain a predicted membrane anchor and high expression levels compared to RpfA, RpfB, RpfC and RpfE could indicate that secretion of this protein is affected to a lesser extent by the loss of glycolylation within the PG. qRT-PCR

was used to confirm RpfC expression, as well as to quantify *rpf* gene expression for the remaining Rpfs.

4.4.2.2 qRT-PCR

Gene expression was confirmed for all *Mtb* Rpfs by qRT-PCR, as demonstrated by the mean expression ratio data. Mean expression ratios were determined by comparison to the housekeeping gene: 16S rRNA. In mycobacterial gene expression work 16S rRNA is a common choice for normalisation (Talaat et al., 2002, Subbian et al., 2011). This gene has a relatively stable expression and is therefore suitable as an internal control for most qRT-PCR, however there are studies which demonstrate that under varying growth conditions 16S rRNA expression levels are no longer stable (Takle et al., 2007). Under the present experimental conditions 16S rRNA is a suitable reference gene as gene expression from bacteria grown under different growth conditions were not being compared.

The reliability of expression data was confirmed by carrying out controls. All cDNA samples produced single peaked melt curves, with each peak matching the corresponding dissociation temperature associated with the Rpf gene amplified. Using cDNA samples from the empty pMIND controls for both wild type and Δ *namH* *M. smegmatis*, Rpf primers were used to run qRT-PCR cycles. No amplification occurred in any of the runs.

The aim was to quantify the gene expression of all *Mtb* *rpf*s. This was evidenced by the Rpf qRT-PCR mean expression data which demonstrates that in both wild type and Δ *namH* *M. smegmatis* the pattern is identical; with the following trend: D>E>C>A>B. Expression of all Rpfs was relatively low, indicative of poor induction regulation by Tc, perhaps due to leaky expression of the pMIND system. The low ratios observed for RpfA and RpfB could

also be attributed to reduced reaction efficiencies, possibly as a result of a high GC content or due to primer design.

Comparison between ELISA and qRT-PCR expression indicated that glycolylation within mycobacterial PG may influence protein binding at the cell wall, and that Δ *namH* *M. smegmatis* displays a reduced level of secreted Rpf proteins in comparison to wild type overexpressing strains (Figure 41). This does not include RpfD, as discussed earlier; *Mtb* RpfD does not have an annotated PG anchor domain and therefore may not bind to the cell wall. RpfD has a predicted LytTR-type HTH domain and a signal sequence (Prosite, entry PS50930). LytTR is a type of DNA binding domain found in some cytoplasmic proteins (Nikolskaya and Galperin, 2002).

Overall the ELISA and qRT-PCR data, demonstrated expression of all 5 *Mtb* Rpfs. ELISA data depicts a varying expression pattern, with generally higher levels observed in wild type *M. smegmatis*, whilst qRT-PCR data showed an identical expression pattern in both wild type and Δ *namH* *M. smegmatis* strains. As stated above, the expression patterns may be influenced by several factors. ELISA sensitivity is limited by antibody recognition, whilst qRT-PCR is exponential and the initial limiting factor of the reaction should be the cDNA sample.

4.4.3 GROWTH STUDIES

4.4.3.1 7H9 MIDDLEBROOK MEDIUM

Growth analysis was employed to determine whether *Mtb* Rpfs are capable of stimulating growth in *M. smegmatis*. All *Mtb* Rpfs were found to stimulate growth in wild type *M. smegmatis* as evidenced by Figure 43. A clear trend was observed; all Rpf over-expressing strains appear to produce a higher final OD. Data analysis demonstrated a consistent and statistically significant increase in growth rate by RpfA, RpfB and RpfC (shown in Table 14). RpfA

showed the greatest change in growth rate; at $0.22/h^{-1}$ compared to $0.19/h^{-1}$ for pMIND (Table 14). The apparent lag phase data demonstrate that in wild type *M. smegmatis* RpfC, RpfD and RpfE resulted in the greatest reduction; 18 hours, compared to 20 hours observed in the pMIND strain (Table 14).

Growth characterisation was performed in Δ *namH M. smegmatis* *Mtb* Rpf strains in 7H9 to determine whether glycolylation plays a role in Rpf induced growth stimulation. Glycolylation does not influence Rpf induced growth stimulation, this was shown through the growth curves in Figure 44, and the corresponding statistical analysis in Table 15. None of the *Mtb* Rpfs produced a higher final OD in comparison to the Δ *namH M. smegmatis* pMIND control. Over-expression of RpfA resulted in an increased growth rate; $0.18/h^{-1}$ compared to $0.16/h^{-1}$ for the Δ *namH* pMIND control (Table 15). This was also observed for RpfB.

All together these findings indicate that *Mtb* Rpfs are capable of stimulating growth in wild type and Δ *namH M. smegmatis*. Therefore glycolylation of the mycobacterial PG did not appear to play a role in Rpf associated growth stimulation. RpfA and RpfB produced the greatest increase in growth rate in both wild type and Δ *namH M. smegmatis*. Previous work had demonstrated growth stimulation of growing cultures by Rpfs but *Mtb* Rpfs have not previously been shown to elicit the same response in *M. smegmatis* (Mukamolova et al., 2002b).

4.4.3.2 SAUTON'S

In order to investigate the effect of *Mtb* Rpfs on *M. smegmatis* in an environment where Rpf stimulation would be more advantageous growth analysis in Sauton's medium was carried out. The aim of this experiment was to examine the effects of Rpf on wild type and Δ *namH M. smegmatis* when Rpf stimulation may be more beneficial, and hence any growth alteration should be more

evident. Due to the reduced growth rate and increased clumping, cultures could not be grown in the 100 well plates necessary for Bioscreen analysis, therefore 10ml cultures were hand measured. Whilst each experiment contained replicas and several independent experiments were performed, the lack of data points and large replica numbers prevented detailed statistical analysis.

RpfA and RpfB appear to alter the growth characteristics more significantly than the remaining *Mtb* Rpfs. RpfA, in both wild type and Δ *namH* *M. smegmatis* resulted in a curve with a visibly reduced lag phase and potentially an increased growth rate (as determined by visual examination of Figure 45 and Figure 46). This fits well with the 7H9 observations of RpfA, which consistently showed an increased growth rate.

Overall when *M. smegmatis* was grown in Sautons medium RpfA and RpfB were found to stimulate growth in early log phase and potentially reduce the lag phase as well as increase the growth rate. These results are independent of the presence of N-glycolylation and correlate well with the 7H9 growth data, all of which led to the conclusion that Rpf growth stimulation is not affected by glycolylation of the cell wall. Glycolylation may therefore instead play a role in intracellular survival, antimicrobial resistance or immune response (Raymond et al., 2005, Coulombe et al., 2009).

Additionally, by comparing the growth stimulation assays with the protein quantification data it can be concluded that Rpf growth stimulation (both in wild type and Δ *namH* *M. smegmatis*) is not reflective of protein expression levels. RpfB is the most poorly expressed protein (by qRT-PCR, Figure 42), yet when wild type and Δ *namH* *M. smegmatis* strains over-expressing RpfB are grown in either Sauton's or 7H9 medium this resulted in an increased growth rate to a greater extent than the most highly expressed protein; RpfD (Figure 45 and Figure 46). However these results could be

influenced by poor reaction efficiency of RpfB in qRT-PCR, most likely due to primer design or they could be a result of the distinctive functions of the different Rpf proteins.

4.4.4 RESUSCITATION OF NON-CULTURABLE CELLS

An *M. smegmatis* non-culturability model (Shleevea et al., 2004) was implemented in order to investigate the resuscitation potential of the individual *Mtb* Rpfs, as well as to determine the role of glycolylation in Rpf induced mycobacterial resuscitation. This was determined by quantification of the number of viable cells by MPN in liquid medium. Optimisation of the formation of Rpf-dependent cells was carried out before assessment of resuscitation media. All wild type *M. smegmatis* strains were used to examine the resuscitation potential of the individual *Mtb* Rpfs in *M. smegmatis* by MPN. The MPN data showed that RpfD followed by RpfA produce the greatest levels of resuscitation. RpfB, RpfC and RpfE all produced much lower levels of resuscitation. RpfD Log₁₀ MPN values were comparable to those of *M. luteus* Rpf (Figure 48). The resuscitation data did not correlate with the qRT-PCR expression data and therefore indicated that MPN values represent the individual Rpf resuscitation potential; RpfE had relatively high expression levels, as did RpfC (by qRT-PCR, Figure 42), yet their MPN values were up-to 3.6 fold lower than those observed for RpfD (Figure 48).

Optimisation of Rpf-dependent cell formation for Δ *namH* *M. smegmatis* failed to produce fully non-culturable or Rpf-dependent cultures under any conditions (Table 16). This could have been due to a weakened cell wall structure as a result of reduced hydrogen bonding, which may prevent structural changes necessary for the formation of these cells (Raymond et al., 2005). Or alternatively, due to the increased clumping in Δ *namH* *M. smegmatis*, cells within these clumps may have been present in a micro-environment,

shielded from the harsh growth environment of the mHdeB medium and thus a proportion of cells remained culturable. This model of non-culturability was highly variable and produced cultures which remained culturable after incubation or cells which failed to resuscitate and were therefore no longer viable. These findings suggest that this model did not fully replicate *in vivo* NRP but may ultimately lead to cell death, the timing of isolation for resuscitation when cells are no longer culturable but remain viable was therefore extremely critical.

Overall RpfA produced the greatest growth stimulation as determined by increased growth rate; this was observed for both wild type and Δ *namH* *M. smegmatis* strains whether grown in Sauton's or 7H9 medium. RpfD produced the greatest level of resuscitation in non-culturable cells and qRT-PCR expression levels of this protein were also found to be higher than the remaining Rpfs. However, resuscitation patterns did not correspond to gene expression for the remaining Rpfs.

4.5 CONCLUSION

The overall aim of this chapter was to investigate the role of glycolylation in Rpf-associated growth stimulation and resuscitation. Individual *Mtb* Rpf overexpressing strains were generated in wild type and Δ *namH* *M. smegmatis*, expression was then confirmed and quantified by ELISA and qRT-PCR. Growth analysis demonstrated that over-expression of *Mtb* RpfA and RpfB in wild type and Δ *namH* *M. smegmatis* resulted in an increased growth rate when grown in either Sauton's or 7H9 media. This demonstrated that glycolylation of mycobacterial PG did not play a role in Rpf-associated growth stimulation. Rpf induced Δ *namH* *M. smegmatis* resuscitation data could not be produced due to the inability of this strain to form Rpf-dependent cells. However, MPN values for wild type *M. smegmatis* strains showed variability in

individual Rpf resuscitation potential, indicating the diversity of the different proteins. *Mtb* RpfA showed the greatest growth stimulation in both wild type and Δ *namH* *M. smegmatis* whilst RpfD had the greatest resuscitation index.

CHAPTER 5:
GENERATION AND PHENOTYPIC CHARACTERISATION OF
MYCOBACTERIUM TUBERCULOSIS *NAMH* DELETION
MUTANT

5.1 INTRODUCTION

This chapter describes the generation of a *namH* deletion mutant in *Mycobacterium tuberculosis* ($\Delta namH$), to investigate the role of PG N-glycolylation in *Mtb* intracellular survival and antimicrobial killing.

5.1.1 GENERATION OF AN *MTB* KNOCKOUT MUTANT

Historically, generation of defined mutants within mycobacteria has been problematic. This was due to a lack of genetic transfer systems, one of the first breakthroughs using allelic exchange allowed insertional inactivation of a leucine biosynthetic gene (Balasubramanian et al., 1996). Another notable achievement in this area was the use of transposon mutagenesis; using a temperature sensitive plasmid containing a transposon an *M. smegmatis* strain containing multiple insertional mutations was generated (Guilhot et al., 1994).

The methodology developed by Parish and Stoker (Parish and Stoker, 2000) allows the construction of unmarked deletion mutants in mycobacteria, resulting in knockout strains without the presence of antibiotic resistance markers. This technique is more advantageous than generation of marked deletion mutations as it minimises possible polar effects and influence of antibiotic resistance markers.

The method is based on homologous recombination and requires cloning of flanking regions of a gene of interest and their assembly in a suicide vector. Homologous recombination allows genetic recombination of similar or identical DNA sequences, whilst use of a suicide vector prevents replication within mycobacteria. Single and double cross-overs refer to the number of recombination

events; hence a single cross-over has had only one and double cross-overs have had two. This method, uses a suicide plasmid to deliver the recombination substrate to the cell, these plasmids do not contain a mycobacterial origin of replication and thus cannot replicate in *Mtb*. This method allows relatively straight forward generation of unmarked double cross-over mutants in mycobacteria (Parish and Stoker, 2000).

The flanking regions of *namH* (*rv3817* and *rv3819*, respectively) were amplified and the restriction sites shown in Figure 49 were introduced in order to generate the $\Delta namH$ mutant. Also shown in this figure is the operon Rv3818-3819 and the fragments used to generate the knockout mutant (fragment one (FR1) and fragment 2 (FR2), upstream and downstream of *namH* respectively). As depicted in Figure 50, each fragment was initially cloned into separate vectors.

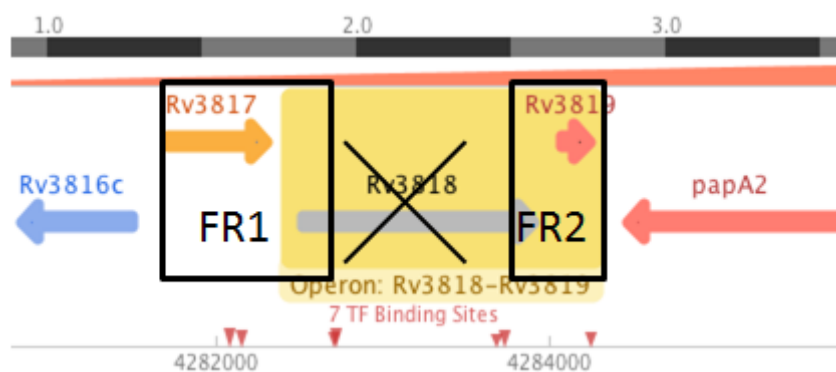


FIGURE 49: $\Delta NAMH$ KNOCKOUT CONSTRUCT STRUCTURE

Each fragment was initially cloned into separate plasmids using the restriction enzymes shown above. Each fragment overlapped *namH* by approximately 100 base pairs. Operon information was adapted from TBDB (Reddy et al., 2009).

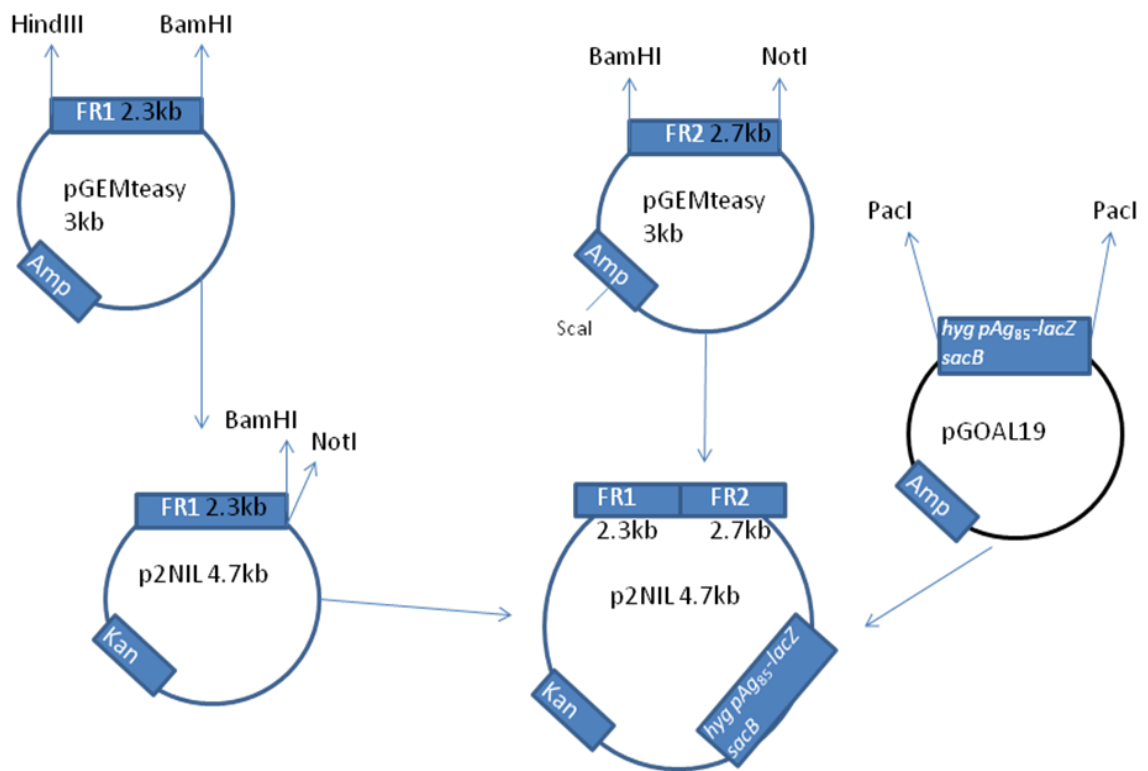


FIGURE 50: SCHEMATIC SHOWING GENERATION OF AN *MTB* Δ *NAMH* MUTANT

The schematic shows the molecular biology required for construction of screening vectors, manipulation vectors and insertion of the PACI cassette from pGOAL19, including the restriction enzymes and antibiotic resistance needed for each step.

Figure 50 provides a general schematic of the processes involved in the construction for a Δ *namH* *MtB* mutant. The construct was confirmed by multiple restriction digests and analysed by gel electrophoresis

5.1.2 SOUTHERN HYBRIDISATION

Southern hybridisation is commonly used alongside PCR for analysing DNA fragments and confirmation of gene deletion. Digoxigenin (DIG, a steroid which is not present in DNA) is widely used for labelling of DNA probes, enabling hybridisation and detection through immunological enzymatic reactions using specific anti-DIG antibodies (Holtke and Kessler, 1990). Use of radioactive

probes was once commonplace in this field, however since the introduction of DIG labelling technology this has eliminated the need for this (Holtke and Kessler, 1990). Other methods originally employed, used biotin or allylamino labels; however they had certain limitations related to specificity and efficiency of labelling (Theissen et al., 1989, Langer et al., 1981).

DIG labelling is a highly specific and sensitive technique with a wide spectrum of applications, including colony and *in situ* hybridisations (Holtke et al., 1990, Kessler et al., 1990). Commercially available kits, such as DIG High Prime DNA Labelling and Detection Starter Kit I (Roche) allow straight forward, rapid results and are highly sensitive. This kit uses random priming which is advantageous; however it is more suited to higher DNA concentration. Exposure and detection is performed by the addition of NBT/BCIP, supplied with the kit. Other methods are available for instances where only low DNA concentrations are available. The combination of this technique with PCR allows reliable and conclusive DNA analysis.

5.1.3 *MTB*; INTRACELLULAR SURVIVAL AND REPLICATION

As mentioned in the introduction *Mtb* is able to replicate in macrophages but the current understanding of the mitigating factors governing the development of tuberculosis is incomplete. Frequently used model systems for *Mtb* infection, excluding animal studies, are macrophages. Initially it was assumed that activated macrophages were capable of killing *Mtb*; however this was difficult to demonstrate *in vitro* (Fenton and Vermeulen, 1996). If killing was possible then it could be postulated that this would be a result of species such as reactive oxygen or reactive nitrogen intermediates present within phagolysosomes. Several studies, using activated murine macrophages demonstrated mycobacterial

growth inhibition directly related to the generation of reactive nitrogen intermediates (Chan et al., 1992, Denis, 1991).

Mycobacteria as well as host genotypes have been found to affect the development of tuberculosis, therefore macrophage infection studies can be a useful means of assessing intracellular survival for different *Mtb* strains (Caws et al., 2008). No single system will replicate the *in vivo* setting of *Mtb* infection and therefore there is no standard system as a method for infection studies. Whilst macrophage infection studies are useful in analysing bacterial survival intracellularly, they do not provide data regarding host interactions, disease progression and pathogenesis. However, animal models also have their draw backs; firstly costs, which will be high, and secondly different animal models are more suited to different aspects of tuberculosis pathogenesis (Parrish et al., 1998). Therefore, taking into consideration all methods, advantages and drawbacks initial studies were carried out using a macrophage model.

Both primary and cell line macrophages are used in infection studies, primary cells are isolated directly from tissues and cell lines are primary cells which have been passaged. Passaged macrophages become more homogenous and are more commonly used due to their low cost, ease of use as well as being readily available (Kaur and Dufour, 2012). However, they also have drawbacks; serial passage can lead to variations in phenotypic and genotypic profiles (Kaur and Dufour, 2012).

IFN- γ production leads to macrophage activation and activated macrophages have been shown to produce reactive nitrogen intermediates and reactive oxygen species in murine infection studies, this can be replicated *in vitro* by exposure to IFN- γ (Manganelli et al., 2001, Chan et al., 1992). *Mtb* replicates well in unactivated macrophages and as a result, uninfected macrophages

have been used as a model of initial TB infection in previous studies (Bodnar et al., 2001, Rengarajan et al., 2005)

5.1.4 *MTB* DRUG SUSCEPTIBILITY

As previously discussed there are four front-line anti-tuberculosis drugs currently in use. These are: Rifampicin (Rif), Pyrazinamide (PZA), Isoniazid (INZ) and Ethambutol (EMB), targeting; DNA replication, *trans*-translation, and cell wall synthesis (respectively). Minimum inhibitory concentration is the lowest concentration of a drug that will prevent detectable growth of a microorganism. The minimum inhibitory concentrations (MICs) for the drugs list above are:

TABLE 17: MICs OF THE FRONT-LINE ANTI-TUBERCULOSIS DRUGS

	MIC mg/L
RIF¹	0.25
EMB¹	1-2
INZ¹	0.1
PZA²	50-100
Strep³	2

¹(Banfi et al., 2003), ²(Zhang and Mitchison, 2003), ³(Suo et al., 1988)

Antimicrobial killing assays examined the susceptibility of mycobacteria to a variety of drugs by determining the percentage killed. By using a combination of drugs and assessing antimicrobial killing upon different *Mtb* strains, any variations between strains could provide genotypic data on *Mtb* survival.

5.1.5 AIMS

To understand the biological role of N-glycolylation in *Mtb* replication and antimicrobial tolerance the following objectives were undertaken:

- To generate a $\Delta namH$ *Mtb* mutant
- To characterise $\Delta namH$ *Mtb* growth *in vitro* and in cultured macrophages
- To compare antimicrobial killing of wild type and $\Delta namH$ *Mtb*

5.2 MATERIALS AND METHODS

5.2.1 BACTERIAL STRAINS

The bacterial strains used in this chapter are shown below.

TABLE 18: BACTERIAL STRAINS

Strain	Description	Source
<i>Mycobacterium tuberculosis</i> H37Rv	Laboratory strain	Laboratory stock
<i>Mycobacterium tuberculosis</i> H37Rv Δ <i>namH</i>	Laboratory strain with a <i>namH</i> deletion	This study
<i>Mycobacterium tuberculosis</i> H37Rv Δ <i>namH</i> pRBexint- <i>namH</i>	Complementation strain of <i>namH</i> deletion	This study

TABLE 19: PRIMERS SEQUENCES AND THE RESULTING AMPLICON SIZES

Primer	Amplicon Size (kb)	Sequence
FR1 (<i>rv3817</i>)	2.3	F:CCAC <i>AAGCTT</i> GTATTCTCCTTCACCTCTCA R:CAC <i>GGATCC</i> TGCGTGACCAACGCTTGTGAC
FR2 (<i>rv3819</i>)	2.7	F:ACAGCA <i>GGATCC</i> AGTTCACGGCCATGAATGCAGT TCT R:CAATCTA <i>GCGGCCGCT</i> TAGGCAAGCCCGCCGCC GC
FR1check	N/A	ATGGGCTCGCTGAGCGCGGGCGC
FR2check	N/A	ACCGGCACGGTGATCGGCACCA
<i>namH</i> test	0.5	F:ATGAGCGGCGTGCCAAGCTGG R:ACGAATGATAGCGGCGCAGCGT
<i>namH</i>	1.5	F:CGAAAGCTCGAGGTGCAGGTCACAAGCGTTGGT R:CGTAGAGGATCCTCATGGCCGTGAACTGCGTAG

*Inserted restriction sites are shown in italic; red corresponds to *Hind III*, green to *BamH I* and blue to *Not I*.

5.2.2 GENERATION OF A Δ *NAMH* MUTANT IN *MTB* H37Rv

Generation of a *namH* mutant of *Mtb* was performed based on previously published work by Parish and Stoker (Parish and Stoker, 2000). The flanking regions (*rv3817* (FR1) and *rv3819* (FR2), shown in Figure 49) were initially amplified from *Mtb* gDNA, digested with the enzymes shown in Figure 49 and highlighted in Table 19 and cloned into a standard *E. coli* vector (pGEM®-T Easy vector system). Generated constructs were then transformed into DH5 α cells, white colonies were selected for by plating onto 50 μ g/ml ampicillin, 50 μ g/ml X-gal and 100mM IPTG containing plates and successful clones were sequenced to exclude any PCR errors.

The verified fragments were assembled in pNIL2 plasmid; FR1 from FR1pGEM-T easy was digested with *Bam*HI and *Hind*III, gel extracted and purified (using QIAEX II extraction kit (Qiagen)) before being ligated into the similarly digested and purified pNIL2 vector, transformed and checked for the correct insert. A clone containing the correct insert was then cut using *Bam*HI and *Not*I and used to insert *Bam*HI, *Not*I and *Sca*I digested and gel purified FR2 from FR2pGEMeasy. Ligation mix was then transformed and plated onto 50 μ g/ml kanamycin plates and the resulting clones checked for the correct inserts by a 13 enzyme digest.

Once confirmed, a *Pac*I cassette containing a series of marker genes: hygromycin resistance gene, *sacB* gene and *lacZ* gene (*hyg*, pAg₈₅-*lacZ* and -*sacB*) was cloned into restriction sites at the final stage. This final construct was transformed as above and plated onto 80 μ g/ml X-gal, 50 μ g/ml kanamycin, 100mM IPTG containing LA plates; blue transformants were selected and diagnostic digestions were performed. A Δ *namH* candidate was then used to electroporate *Mtb* as previously described (Chapter 2).

5.2.2.1 SELECTION OF SINGLE AND DOUBLE CROSS-OVERS

All *Mtb* work was performed in a Category 3 suite facility within class I or II microbiological safety cabinets following the relevant Codes of Practice. After electroporation, samples were plated onto 7H10 agar plates containing 10% (w/v) ADC, 2% (w/v) sucrose and 80µg/ml X-gal and grown at 37°C for a minimum of 3 weeks. Once blue colonies became visible plates were regularly checked. Colonies were picked once they were large enough to inoculate multiple cultures and streak out onto 7H10 plates. 7H9 medium containing 10% (w/v) ADC, 0.05% (w/v) Tween 80 and either with or without the presence of kanamycin (50µg/ml) were inoculated. These were incubated at 37°C until they reached stationary phase, in the presence of kanamycin no growth was observed.

Frozen stocks were prepared from the growing culture and 7H10 plates containing 10% (w/v) ADC and 2% (w/v) sucrose were inoculated. These were incubated as before and 50 colonies were picked and streaked onto 7H10 (containing 10% (w/v) ADC, 2% (w/v) sucrose and 80µg/ml X-gal) with and without 50µg/ml kanamycin. These were numbered 1 to 50 and only white colonies which did not grow in the presence of kanamycin but produced colonies on plates without antibiotic were then picked for further analysis.

5.2.2.2 HEAT KILLING OF *MTB*

Colonies growing on plates without antibiotic (described above) and therefore deemed to be $\Delta namH$ double cross overs, were picked and resuspended in 100µl of H₂O. Samples were then heat killed using a dry block at 95°C for a minimum of 30 minutes. Samples could then be removed from the Cat3 facility and used for PCR reactions (Chapter 2).

5.2.3 *MTB* GENOMIC DNA PURIFICATION

Stationary phase cultures were harvested at 2500xg for 15 minutes; pellets were resuspended in 1ml of TE buffer before re-centrifugation (as described above). Samples were frozen at -80°C for a minimum of 4 hours. Samples were then resuspended in 1ml of TE buffer; an equal volume of chloroform:methanol (2:1) was added to each sample and mixed gently for 5 minutes.

Phase separation was aided by centrifugation at 2500xg for 20 minutes on a bench top centrifuge. The phases were removed by pipette (bacteria were present at the interface between phases). Tubes were left uncapped for 10 to 15 minutes within the microbiological safety cabinet. A further 1ml of TE buffer was added and samples placed on a vortex briefly. 0.1 volume of 1M Tris HCl; pH9 was added and lysozyme (at a final concentration of 100µg/ml) was added.

Samples were incubated at 37°C for 12 to 16 hours. 0.1 volume of 10% (w/v) SDS and 0.01 volume of proteinase K (10mg/ml) were added and mixed by inversion, samples were incubated at 55°C on a dry block for 3 hours. An equal volume of phenol;chloroform;Isoamyl alcohol (25:24:1) was added and incubated for 30 minutes before centrifugation at 12,000xg for 30 minutes. The aqueous layer was transferred to a fresh tube and this process repeated. The aqueous phase was transferred to a fresh tube, and at this stage samples were safe to remove from the Category 3 suite facility. All samples were swabbed with 70% EtOH before removal.

5.2.4 DIAGNOSTIC PCR

Diagnostic PCRs of all *Mtb* knockout mutant candidates were performed as described in Chapter 2. Primers designed for confirmation of *namH* deletion can be found in Table 19.

5.2.5 SOUTHERN HYBRIDISATION

Southern hybridisation was performed using DIG High Prime DNA Labelling and Detection Starter Kit I (Roche).

5.2.5.1 DIG LABELLING

1µg of Fragment 2 DNA (used for the construction of $\Delta namH$ mutant), in a final volume of 16µl, was denatured at 95°C on a dry block before chilling on ice briefly. DIG-High Prime solution was well mixed and a 4µl aliquot taken and mixed with the template DNA (Fragment 2 in this case). This was then incubated at 37°C before inactivation at 65°C for 10 minutes. The same was carried out for the DNA Ladder Mix (Generuler™, Thermo Scientific). Both samples were then stored at -20°C.

5.2.5.2 TRANSFER TO POSITIVELY CHARGED NYLON MEMBRANE

Appropriate restriction enzymes were selected and digestion of 1µg gDNA was carried out overnight. Digested samples were then separated by DNA gel electrophoresis, using a 1% (w/v) agarose gel. This gel was used to transfer the DNA fragments to a positively charged nylon membrane (Roche). The gel was briefly depurinated in 0.25M HCl with slow agitation. The following assembly was then performed:

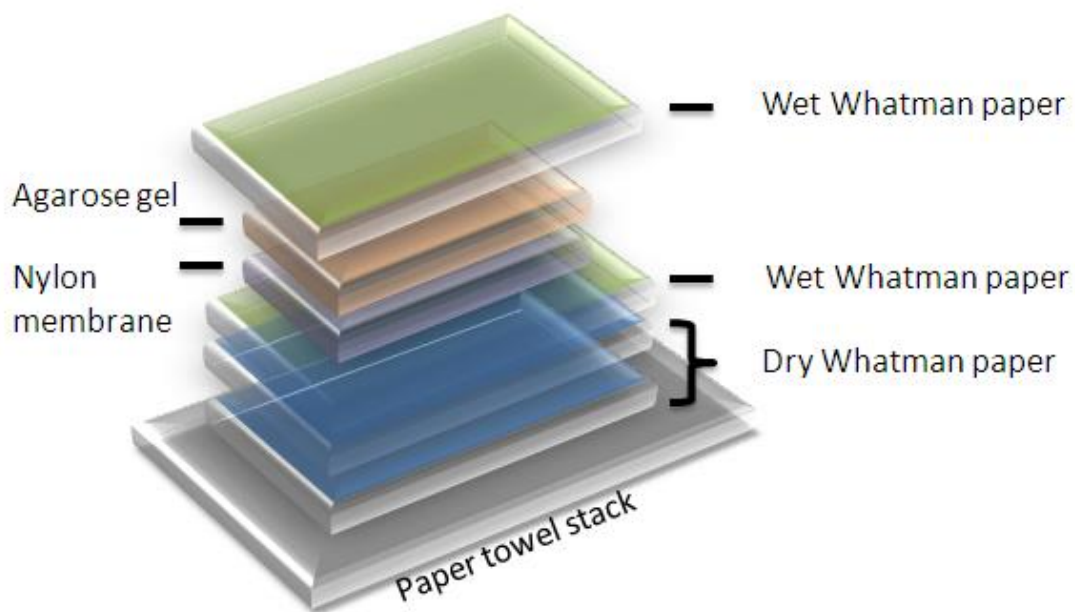


FIGURE 51: ASSEMBLY FOR SOUTHERN HYBRIDISATION TRANSFER TO NYLON MEMBRANE

0.4M NaOH transfer buffer was used to soak pre-cut Whatman paper, nylon membrane and depurinated agarose gel. These were then assembled as shown above. Once the gel had been carefully placed onto the membrane all bubbles were gently removed and using a pencil the wells within the gel were marked on the underlying membrane. These wells could then be cut off using a scalpel and covered with a thin piece of Clingfilm. Once assembled a large piece of Whatman paper (the width being roughly equal to the length of the gel), with each end placed in transfer buffer, was placed on top of the above construction and firmly pressed down.

Once the transfer apparatus (as shown in Figure 51) had been assembled and the final piece of Whatman paper (soaked in transfer buffer and each end placed in containers of this buffer) had been added, transfer was left to occur for 2 hours. This was then be disassembled and the nylon membrane used for further work.

5.2.5.3 UV-CROSSLINKING

Nylon membranes containing transferred DNA fragments were UV-cross-linked using a UV Straterlinker™ 2400 (Invitrogen). The automated crosslinking option was performed twice.

5.2.5.4 HYBRIDISATION AND IMMUNOLOGICAL DETECTION

DIG Easy Hyb buffer (10ml/100cm² membrane) was heated to hybridisation temperature (42°C), calculated based on GC content and percentage homology of the probe to the target, and the membrane was pre-hybridised for 30 minutes with constant agitation. DIG-labelled DNA probe was then denatured for 5 minutes before rapid cooling; this was added (25ng/ml) to pre-heated DIG Easy Hyb buffer (3.5ml/100cm² membrane) and mixed well. Pre-hybridisation solution could then be removed and the probe containing hybridisation solution was added, this was incubated overnight with agitation. Two 5 minute washes in 2xSSC buffer (containing 0.1% (w/v) SDS) at room temperature were carried out before two 15 minute washes in pre-warmed 0.5xSSC (containing 0.1% (w/v) SDS).

The membrane was then briefly washed in washing buffer before incubating in 100ml blocking solution for 30 minutes at room temperature. 20ml of Antibody solution was added and incubated for 30 minutes, followed by two 15 minute washes in washing buffer before brief equilibration in Detection buffer. 10ml of colour substrate solution was added, and incubation was performed for up to 4 hours. Termination of the reaction was carried out by thorough washing in H₂O.

5.2.6 GROWTH STUDIES

All *Mtb* cultivation was carried out in a Category 3 suite, using microbiological safety cabinets (Class I and II) and following the Codes Of Practice and Standard Operating Procedures necessary. Strains were grown in either 7H9 or Sautons liquid media, containing 0.05% (w/v) Tween 80 (as described in Chapter 2) or on 7H10 solid agar (Chapter 2), all containing 10% (v/v) ADC. Starter cultures were inoculated by defrosting an aliquot of frozen stock

and inoculating 5ml of medium with 300µl of this. Primary cultures were then grown until the OD_{600nm} reached 0.5, 50µl of these cultures were then used to inoculate a secondary culture as before. Once these cultures had reached OD_{600nm} 0.5 they were used to inoculate 10ml cultures in 50ml falcons. These were then grown for up to 3 weeks, with regular OD sampling. Each independent experiment contained a minimum of duplicate biological replicas.

5.2.7 MACROPHAGE INFECTION STUDIES

J774A.1 murine macrophages were used in this study (ATCC™: TIB-67™). Cells were grown in Dulbecco's Modified Eagle's Medium (DMEM) supplemented with 5mM L-glutamine and 10% (v/v) Foetal Calf Serum (FCS). Growth conditions were as follows: stationary incubation at 37°C and 5% CO₂. Murine macrophages have a doubling time of approximately 17 hours, therefore cultures for infection studies were seeded at 1x10⁵ cells/ml and left to adhere and grow overnight.

Macrophage infections were then infected at MOIs of 0.5 and 1. Multiplicity of Infection (MOI) was calculated based on the assumption of macrophage counts doubling overnight. Hence 2x10⁵ cells/ml should be present, therefore for an MOI of 1; 2x10⁵ cells/ml of *Mtb* cells were added. Cultures for *Mtb* infection studies were prepared as described above, when the tertiary cultures reached an OD of 0.5 cultures were washed twice in sterile PBS before resuspending in 10ml DMEM and 1ml aliquots frozen at -80°C. The next day aliquots of both wild type and $\Delta namH$ *Mtb* were defrosted and used for CFU counts (Chapter 2). Plates were then incubated for up to 3.

1ml *Mtb* DMEM aliquots were then defrosted, centrifuged at 12,000xg for 10 minutes and pellets were resuspended in 1ml of fresh DMEM. A single cell suspension was generated by passing

the sample repeatedly through a blunt ended needle (Harvard Apparatus). Each well within the 24-well plate (Nucleon) contained 1ml of 2×10^5 cells/ml of macrophages adhered to the bottom of the well, the medium was removed and replaced with fresh DMEM, wells were then infected at MOIs of 0.5 and 1 with wild type and $\Delta namH Mtb$ (each sample was prepared in triplicate). Plates were then incubated for 4 hours, after which wells were emptied and washed once in fresh medium before fresh medium added for further incubation. Several time points were taken for CFU analysis. 10mm glass coverslips were also placed in several wells prior to macrophage seeding so that microscope images could be taken.

5.2.7.1 CELL LYSIS

In order to lyse macrophages for intracellular bacterial cell counts, media was first removed by pipetting and wells were gently washed with fresh medium before 200 μ l of PBS containing 0.2% (w/v) Triton X-100 was added and incubated for 5 minutes. Using a pipette wells were then scraped before the sample was transferred to a 96 well microtitre plate for serial dilution and CFU plating.

5.2.8 MICROSCOPY

5.2.8.1 PREPARING COVERSGLIPS

All coverslips were sterilised by overnight treatment with 19-20 % (v/v) formaldehyde. Coverslips were placed in an open petri dish which could then be added to a container with paper towels soaked in 10ml of formaldehyde. This was closed and left within a safety cabinet overnight. The following day the petri dish was removed from the box and left to dry within the cabinet for a minimum of 2 hours. All waste was disposed of following the relevant SOPs. Coverslips could then be removed from the Category 3 facility.

Using the commercially available TB Quick Stain Kit (BD), coverslips were first treated for 5 minutes in Carbofuchsin reagent before thorough washing in distilled water. Slips were then immersed in methylene blue reagent for 1 minute before washing again, coverslips could then be mounted using 10% (w/v) glycerol onto slides for microscopy.

5.2.8.2 MICROSCOPE SETTINGS AND IMAGE ANALYSIS

A Nikon Diaphot 200 inverted microscope with 100w high pressure mercury vapour lamp was used for all images. Images were taken with a high speed Peltier-cooled Retiga Exi Fast 1394 camera (QImaging, Surrey, BC). The software used was: InVivo v3.2.2 build 48 (Media Cybernetics, U.S.A) and ImageJ v1.4q (Staal et al., 2004) was used for image analysis. All images were stored as 12 bit tagged image files (tif) for further analysis.

5.2.9 ANTIMICROBIAL KILLING AND RECOVERY

5.2.9.1 ANTIMICROBIAL KILLING ASSAYS

Mtb H37Rv wild type and $\Delta namH$ pre-cultures were grown till OD 0.5, these were then used to inoculate 5ml 7H9 cultures (prepared as previously described, Chapter 2) with the addition of one of the following antimicrobial agents at the shown concentration:

TABLE 20: ANTIMICROBIAL CONCENTRATIONS FOR PERCENTAGE KILLING EXPERIMENTS

Antimicrobial Agent	Concentration ($\mu\text{g/ml}$)
Isoniazid	1
Rifampicin	1
Streptomycin	10

CFU plates were prepared once cultures were inoculated; each sample was prepared in triplicate and after 5 days growth at 37°C, with 100rpm shaking CFUs were taken again. Cultures were then used to set up MPN plates for resuscitation.

5.2.9.2 *MTB* CULTURE SUPERNATANT PREPARATION

Mtb culture supernatant (SN) was prepared by growing wild type *Mtb* in 7H9 with 10% (v/v) OADC and 0.05% (w/v) Tween 80 (Chapter 2) till the OD was between 0.6 and 0.8; cells were then harvested by centrifugation at 2500xg for 20 minutes. The SN was carefully removed by pipetting and filtered twice (1L filter unit 0.2µm pore size, Fisher Scientific). The resulting SN could then be removed from the Category 3 suite and aliquoted. These aliquots were then immersed in liquid Nitrogen and vacuum dried. Once dry, samples could be stored at -80°C, when needed they were resuspended in sterile H₂O on ice and incubated for 30 minutes before use.

100µl of diluted Sautons medium (Chapter 2) was used to prepare a 96-well resuscitation plate. The initial row was inoculated with 10µl of antimicrobial treated cultures; these were then serially diluted within the plate. A second plate contained 100µl aliquots of culture SN, the same procedure was performed. Plates were incubated, static and at 37°C for up to 3 weeks. MPN and RI were calculated as previously described (Chapter 4).

5.3 RESULTS

5.3.1 GENERATION AND CONFIRMATION OF AN *MTB* Δ NAMH MUTANT

5.3.1.1 DIAGNOSTIC DIGESTIONS AND PCR REACTIONS

An unmarked double crossover knockout mutant in *Mtb* was generated using a method published by Parish and Stoker in 2000. Before insertion of a *PACI* marker cassette (needed for selection of single and double crossovers) a positive FR12pNIL2 clone was assessed by multiple diagnostic restriction digests. The selected enzymes and the corresponding fragment sizes calculated (Vincze et al., 2003) are shown below in Table 21.

TABLE 21: DIAGNOSTIC RESTRICTION DIGESTS OF FR12PNIL2 AND THEIR CALCULATED SIZES

Lane No. In Figure	Enzyme/s	Fragment size/bp
1	EcoRI	5586, 1559, 1587, 852
2	Sall	8806, 509, 161, 148
3	NheI	9624
4	XhoI	4890, 4734
5	NcoI	9624
6	NotI and BamHI	6895, 2729
7	NotI	9624
8	HindIII and NotI	5195, 4429
9	HindIII and BamHI	7158, 2466
10	MluI	6458, 3166
11	KpnI	6622, 3002

The resulting fragments were analysed by gel electrophoresis and the results are shown in Figure 52, the lane number of the gel corresponds to the number listed in Table 21.

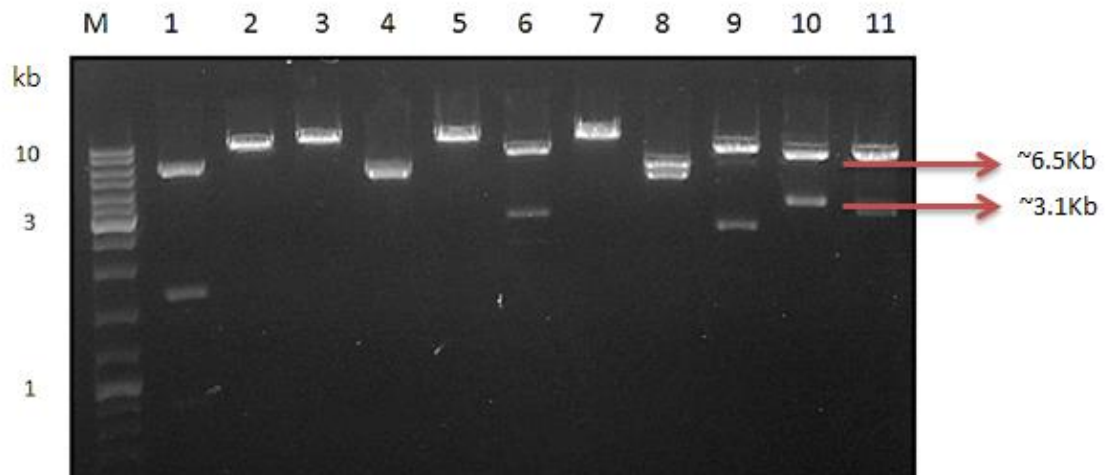


FIGURE 52: DNA GEL SHOWING RESTRICTION DIGESTED DNA FRAGMENTS OF FR12pNIL2

FR12pNIL2 DNA samples were digested using the restriction enzymes shown in Table 21 and the calculated fragment sizes are also shown. Samples were analysed on a 1% (w/v) agarose gel, and ran at 90V for 45 minutes. A 10kb DNA ladder (GeneRuler™) shown in the first lane, was loaded for mass determination. An example of digestion product sizes is shown.

From Figure 52, and taking the masses shown in Table 21 into consideration, it can be concluded that the FR12pNIL2 candidate selected and analysed by digestion contains the correct fragments. All enzymes produced DNA fragments of the expected molecular weights, as determined by gel electrophoresis. Several smaller (<500bp) fragments were not visible by DNA gel electrophoresis, however, the remaining bands matched the correct molecular weights and therefore it can be assumed that the low molecular weight bands are not visible.

An example being lane 10 (*MpnI* digested DNA) which was predicted in Table 21 to produce bands at roughly 6.5kb and 3kb. From Figure 52 there are two bands visible in lane 10, if these are used in reference to the DNA ladder it can be observed that the low molecular weight band is approximately 3kb whilst the larger band appears below the 8kb marker. *EcoRI*, predicted to produce fragments of the following sizes: 5586, 1559, 1587 and 852 is also confirmed; in Figure 52, lane 1 the following digestion bands can be seen, 6Kb, 1.5Kb and 900bp. The two bands at ~1.5Kb are too similar in mass to be separated by gel electrophoresis.

Having confirmed the correct assembly of the knockout construct the marker cassette (*PACI*) could then be inserted. A single digest was carried out to confirm the presence of this cassette before electroporation in *Mtb* (data not shown). After electroporation into *Mtb*, single crossovers were selected by growth on 7H10 plates containing sucrose and x-gal. Blue colonies were picked for inoculation of non-antibiotic containing medium for several generations.

Double cross-overs were selected for by picking single colonies and re-streaking them. Clones which produced white colonies on non-antibiotic containing 7H10 x-gal plates but did not produce any growth on corresponding Kanamycin plates were selected. 50 colonies were plated. From these, 48 were heat killed and removed from the Category 3 suite and analysed by PCR and gel electrophoresis.

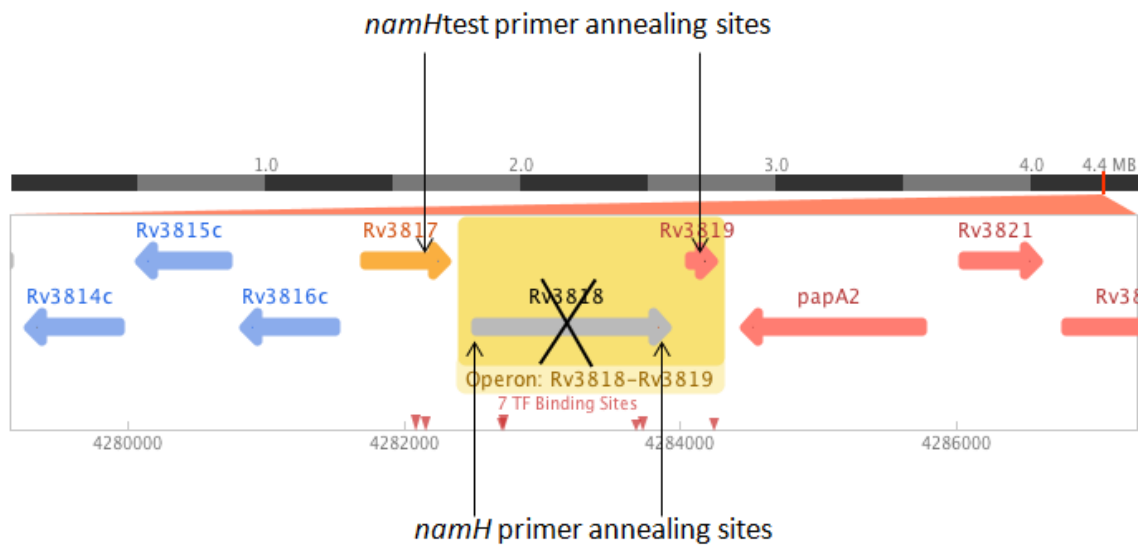


FIGURE 53: SCHEMATIC OF DIAGNOSTIC PRIMER SITES IN *MTB NAMH* MUTANT

A schematic showing the primer annealing sites of DNA amplification for diagnostic PCR assays in $\Delta namH$ *Mtb*. Operon orientation was adapted from TBDB website (Reddy et al., 2009).

Two primer sets were used to determine whether *namH* had been successfully knocked out, a schematic demonstrating where these two primer pairs anneal is shown in Figure 53. The first primer pair (*namH*, Table 19) amplified *namH* and therefore would only produce bands in candidates still carrying a *namH* gene. This eliminated 44 of the 48 candidates (data not shown), the remaining four candidates were then analysed using a second set of primers (*namHtest*, Table 19).

TABLE 22: AMPLICON SIZES IN WT AND $\Delta NAMH$ *MTB* USING DIFFERENT PRIMERS

Primer pair	Size of product in WT	Size of product in $\Delta namH$
<i>namH</i>	1.5kb	200bp
<i>namHtest</i>	2kb	500bp

This primer pair was designed to recognise sequences upstream and downstream of *namH*, therefore PCR products could be generated from wild type and mutant genomes. Hence if the *namH* gene had been successfully knocked out a 500bp band should be visible (amplicon sizes are shown in Table 22. For each PCR reaction a positive (FR12pNIL2 DNA) and negative (*Mtb* gDNA) control were ran alongside.

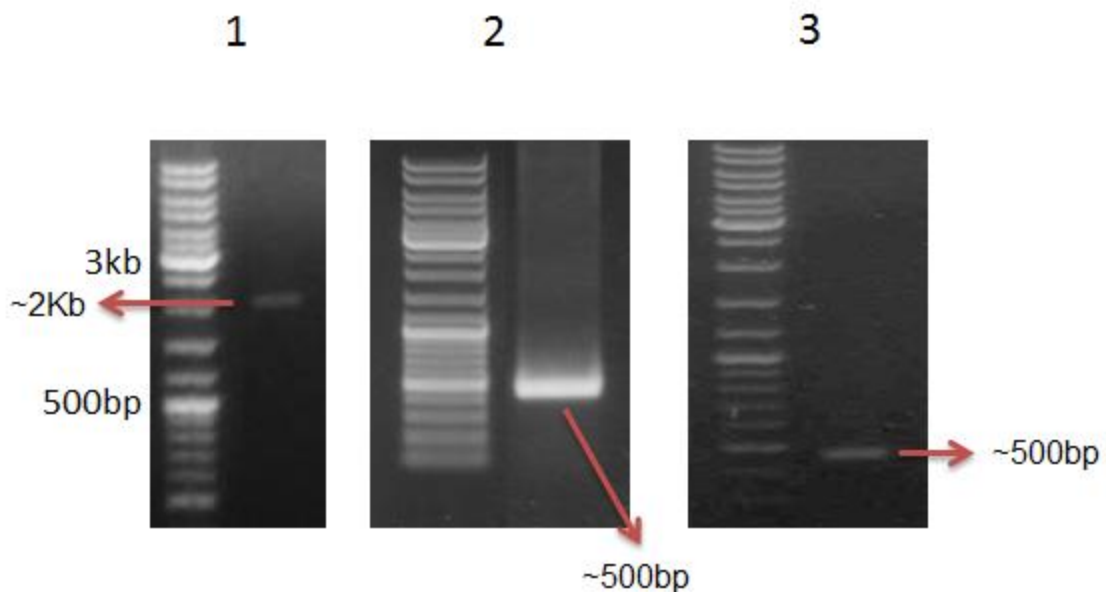


FIGURE 54: DNA GELS SHOWING PCR PRODUCTS USING *NAMH*TEST PRIMERS

The above lanes are as follows: 1) *Mtb* gDNA (negative), 2) FR12pNIL2 DNA (positive) and 3) $\Delta namH$ *Mtb* candidate 6 DNA were used for PCR amplification using *namH*test primers. Amplification was performed using GoTaq polymerase, the cycle conditions were performed as previously described (Chapter 2). A 500bp band was expected if *namH* has successfully been knocked-out; if still present an approximate 2kb band was expected.

Figure 54 demonstrated that *Mtb* $\Delta namH$ candidate 6 (Figure 54; 3) contained a band of roughly 500bp, which was expected if *namH* had successfully been deleted. When using primer set 1 (designed to amplify *namH*) the low molecular weight of the band made it difficult to distinguish it from primer dimers (data not shown). However, if this candidate contained a single crossover this band

would also be present and potentially, due to PCR problems no band corresponding to *namH* may have been observed. Therefore to be completely certain that this candidate was in fact a double crossover, a series of Southern blots, using a variety of enzymes were carried out.

5.3.1.2 SOUTHERN HYBRIDISATION

Using the following restriction enzymes: *StuI*, *NheI* and *Clal* a range of DNA fragments were generated using candidate $\Delta namH$ *Mtb* gDNA. These were analysed and compared to wild type *Mtb* gDNA fragments by Southern hybridisation. The commercially available kit; DIG High Prime DNA Labelling and Detection Starter Kit I (Roche) was used for all Southern blots. Fragment 2 DNA from the knockout construct was used as a probe to detect *namH* or the lack of. The variety of enzymes and their corresponding fragment masses in both wild type and $\Delta namH$ are shown in Table 23.

TABLE 23: RESTRICTION DIGEST FRAGMENT SIZES PREDICATED FOR WILD TYPE *MTB* AND $\Delta NAMH$ *MTB*

Enzyme	WT Size (Kb)	$\Delta namH$ Size (Kb)
StuI	6.7	5.2
NheI	6.8	5.3
Clal	7.9	10

Using NEB online free software (Vincze et al., 2003) and the DNA sequences of both wild type and $\Delta namH$ *Mtb* the above enzymes were chosen for their suitability. *StuI* and *NheI* do not cut within *namH* and therefore a smaller product is expected for $\Delta namH$ whereas *Clal* cuts within *namH* and hence a larger fragment is

predicted for $\Delta namH$ than wild type. The enzymes shown in Table 23 were selected based on the size of the fragments produced, the site where they cut and their availability. The corresponding Southern blots are shown in Figure 55.

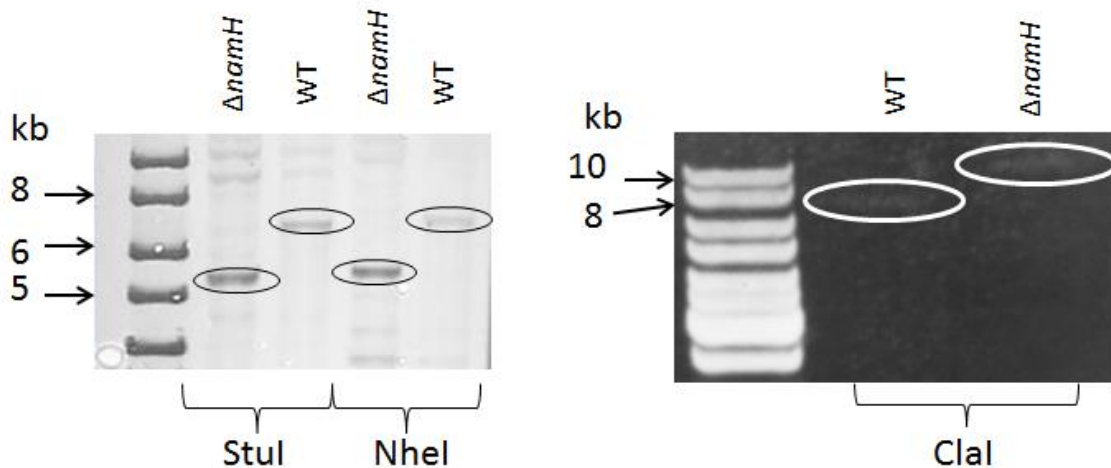


FIGURE 55: SOUTHERN BLOTS OF WILD TYPE AND $\Delta NAMH$ *MTB* DIGESTED gDNA

Using the restriction enzymes *Stul*, *NheI* and *ClaI*, gDNA from a $\Delta namH$ *Mtb* candidate as well as from wild type *Mtb* was digested, separated by electrophoresis, transferred to a positively charged membrane and probed with a DIG labelled DNA fragment. Using anti-DIG antibodies and enzyme-linked substrate the blots were then placed into a colour detection solution. The corresponding calculated masses for each enzyme and each strain are shown in Table 23. Bands of interest have been circled. The figure on the right (*ClaI* digestion) has been inverted to improve appearance of bands.

Figure 55 shows the results from two southern blots using three different enzymes; *Stul*, *NheI* and *ClaI*. *Stul* and *NheI* were predicted to produce very similarly sized DNA fragments (6.6kb and 6.8kb in WT, 5.2kb and 5.3kb in $\Delta namH$); this was clearly observed in the above figure, bands above the 5kb marker were observed in $\Delta namH$ fragments and bands between 6 and 8kb were observed in WT fragments. Due to some weak unspecific

background bands there was a clear difference in digestion pattern for the two enzymes.

ClaI on the other hand was predicted to produce a larger DNA fragment (10Kb, Table 23) than in wild type *Mtb* (~8Kb, Table 23), again this is visible in Figure 55 with $\Delta namH$ fragments producing a band at roughly 10kb and WT fragments producing a bands around the 8kb marker. For all three enzymes the calculated masses for both wild type and $\Delta namH$ *Mtb* gDNA (Table 23) were shown by Southern blot (Figure 55). After successful generation of a $\Delta namH$ mutant, candidate 6 could then be used for characterisation of *namH* in *Mtb*.

5.3.2 $\Delta NAMH$ *MTB* HAS A SLIGHT GROWTH DEFECT AND INCREASED CLUMPING

Wild type and $\Delta namH$ *Mtb* were grown in 7H9 and Sautons media (as described in Chapter 2) in order to investigate whether the mutant had a growth defect.

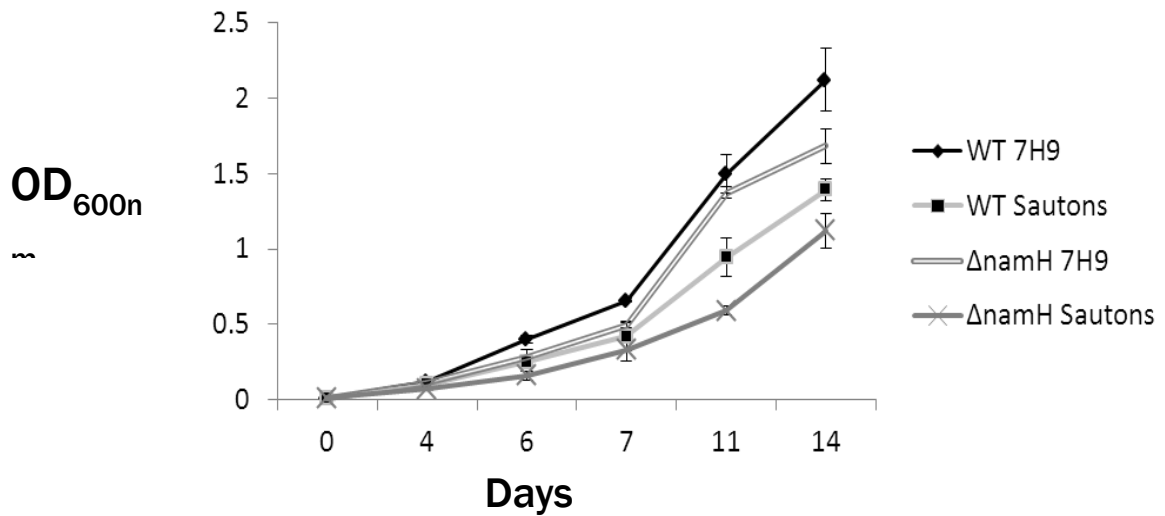


FIGURE 56: WILD TYPE AND $\Delta NAMH$ *Mtb* GROWTH ANALYSIS IN 7H9 AND SAUTONS MEDIA

10ml cultures were all inoculated from pre-cultures grown till OD 0.5, samples were hand measured using a spectrophotometer in 1.5ml disposable cuvettes (Chapter 2). A medium specific blank was used at all stages, and once cells reached OD 0.5 samples were diluted before measurements were taken. P values at the highest OD were 0.06 and 0.05 in 7H9 and Sauton's media respectively.

As cultures entered the stationary phase there was a significant increase in cell clumping within $\Delta namH$ *Mtb* compared to the WT strain, this was exaggerated when grown in Sautons medium. From Figure 56 a slight growth defect can be observed for $\Delta namH$ *Mtb* when grown in either medium, producing a lower final OD and, based on the curves alone, an altered growth rate. Overall it appears that $\Delta namH$ *Mtb*, in either 7H9 or Sautons media, has a slightly altered growth phenotype and increased clumping.

Colony morphology of both WT and $\Delta namH$ *Mtb* appears very similar when grown on solid medium; as shown in Figure 57.

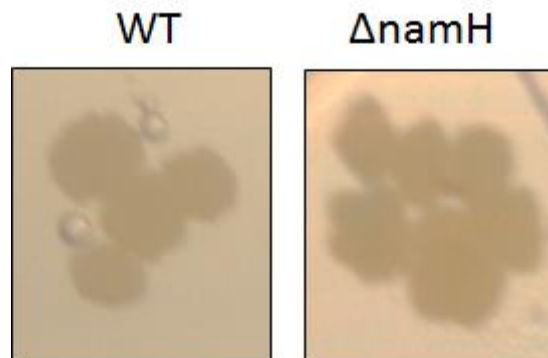


FIGURE 57: SINGLE COLONY IMAGES OF WILD TYPE AND Δ NAMH *MtB*

Images of wild type and Δ *namH* *Mtb* single colonies grown on 7H10 agar containing 10% (w/v) ADC are shown in the above figure.

Both strains appear to have a ruffled edge, and although not visible in these images both strains had rough colony morphology.

5.3.3 DOES GLYCOLYLATION PLAY A ROLE IN INTRACELLULAR SURVIVAL?

The ability of *Mtb* to overcome the host immune response is a key factor in the survival of this bacterium. Interactions of *Mtb* with host immune cells, is still not fully understood, *Mtb* is able to survive and replicate within these cells. Previous studies using a Δ *namH* *M. smegmatis* mutant showed increased susceptibility to cell wall enzymes; it was hypothesized that this modification may play a role in *Mtb* intracellular survival.

J774 murine macrophages were used for triplicate infection studies to investigate the role of glycolylation in intracellular survival and replication. Each experiment contained triplicate biological replicas; negative controls were also implemented to assess contamination. Small coverslips were placed in several wells for each experiment prior to macrophage seeding; this allowed imaging of the cells at different stages of infection.

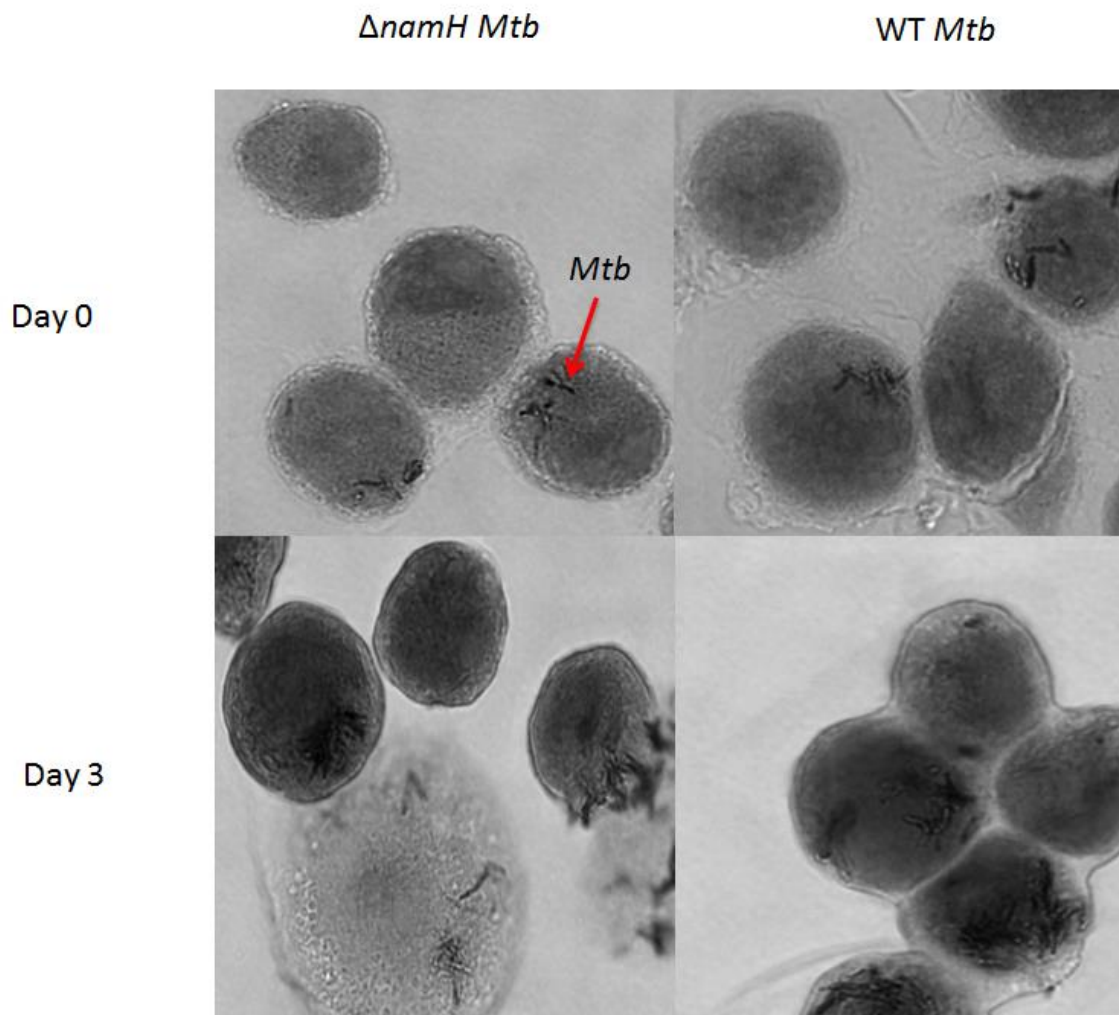


FIGURE 58: PHASE CONTRAST MICROSCOPY IMAGES OF MACROPHAGE INFECTION AT MOI 1

After slide sterilisation using 19-20% formaldehyde samples were removed from the Category 3 suite and stained using TB Quick Stain Kit (Roche) before being mounted. A Nikon Diaphot 200 inverted microscope with 100w high pressure mercury vapour lamp was used for all images. Images were taken with a high speed Peltier-cooled Retiga Exi Fast 1394 camera (QImaging, Surrey, BC). The software used was: InVivo v3.2.2 build 48 (Media Cybernetics, U.S.A) and ImageJ v1.4q (Staal et al., 2004) was used for image analysis.

Images for wild type and *ΔnamH Mtb* macrophage infection studies at MOI 1, after 4 hours infection (Figure 58; Day 0) and on Day 3 are shown in Figure 58. After 4 hours of infection on Day 0, in both wild type and *ΔnamH Mtb* infected macrophages, both infected and

uninfected macrophages were observed, there were also no extracellular bacteria identified.

After 3 days however, there was a clear increase in *Mtb* (probably due to multiplication) in both wild type and $\Delta namH$ *Mtb* infected macrophages, as expected. Intact macrophages were still visible after 3 days of infection and an uninfected cell can be observed in Figure 58; $\Delta namH$ *Mtb* Day 3. However, it was also clear that the infection had progressed resulting in macrophages lysis; an erupting macrophage can be seen releasing intracellular *Mtb* cells in the same image.

To determine whether glycolylation affected the survival and replication of *Mtb* in macrophages, wild type and $\Delta namH$ *Mtb* infected cells were washed of any extracellular bacteria before lysis, and CFU plating was carried out at different time points throughout the infection.

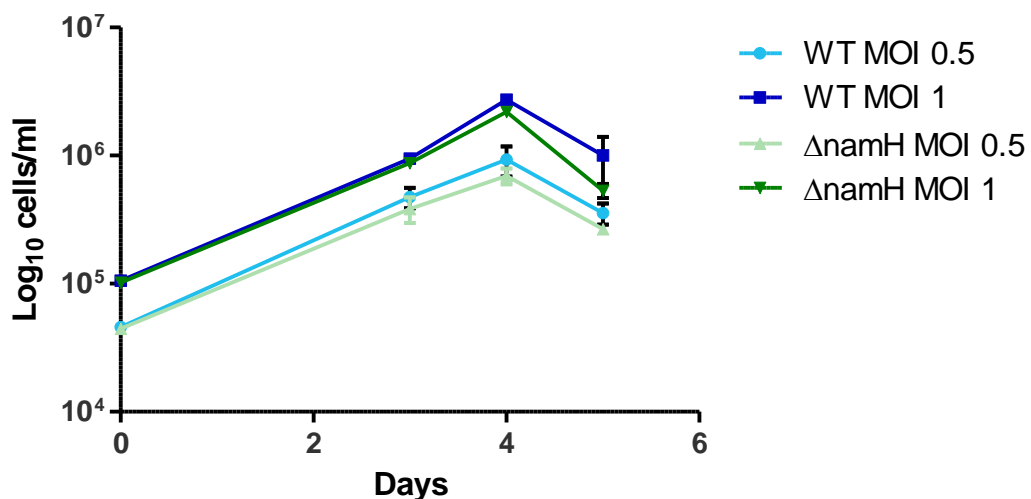


FIGURE 59: MACROPHAGE SURVIVAL AND REPLICATION DATA FOR WILD TYPE AND $\Delta NAMH$ *MTB*

Wild type and $\Delta namH$ *Mtb* Macrophage infections were performed at MOIs of 0.5 and 1. CFUs were taken after 4 hours of infection on day 0, day 3, day 4 and day 5. Extracellular bacteria were removed by washing prior to cell lysis. Experiments were performed in triplicate and each contained triplicate biological replicas.

Figure 59 shows the average CFU data for multiple macrophage infections, the error bars represent the standard mean error from all individual replicas. In the early stages of infection, at both MOIs there appeared to be a very similar trend in replication for both wild type and $\Delta namH$ *Mtb*. However, at the later stages (Figure 59; Day 5) there was a slight drop in cell numbers at MOI 1 for $\Delta namH$ *Mtb*. This was not replicated at MOI 0.5. The error bars and p values (0.62 and 0.78, MOI 0.5 and 1 respectively) at day 5 indicate that this difference was not statistically significant.

5.3.4 ANTIMICROBIAL KILLING

As mentioned above, previously published work on an *M. smegmatis namH* knockout mutant led to the finding that N-glycosylation may be a cause of decreased susceptibility to β -lactam antibiotics and lysozyme (Raymond et al., 2005). This led to the hypothesis that this may also be true in *Mtb* and hence may affect antimicrobial effectiveness. Therefore a variety of antimicrobial treatments were used to assess whether glycosylation affects antimicrobial killing in *Mtb*. The results shown below are preliminary data from three biological samples per assay; CFUs were calculated by averaging triplicate replicas.

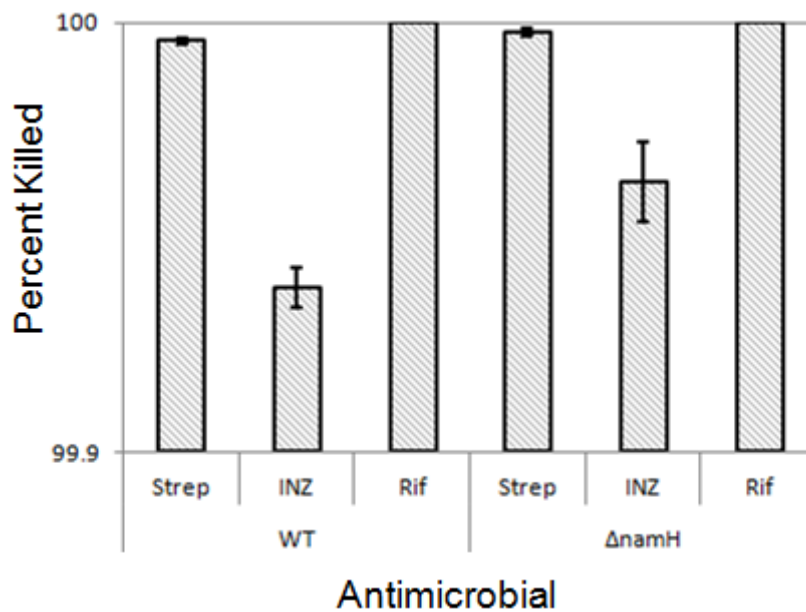


FIGURE 60: PERCENTAGE KILLING IN WILD TYPE AND $\Delta NAMH$ *MTB* AGAINST ANTIMICROBIAL TREATMENT

CFU numbers of cultures from pre- and post-antimicrobial treatment (after 5 days incubation) were used to calculate percentage killing. Antimicrobials streptomycin, isoniazid and rifampicin were used at the following concentrations ($\mu\text{g/ml}$): 10, 1 and 1 respectively. 7H9 medium, containing 10% (w/v) ADC and 0.05% (w/v) Tween 80, was used for all cultures. 5ml cultures (in 20ml universals) were grown for 5 days at 37°C with 100rpm shaking. Each sample was prepared in triplicate. The limit of detection was 25 cells/ml.

Almost all samples reached 100% killed, however there was a slight reduction when treated with INZ. All cultures treated with 1 $\mu\text{g/ml}$ Rifampicin, for both wild type and $\Delta namH$ *Mtb* strains, resulted in no visible cells on solid medium (Figure 60). Streptomycin treatment (10 $\mu\text{g/ml}$) resulted in <0.01% survival for both wild type and $\Delta namH$ *Mtb* after 5 days incubation. Isoniazid treatment resulted in the lowest percentage of cells killed in both strains (although still greater than 99%); there was a greater survival observed for wild type *Mtb* (Figure 60). More work is required to determine whether this effect is significant and highly reproducible. After 5 days treatment these samples were used to prepare MPN resuscitation plates.

5.3.5 DOES GLYCOLYLATION PLAY A ROLE IN *Mtb* RECOVERY AFTER ANTIMICROBIAL TREATMENT?

Due to the altered growth phenotype of the $\Delta namH$ *Mtb* strain, increased cell clumping and hypothesised weakened cell wall structure (potentially important for recovery) MPN plates of antimicrobial treated *Mtb* cultures were used to assess the role of N-glycolylation in *Mtb* recovery. MPN plates were set up as follows: a plate containing diluted Sauton's medium (Chapter 2) was used as a control for growth of viable cells after treatment, a second plate containing *Mtb* culture SN was used to determine resuscitation potential of the different strains. Triplicate biological replicas were plated for each strain and three independent experiments were carried out.

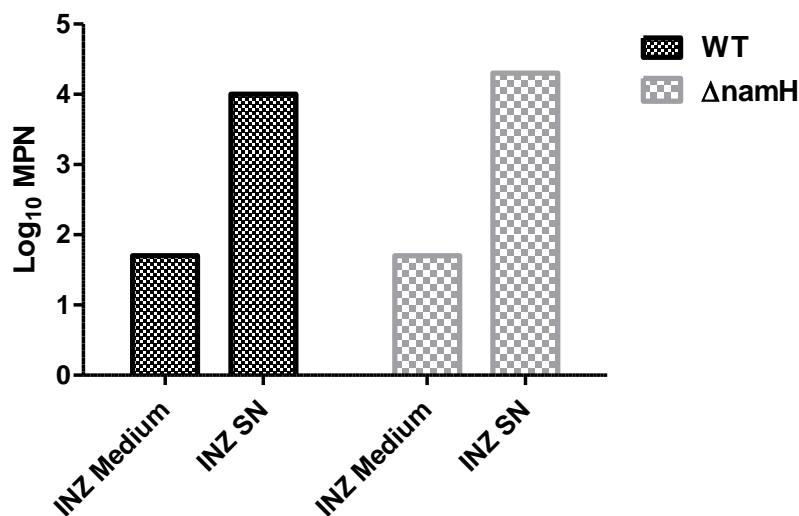


FIGURE 61: LOG₁₀ MPN DATA FOR WT AND $\Delta NAMH$ *Mtb* AFTER ISONIAZID TREATMENT

100 μ l of medium was inoculated with 10 μ l neat culture, plates were incubated statically at 37°C for up to 3 weeks. No resuscitation was observed for Rif or Strep treated cultures. The limit of detection was 10 cells/ml.

MPN plates inoculated from *Mtb* cultures after treatment with either rifampicin or streptomycin did not result in growth, in medium or

culture SN. Isoniazid treated cultures produced MPN counts in plates containing diluted Sauton's medium; indicative of a culturable cell population. However, for both wild type and $\Delta namH$ *Mtb*, MPN counts were much higher when culture SN was added (Figure 61). MPN numbers from bacteria cultured in diluted Sauton's medium show similar values for both wild type and $\Delta namH$ *Mtb*, yet $\Delta namH$ *Mtb* produces a slightly greater resuscitation value when culture SN is added (Figure 61).

TABLE 24: RESUSCITATION INDEX AND CFU COUNTS AFTER INZ TREATMENT

Strain	Log ₁₀ CFU	Resuscitation Index (RI)	
		Medium	Supernatant (SN)
WT <i>Mtb</i>	1.4±0.29	1.2	2.9
$\Delta namH$ <i>Mtb</i>	1.16±0.5	1.5	3.6

Table 24 shows the Log₁₀ CFU counts and RI calculated from Log₁₀ MPN data shown in Figure 61. When grown in either diluted Sauton's medium or culture SN $\Delta namH$ *Mtb* has a greater RI despite a lower initial CFU count.

5.4 DISCUSSION

A *namH* deletion mutant of *Mtb* was generated using the technique previously described by Parish and Stoker (Parish and Stoker, 2000). The gene of interest; *namH* encodes a Rieske type monooxygenase responsible for the production of glycolylated muramyl peptidoglycan precursors which are then incorporated into the existing PG (Raymond et al., 2005). By deleting the *namH* gene and thus producing an *Mtb* strain containing N-Ac-Muramyl PG only it was possible to specifically investigate the role of this cell wall modification in cell growth, morphology, intracellular survival and replication as well as potential roles in recovery after antimicrobial treatment.

Previous work, using $\Delta namH$ *M. smegmatis* demonstrated that N-glycolylation is important for mycobacterial sensitivity to some cell wall hydrolases (Raymond et al., 2005). It was therefore hypothesised that an *Mtb* mutant lacking this modification may have a reduced ability to survive and replicate *in vivo*. Macrophage experiments were designed as a first step in addressing this hypothesis. Due to the predicted reduction in hydrogen bonding within the cell wall and the potential instability, this led to the hypothesis that $\Delta namH$ *Mtb* may have an altered growth phenotype and a reduced resuscitation potential.

5.4.1 $\Delta NAMH$ *MTB* MUTANT CONFIRMATION

The *namH* deletion was confirmed using two independent approaches. Firstly, PCR; after electroporation successful transformants were picked for further analysis, 48 potential double crossover candidates were assessed by PCR. The majority of candidates were ruled out by PCR; using primers which amplified *namH*. All remaining candidates were then used in a second PCR reaction with primers specifically designed to amplify upstream and

downstream from *namH*. The results from this experiment showed the expected band in the negative control, the positive control FR12pNIL2 showed the expected 500bp band as did the *namH Mtb* mutant candidate. The transformation efficiency was calculated to be 8.3%.

Secondly, this *namH* mutant candidate was confirmed by Southern hybridisation. Three different restriction enzymes were used and the observed bands, from all enzymes corresponded well to the calculated sizes. Previous studies have demonstrated that *M. smegmatis namH* is non-essential and *Mtb namH* was predicted, likewise to be non-essential (Raymond et al., 2005, Sasseti et al., 2003). Generation of the *namH Mtb* mutant demonstrated the non-essentiality of *namH*.

5.4.2 GROWTH CHARACTERISATION

In Chapter 4 the role of glycolylation in *M. smegmatis* using a $\Delta namH$ mutant was investigated; severe clumping and a greatly reduced growth rate that was exaggerated when grown in Sauton's medium was observed. It was therefore predicted that a $\Delta namH Mtb$ knockout strain would have similar growth characteristics. The growth of $\Delta namH Mtb$ in 7H9 medium produced a growth curve with a very similar pattern to wild type *Mtb* in Sautons medium.

$\Delta namH Mtb$ cultures had a tendency to clump, which was more pronounced in Sautons medium and at higher ODs, the growth pattern and clumping observed fitted well with the prior *M. smegmatis* data. A possible reason for clumping could be due to reduced cell wall stability which may influence cell aggregation; alternatively the overall architecture of the cell wall may have been altered affecting the hydrophobicity of the cell.

5.4.3 $\Delta NAMH MTB$ INTRACELLULAR SURVIVAL

Previously published work identified glycolylated muropeptides as potent initiators of the host innate immune response, however the role of glycolylation in host immune interactions is not fully understood (Coulombe et al., 2009). It is known that glycolylation plays a role in sensitivity to muralytic enzymes such as lysozyme and could lead to a reduced stability of the cell wall (Raymond et al., 2005).

It is also well established that muramyl dipeptide (MDP) is the smallest muropeptide structure with adjuvant activity, and that this proceeds via NOD2 receptors (Girardin et al., 2003b). However, researchers recently demonstrated that identified N-glycolyl MDP as a more potent NOD2 stimulator (Coulombe et al., 2009). J774 macrophage infection studies were used as a means of assessing the role of N-glycolylation in *Mtb* intracellular survival, it was predicted that $\Delta namH$ *Mtb* would have reduced survival and replication in comparison to wild type *Mtb*.

Mtb macrophage infections were inoculated at MOIs of 0.5 and 1 and after 3 days there was clear multiplication. Microscopy images showed a large increase in the amount of intracellular bacteria as well as some uninfected and dead macrophages and CFU data also indicated replication at this stage. CFU counts showed a continuation of replication at day 4 but a drop in cells at day 5. This trend was found at both MOIs and in both wild type and $\Delta namH$ *Mtb*.

Therefore N-glycolylation of the *Mtb* cell wall did not play a role in intracellular survival and replication. However, this does not mean the role of N-glycolylation in survival and replication of *Mtb in vivo* is fully understood. This modification has already been shown to be important for immune response and could therefore play a larger role in host interactions and survival (Coulombe et al., 2009). A

more complex model may therefore be useful in investigating this role further.

5.4.4 ANTIMICROBIAL KILLING

It is well established that modification of the PG structure within bacteria can be beneficial and enable antibiotic resistance. Well-documented examples of this include de-acetylation and O-acetylation of the PG resulting in resistance to cell wall hydrolases (Laaberki et al., 2011, Zipperle et al., 1984, Bera et al., 2006). It has also been found that glycolylation of the mycobacterial cell wall reduces sensitivity to β -lactam antibiotics and cell wall hydrolases such as lysozyme (Raymond et al., 2005). It was therefore postulated that $\Delta namH$ *Mtb* may have an increased sensitivity to antimicrobial treatments; specifically those that target the cell wall. The susceptibility of *Mtb* to antimicrobials with a variety of targets was carried out to investigate whether any differences in antimicrobial killing was solely due to this modification or perhaps the stability of the cell in general.

Rifampicin treatment in both wild type and $\Delta namH$ *Mtb* was investigated; no major difference was expected as this drug targets DNA replication. There was no observed difference between wild type and $\Delta namH$ *Mtb*. Treatment with streptomycin resulted in high percentage killing in both wild type and $\Delta namH$ *Mtb*; however there was a slightly higher percentage survival observed for wild type *Mtb*. This drug targets protein synthesis but due to the low survival in both strains it is difficult to conclude whether there is a significant difference. Finally, isoniazid treatment resulted in the highest percentage survival, there was a lower survival rate observed in $\Delta namH$ *Mtb* compared to WT. This drug targets cell wall synthesis and it was therefore predicted that $\Delta namH$ *Mtb* would be more susceptible to this drug than WT.

It appears, based on percentage killing data, that N-glycolylation plays a role in *Mtb* susceptibility to cell wall targeted antimicrobials. However, further work would have to be carried out to determine whether $\Delta namH$ *Mtb* is more susceptible to drugs with alternative targets due to the low level of survival. As mentioned previously deletion of *namH* is thought to affect the stability and potentially the overall conformation of the cell wall, these changes may affect drug up-take due to permeability alterations, interactions with the cell wall and due to clumping may shield a minority of cells from the environment.

5.4.5 THE ROLE OF GLYCOLYLATION IN *MTB* RESUSCITATION

Unfortunately, using the previously discussed non-culturability model (Shleeva et al., 2004), it was not possible to investigate the role of glycolylation in resuscitation using $\Delta namH$ *M. smegmatis* (Chapter 4). Non-culturability models in *Mtb* require several months for the production of non-culturable cells. However, previous work in the laboratory has demonstrated the production of Rpf-dependent cells through antimicrobial treatment. Therefore by using *Mtb* cultures after antimicrobial treatment and assessing their recovery by MPN, the role of glycolylation in the generation of Rpf-dependent cells could be investigated. Plates were prepared using diluted Sauton's medium or culture SN. Cultures producing growth in medium only were classed as culturable but MPN counts from culture SN plates using these cultures were still be used to examine recovery.

Culture SN, both of *Mtb* and other bacteria (i.e. *M. luteus*) is commonly used to stimulate resuscitation from dormancy, as it is a source of Rpf proteins amongst other agents (Votyakova et al., 1994, Sun and Zhang, 1999). Cultures treated with rifampicin and streptomycin did not produce any growth in liquid medium; Rpf-

dependent cells were not produced, this was true for both wild type and *ΔnamH Mtb*.

On one hand it was predicted, owing to the reduced survival of *ΔnamH Mtb* against isoniazid and the predicted reduced resuscitation ability; as a result of a weakened cell wall structure and potentially due to glycolylated muropeptides playing a role in mycobacterial resuscitation, that *ΔnamH Mtb* would produce lower MPN counts in comparison to wild type *Mtb*. However, due to the weakened cell wall architecture and the cell wall target of INZ it was also predicted that Rpf-dependent cells would be produced in *ΔnamH Mtb*. When grown in the presence of culture SN there was a slight increase in resuscitation of INZ treated *ΔnamH Mtb*.

Overall, it appears that *ΔnamH Mtb* cells, despite increased susceptibility to isoniazid are capable of recovery to a greater extent than wild type *Mtb*. A potential explanation for this observation could be due to clumping, as this was observed during *ΔnamH Mtb* growth studies. Clumping of the cells may protect some cells from damage and thus when placed into favourable medium (i.e. containing Rpfs) they are able to replicate again.

Overall the MPN counts for wild type and *ΔnamH Mtb* are too similar to draw any drastic conclusions. It may be that *ΔnamH Mtb* is capable of recovery, to the same extent as wild type *Mtb* or perhaps there was a population of cells, hidden from environmental stresses within *ΔnamH* clumps that produce high MPN values when grown in culture SN. Overall it cannot be concluded whether glycolylation is important for resuscitation in *Mtb*.

5.5 CONCLUSION

A $\Delta namH$ *Mtb* knockout was generated in order to investigate the biological role of glycolylated murein in *Mtb*. Once this mutant was confirmed by PCR and Southern hybridisation growth phenotypes were examined. A slight growth defect and an increase in clumping were observed, both of these observations fitted well with the previous *M. smegmatis* data. The role of this modification was then investigated in intracellular survival and replication using J774 macrophages. It was hypothesised that the loss of this modification and subsequent predicted reduction in hydrogen bonding, as well as increased susceptibility to muralytic enzymes would result in a reduced survival capability of $\Delta namH$ *Mtb*. Whilst a slight drop in cell count was observed consistently at the later stages of infection for $\Delta namH$ *Mtb*, these values were not statistically significant and hence: macrophage data indicated that N-glycolylation of the PG did not play a role in intracellular replication and survival. Initial data suggested non-glycolylated *Mtb* was more susceptible to antimicrobials with cell wall targets, but resuscitation potential remains unclear.

CHAPTER 6: FINAL CONCLUSIONS AND FUTURE WORK

6.1 FINAL CONCLUSIONS

Glycolylation of the mycobacterial PG was first identified in the 1970's by Takayama et al, initial studies examining the extent of this modification demonstrated a purely glycolylated mycobacterial PG (Takayama et al., 1970). However, more recent findings have shown that these original results were skewed as a consequence of drug treatment with D-cycloserine to enrich the intracellular pool of precursors (Mahapatra et al., 2005). By examining the intracellular pool of PG precursors, both in the presence and absence of drug treatment and analysing precursors and mature PG by MS, the effects could clearly be observed; when D-cycloserine treated *M. tuberculosis* PG precursors were analysed they were found to be solely comprised of UDP-glycolyl muramyl-tripeptide whereas *M. smegmatis*, under the same treatment, was found to contain a mixture of glycolylated and acetylated precursors (Mahapatra et al., 2005). The reverse was observed when vancomycin treatment was used. Ultimately the authors demonstrated a MurNGlyc to MurNAc ratio of 7:3 within mature *M. tuberculosis* PG when isolated in the absence of drug treatment.

Owing to the insensitivity of *M. tuberculosis* to β -lactams as well as the urgent need for new drug regimens, the role of glycolylation in mycobacterial intracellular survival, cell wall architecture and potentially resuscitation has been of interest in recent years. With the advent of microbial molecular biology, particularly within mycobacterial genetics, a study examining the antimicrobial sensitivity of a $\Delta namH$ *M. smegmatis* strain showed an increased susceptibility to β -lactam antibiotics (Raymond et al., 2005). This led to the hypothesis that this modification, due to the increased free hydroxyl groups, may result in greater cell wall stability as a result of additional hydrogen bonding. Alternatively the addition of

this functional group could affect the binding of cell wall drugs and hence a knockout may be more susceptible to drug treatment.

The aims of this study were to investigate the role of mycobacterial N-glycolylation in Rpf-mediated growth stimulation and resuscitation. This was carried out using the following objectives: Are *Mtb* Rpfs adapted to cleaving N-glycolylated PG? This was analysed by (1) attempting to generate glycolylated PG in *E. coli* and examining the resulting Rpf muropeptide products and (2) by over-expressing all five individual *Mtb* Rpfs in a $\Delta namH$ *M. smegmatis* mutant to determine *Mtb* Rpf growth stimulation and resuscitation effects. A further aim of this study was to assess the role of *Mtb* N-glycolylation in intracellular survival; this was carried out through the generation of a $\Delta namH$ *Mtb* mutant and assessed by murine macrophage infection studies. Investigation into the role of N-glycolylation in antimicrobial susceptibility was investigated by antimicrobial killing assays.

Overall *Mtb* Rpfs were not shown to be adapted to, or more efficient at cleaving bacteria containing N-glycolylated PG. *Mtb* Rpfs were shown to be capable of growth stimulation and resuscitation in wild type *M. smegmatis*. They were also able to stimulate growth in $\Delta namH$ *M. smegmatis*; *Mtb* RpfA showed the greatest growth stimulation in both wild type and $\Delta namH$ *M. smegmatis*. It was also demonstrated that whilst *M. smegmatis* contains endogenous Rpfs these did not result in resuscitation and a WT pMIND negative control was used throughout. A limitation of these investigations was the inability to of $\Delta namH$ *M. smegmatis* to reach non-culturability using the *M. smegmatis* method by Shleeva., et al. Hence, the effect of N-glycolylation in Rpf-mediated resuscitation could not be determined. However, MPN values for wild type *M. smegmatis* strains showed variability in individual Rpf resuscitation potential, indicating the diversity of the different proteins; RpfD had the greatest resuscitation index.

Macrophage infection studies demonstrated that glycolylation of *Mtb* PG had no effect on intracellular replication and survival, however antimicrobial killing showed an increased susceptibility to the cell wall targeted antimicrobial, isoniazid. These findings indicate that mycobacterial N-glycolylation may not have a role in intracellular survival, Rpf-associated growth stimulation or muralytic activity but potentially may be important for cell wall stability and antimicrobial susceptibility. Recent work has also shown that N-glycolylation may be important for mediating an immune response (Coulombe et al., 2009).

6.2 FUTURE WORK

As previously discussed, in order to achieve glycolylated PG in *E. coli* a system expressing a higher level of soluble protein would be required. One possible way that this solubility issue could be overcome would be to try an alternative tag, such as glutathione-S-transferase (GST), thioredoxin (Trx), or N utilization substance A (NusA) or to use an alternative expression host such as Origami™ B or Rosetta™, allowing a more controllable level of expression (Novagen, 2003a). Additionally, further work to produce a construct co-overexpressing soluble Rv3818 and Rv3819 could be investigated. However, with recent work having demonstrated *Mtb* Rpf muralytic activity in wild type *E. coli*, generation of a NamH overexpressing strain may not be necessary; analysis of Rpf muropeptide products could potentially be investigated using wild type *E. coli*.

In order to determine the role of mycobacterial N-glycolylation in Rpf-mediated resuscitation an alternative non-culturability model would need to be implemented. However, if the clumping of $\Delta namH$ *M. smegmatis* shields cells from harsh environments then finding a suitable non-culturability model may prove quite difficult. There are

several options to consider: a recent study using *M. smegmatis* cells grown in nitrogen minimal medium produced bacteria with low-metabolic activity and increased antibiotic resistance which were unable to form colonies on solid media. These cultures could still be resuscitated after storage for prolonged periods of time (Anuchin et al., 2009). Previous work has also demonstrated *M. smegmatis* entry into a dormancy-like, drug-resistant state under oxygen-limiting conditions (Lim and Dick, 2001). Therefore investigations into and optimisation of a new model would need to be carefully addressed.

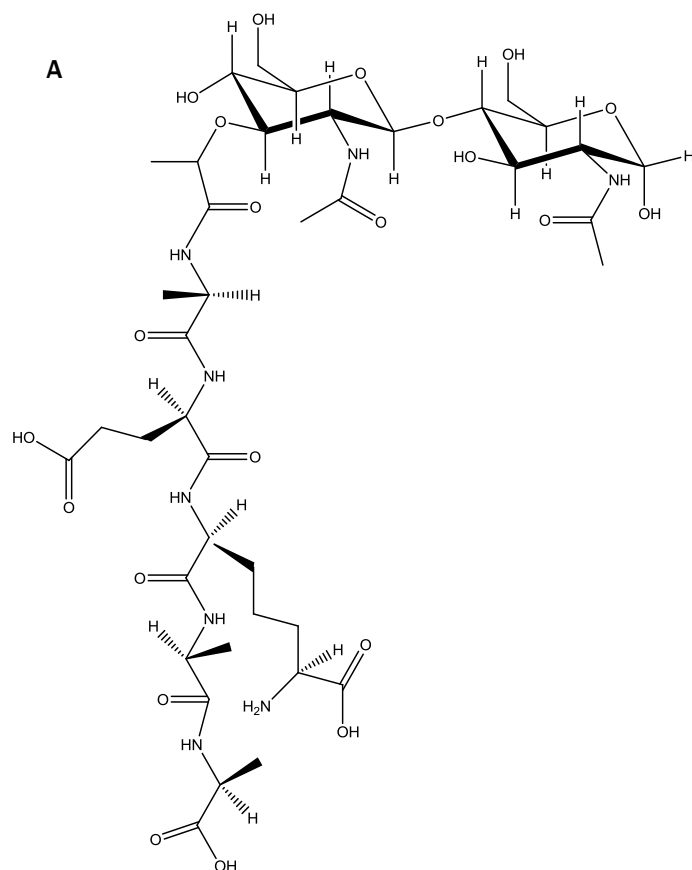
Further investigation into the role of *Mtb* N-glycolylation on long term survival, adaptation to a dormancy-like state and resuscitation could be carried out by implementing an *Mtb in vitro* dormancy model. An example of which is a multiple stress model (Deb et al., 2009), which uses low oxygen (5%), high CO₂ (10%), nutrient starvation and acidic pH (5.0); *Mtb* lost culturability and acid fastness, accumulated triacylglycerol (TG) and wax esters (WE) and then developed phenotypic antibiotic resistance. Alternatively Wayne's NRP model or nutrient starvation could be implemented (Betts et al., 2002, Wayne and Hayes, 1996). Again, these methods all have their own drawbacks and careful optimisation would be necessary.

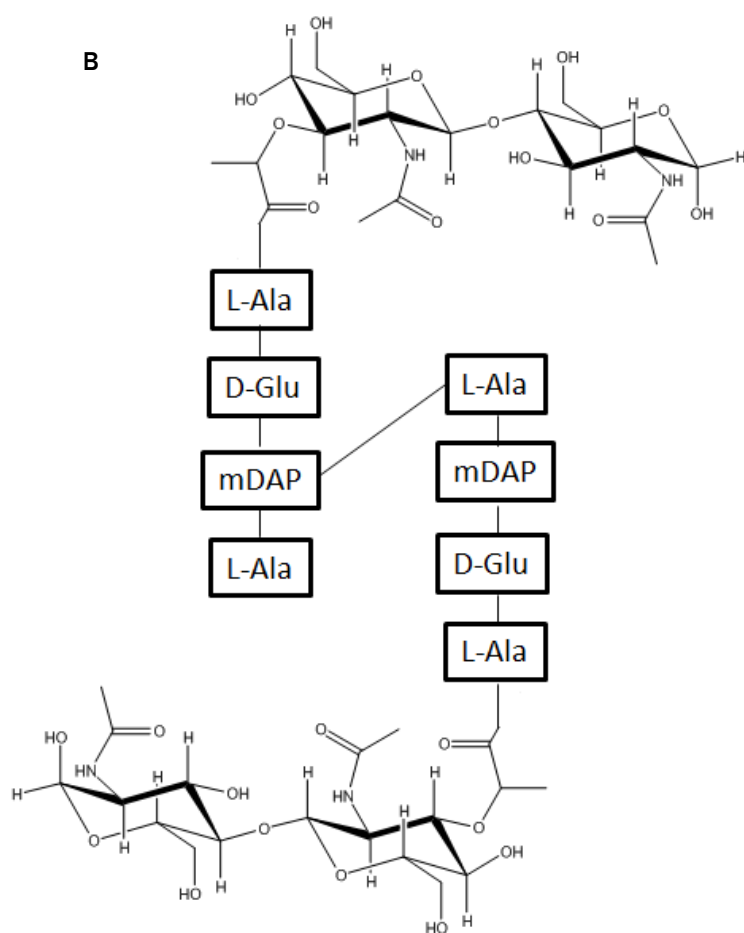
Finally, the role of peptidoglycan glycolylation in *Mtb* intracellular survival remains unknown. These investigations demonstrated that this modification does not play a role in intracellular survival in cultured macrophages. However, as previous studies have demonstrated that N-glycolyl muramyl dipeptides may have an important role in mediating host immune response (Coulombe et al., 2009) further investigations into $\Delta namH$ *Mtb* survival in an animal model may address these issues. Alternatively INF γ activated macrophage experiments could be performed in order to assess intracellular survival.

APPENDICES

APPENDIX 1: MUROPEPTIDE SCHEMATICS AND FRAGMENTATION

FIGURE 62: MUROPEPTIDE SCHEMATIC

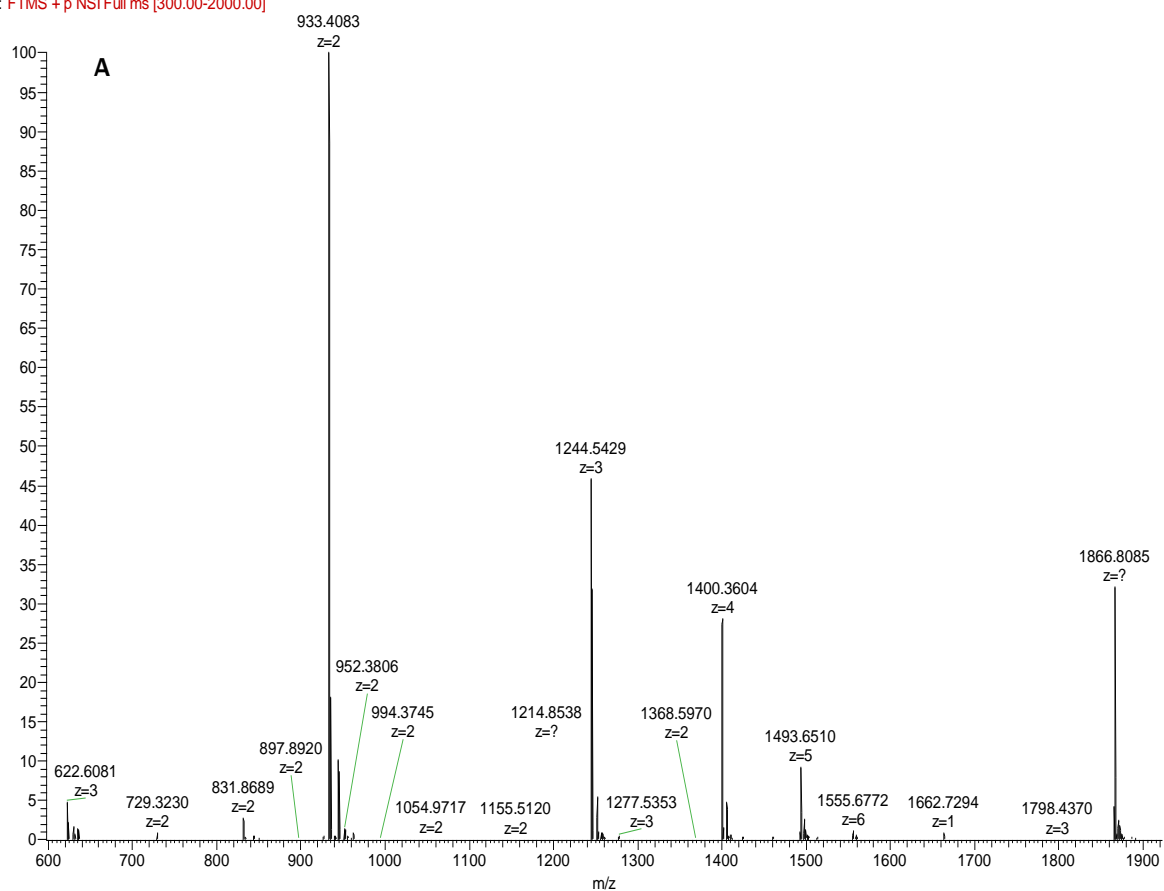




Structural schematics of mucopeptides: A) Disaccharide Pentapeptide is shown (NAG-NAM-L-Ala-D-Glu-mDAP-L-Ala-L-Ala) and B) Disaccharide Tetrapeptide-Disaccharide Tetrapeptide (4-3 cross-links) are shown.

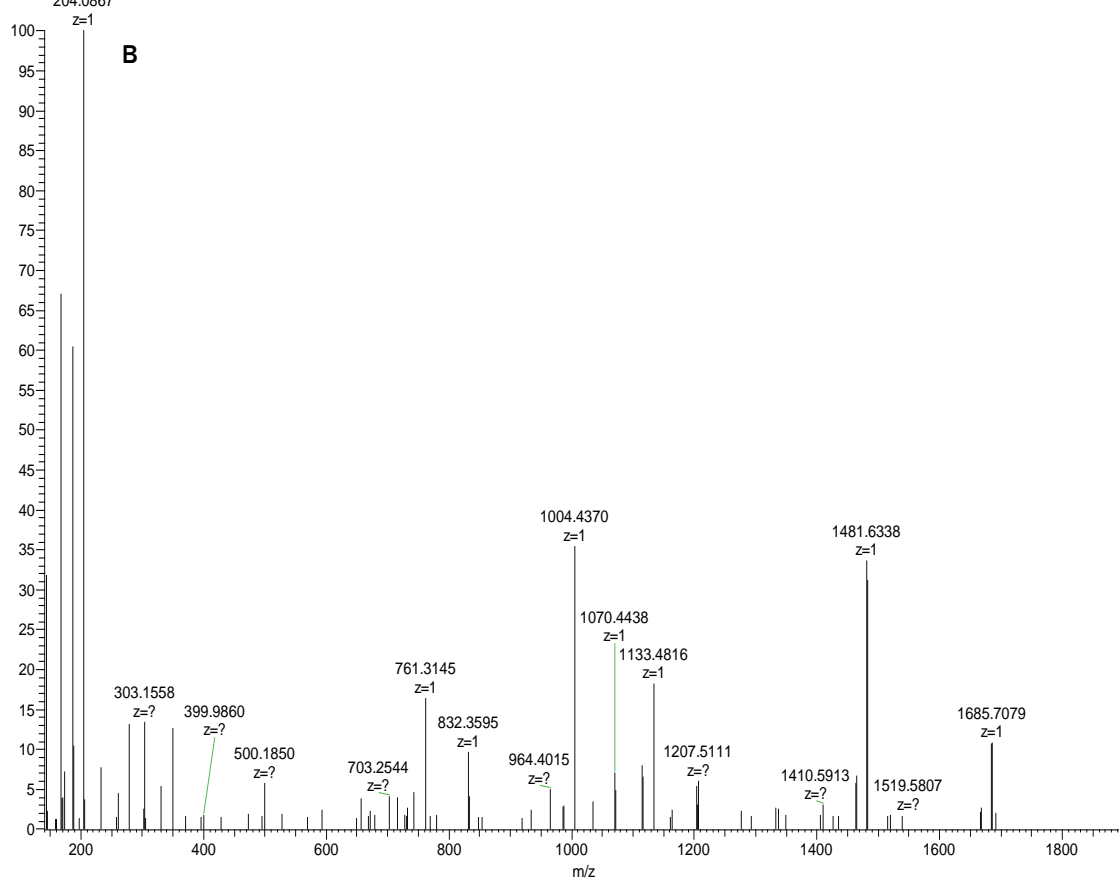
FIGURE 63: MASS SPECTRUM AND FRAGMENTATION OF MUTANOLYSIN RELEASED MUROPEPTIDES FROM *E. COLI* PG

120711_001_UL01219-EC-37 #747-1171 RT: 10.38-13.76 AV: 83 NL: 2.42E7
F: FTMS + p NSI Full ms [300.00-2000.00]



A mucopeptide sample collected via rp-HPLC from mutanolysin digested *E. coli* PG was analysed by MS (A) and the peak at 944 was further analysed by Tandem MS (B).

120711_001_UL01219-EC-37 #894 RT: 11.61 AV: 1 NL: 6.55E4
T: FTMS + c NSI d Full ms2 944.40@hcd42.50 [140.00-1900.00]
204.0867



(B) Tandem MS fragmentation was performed and the resulting ions compared to known mucopeptide molecular ions.

APPENDIX 2: QRT-PCR MELTING CURVES

FIGURE 64: MELTING CURVES FOR WILD TYPE AND Δ NAMH *M. SMEGMATIS* PMIND-RPFA-E CDNA SAMPLES AND *MTB* gDNA STANDARDS USING 16S rRNA PRIMERS

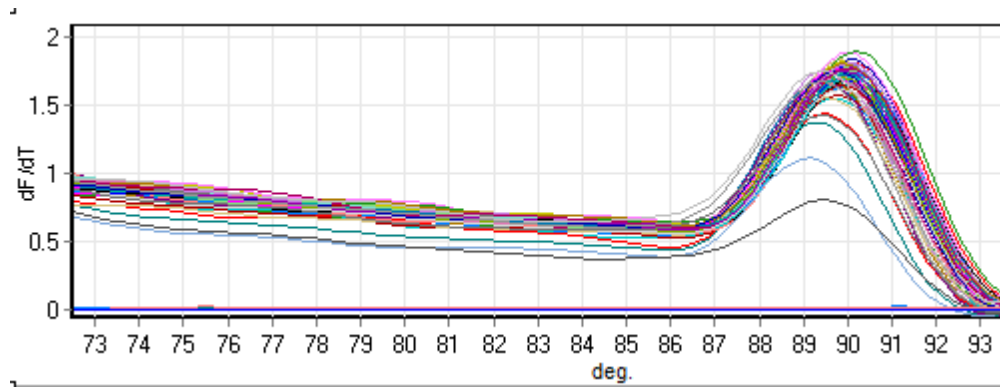


FIGURE 65: MELTING CURVES FOR WILD TYPE AND Δ NAMH *M. SMEGMATIS* PMIND-RPFA CDNA SAMPLES AND *MTB* gDNA STANDARDS USING RPFA PRIMERS

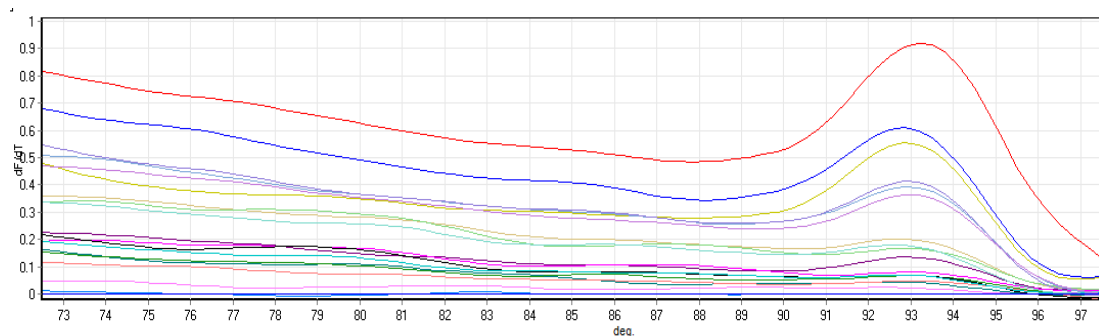


FIGURE 66: MELTING CURVES FOR WILD TYPE AND Δ NAMH *M. SMEGMATIS* PMIND-RPFB CDNA SAMPLES AND *MTB* gDNA STANDARDS USING RPFB PRIMERS

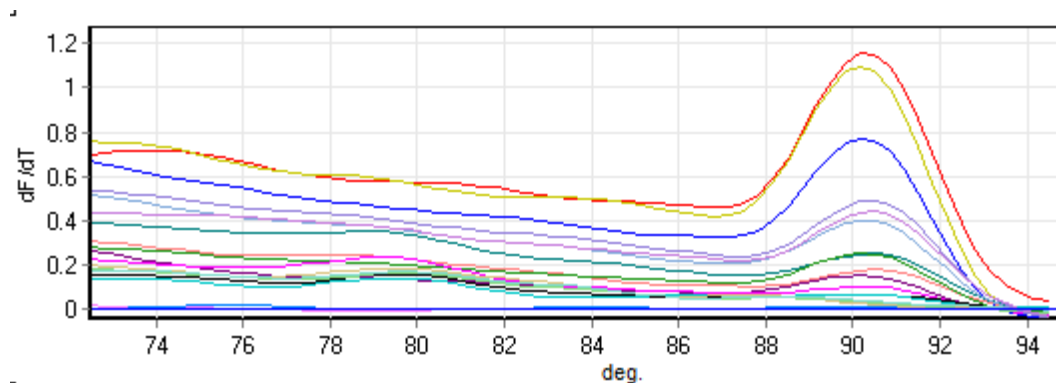


FIGURE 67: MELTING CURVES FOR WILD TYPE AND Δ NAMH *M. SMEGMATIS* PMIND-RPFC CDNA SAMPLES AND *MTB* GDNA STANDARDS USING RPFC PRIMERS

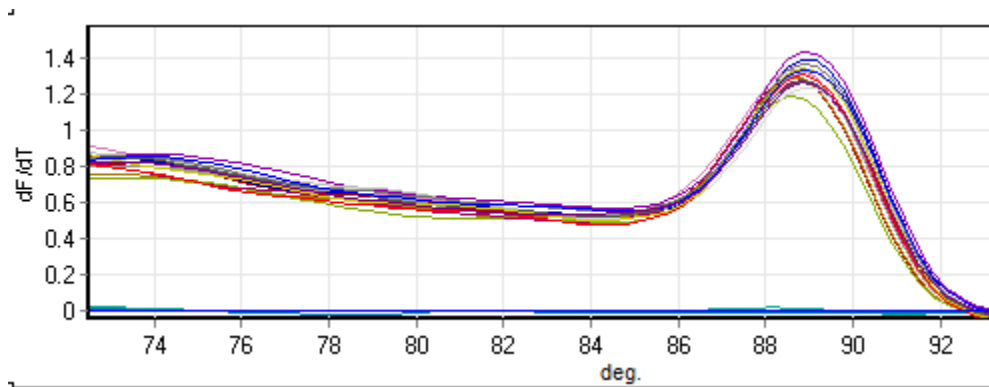


FIGURE 68: MELTING CURVES FOR WILD TYPE AND Δ NAMH *M. SMEGMATIS* PMIND-RPFD CDNA SAMPLES AND *MTB* GDNA STANDARDS USING RPFD PRIMERS

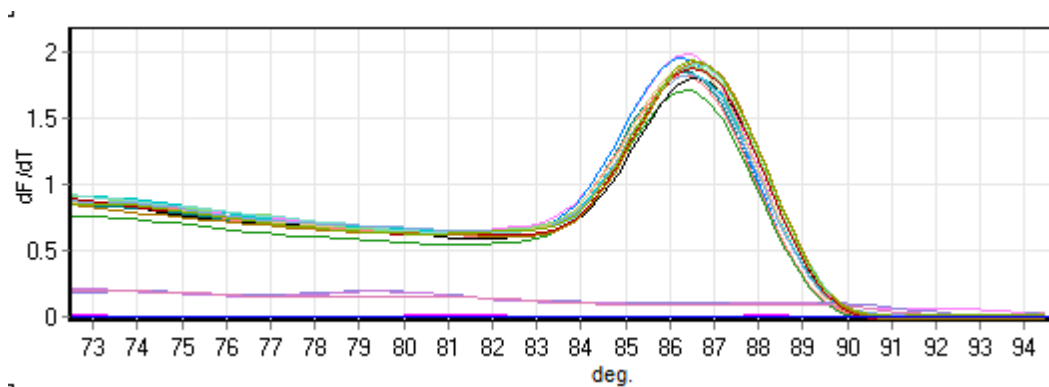
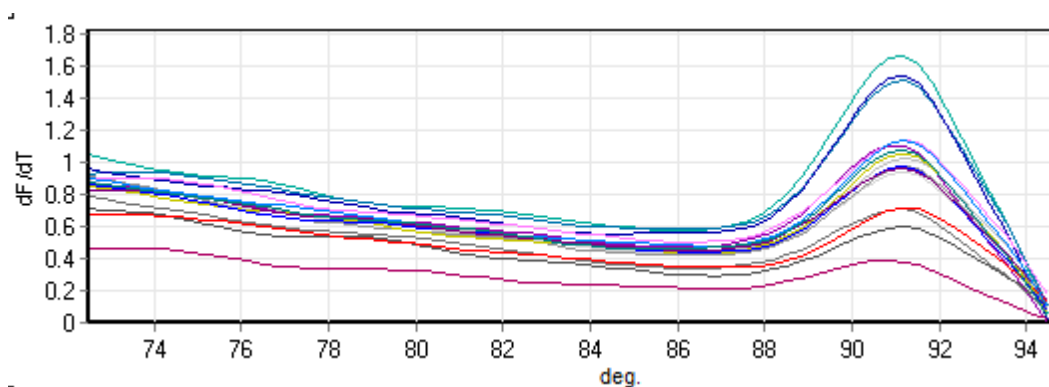


FIGURE 69: MELTING CURVES FOR WILD TYPE AND Δ NAMH *M. SMEGMATIS* PMIND-RPFE CDNA SAMPLES AND *MTB* GDNA STANDARDS USING RPFE PRIMERS



REFERENCES

- ABRAMOVITCH, R. B., ROHDE, K. H., HSU, F. F. & RUSSELL, D. G. 2011. aprABC: a Mycobacterium tuberculosis complex-specific locus that modulates pH-driven adaptation to the macrophage phagosome. *Mol Microbiol*, 80, 678-94.
- ACHTMAN, M. 2008. Evolution, population structure, and phylogeography of genetically monomorphic bacterial pathogens. *Annu Rev Microbiol*, 62, 53-70.
- ADAMS, K. N., TAKAKI, K., CONNOLLY, L. E., WIEDENHOFT, H., WINGLEE, K., HUMBERT, O., EDELSTEIN, P. H., COSMA, C. L. & RAMAKRISHNAN, L. 2011. Drug tolerance in replicating mycobacteria mediated by a macrophage-induced efflux mechanism. *Cell*, 145, 39-53.
- AMANO, K. & WILLIAMS, J. C. 1983. Peptidoglycan of Legionella pneumophila: apparent resistance to lysozyme hydrolysis correlates with a high degree of peptide cross-linking. *J Bacteriol*, 153, 520-6.
- ANDRIES, K., VERHASSELT, P., GUILLEMONT, J., GOHLMANN, H. W., NEEFS, J. M., WINKLER, H., VAN GESTEL, J., TIMMERMAN, P., ZHU, M., LEE, E., WILLIAMS, P., DE CHAFFOY, D., HUITRIC, E., HOFFNER, S., CAMBAU, E., TRUFFOT-PERNOT, C., LOUNIS, N. & JARLIER, V. 2005. A diarylquinoline drug active on the ATP synthase of Mycobacterium tuberculosis. *Science*, 307, 223-7.
- ANUCHIN, A. M., MULYUKIN, A. L., SUZINA, N. E., DUDA, V. I., EL-REGISTAN, G. I. & KAPRELYANTS, A. S. 2009. Dormant forms of Mycobacterium smegmatis with distinct morphology. *Microbiology*, 155, 1071-9.
- ARBELOA, A., HUGONNET, J. E., SENTILHES, A. C., JOSSEAUME, N., DUBOST, L., MONSEMPES, C., BLANOT, D., BROUARD, J. P. & ARTHUR, M. 2004. Synthesis of mosaic peptidoglycan cross-bridges by hybrid peptidoglycan assembly pathways in gram-positive bacteria. *J Biol Chem*, 279, 41546-56.
- ARNVIG, K. & YOUNG, D. 2012. Non-coding RNA and its potential role in Mycobacterium tuberculosis pathogenesis. *RNA Biol*, 9, 427-36.
- BALASUBRAMANIAN, V., PAVELKA, M. S., JR., BARDAROV, S. S., MARTIN, J., WEISBROD, T. R., MCADAM, R. A., BLOOM, B. R. & JACOBS, W. R., JR. 1996. Allelic exchange in Mycobacterium tuberculosis with long linear recombination substrates. *J Bacteriol*, 178, 273-9.
- BANERJEE, A., DUBNAU, E., QUEMARD, A., BALASUBRAMANIAN, V., UM, K. S., WILSON, T., COLLINS, D., DE LISLE, G. & JACOBS, W. R., JR. 1994. inhA, a gene encoding a target for isoniazid and ethionamide in Mycobacterium tuberculosis. *Science*, 263, 227-30.
- BANFI, E., SCIALINO, G. & MONTI-BRAGADIN, C. 2003. Development of a microdilution method to evaluate Mycobacterium tuberculosis drug susceptibility. *J Antimicrob Chemother*, 52, 796-800.
- BARRY, C. E., 3RD, BOSHOFF, H. I., DARTOIS, V., DICK, T., EHRT, S., FLYNN, J., SCHNAPPINGER, D., WILKINSON, R. J. & YOUNG, D. 2009. The spectrum of latent tuberculosis: rethinking the biology and intervention strategies. *Nat Rev Microbiol*, 7, 845-55.
- BARTHE, P., MUKAMOLOVA, G. V., ROUMESTAND, C. & COHEN-GONSAUD, M. 2010. The structure of PknB extracellular PASTA domain from mycobacterium tuberculosis suggests a ligand-dependent kinase activation. *Structure*, 18, 606-15.
- BERA, A., BISWAS, R., HERBERT, S. & GOTZ, F. 2006. The presence of peptidoglycan O-acetyltransferase in various staphylococcal species correlates with lysozyme resistance and pathogenicity. *Infect Immun*, 74, 4598-604.
- BERNSTEIN, J., LOTT, W. A., STEINBERG, B. A. & YALE, H. L. 1952. Chemotherapy of experimental tuberculosis. V. Isonicotinic acid hydrazide (nydrazid) and related compounds. *Am Rev Tuberc*, 65, 357-64.

- BETTS, J. C., LUKEY, P. T., ROBB, L. C., MCADAM, R. A. & DUNCAN, K. 2002. Evaluation of a nutrient starvation model of *Mycobacterium tuberculosis* persistence by gene and protein expression profiling. *Mol Microbiol*, 43, 717-31.
- BIKETOV, S., POTAPOV, V., GANINA, E., DOWNING, K., KANA, B. D. & KAPRELYANTS, A. 2007. The role of resuscitation promoting factors in pathogenesis and reactivation of *Mycobacterium tuberculosis* during intra-peritoneal infection in mice. *BMC Infect Dis*, 7, 146.
- BLACKBURN, N. T. & CLARKE, A. J. 2000. Assay for lytic transglycosylases: a family of peptidoglycan lyases. *Anal Biochem*, 284, 388-93.
- BLAKEMORE, R., STORY, E., HELB, D., KOP, J., BANADA, P., OWENS, M. R., CHAKRAVORTY, S., JONES, M. & ALLAND, D. 2010. Evaluation of the analytical performance of the Xpert MTB/RIF assay. *J Clin Microbiol*, 48, 2495-501.
- BLOKPOEL, M. C., MURPHY, H. N., O'TOOLE, R., WILES, S., RUNN, E. S., STEWART, G. R., YOUNG, D. B. & ROBERTSON, B. D. 2005. Tetracycline-inducible gene regulation in mycobacteria. *Nucleic Acids Res*, 33, e22.
- BODNAR, K. A., SERBINA, N. V. & FLYNN, J. L. 2001. Fate of *Mycobacterium tuberculosis* within murine dendritic cells. *Infect Immun*, 69, 800-9.
- BOEHME, C. C., NABETA, P., HILLEMANN, D., NICOL, M. P., SHENAI, S., KRAPP, F., ALLEN, J., TAHIRLI, R., BLAKEMORE, R., RUSTOMJEE, R., MILOVIC, A., JONES, M., O'BRIEN, S. M., PERSING, D. H., RUESCH-GERDES, S., GOTUZZO, E., RODRIGUES, C., ALLAND, D. & PERKINS, M. D. 2010. Rapid molecular detection of tuberculosis and rifampin resistance. *N Engl J Med*, 363, 1005-15.
- BONECA, I. G. 2005. The role of peptidoglycan in pathogenesis. *Curr Opin Microbiol*, 8, 46-53.
- BOSHOFF, H. I., MYERS, T. G., COPP, B. R., MCNEIL, M. R., WILSON, M. A. & BARRY, C. E., 3RD 2004. The transcriptional responses of *Mycobacterium tuberculosis* to inhibitors of metabolism: novel insights into drug mechanisms of action. *J Biol Chem*, 279, 40174-84.
- BOTH, D., SCHNEIDER, G. & SCHNELL, R. 2011. Peptidoglycan remodeling in *Mycobacterium tuberculosis*: comparison of structures and catalytic activities of RipA and RipB. *J Mol Biol*, 413, 247-60.
- BRENNAN, P. J. & NIKAIIDO, H. 1995. The envelope of mycobacteria. *Annu Rev Biochem*, 64, 29-63.
- BRITTON, W. J., HELLQVIST, L., BASTEN, A. & RAISON, R. L. 1985. *Mycobacterium leprae* antigens involved in human immune responses. I. Identification of four antigens by monoclonal antibodies. *J Immunol*, 135, 4171-7.
- BROSCH, R., GORDON, S. V., MARMIESSE, M., BRODIN, P., BUCHRIESER, C., EIGLMEIER, K., GARNIER, T., GUTIERREZ, C., HEWINSON, G., KREMER, K., PARSONS, L. M., PYM, A. S., SAMPER, S., VAN SOOLINGEN, D. & COLE, S. T. 2002. A new evolutionary scenario for the *Mycobacterium tuberculosis* complex. *Proc Natl Acad Sci U S A*, 99, 3684-9.
- BRUDEY, K., DRISCOLL, J. R., RIGOUTS, L., PRODINGER, W. M., GORI, A., AL-HAJOJ, S. A., ALLIX, C., ARISTIMUNO, L., ARORA, J., BAUMANIS, V., BINDER, L., CAFRONE, P., CATALDI, A., CHEONG, S., DIEL, R., ELLERMEIER, C., EVANS, J. T., FAUVILLE-DUFAUX, M., FERDINAND, S., GARCIA DE VIEDMA, D., GARZELLI, C., GAZZOLA, L., GOMES, H. M., GUTTIEREZ, M. C., HAWKEY, P. M., VAN HELDEN, P. D., KADIVAL, G. V., KREISWIRTH, B. N., KREMER, K., KUBIN, M., KULKARNI, S. P., LIENS, B., LILLEBAEK, T., HO, M. L., MARTIN, C., MOKROUSOV, I., NARVSKAIA, O., NGEOW, Y. F., NAUMANN, L., NIEMANN, S., PARWATI, I., RAHIM, Z., RASOLOFO-RAZANAMPARANY, V., RASOLONAVALONA, T., ROSSETTI, M. L., RUSCH-GERDES, S., SAJDUDA, A., SAMPER, S., SHEMYAKIN, I. G., SINGH, U. B., SOMOSKOVI, A., SKUCE, R. A., VAN SOOLINGEN, D., STREICHER, E. M., SUFFYS, P. N., TORTOLI, E., TRACEVSKA, T., VINCENT, V., VICTOR, T. C., WARREN, R. M., YAP, S. F., ZAMAN, K., PORTAELS, F., RASTOGI, N. & SOLA, C. 2006. *Mycobacterium*

- tuberculosis complex genetic diversity: mining the fourth international spoligotyping database (SpolDB4) for classification, population genetics and epidemiology. *BMC Microbiol*, 6, 23.
- CARDONA, P. J. & RUIZ-MANZANO, J. 2004. On the nature of Mycobacterium tuberculosis-latent bacilli. *Eur Respir J*, 24, 1044-51.
- CATTAMANCHI, A., SMITH, R., STEINGART, K. R., METCALFE, J. Z., DATE, A., COLEMAN, C., MARSTON, B. J., HUANG, L., HOPEWELL, P. C. & PAI, M. 2011. Interferon-gamma release assays for the diagnosis of latent tuberculosis infection in HIV-infected individuals: a systematic review and meta-analysis. *J Acquir Immune Defic Syndr*, 56, 230-8.
- CAWS, M., THWAITES, G., DUNSTAN, S., HAWN, T. R., LAN, N. T., THUONG, N. T., STEPNIIEWSKA, K., HUYEN, M. N., BANG, N. D., LOC, T. H., GAGNEUX, S., VAN SOOLINGEN, D., KREMER, K., VAN DER SANDE, M., SMALL, P., ANH, P. T., CHINH, N. T., QUY, H. T., DUYEN, N. T., THO, D. Q., HIEU, N. T., TOROK, E., HIEN, T. T., DUNG, N. H., NHU, N. T., DUY, P. M., VAN VINH CHAU, N. & FARRAR, J. 2008. The influence of host and bacterial genotype on the development of disseminated disease with Mycobacterium tuberculosis. *PLoS Pathog*, 4, e1000034.
- CHAMAILLARD, M., HASHIMOTO, M., HORIE, Y., MASUMOTO, J., QIU, S., SAAB, L., OGURA, Y., KAWASAKI, A., FUKASE, K., KUSUMOTO, S., VALVANO, M. A., FOSTER, S. J., MAK, T. W., NUNEZ, G. & INOHARA, N. 2003. An essential role for NOD1 in host recognition of bacterial peptidoglycan containing diaminopimelic acid. *Nat Immunol*, 4, 702-7.
- CHAN, E. D., STRAND, M. J. & ISEMAN, M. D. 2009. Multidrug-resistant tuberculosis (TB) resistant to fluoroquinolones and streptomycin but susceptible to second-line injection therapy has a better prognosis than extensively drug-resistant TB. *Clin Infect Dis*, 48, e50-2.
- CHAN, J., XING, Y., MAGLIOZZO, R. S. & BLOOM, B. R. 1992. Killing of virulent Mycobacterium tuberculosis by reactive nitrogen intermediates produced by activated murine macrophages. *J Exp Med*, 175, 1111-22.
- CHAO, M. C., KIESER, K. J., MINAMI, S., MAVRICI, D., ALDRIDGE, B. B., FORTUNE, S. M., ALBER, T. & RUBIN, E. J. 2013. Protein complexes and proteolytic activation of the cell wall hydrolase RipA regulate septal resolution in mycobacteria. *PLoS Pathog*, 9, e1003197.
- CIUCANU, I., ; KEREK, F 1984. A SIMPLE AND RAPID METHOD FOR THE PERMETHYLATION OF CARBOHYDRATES. *CARBOHYDRATE RESEARCH*, 131, 209-217.
- COHEN-GONSAUD, M., BARTHE, P., BAGNERIS, C., HENDERSON, B., WARD, J., ROUMESTAND, C. & KEEP, N. H. 2005. The structure of a resuscitation-promoting factor domain from Mycobacterium tuberculosis shows homology to lysozymes. *Nat Struct Mol Biol*, 12, 270-3.
- COLANGELI, R., HELB, D., SRIDHARAN, S., SUN, J., VARMA-BASIL, M., HAZBON, M. H., HARBACHEUSKI, R., MEGJUGORAC, N. J., JACOBS, W. R., JR., HOLZENBURG, A., SACCHETTINI, J. C. & ALLAND, D. 2005. The Mycobacterium tuberculosis iniA gene is essential for activity of an efflux pump that confers drug tolerance to both isoniazid and ethambutol. *Mol Microbiol*, 55, 1829-40.
- COLE, S. T. (ed.) 2005. *Tuberculosis and the Tubercle Bacillus*: American Society for Microbiology.
- COMMANDEUR, S., VAN MEIJGAARDEN, K. E., LIN, M. Y., FRANKEN, K. L., FRIGGEN, A. H., DRIJFHOUT, J. W., OFTUNG, F., KORSVOLD, G. E., GELUK, A. & OTTENHOFF, T. H. 2011. Identification of human T-cell responses to Mycobacterium tuberculosis resuscitation-promoting factors in long-term latently infected individuals. *Clin Vaccine Immunol*, 18, 676-83.
- COULOMBE, F., DIVANGAHI, M., VEYRIER, F., DE LESELEUC, L., GLEASON, J. L., YANG, Y., KELLIHER, M. A., PANDEY, A. K., SASSETTI, C. M., REED, M. B. & BEHR, M. A. 2009.

- Increased NOD2-mediated recognition of N-glycolyl muramyl dipeptide. *J Exp Med*, 206, 1709-16.
- CRICK, D. C., MAHAPATRA, S. & BRENNAN, P. J. 2001. Biosynthesis of the arabinogalactan-peptidoglycan complex of *Mycobacterium tuberculosis*. *Glycobiology*, 11, 107R-118R.
- CUEVAS, L. E., BROWNING, R., BOSSUYT, P., CASENGHI, M., COTTON, M. F., CRUZ, A. T., DODD, L. E., DROBNIOWSKI, F., GALE, M., GRAHAM, S. M., GRZEMSKA, M., HEINRICH, N., HESSELING, A. C., HUEBNER, R., JEAN-PHILIPPE, P., KABRA, S. K., KAMPMANN, B., LEWINSOHN, D., LI, M., LIENHARDT, C., MANDALAKAS, A. M., MARAIS, B. J., MENZIES, H. J., MONTEPIEDRA, G., MWANSAMBO, C., OBERHELMAN, R., PALUMBO, P., RUSSEK-COHEN, E., SHAPIRO, D. E., SMITH, B., SOTO-CASTELLARES, G., STARKE, J. R., SWAMINATHAN, S., WINGFIELD, C. & WORRELL, C. 2012. Evaluation of tuberculosis diagnostics in children: 2. Methodological issues for conducting and reporting research evaluations of tuberculosis diagnostics for intrathoracic tuberculosis in children. Consensus from an expert panel. *J Infect Dis*, 205 Suppl 2, S209-15.
- CUEVAS, L. E., YASSIN, M. A., AL-SONBOLI, N., LAWSON, L., ARBIDE, I., AL-AGHBARI, N., SHERCHAND, J. B., AL-ABSI, A., EMENYONU, E. N., MERID, Y., OKOBI, M. I., ONUOHA, J. O., ASCHALEW, M., ASEFFA, A., HARPER, G., DE CUEVAS, R. M., KREMER, K., VAN SOOLINGEN, D., NATHANSON, C. M., JOLY, J., FARAGHER, B., SQUIRE, S. B. & RAMSAY, A. 2011. A multi-country non-inferiority cluster randomized trial of frontloaded smear microscopy for the diagnosis of pulmonary tuberculosis. *PLoS Med*, 8, e1000443.
- D'ORDINE, R. L., RYDEL, T. J., STOREK, M. J., STURMAN, E. J., MOSHIRI, F., BARTLETT, R. K., BROWN, G. R., EILERS, R. J., DART, C., QI, Y., FLASINSKI, S. & FRANKLIN, S. J. 2009. Dicamba monooxygenase: structural insights into a dynamic Rieske oxygenase that catalyzes an exocyclic monooxygenation. *J Mol Biol*, 392, 481-97.
- DAHL, J. L., KRAUS, C. N., BOSHOFF, H. I., DOAN, B., FOLEY, K., AVARBOCK, D., KAPLAN, G., MIZRAHI, V., RUBIN, H. & BARRY, C. E., 3RD 2003. The role of RelMtb-mediated adaptation to stationary phase in long-term persistence of *Mycobacterium tuberculosis* in mice. *Proc Natl Acad Sci U S A*, 100, 10026-31.
- DAVIES, A. P., DHILLON, A. P., YOUNG, M., HENDERSON, B., MCHUGH, T. D. & GILLESPIE, S. H. 2008. Resuscitation-promoting factors are expressed in *Mycobacterium tuberculosis*-infected human tissue. *Tuberculosis (Edinb)*, 88, 462-8.
- DE JONGE, B. L., WIENTJES, F. B., JURIDA, I., DRIEHUIS, F., WOUTERS, J. T. & NANNINGA, N. 1989. Peptidoglycan synthesis during the cell cycle of *Escherichia coli*: composition and mode of insertion. *J Bacteriol*, 171, 5783-94.
- DE PEDRO, M. A., HÖLTJE, J. V., LÖFFELHARDT, W. & FEDERATION OF EUROPEAN MICROBIOLOGICAL SOCIETIES. 1993. *Bacterial growth and lysis : metabolism and structure of the bacterial sacculus*, New York, Plenum Press.
- DEB, C., LEE, C. M., DUBEY, V. S., DANIEL, J., ABOMOELAK, B., SIRAKOVA, T. D., PAWAR, S., ROGERS, L. & KOLATTUKUDY, P. E. 2009. A novel in vitro multiple-stress dormancy model for *Mycobacterium tuberculosis* generates a lipid-loaded, drug-tolerant, dormant pathogen. *PLoS One*, 4, e6077.
- DENIS, M. 1991. Involvement of cytokines in determining resistance and acquired immunity in murine tuberculosis. *J Leukoc Biol*, 50, 495-501.
- DHARMADHIKARI, A. S. & NARDELL, E. A. 2008. What animal models teach humans about tuberculosis. *Am J Respir Cell Mol Biol*, 39, 503-8.
- DHEDA, K., BOOTH, H., HUGGETT, J. F., JOHNSON, M. A., ZUMLA, A. & ROOK, G. A. 2005. Lung remodeling in pulmonary tuberculosis. *J Infect Dis*, 192, 1201-9.
- DOVER, L. G., ALDERWICK, L. J., BROWN, A. K., FUTTERER, K. & BESRA, G. S. 2007. Regulation of cell wall synthesis and growth. *Curr Mol Med*, 7, 247-76.
- DOWNING, K. J., MISCHENKO, V. V., SHLEEVA, M. O., YOUNG, D. I., YOUNG, M., KAPRELYANTS, A. S., APT, A. S. & MIZRAHI, V. 2005. Mutants of *Mycobacterium tuberculosis* lacking

- three of the five rpf-like genes are defective for growth in vivo and for resuscitation in vitro. *Infect Immun*, 73, 3038-43.
- DRAPER, P., KANDLER, O. & DARBRE, A. 1987. Peptidoglycan and arabinogalactan of *Mycobacterium leprae*. *J Gen Microbiol*, 133, 1187-94.
- DYER, K. A. 1992. Reshaping our views of death and dying. *JAMA*, 267, 1265, 1269-70.
- ENDL, J., SEIDL, P. H., FIEDLER, F. & SCHLEIFER, K. H. 1984. Determination of cell wall teichoic acid structure of staphylococci by rapid chemical and serological screening methods. *Arch Microbiol*, 137, 272-80.
- FENTON, M. J. & VERMEULEN, M. W. 1996. Immunopathology of tuberculosis: roles of macrophages and monocytes. *Infect Immun*, 64, 683-90.
- FERGUSON, J. S., WEIS, J. J., MARTIN, J. L. & SCHLESINGER, L. S. 2004. Complement protein C3 binding to *Mycobacterium tuberculosis* is initiated by the classical pathway in human bronchoalveolar lavage fluid. *Infect Immun*, 72, 2564-73.
- FERRARO, D. J., GAKHAR, L. & RAMASWAMY, S. 2005. Rieske business: structure-function of Rieske non-heme oxygenases. *Biochem Biophys Res Commun*, 338, 175-90.
- FIRMANI, M. A. & RILEY, L. W. 2002. *Mycobacterium tuberculosis* CDC1551 is resistant to reactive nitrogen and oxygen intermediates in vitro. *Infect Immun*, 70, 3965-8.
- FLYNN, J. L. & CHAN, J. 2001. Tuberculosis: latency and reactivation. *Infect Immun*, 69, 4195-201.
- FONTAN, P. A., ARIS, V., ALVAREZ, M. E., GHANNY, S., CHENG, J., SOTEROPOULOS, P., TREVANI, A., PINE, R. & SMITH, I. 2008. *Mycobacterium tuberculosis* sigma factor E regulon modulates the host inflammatory response. *J Infect Dis*, 198, 877-85.
- FRIEDEN, T. R., STERLING, T. R., MUNSIFF, S. S., WATT, C. J. & DYE, C. 2003. Tuberculosis. *Lancet*, 362, 887-99.
- GALLY, D. L., HANCOCK, I. C., HARWOOD, C. R. & ARCHIBALD, A. R. 1991. Cell wall assembly in *Bacillus megaterium*: incorporation of new peptidoglycan by a monomer addition process. *J Bacteriol*, 173, 2548-55.
- GARCIA-FRUITOS, E., GONZALEZ-MONTALBAN, N., MORELL, M., VERA, A., FERRAZ, R. M., ARIS, A., VENTURA, S. & VILLAVERDE, A. 2005. Aggregation as bacterial inclusion bodies does not imply inactivation of enzymes and fluorescent proteins. *Microb Cell Fact*, 4, 27.
- GASTEIGER, E., GATTIKER, A., HOOGLAND, C., IVANYI, I., APPEL, R. D. & BAIROCH, A. 2003. ExpASY: The proteomics server for in-depth protein knowledge and analysis. *Nucleic Acids Res*, 31, 3784-8.
- GENGENBACHER, M. & KAUFMANN, S. H. 2012. *Mycobacterium tuberculosis*: success through dormancy. *FEMS Microbiol Rev*, 36, 514-32.
- GILL, W. P., HARIK, N. S., WHIDDON, M. R., LIAO, R. P., MITTLER, J. E. & SHERMAN, D. R. 2009. A replication clock for *Mycobacterium tuberculosis*. *Nat Med*, 15, 211-4.
- GIRARDIN, S. E., BONECA, I. G., CARNEIRO, L. A., ANTIGNAC, A., JEHANNO, M., VIALA, J., TEDIN, K., TAHA, M. K., LABIGNE, A., ZHRINGER, U., COYLE, A. J., DISTEFANO, P. S., BERTIN, J., SANSONETTI, P. J. & PHILPOTT, D. J. 2003a. Nod1 detects a unique muropeptide from gram-negative bacterial peptidoglycan. *Science*, 300, 1584-7.
- GIRARDIN, S. E., BONECA, I. G., VIALA, J., CHAMAILLARD, M., LABIGNE, A., THOMAS, G., PHILPOTT, D. J. & SANSONETTI, P. J. 2003b. Nod2 is a general sensor of peptidoglycan through muramyl dipeptide (MDP) detection. *J Biol Chem*, 278, 8869-72.
- GLAUNER, B. 1988. Separation and quantification of muropeptides with high-performance liquid chromatography. *Anal Biochem*, 172, 451-64.
- GLAUNER, B., HOLTJE, J. V. & SCHWARZ, U. 1988. The composition of the murein of *Escherichia coli*. *J Biol Chem*, 263, 10088-95.
- GOLD, B., PINGLE, M., BRICKNER, S. J., SHAH, N., ROBERTS, J., RUNDELL, M., BRACKEN, W. C., WARRIER, T., SOMERSAN, S., VENUGOPAL, A., DARBY, C., JIANG, X., WARREN, J. D.,

- FERNANDEZ, J., OUERFELLI, O., NUERMBERGER, E. L., CUNNINGHAM-BUSSEL, A., RATH, P., CHIDAWANYIKA, T., DENG, H., REALUBIT, R., GLICKMAN, J. F. & NATHAN, C. F. 2012. Nonsteroidal anti-inflammatory drug sensitizes Mycobacterium tuberculosis to endogenous and exogenous antimicrobials. *Proc Natl Acad Sci U S A*, 109, 16004-11.
- GORDON, S. V., BROSCHE, R., BILLAULT, A., GARNIER, T., EIGLMEIER, K. & COLE, S. T. 1999. Identification of variable regions in the genomes of tubercle bacilli using bacterial artificial chromosome arrays. *Mol Microbiol*, 32, 643-55.
- GORDON, S. V., EIGLMEIER, K., GARNIER, T., BROSCHE, R., PARKHILL, J., BARRELL, B., COLE, S. T. & HEWINSON, R. G. 2001. Genomics of Mycobacterium bovis. *Tuberculosis (Edinb)*, 81, 157-63.
- GOUDE, R., AMIN, A. G., CHATTERJEE, D. & PARISH, T. 2009. The arabinosyltransferase EmbC is inhibited by ethambutol in Mycobacterium tuberculosis. *Antimicrob Agents Chemother*, 53, 4138-46.
- GRIFFITH, D. E., AKSAMIT, T., BROWN-ELLIOTT, B. A., CATANZARO, A., DALEY, C., GORDIN, F., HOLLAND, S. M., HORSBURGH, R., HUITT, G., IADEMARCO, M. F., ISEMAN, M., OLIVIER, K., RUOSS, S., VON REYN, C. F., WALLACE, R. J., JR. & WINTHROP, K. 2007. An official ATS/IDSA statement: diagnosis, treatment, and prevention of nontuberculous mycobacterial diseases. *Am J Respir Crit Care Med*, 175, 367-416.
- GUILHOT, C., OTAL, I., VAN ROMPAEY, I., MARTIN, C. & GICQUEL, B. 1994. Efficient transposition in mycobacteria: construction of Mycobacterium smegmatis insertional mutant libraries. *J Bacteriol*, 176, 535-9.
- GUPTA, K. R., SRIVASTAVA, R. 2012. Resuscitation Promoting Factors: a Family of Microbial Proteins in Survival and Resuscitation of Dormant Mycobacteria. *Indian J Microbiol*, 52, 114-121.
- GUPTA, R., LAVOLLAY, M., MAINARDI, J. L., ARTHUR, M., BISHAI, W. R. & LAMICHHANE, G. 2010a. The Mycobacterium tuberculosis protein LdtMt2 is a nonclassical transpeptidase required for virulence and resistance to amoxicillin. *Nat Med*, 16, 466-9.
- GUPTA, R. K., SRIVASTAVA, B. S. & SRIVASTAVA, R. 2010b. Comparative expression analysis of rpf-like genes of Mycobacterium tuberculosis H37Rv under different physiological stress and growth conditions. *Microbiology*, 156, 2714-22.
- GUPTA, U. D. & KATOCH, V. M. 2009. Animal models of tuberculosis for vaccine development. *Indian J Med Res*, 129, 11-8.
- HARRIS, R. F. & SOMMERS, L. E. 1968. Plate-dilution frequency technique for assay of microbial ecology. *Appl Microbiol*, 16, 330-4.
- HAYASHI, K. 1975. A rapid determination of sodium dodecyl sulfate with methylene blue. *Anal Biochem*, 67, 503-6.
- HEID, C. A., STEVENS, J., LIVAK, K. J. & WILLIAMS, P. M. 1996. Real time quantitative PCR. *Genome Res*, 6, 986-94.
- HERSHKOVITZ, I., DONOGHUE, H. D., MINNIKIN, D. E., BESRA, G. S., LEE, O. Y., GERNAEY, A. M., GALILI, E., ESHED, V., GREENBLATT, C. L., LEMMA, E., BAR-GAL, G. K. & SPIGELMAN, M. 2008. Detection and molecular characterization of 9,000-year-old Mycobacterium tuberculosis from a Neolithic settlement in the Eastern Mediterranean. *PLoS One*, 3, e3426.
- HETT, E. C., CHAO, M. C., DENG, L. L. & RUBIN, E. J. 2008. A mycobacterial enzyme essential for cell division synergizes with resuscitation-promoting factor. *PLoS Pathog*, 4, e1000001.
- HETT, E. C. & RUBIN, E. J. 2008. Bacterial growth and cell division: a mycobacterial perspective. *Microbiol Mol Biol Rev*, 72, 126-56, table of contents.
- HOLTJE, J. V. & TOMASZ, A. 1975. Lipoteichoic acid: a specific inhibitor of autolysin activity in Pneumococcus. *Proc Natl Acad Sci U S A*, 72, 1690-4.

- HOLTKE, H. J. & KESSLER, C. 1990. Non-radioactive labeling of RNA transcripts in vitro with the hapten digoxigenin (DIG); hybridization and ELISA-based detection. *Nucleic Acids Res*, 18, 5843-51.
- HOLTKE, H. J., SEIBL, R., BURG, J., MUHLEGGGER, K. & KESSLER, C. 1990. Non-radioactive labeling and detection of nucleic acids. II. Optimization of the digoxigenin system. *Biol Chem Hoppe Seyler*, 371, 929-38.
- HOMOLKA, S., NIEMANN, S., RUSSELL, D. G. & ROHDE, K. H. 2010. Functional genetic diversity among Mycobacterium tuberculosis complex clinical isolates: delineation of conserved core and lineage-specific transcriptomes during intracellular survival. *PLoS Pathog*, 6, e1000988.
- HONG, X. & HOPFINGER, A. J. 2004a. Construction, molecular modeling, and simulation of Mycobacterium tuberculosis cell walls. *Biomacromolecules*, 5, 1052-65.
- HONG, X. & HOPFINGER, A. J. 2004b. Molecular modeling and simulation of Mycobacterium tuberculosis cell wall permeability. *Biomacromolecules*, 5, 1066-77.
- HORVATH, C. G., PREISS, B. A. & LIPSKY, S. R. 1967. Fast liquid chromatography: an investigation of operating parameters and the separation of nucleotides on pellicular ion exchangers. *Anal Chem*, 39, 1422-8.
- HU, Y., MANGAN, J. A., DHILLON, J., SOLE, K. M., MITCHISON, D. A., BUTCHER, P. D. & COATES, A. R. 2000. Detection of mRNA transcripts and active transcription in persistent Mycobacterium tuberculosis induced by exposure to rifampin or pyrazinamide. *J Bacteriol*, 182, 6358-65.
- JACOBS, C., HUANG, L. J., BARTOWSKY, E., NORMARK, S. & PARK, J. T. 1994. Bacterial cell wall recycling provides cytosolic muropeptides as effectors for beta-lactamase induction. *EMBO J*, 13, 4684-94.
- JARLIER, V. & NIKAIIDO, H. 1994. Mycobacterial cell wall: structure and role in natural resistance to antibiotics. *FEMS Microbiol Lett*, 123, 11-8.
- JASSAL, M. & BISHAI, W. R. 2009. Extensively drug-resistant tuberculosis. *Lancet Infect Dis*, 9, 19-30.
- JO, E. K., PARK, J. K. & DOCKRELL, H. M. 2003. Dynamics of cytokine generation in patients with active pulmonary tuberculosis. *Curr Opin Infect Dis*, 16, 205-10.
- JOUANGUY, E., ALTARE, F., LAMHAMEDI, S., REVY, P., EMILE, J. F., NEWPORT, M., LEVIN, M., BLANCHE, S., SEBOUN, E., FISCHER, A. & CASANOVA, J. L. 1996. Interferon-gamma-receptor deficiency in an infant with fatal bacille Calmette-Guerin infection. *N Engl J Med*, 335, 1956-61.
- KALISZAN, R., WICZLING, P. & MARKUSZEWSKI, M. J. 2004. pH gradient reversed-phase HPLC. *Anal Chem*, 76, 749-60.
- KANA, B. D., GORDHAN, B. G., DOWNING, K. J., SUNG, N., VOSTROKTUNOVA, G., MACHOWSKI, E. E., TSENOVA, L., YOUNG, M., KAPRELYANTS, A., KAPLAN, G. & MIZRAHI, V. 2008. The resuscitation-promoting factors of Mycobacterium tuberculosis are required for virulence and resuscitation from dormancy but are collectively dispensable for growth in vitro. *Mol Microbiol*, 67, 672-84.
- KANA, B. D. & MIZRAHI, V. 2010. Resuscitation-promoting factors as lytic enzymes for bacterial growth and signaling. *FEMS Immunol Med Microbiol*, 58, 39-50.
- KANETSUNA, F. 1980. Effect of lysozyme on mycobacteria. *Microbiol Immunol*, 24, 1151-62.
- KANG, P., MECHREF, Y., KLOUCKOVA, I. & NOVOTNY, M. V. 2005. Solid-phase permethylation of glycans for mass spectrometric analysis. *Rapid Commun Mass Spectrom*, 19, 3421-8.
- KAPRELYANTS, A. S., GOTTSCHAL, J. C. & KELL, D. B. 1993. Dormancy in non-sporulating bacteria. *FEMS Microbiol Rev*, 10, 271-85.
- KARAKOUSIS, P. C., YOSHIMATSU, T., LAMICHHANE, G., WOOLWINE, S. C., NUERMBERGER, E. L., GROSSET, J. & BISHAI, W. R. 2004. Dormancy phenotype displayed by extracellular

- Mycobacterium tuberculosis within artificial granulomas in mice. *J Exp Med*, 200, 647-57.
- KATO-MAEDA, M., RHEE, J. T., GINGERAS, T. R., SALAMON, H., DRENKOW, J., SMITTIPAT, N. & SMALL, P. M. 2001. Comparing genomes within the species Mycobacterium tuberculosis. *Genome Res*, 11, 547-54.
- KAUFMANN, S. H. 2008. Tuberculosis: Deadly combination. *Nature*, 453, 295-6.
- KAUR, G. & DUFOUR, J. M. 2012. Cell lines: Valuable tools or useless artifacts. *Spermatogenesis*, 2, 1-5.
- KEILER, K. C. 2008. Biology of trans-translation. *Annu Rev Microbiol*, 62, 133-51.
- KESSLER, C., HOLTKE, H. J., SEIBL, R., BURG, J. & MUHLEGGGER, K. 1990. Non-radioactive labeling and detection of nucleic acids. I. A novel DNA labeling and detection system based on digoxigenin: anti-digoxigenin ELISA principle (digoxigenin system). *Biol Chem Hoppe Seyler*, 371, 917-27.
- KLEINERT, S., TONY, H. P., KRUEGER, K., DETERT, J., MIELKE, F., ROCKWITZ, K., SCHWENKE, R., BURMESTER, G. R., DIEL, R., FEUCHTENBERGER, M. & KNEITZ, C. 2012. Screening for latent tuberculosis infection: performance of tuberculin skin test and interferon-gamma release assays under real-life conditions. *Ann Rheum Dis*, 71, 1791-5.
- KNECHEL, N. A. 2009. Tuberculosis: pathophysiology, clinical features, and diagnosis. *Crit Care Nurse*, 29, 34-43; quiz 44.
- KOH, W. J., KWON, O. J. & LEE, K. S. 2002. Nontuberculous mycobacterial pulmonary diseases in immunocompetent patients. *Korean J Radiol*, 3, 145-57.
- KRAFT, A. R., TEMPLIN, M. F. & HOLTJE, J. V. 1998. Membrane-bound lytic endotransglycosylase in Escherichia coli. *J Bacteriol*, 180, 3441-7.
- KROGH, A., LARSSON, B., VON HEIJNE, G. & SONNHAMMER, E. L. 2001. Predicting transmembrane protein topology with a hidden Markov model: application to complete genomes. *J Mol Biol*, 305, 567-80.
- KRULWICH, T. A., ENSIGN, J. C., TIPPER, D. J. & STROMINGER, J. L. 1967. Sphere-rod morphogenesis in Arthrobacter crystallopoietes. I. Cell wall composition and polysaccharides of the peptidoglycan. *J Bacteriol*, 94, 734-40.
- LAABERKI, M. H., PFEFFER, J., CLARKE, A. J. & DWORKIN, J. 2011. O-Acetylation of peptidoglycan is required for proper cell separation and S-layer anchoring in Bacillus anthracis. *J Biol Chem*, 286, 5278-88.
- LANGER, P. R., WALDROP, A. A. & WARD, D. C. 1981. Enzymatic synthesis of biotin-labeled polynucleotides: novel nucleic acid affinity probes. *Proc Natl Acad Sci U S A*, 78, 6633-7.
- LAVOLLAY, M., ARTHUR, M., FOURGEAUD, M., DUBOST, L., MARIE, A., VEZIRIS, N., BLANOT, D., GUTMANN, L. & MAINARDI, J. L. 2008. The peptidoglycan of stationary-phase Mycobacterium tuberculosis predominantly contains cross-links generated by L,D-transpeptidation. *J Bacteriol*, 190, 4360-6.
- LAWN, S. D., WOOD, R. & WILKINSON, R. J. 2011. Changing concepts of "latent tuberculosis infection" in patients living with HIV infection. *Clin Dev Immunol*, 2011.
- LAWN, S. D. & ZUMLA, A. I. 2011. Tuberculosis. *Lancet*, 378, 57-72.
- LEVIN, M. E. & HATFULL, G. F. 1993. Mycobacterium smegmatis RNA polymerase: DNA supercoiling, action of rifampicin and mechanism of rifampicin resistance. *Mol Microbiol*, 8, 277-85.
- LI, M. S., MONAHAN, I. M., WADDELL, S. J., MANGAN, J. A., MARTIN, S. L., EVERETT, M. J. & BUTCHER, P. D. 2001. cDNA-RNA subtractive hybridization reveals increased expression of mycocerosic acid synthase in intracellular Mycobacterium bovis BCG. *Microbiology*, 147, 2293-305.
- LI, Z., CLARKE, A. J. & BEVERIDGE, T. J. 1998. Gram-negative bacteria produce membrane vesicles which are capable of killing other bacteria. *J Bacteriol*, 180, 5478-83.

- LIM, A. & DICK, T. 2001. Plate-based dormancy culture system for Mycobacterium smegmatis and isolation of metronidazole-resistant mutants. *FEMS Microbiol Lett*, 200, 215-9.
- LIPSCOMB, J. D. & HOFFMAN, B. M. 2005. Allosteric control of O₂ reactivity in Rieske oxygenases. *Structure*, 13, 684-5.
- M. MADIGAN, J. M., P. DUNLAP AND D. CLARK 2009. *Biology of Microorganisms*, Pearson Benjamin Cummings.
- MAGNET, S., DUBOST, L., MARIE, A., ARTHUR, M. & GUTMANN, L. 2008. Identification of the L,D-transpeptidases for peptidoglycan cross-linking in Escherichia coli. *J Bacteriol*, 190, 4782-5.
- MAHAPATRA, S., CRICK, D. C., MCNEIL, M. R. & BRENNAN, P. J. 2008. Unique structural features of the peptidoglycan of Mycobacterium leprae. *J Bacteriol*, 190, 655-61.
- MAHAPATRA, S., SCHERMAN, H., BRENNAN, P. J. & CRICK, D. C. 2005. N Glycolylation of the nucleotide precursors of peptidoglycan biosynthesis of Mycobacterium spp. is altered by drug treatment. *J Bacteriol*, 187, 2341-7.
- MAJLESSI, L., BRODIN, P., BROSCHE, R., ROJAS, M. J., KHUN, H., HUERRE, M., COLE, S. T. & LECLERC, C. 2005. Influence of ESAT-6 secretion system 1 (RD1) of Mycobacterium tuberculosis on the interaction between mycobacteria and the host immune system. *J Immunol*, 174, 3570-9.
- MAKAROV, V., MANINA, G., MIKUSOVA, K., MOLLMANN, U., RYABOVA, O., SAINT-JOANIS, B., DHAR, N., PASCA, M. R., BURONI, S., LUCARELLI, A. P., MILANO, A., DE ROSSI, E., BELANOVA, M., BOBOVSKA, A., DIANISKOVA, P., KORDULAKOVA, J., SALA, C., FULLAM, E., SCHNEIDER, P., MCKINNEY, J. D., BRODIN, P., CHRISTOPHE, T., WADDELL, S., BUTCHER, P., ALBRETHSEN, J., ROSENKRANDS, I., BROSCHE, R., NANDI, V., BHARATH, S., GAONKAR, S., SHANDIL, R. K., BALASUBRAMANIAN, V., BALGANESH, T., TYAGI, S., GROSSET, J., RICCARDI, G. & COLE, S. T. 2009. Benzothiazinones kill Mycobacterium tuberculosis by blocking arabinan synthesis. *Science*, 324, 801-4.
- MANGAN, J. A., SOLE, K. M., MITCHISON, D. A. & BUTCHER, P. D. 1997. An effective method of RNA extraction from bacteria refractory to disruption, including mycobacteria. *Nucleic Acids Res*, 25, 675-6.
- MANGANELLI, R., VOSKUIL, M. I., SCHOOLNIK, G. K. & SMITH, I. 2001. The Mycobacterium tuberculosis ECF sigma factor sigmaE: role in global gene expression and survival in macrophages. *Mol Microbiol*, 41, 423-37.
- MARRAKCHI, H., LANEELLE, G. & QUEMARD, A. 2000. InhA, a target of the antituberculous drug isoniazid, is involved in a mycobacterial fatty acid elongation system, FAS-II. *Microbiology*, 146 (Pt 2), 289-96.
- MASSCHALCK, B., VAN HOUTDT, R., VAN HAVER, E. G. & MICHIELS, C. W. 2001. Inactivation of gram-negative bacteria by lysozyme, denatured lysozyme, and lysozyme-derived peptides under high hydrostatic pressure. *Appl Environ Microbiol*, 67, 339-44.
- MATSUHASHI, M. 1966. [Biosynthesis in the bacterial cell wall]. *Tanpakushitsu Kakusan Koso*, 11, 875-86.
- MATTEELLI, A., CARVALHO, A. C., DOOLEY, K. E. & KRITSKI, A. 2010. TMC207: the first compound of a new class of potent anti-tuberculosis drugs. *Future Microbiol*, 5, 849-58.
- MAZUREK, G. H., JEREB, J., VERNON, A., LOBUE, P., GOLDBERG, S. & CASTRO, K. 2010. Updated guidelines for using Interferon Gamma Release Assays to detect Mycobacterium tuberculosis infection - United States, 2010. *MMWR Recomm Rep*, 59, 1-25.
- MCCUNE, R. M., JR., MCDERMOTT, W. & TOMPSETT, R. 1956. The fate of Mycobacterium tuberculosis in mouse tissues as determined by the microbial enumeration technique. II. The conversion of tuberculous infection to the latent state by the administration of pyrazinamide and a companion drug. *J Exp Med*, 104, 763-802.

- MCCUNE, R. M., JR. & TOMPSETT, R. 1956. Fate of Mycobacterium tuberculosis in mouse tissues as determined by the microbial enumeration technique. I. The persistence of drug-susceptible tubercle bacilli in the tissues despite prolonged antimicrobial therapy. *J Exp Med*, 104, 737-62.
- MCNEIL, M., DAFTE, M. & BRENNAN, P. J. 1990. Evidence for the nature of the link between the arabinogalactan and peptidoglycan of mycobacterial cell walls. *J Biol Chem*, 265, 18200-6.
- MCNERNEY, R., MAEURER, M., ABUBAKAR, I., MARAIS, B., MCHUGH, T. D., FORD, N., WEYER, K., LAWN, S., GROBUSCH, M. P., MEMISH, Z., SQUIRE, S. B., PANTALEO, G., CHAKAYA, J., CASENGHI, M., MIGLIORI, G. B., MWABA, P., ZIJENAH, L., HOELSCHER, M., COX, H., SWAMINATHAN, S., KIM, P. S., SCHITO, M., HARARI, A., BATES, M., SCHWANK, S., O'GRADY, J., PLETSCHETTE, M., DITUI, L., ATUN, R. & ZUMLA, A. 2012. Tuberculosis diagnostics and biomarkers: needs, challenges, recent advances, and opportunities. *J Infect Dis*, 205 Suppl 2, S147-58.
- METCALFE, C., MACDONALD, I. K., MURPHY, E. J., BROWN, K. A., RAVEN, E. L. & MOODY, P. C. 2008. The tuberculosis prodrug isoniazid bound to activating peroxidases. *J Biol Chem*, 283, 6193-200.
- MIESEL, L., ROZWARSKI, D. A., SACCHETTINI, J. C. & JACOBS, W. R., JR. 1998. Mechanisms for isoniazid action and resistance. *Novartis Found Symp*, 217, 209-20; discussion 220-1.
- MOSTOWY, S., COUSINS, D., BRINKMAN, J., ARANAZ, A. & BEHR, M. A. 2002. Genomic deletions suggest a phylogeny for the Mycobacterium tuberculosis complex. *J Infect Dis*, 186, 74-80.
- MUKADI, Y. D., MAHER, D. & HARRIES, A. 2001. Tuberculosis case fatality rates in high HIV prevalence populations in sub-Saharan Africa. *AIDS*, 15, 143-52.
- MUKAMOLOVA, G. V., KAPRELYANTS, A. S., YOUNG, D. I., YOUNG, M. & KELL, D. B. 1998a. A bacterial cytokine. *Proc Natl Acad Sci U S A*, 95, 8916-21.
- MUKAMOLOVA, G. V., MURZIN, A. G., SALINA, E. G., DEMINA, G. R., KELL, D. B., KAPRELYANTS, A. S. & YOUNG, M. 2006. Muralytic activity of Micrococcus luteus Rpf and its relationship to physiological activity in promoting bacterial growth and resuscitation. *Mol Microbiol*, 59, 84-98.
- MUKAMOLOVA, G. V., TURAPOV, O., MALKIN, J., WOLTMANN, G. & BARER, M. R. 2010. Resuscitation-promoting factors reveal an occult population of tubercle Bacilli in Sputum. *Am J Respir Crit Care Med*, 181, 174-80.
- MUKAMOLOVA, G. V., TURAPOV, O. A., KAZARIAN, K., TELKOV, M., KAPRELYANTS, A. S., KELL, D. B. & YOUNG, M. 2002a. The rpf gene of Micrococcus luteus encodes an essential secreted growth factor. *Mol Microbiol*, 46, 611-21.
- MUKAMOLOVA, G. V., TURAPOV, O. A., YOUNG, D. I., KAPRELYANTS, A. S., KELL, D. B. & YOUNG, M. 2002b. A family of autocrine growth factors in Mycobacterium tuberculosis. *Mol Microbiol*, 46, 623-35.
- MUKAMOLOVA, G. V., YANOPOLSKAYA, N. D., KELL, D. B. & KAPRELYANTS, A. S. 1998b. On resuscitation from the dormant state of Micrococcus luteus. *Antonie Van Leeuwenhoek*, 73, 237-43.
- MURRAY, J. F. 2004. Mycobacterium tuberculosis and the cause of consumption: from discovery to fact. *Am J Respir Crit Care Med*, 169, 1086-8.
- NERLICH, A. G., HAAS, C. J., ZINK, A., SZEIMIES, U. & HAGEDORN, H. G. 1997. Molecular evidence for tuberculosis in an ancient Egyptian mummy. *Lancet*, 350, 1404.
- NICOD, L. P. 2007. Immunology of tuberculosis. *Swiss Med Wkly*, 137, 357-62.
- NIKITUSHKIN, V. D., DEMINA, G. R., SHLEEVA, M. O. & KAPRELYANTS, A. S. 2013. Peptidoglycan fragments stimulate resuscitation of "non-culturable" mycobacteria. *Antonie Van Leeuwenhoek*, 103, 37-46.

- NIKOLSKAYA, A. N. & GALPERIN, M. Y. 2002. A novel type of conserved DNA-binding domain in the transcriptional regulators of the AlgR/AgrA/Lytr family. *Nucleic Acids Res*, 30, 2453-9.
- NOVAGEN 2003a. pET System Manual. 10 ed. Germany: Brookhaven Science Associates.
- NOVAGEN 2003b. pET System Manual. 10th ed.: Novagen.
- O'SULLIVAN, D. M., NICOARA, S. C., MUTETWA, R., MUNGOFA, S., LEE, O. Y., MINNIKIN, D. E., BARDWELL, M. W., CORBETT, E. L., MCNERNEY, R. & MORGAN, G. H. 2012. Detection of Mycobacterium tuberculosis in sputum by gas chromatography-mass spectrometry of methyl mycocerosates released by thermochemolysis. *PLoS One*, 7, e32836.
- OLIJHOEK, A. J., KLENCKE, S., PAS, E., NANNINGA, N. & SCHWARZ, U. 1982. Volume growth, murein synthesis, and murein cross-linkage during the division cycle of Escherichia coli PA3092. *J Bacteriol*, 152, 1248-54.
- ONAKA, H., MORI, Y., IGARASHI, Y. & FURUMAI, T. 2011. Mycolic acid-containing bacteria induce natural-product biosynthesis in Streptomyces species. *Appl Environ Microbiol*, 77, 400-6.
- ORME, I. M. 1988. A mouse model of the recrudescence of latent tuberculosis in the elderly. *Am Rev Respir Dis*, 137, 716-8.
- OTTOLENGHI, A. C., CAPARROS, M. & DE PEDRO, M. A. 1993. Peptidoglycan tripeptide content and cross-linking are altered in Enterobacter cloacae induced to produce AmpC beta-lactamase by glycine and D-amino acids. *J Bacteriol*, 175, 1537-42.
- PALANISAMY, G. S., DUTEAU, N., EISENACH, K. D., CAVE, D. M., THEUS, S. A., KREISWIRTH, B. N., BASARABA, R. J. & ORME, I. M. 2009. Clinical strains of Mycobacterium tuberculosis display a wide range of virulence in guinea pigs. *Tuberculosis (Edinb)*, 89, 203-9.
- PARISH, T. & STOKER, N. G. 2000. Use of a flexible cassette method to generate a double unmarked Mycobacterium tuberculosis tlyA plcABC mutant by gene replacement. *Microbiology*, 146 (Pt 8), 1969-75.
- PARISH, T. & STOKER, N. G. 1998. *Mycobacteria Protocols*[SPRINGER VERLAG GMBH.
- PARRISH, N. M., DICK, J. D. & BISHAI, W. R. 1998. Mechanisms of latency in Mycobacterium tuberculosis. *Trends Microbiol*, 6, 107-12.
- PATEL, K., JHAMB, S. S. & SINGH, P. P. 2011. Models of latent tuberculosis: their salient features, limitations, and development. *J Lab Physicians*, 3, 75-9.
- PETERSEN, T. N., BRUNAK, S., VON HEIJNE, G. & NIELSEN, H. 2011. SignalP 4.0: discriminating signal peptides from transmembrane regions. *Nat Methods*, 8, 785-6.
- PETIT, J. F., ADAM, A., WIETZEBIN-FALSZPAN, J., LEDERER, E. & GHUYSEN, J. M. 1969. Chemical structure of the cell wall of Mycobacterium smegmatis. I. Isolation and partial characterization of the peptidoglycan. *Biochem Biophys Res Commun*, 35, 478-85.
- PFAFFL, M. W. 2004. Quantification strategies in real-time PCR. In: BUSTIN, S. A. (ed.) *A-Z of quantitative PCR*.
- PFANZAGL, B., ZENKER, A., PITTENAUER, E., ALLMAIER, G., MARTINEZ-TORRECUADRADA, J., SCHMID, E. R., DE PEDRO, M. A. & LOFFELHARDT, W. 1996. Primary structure of cyanelle peptidoglycan of Cyanophora paradoxa: a prokaryotic cell wall as part of an organelle envelope. *J Bacteriol*, 178, 332-9.
- PFENNINGER, A., KARAS, M., FINKE, B., STAHL, B. & SAWATZKI, G. 1999. Matrix optimization for matrix-assisted laser desorption/ionization mass spectrometry of oligosaccharides from human milk. *J Mass Spectrom*, 34, 98-104.
- PRICE, N. P. 2008. Permethylated linkage analysis techniques for residual carbohydrates. *Appl Biochem Biotechnol*, 148, 271-6.
- PROVVEDI, R., BOLDRIN, F., FALCIANI, F., PALU, G. & MANGANELLI, R. 2009. Global transcriptional response to vancomycin in Mycobacterium tuberculosis. *Microbiology*, 155, 1093-102.

- RAMAN, S., HAZRA, R., DASCHER, C. C. & HUSSON, R. N. 2004. Transcription regulation by the Mycobacterium tuberculosis alternative sigma factor SigD and its role in virulence. *J Bacteriol*, 186, 6605-16.
- RAYMOND, J. B., MAHAPATRA, S., CRICK, D. C. & PAVELKA, M. S., JR. 2005. Identification of the namH gene, encoding the hydroxylase responsible for the N-glycolylation of the mycobacterial peptidoglycan. *J Biol Chem*, 280, 326-33.
- REDDY, T. B., RILEY, R., WYMORE, F., MONTGOMERY, P., DECAPRIO, D., ENGELS, R., GELLESCH, M., HUBBLE, J., JEN, D., JIN, H., KOEHRSEN, M., LARSON, L., MAO, M., NITZBERG, M., SISK, P., STOLTE, C., WEINER, B., WHITE, J., ZACHARIAH, Z. K., SHERLOCK, G., GALAGAN, J. E., BALL, C. A. & SCHOOLNIK, G. K. 2009. TB database: an integrated platform for tuberculosis research. *Nucleic Acids Res*, 37, D499-508.
- RENGARAJAN, J., BLOOM, B. R. & RUBIN, E. J. 2005. Genome-wide requirements for Mycobacterium tuberculosis adaptation and survival in macrophages. *Proc Natl Acad Sci U S A*, 102, 8327-32.
- RIBEIRO, A. L., DEGIACOMI, G., EWANN, F., BURONI, S., INCANDELA, M. L., CHIARELLI, L. R., MORI, G., KIM, J., CONTRERAS-DOMINGUEZ, M., PARK, Y. S., HAN, S. J., BRODIN, P., VALENTINI, G., RIZZI, M., RICCARDI, G. & PASCA, M. R. 2011. Analogous mechanisms of resistance to benzothiazinones and dinitrobenzamides in Mycobacterium smegmatis. *PLoS One*, 6, e26675.
- RICHELDI, L., EWER, K., LOSI, M., BERGAMINI, B. M., ROVERSI, P., DEEKS, J., FABBRI, L. M. & LALVANI, A. 2004. T cell-based tracking of multidrug resistant tuberculosis infection after brief exposure. *Am J Respir Crit Care Med*, 170, 288-95.
- RICKMAN, L., SCOTT, C., HUNT, D. M., HUTCHINSON, T., MENENDEZ, M. C., WHALAN, R., HINDS, J., COLSTON, M. J., GREEN, J. & BUXTON, R. S. 2005. A member of the cAMP receptor protein family of transcription regulators in Mycobacterium tuberculosis is required for virulence in mice and controls transcription of the rpfA gene coding for a resuscitation promoting factor. *Mol Microbiol*, 56, 1274-86.
- RUGGIERO, A., MARASCO, D., SQUEGLIA, F., SOLDINI, S., PEDONE, E., PEDONE, C. & BERISIO, R. 2010. Structure and functional regulation of RipA, a mycobacterial enzyme essential for daughter cell separation. *Structure*, 18, 1184-90.
- RUGGIERO, A., SQUEGLIA, F., PIRONE, L., CORREALE, S. & BERISIO, R. 2011. Expression, purification, crystallization and preliminary X-ray crystallographic analysis of a major fragment of the resuscitation-promoting factor RpfB from Mycobacterium tuberculosis. *Acta Crystallogr Sect F Struct Biol Cryst Commun*, 67, 164-8.
- RUGGIERO, A., TIZZANO, B., GEERLOF, A., PEDONE, E., PEDONE, C., WILMANNNS, M. & BERISIO, R. 2007. Expression, purification, crystallization and preliminary X-ray crystallographic analysis of a resuscitation-promoting factor from Mycobacterium tuberculosis. *Acta Crystallogr Sect F Struct Biol Cryst Commun*, 63, 870-3.
- RUGGIERO, A., TIZZANO, B., PEDONE, E., PEDONE, C., WILMANNNS, M. & BERISIO, R. 2009. Crystal structure of the resuscitation-promoting factor (DeltaDUF)RpfB from M. tuberculosis. *J Mol Biol*, 385, 153-62.
- RUSSELL-GOLDMAN, E., XU, J., WANG, X., CHAN, J. & TUFARIELLO, J. M. 2008. A Mycobacterium tuberculosis Rpf double-knockout strain exhibits profound defects in reactivation from chronic tuberculosis and innate immunity phenotypes. *Infect Immun*, 76, 4269-81.
- SALTON, M. R. J. 1964. *The Bacterial Cell Wall*, New York, Elsevier
- SASSETTI, C. M., BOYD, D. H. & RUBIN, E. J. 2003. Genes required for mycobacterial growth defined by high density mutagenesis. *Mol Microbiol*, 48, 77-84.
- SCANGA, C. A., MOHAN, V. P., JOSEPH, H., YU, K., CHAN, J. & FLYNN, J. L. 1999. Reactivation of latent tuberculosis: variations on the Cornell murine model. *Infect Immun*, 67, 4531-8.

- SCHLEIFER, K. H. & KANDLER, O. 1972. Peptidoglycan types of bacterial cell walls and their taxonomic implications. *Bacteriol Rev*, 36, 407-77.
- SEDDON, J. A., HESSELING, A. C., MARAIS, B. J., MCILLERON, H., PELOQUIN, C. A., DONALD, P. R. & SCHAAP, H. S. 2012. Paediatric use of second-line anti-tuberculosis agents: a review. *Tuberculosis (Edinb)*, 92, 9-17.
- SEGALA, E., SOUGAKOFF, W., NEVEJANS-CHAUFFOUR, A., JARLIER, V. & PETRELLA, S. 2012. New mutations in the mycobacterial ATP synthase: new insights into the binding of the diarylquinoline TMC207 to the ATP synthase C-ring structure. *Antimicrob Agents Chemother*, 56, 2326-34.
- SESTER, M., SOTGIU, G., LANGE, C., GIEHL, C., GIRARDI, E., MIGLIORI, G. B., BOSSINK, A., DHEDA, K., DIEL, R., DOMINGUEZ, J., LIPMAN, M., NEMETH, J., RAVN, P., WINKLER, S., HUITRIC, E., SANDGREN, A. & MANISSERO, D. 2011. Interferon-gamma release assays for the diagnosis of active tuberculosis: a systematic review and meta-analysis. *Eur Respir J*, 37, 100-11.
- SHAH, I. M. & DWORKIN, J. 2010. Induction and regulation of a secreted peptidoglycan hydrolase by a membrane Ser/Thr kinase that detects muropeptides. *Mol Microbiol*, 75, 1232-43.
- SHAH, I. M., LAABERKI, M. H., POPHAM, D. L. & DWORKIN, J. 2008. A eukaryotic-like Ser/Thr kinase signals bacteria to exit dormancy in response to peptidoglycan fragments. *Cell*, 135, 486-96.
- SHAILA, M. S., GOPINATHAN, K. P. & RAMAKRISHNAN, T. 1973. Protein synthesis in Mycobacterium tuberculosis H37Rv and the effect of streptomycin in streptomycin-susceptible and -resistant strains. *Antimicrob Agents Chemother*, 4, 205-13.
- SHI, W., ZHANG, X., JIANG, X., YUAN, H., LEE, J. S., BARRY, C. E., 3RD, WANG, H., ZHANG, W. & ZHANG, Y. 2011. Pyrazinamide inhibits trans-translation in Mycobacterium tuberculosis. *Science*, 333, 1630-2.
- SHLEEVA, M., MUKAMOLOVA, G. V., YOUNG, M., WILLIAMS, H. D. & KAPRELYANTS, A. S. 2004. Formation of 'non-culturable' cells of Mycobacterium smegmatis in stationary phase in response to growth under suboptimal conditions and their Rpf-mediated resuscitation. *Microbiology*, 150, 1687-97.
- SHLEEVA, M. O., BAGRAMYAN, K., TELKOV, M. V., MUKAMOLOVA, G. V., YOUNG, M., KELL, D. B. & KAPRELYANTS, A. S. 2002. Formation and resuscitation of "non-culturable" cells of Rhodococcus rhodochrous and Mycobacterium tuberculosis in prolonged stationary phase. *Microbiology*, 148, 1581-91.
- SIGRIST, C. J., DE CASTRO, E., CERUTTI, L., CUCHE, B. A., HULO, N., BRIDGE, A., BOUGUELERET, L. & XENARIOS, I. 2013. New and continuing developments at PROSITE. *Nucleic Acids Res*, 41, D344-7.
- SMEULDERS, M. J., KEER, J., SPEIGHT, R. A. & WILLIAMS, H. D. 1999. Adaptation of Mycobacterium smegmatis to stationary phase. *J Bacteriol*, 181, 270-83.
- SMITH, N. H., HEWINSON, R. G., KREMER, K., BROSCHE, R. & GORDON, S. V. 2009. Myths and misconceptions: the origin and evolution of Mycobacterium tuberculosis. *Nat Rev Microbiol*, 7, 537-44.
- STAAL, J., ABRAMOFF, M. D., NIEMEIJER, M., VIERGEVER, M. A. & VAN GINNEKEN, B. 2004. Ridge-based vessel segmentation in color images of the retina. *IEEE Trans Med Imaging*, 23, 501-9.
- STAHLBERG, A., HAKANSSON, J., XIAN, X., SEMB, H. & KUBISTA, M. 2004. Properties of the reverse transcription reaction in mRNA quantification. *Clin Chem*, 50, 509-15.
- STEAD, W. W., EISENACH, K. D., CAVE, M. D., BEGGS, M. L., TEMPLETON, G. L., THOEN, C. O. & BATES, J. H. 1995. When did Mycobacterium tuberculosis infection first occur in the New World? An important question with public health implications. *Am J Respir Crit Care Med*, 151, 1267-8.

- STEINGART, K. R., HENRY, M., LAAL, S., HOPEWELL, P. C., RAMSAY, A., MENZIES, D., CUNNINGHAM, J., WELDINGH, K. & PAI, M. 2007. Commercial serological antibody detection tests for the diagnosis of pulmonary tuberculosis: a systematic review. *PLoS Med*, 4, e202.
- STEWART-TULL, D. E. & WHITE, R. G. 1964. The Occurrence of Muramic Acid in Wax D Preparations of Mycobacteria. *J Gen Microbiol*, 34, 43-9.
- STORLA, D. G., YIMER, S. & BJUNE, G. A. 2008. A systematic review of delay in the diagnosis and treatment of tuberculosis. *BMC Public Health*, 8, 15.
- SUBBIAN, S., TSENOVA, L., O'BRIEN, P., YANG, G., KOO, M. S., PEIXOTO, B., FALLOWS, D., DARTOIS, V., MULLER, G. & KAPLAN, G. 2011. Phosphodiesterase-4 inhibition alters gene expression and improves isoniazid-mediated clearance of Mycobacterium tuberculosis in rabbit lungs. *PLoS Pathog*, 7, e1002262.
- SUN, Z. & ZHANG, Y. 1999. Spent culture supernatant of Mycobacterium tuberculosis H37Ra improves viability of aged cultures of this strain and allows small inocula to initiate growth. *J Bacteriol*, 181, 7626-8.
- SUO, J., CHANG, C. E., LIN, T. P. & HEIFETS, L. B. 1988. Minimal inhibitory concentrations of isoniazid, rifampin, ethambutol, and streptomycin against Mycobacterium tuberculosis strains isolated before treatment of patients in Taiwan. *Am Rev Respir Dis*, 138, 999-1001.
- SWARTZ, M. E. 2005. UPLC: An Introduction and Review. *Journal of liquid chromatography*, 28, 1253-1263.
- TABARSI, P., BAGHAEI, P., FARNIA, P., MANSOURI, N., CHITSAZ, E., SHEIKHOESLAM, F., MARJANI, M., ROUHANI, N., MIRSAEIDI, M., ALIPANAH, N., AMIRI, M., MASJEDI, M. R. & MANSOURI, D. 2009. Nontuberculous mycobacteria among patients who are suspected for multidrug-resistant tuberculosis-need for earlier identification of nontuberculous mycobacteria. *Am J Med Sci*, 337, 182-4.
- TAKAYAMA, K., DAVID, H. L., WANG, L. & GOLDMAN, D. S. 1970. Isolation and characterization of uridine diphosphate-N-glycolylmuramyl-L-alanyl-gamma-D-glutamyl-meso-alpha,alpha'-diamino pimelic acid from Mycobacterium tuberculosis. *Biochem Biophys Res Commun*, 39, 7-12.
- TAKAYAMA, K. & KILBURN, J. O. 1989. Inhibition of synthesis of arabinogalactan by ethambutol in Mycobacterium smegmatis. *Antimicrob Agents Chemother*, 33, 1493-9.
- TAKAYAMA, K., WANG, L. & DAVID, H. L. 1972. Effect of isoniazid on the in vivo mycolic acid synthesis, cell growth, and viability of Mycobacterium tuberculosis. *Antimicrob Agents Chemother*, 2, 29-35.
- TAKLE, G. W., TOTH, I. K. & BRURBERG, M. B. 2007. Evaluation of reference genes for real-time RT-PCR expression studies in the plant pathogen Pectobacterium atrosepticum. *BMC Plant Biol*, 7, 50.
- TALAAAT, A. M., HOWARD, S. T., HALE, W. T., LYONS, R., GARNER, H. & JOHNSTON, S. A. 2002. Genomic DNA standards for gene expression profiling in Mycobacterium tuberculosis. *Nucleic Acids Res*, 30, e104.
- TELENTI, A., IMBODEN, P., MARCHESI, F., SCHMIDHEINI, T. & BODMER, T. 1993. Direct, automated detection of rifampin-resistant Mycobacterium tuberculosis by polymerase chain reaction and single-strand conformation polymorphism analysis. *Antimicrob Agents Chemother*, 37, 2054-8.
- THEISSEN, G., RICHTER, A. & LUKACS, N. 1989. Degree of biotinylation in nucleic acids estimated by a gel retardation assay. *Anal Biochem*, 179, 98-105.
- TORTOLI, E., CICHERO, P., PIERSIMONI, C., SIMONETTI, M. T., GESU, G. & NISTA, D. 1999. Use of BACTEC MGIT 960 for recovery of mycobacteria from clinical specimens: multicenter study. *J Clin Microbiol*, 37, 3578-82.

- TOUBIANA, R., BERLAN, J., SATO, H. & STRAIN, M. 1979. Three types of mycolic acid from *Mycobacterium tuberculosis* Brevanne: implications for structure-function relationships in pathogenesis. *J Bacteriol*, 139, 205-11.
- TRAUB, S., VON AULOCK, S., HARTUNG, T. & HERMANN, C. 2006. MDP and other muropeptides--direct and synergistic effects on the immune system. *J Endotoxin Res*, 12, 69-85.
- TUFARIELLO, J. M., JACOBS, W. R., JR. & CHAN, J. 2004. Individual *Mycobacterium tuberculosis* resuscitation-promoting factor homologues are dispensable for growth in vitro and in vivo. *Infect Immun*, 72, 515-26.
- TUFARIELLO, J. M., MI, K., XU, J., MANABE, Y. C., KESAVAN, A. K., DRUMM, J., TANAKA, K., JACOBS, W. R., JR. & CHAN, J. 2006. Deletion of the *Mycobacterium tuberculosis* resuscitation-promoting factor Rv1009 gene results in delayed reactivation from chronic tuberculosis. *Infect Immun*, 74, 2985-95.
- TUOMANEN, E. & COZENS, R. 1987. Changes in peptidoglycan composition and penicillin-binding proteins in slowly growing *Escherichia coli*. *J Bacteriol*, 169, 5308-10.
- UTRUP, L. J., MOORE, T. D., ACTOR, P. & POUPARD, J. A. 1995. Susceptibilities of nontuberculosis mycobacterial species to amoxicillin-clavulanic acid alone and in combination with antimycobacterial agents. *Antimicrob Agents Chemother*, 39, 1454-7.
- VAN CREVEL, R., OTTENHOFF, T. H. & VAN DER MEER, J. W. 2002. Innate immunity to *Mycobacterium tuberculosis*. *Clin Microbiol Rev*, 15, 294-309.
- VAN RIE, A., WARREN, R., RICHARDSON, M., GIE, R. P., ENARSON, D. A., BEYERS, N. & VAN HELDEN, P. D. 2000. Classification of drug-resistant tuberculosis in an epidemic area. *Lancet*, 356, 22-5.
- VENTURA, M., CANCHAYA, C., TAUCH, A., CHANDRA, G., FITZGERALD, G. F., CHATER, K. F. & VAN SINDEREN, D. 2007. Genomics of Actinobacteria: tracing the evolutionary history of an ancient phylum. *Microbiol Mol Biol Rev*, 71, 495-548.
- VERGNE, I., CHUA, J. & DERETIC, V. 2003. Tuberculosis toxin blocking phagosome maturation inhibits a novel Ca²⁺/calmodulin-PI3K hVPS34 cascade. *J Exp Med*, 198, 653-9.
- VILCHEZE, C., MORBIDONI, H. R., WEISBROD, T. R., IWAMOTO, H., KUO, M., SACCHETTINI, J. C. & JACOBS, W. R., JR. 2000. Inactivation of the inhA-encoded fatty acid synthase II (FASII) enoyl-acyl carrier protein reductase induces accumulation of the FASI end products and cell lysis of *Mycobacterium smegmatis*. *J Bacteriol*, 182, 4059-67.
- VINCZE, T., POSFAI, J. & ROBERTS, R. J. 2003. NEBcutter: A program to cleave DNA with restriction enzymes. *Nucleic Acids Res*, 31, 3688-91.
- VOLLMER, W. & BERTSCHE, U. 2008. Murein (peptidoglycan) structure, architecture and biosynthesis in *Escherichia coli*. *Biochim Biophys Acta*, 1778, 1714-34.
- VOLLMER, W., JORIS, B., CHARLIER, P. & FOSTER, S. 2008. Bacterial peptidoglycan (murein) hydrolases. *FEMS Microbiol Rev*, 32, 259-86.
- VOTYAKOVA, T. V., KAPRELYANTS, A. S. & KELL, D. B. 1994. Influence of Viable Cells on the Resuscitation of Dormant Cells in *Micrococcus luteus* Cultures Held in an Extended Stationary Phase: the Population Effect. *Appl Environ Microbiol*, 60, 3284-91.
- W. C. WILEY, I. H. M. 1955. Time-of-Flight Mass Spectrometer with Improved Resolution. *The Review of Scientific Instruments*, 26, 1150 - 1157.
- WAKAMOTO, Y., DHAR, N., CHAIT, R., SCHNEIDER, K., SIGNORINO-GELO, F., LEIBLER, S. & MCKINNEY, J. D. 2013. Dynamic persistence of antibiotic-stressed mycobacteria. *Science*, 339, 91-5.
- WAKSMAN, S. A., REILLY, H. C. & SCHATZ, A. 1945. Strain Specificity and Production of Antibiotic Substances: V. Strain Resistance of Bacteria to Antibiotic Substances, Especially to Streptomycin. *Proc Natl Acad Sci U S A*, 31, 157-64.

- WALLIS, R. S., PAI, M., MENZIES, D., DOHERTY, T. M., WALZL, G., PERKINS, M. D. & ZUMLA, A. 2010. Biomarkers and diagnostics for tuberculosis: progress, needs, and translation into practice. *Lancet*, 375, 1920-37.
- WALLIS, R. S., PATIL, S., CHEON, S. H., EDMONDS, K., PHILLIPS, M., PERKINS, M. D., JOLOBA, M., NAMALE, A., JOHNSON, J. L., TEIXEIRA, L., DIETZE, R., SIDDIQI, S., MUGERWA, R. D., EISENACH, K. & ELLNER, J. J. 1999. Drug tolerance in *Mycobacterium tuberculosis*. *Antimicrob Agents Chemother*, 43, 2600-6.
- WAYNE, L. G. & HAYES, L. G. 1996. An in vitro model for sequential study of shutdown of *Mycobacterium tuberculosis* through two stages of nonreplicating persistence. *Infect Immun*, 64, 2062-9.
- WAYNE, L. G. & LIN, K. Y. 1982. Glyoxylate metabolism and adaptation of *Mycobacterium tuberculosis* to survival under anaerobic conditions. *Infect Immun*, 37, 1042-9.
- WAYNE, L. G. & SOHASKEY, C. D. 2001. Nonreplicating persistence of *Mycobacterium tuberculosis*. *Annu Rev Microbiol*, 55, 139-63.
- WEJSE, C., GUSTAFSON, P., NIELSEN, J., GOMES, V. F., AABY, P., ANDERSEN, P. L. & SODEMANN, M. 2008. TBscore: Signs and symptoms from tuberculosis patients in a low-resource setting have predictive value and may be used to assess clinical course. *Scand J Infect Dis*, 40, 111-20.
- WELIN, A., WINBERG, M. E., ABDALLA, H., SARND AHL, E., RASMUSSEN, B., STENDAHL, O. & LERM, M. 2008. Incorporation of *Mycobacterium tuberculosis* lipoarabinomannan into macrophage membrane rafts is a prerequisite for the phagosomal maturation block. *Infect Immun*, 76, 2882-7.
- WHO. 2009. Treatment of Tuberculosis: Guidelines. Available: http://whqlibdoc.who.int/publications/2010/9789241547833_eng.pdf.
- WHO 2011. Global Tuberculosis Report 2011.
- WHO 2012. Global Tuberculosis Report 2012.
- WIVAGG, C. N. & HUNG, D. T. 2012. Resuscitation-promoting factors are required for beta-lactam tolerance and the permeability barrier in *Mycobacterium tuberculosis*. *Antimicrob Agents Chemother*, 56, 1591-4.
- WU, S.T, L., C.C. AND LAI, C.H. 2009. Current Situations on Identification of Nontuberculous *Mycobacteria* *J Biomed Lab Sci*, 21, 1-5.
- WYCKOFF, T. J., TAYLOR, J. A. & SALAMA, N. R. 2012. Beyond growth: novel functions for bacterial cell wall hydrolases. *Trends Microbiol*, 20, 540-7.
- YOON, H. J., SONG, Y. G., PARK, W. I., CHOI, J. P., CHANG, K. H. & KIM, J. M. 2004. Clinical manifestations and diagnosis of extrapulmonary tuberculosis. *Yonsei Med J*, 45, 453-61.
- YOSHIDA, T. & MAJORS, R. E. 2006. High-speed analyses using rapid resolution liquid chromatography on 1.8-microm porous particles. *J Sep Sci*, 29, 2421-32.
- YOUNG, K. D. 1996. A simple gel electrophoretic method for analyzing the muropeptide composition of bacterial peptidoglycan. *J Bacteriol*, 178, 3962-6.
- YOUNG, M., ARTSATBANOV, V., BELLER, H. R., CHANDRA, G., CHATER, K. F., DOVER, L. G., GOH, E. B., KAHAN, T., KAPRELYANTS, A. S., KYRPIDES, N., LAPIDUS, A., LOWRY, S. R., LYKIDIS, A., MAHILLON, J., MARKOWITZ, V., MAVROMATIS, K., MUKAMOLOVA, G. V., OREN, A., ROKEM, J. S., SMITH, M. C., YOUNG, D. I. & GREENBLATT, C. L. 2010. Genome sequence of the Fleming strain of *Micrococcus luteus*, a simple free-living actinobacterium. *J Bacteriol*, 192, 841-60.
- ZHANG, M., SALA, C., HARTKOORN, R. C., DHAR, N., MENDOZA-LOSANA, A. & COLE, S. T. 2012. Streptomycin-starved *Mycobacterium tuberculosis* 18b, a drug discovery tool for latent tuberculosis. *Antimicrob Agents Chemother*, 56, 5782-9.
- ZHANG, Y. 2004. Persistent and dormant tubercle bacilli and latent tuberculosis. *Front Biosci*, 9, 1136-56.

- ZHANG, Y., HEYM, B., ALLEN, B., YOUNG, D. & COLE, S. 1992. The catalase-peroxidase gene and isoniazid resistance of *Mycobacterium tuberculosis*. *Nature*, 358, 591-3.
- ZHANG, Y. & MITCHISON, D. 2003. The curious characteristics of pyrazinamide: a review. *Int J Tuberc Lung Dis*, 7, 6-21.
- ZHANG, Y., WADE, M. M., SCORPIO, A., ZHANG, H. & SUN, Z. 2003. Mode of action of pyrazinamide: disruption of *Mycobacterium tuberculosis* membrane transport and energetics by pyrazinoic acid. *J Antimicrob Chemother*, 52, 790-5.
- ZHANG, Y. & YEW, W. W. 2009. Mechanisms of drug resistance in *Mycobacterium tuberculosis*. *Int J Tuberc Lung Dis*, 13, 1320-30.
- ZIPPERLE, G. F., JR., EZZELL, J. W., JR. & DOYLE, R. J. 1984. Glucosamine substitution and muramidase susceptibility in *Bacillus anthracis*. *Can J Microbiol*, 30, 553-9.
- ZUMLA, A. & MAEURER, M. 2012. Rational development of adjunct immune-based therapies for drug-resistant tuberculosis: hypotheses and experimental designs. *J Infect Dis*, 205 Suppl 2, S335-9.